

UC Berkeley

UC Berkeley Electronic Theses and Dissertations

Title

Gold(I)-Mediated Nucleophilic Additions to Allenes: from Enantioselective Catalysis to Supramolecular Chemistry

Permalink

<https://escholarship.org/uc/item/09m0s499>

Author

Wang, Zhan

Publication Date

2012

Peer reviewed|Thesis/dissertation

Gold(I)-Mediated Nucleophilic Additions to Allenes:
from Enantioselective Catalysis to Supramolecular Chemistry

By Zhan Wang

A dissertation submitted in partial satisfaction of the requirements
for the degree of Doctor of Philosophy
in
Chemistry
in the
Graduate Division
of the
University of California, Berkeley

Committee in Charge:

Professor F. Dean Toste
Professor Robert Bergman
Professor Benito de Lumen

Spring 2012

Abstract

Gold(I)-Mediated Nucleophilic Additions to Allenes: From Enantioselective Catalysis to Supramolecular Chemistry

By Zhan Wang

Doctor of Philosophy in Chemistry

Professor F. Dean Toste, Chair

The ability of gold(I) complexes to activate carbon-carbon multiple bonds for the addition of nitrogen and oxygen nucleophiles has emerged as an attractive synthetic method in organic chemistry. While many transformations catalyzed by gold(I) have been reported in recent years, few studies provide insight into the mechanism of gold(I) mediated processes. The first half of this thesis will discuss the development of an enantioselective gold(I)-catalyzed hydroamination of allenes with hydroxylamine and hydrazine nucleophiles and mechanistic studies of this and related systems. The second half of this thesis will cover our efforts to incorporate gold(I) catalysts into supramolecular host-guest complexes and will highlight potential advantages of this novel approach to gold(I) reactions.

Chapter 1. In this chapter, we report a novel enantioselective method for formation of isoxazolidines, pyrazolidines and tetrahydrooxazine heterocycles catalyzed by dinuclear bisphosphine gold(I) complexes. Furthermore, we discuss our efforts toward the development of a dynamic kinetic resolution of C_2 -symmetric allenes via intermolecular asymmetric hydroamination.

Chapter 2. We perform detailed kinetic studies to elucidate the mechanism of two transformations: the gold(I)-catalyzed hydroamination of allenes with hydrazine nucleophiles and the intramolecular hydroamination of dienes in the presence of alcohol co-catalysts. While the hydroamination of allenes proceeds via an outer sphere π -acid mechanism, the related reaction with dienes likely proceeds via a Lewis-acid assisted-Brønsted acid pathway.

Chapter 3. This chapter will focus on our efforts to incorporate catalytically active gold(I) complexes into tetrahedral supramolecular guest of the form Ga_4L_6 . Using such a complex, we catalyze the intramolecular hydroalkoxylation of allenes. We demonstrate that encapsulation of gold(I) increases the rate of reaction relative to Me_3PAuBr and also leads to improved catalyst lifetime.

Chapter 4. Herein we apply the supramolecular host-guest complex with gold(I) and Ga_4L_6 to tandem reactions with enzymes. The encapsulated complex performs as well, if not better than the “free” gold(I) complex in chemoenzymatic processes with a variety of esterase and lipases. In some cases the free gold(I) cations significantly reduce the rate of enzyme catalysis while the encapsulated complex has no effect on enzyme activity.

Table of Contents

Chapter 1: Enantioselective Hydroamination of Allenes with N-O and N-N nucleophiles.....	1
Introduction to Enantioselective Hydroamination.....	2
Results.....	7
Future Work.....	21
Experimental.....	22
References.....	39
Appendix 1A: Additional NMR data.....	41
Appendix 1B: Additional HPLC data.....	72
Chapter 2: Mechanistic Studies of Gold(I)-Catalyzed Hydroamination of Allenes and Dienes. 84	84
Introduction to Mechanisms Proposed for Transition Metal Hydroamination.....	85
Results.....	91
Experimental.....	109
References.....	133
Appendix 2A: Additional NMR and HPLC data.....	136
Chapter 3: Catalysis by Gold(I) Complexes encapsulated in a Supramolecular Host.....	142
Introduction to Supramolecular Catalysis.....	143
Results.....	153
Future Work.....	161
Experimental.....	163
References.....	173
Chapter 4: A Supramolecular Approach to Tandem Catalysis with Enzymes.....	175
Introduction to Chemoenzymatic Transformations.....	176
Results.....	181
Future Work.....	188
Experimental.....	190
References.....	195
Appendix 4A.....	197

Acknowledgements

First and foremost, I thank my advisor Professor Dean Toste for all his advice, support, enthusiasm, and motivation. I could not have picked a better place or better mentor to do my doctoral studies with and my Ph.D. experience has been more than I thought was possible when I started graduate school five years ago. I would also like to express my sincere gratitude to my two other “bosses,” Professor Bob Bergman and Professor Ken Raymond, for all their encouragement and guidance. I truly feel lucky to have been able to be a part of this three lab collaboration and to have worked with all three of my advisors. I am also very grateful for the Hertz Foundation for funding and support throughout my graduate studies.

Over the last few years, I have had the privilege of studying with an extraordinary group of graduate students and post docs in the Toste, Bergman and Raymond groups. These individuals have made graduate school a truly collaborative and rewarding experience for me and the work described in this thesis would not be possible without all of their efforts. In particular, I would like to thank Dr. Rebecca Lalonde, Dr. Melanie Chu, Dr. Giovanni Amarante, Dr. Osamu Kanno, Dr. Vivek Rauniyar, and Dr. Casey Brown for helping me and working with me on various projects. Additionally, I would like to thank Dr. Ellen Sletten, Dr. Alison Narayan, Dr. Rachel Zeldon, and Ms. Jessica Douglas for their friendship through graduate school and for helping to pull me out of the bubble of my own research when I needed it.

I thank my parents for their love and their continue efforts to understand what I study. Google translator may never provide a good definition for “enantioselective hydroamination” but their support for what I do is endless. Finally, I am grateful for Mr. David Adler, who has been a source of inspiration for me throughout grad school and whom I can always count on for love and understanding.

Chapter 1:

Enantioselective Hydroamination of Allenes with Hydroxylamine and Hydrazine Nucleophiles

A portion of this work has been published in Lalonde, R. L.; Wang, J. Z.; Mba, M.; Lackner, A. D.; Toste, F. D. "Gold(I)-Catalyzed Enantioselective Synthesis of Pyrazolidines, Isoxazolidines, and Tetrahydrooxazines." *Angew. Chem. Int. Ed.* **2010**, *49*, 98-601, but has been described here in greater detail.¹

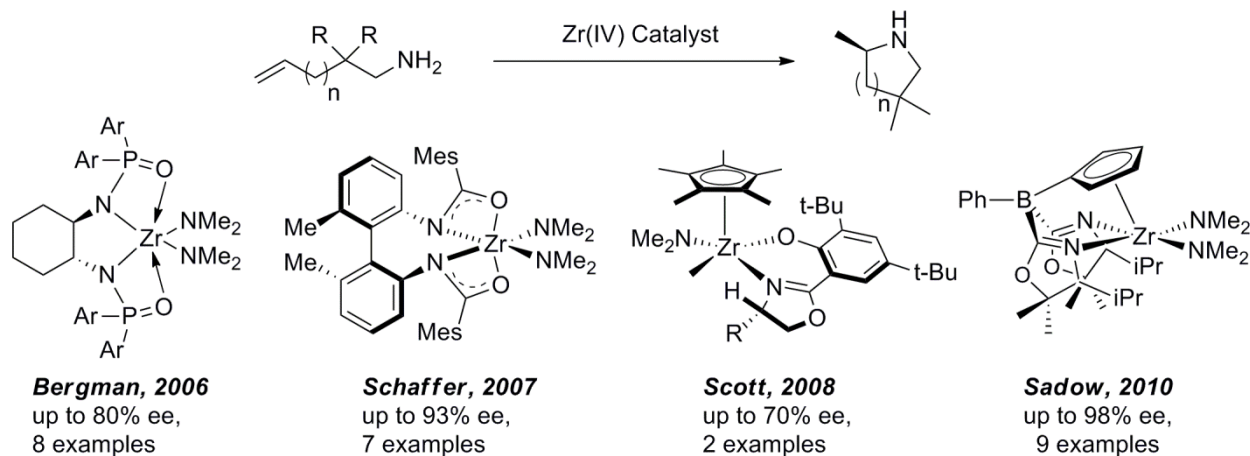
¹ Dr. Miriam Mba performed in the initial reaction. Dr. Rebecca. K. Lalonde performed hydroalkoxylation studies with terminal N-O substrates and hydroamination of hydrazine substrates. Aaron Lackner helped in the preparation of chiral silver salts.

Introduction

In recent years, intramolecular transition metal catalyzed hydroamination of carbon-carbon double bonds has emerged as a powerful method for carbon-nitrogen bond formation.¹ Because hydroamination provides the most direct and atom-efficient method for synthesis of nitrogen-containing heterocycles, development of mild yet general procedures has been the subject of much research in synthetic organic chemistry.² The earliest example of homogeneous transition metal catalyzed olefin hydroamination was reported by Coulson in 1971.³ Since this seminal publication, both early and late metal catalysts have been developed for inter- and intramolecular hydroamination of alkenes and allenes.⁴ In particular, enantioselective hydroamination is a valuable transformation, as many natural products and pharmaceuticals contain chiral amines.

Notable examples of early transition metal catalyzed asymmetric hydroamination include the zirconium(IV) systems developed by Bergman, Schaffer, Scott, and Sadow for the intramolecular addition of primary amines to alkenes to form pyrrolidines.⁵⁻⁸ The first of these reports used zirconium catalysts, generated *in situ* from zirconium tetrakis(dimethyl)amide and diphosphinic amide ligands⁵ (eq 2) to perform the cyclization with up to 80% ee. Recently, Sadow utilized a Zr(IV)-oxazolidine borate complex for enantioselective hydroamination. This complex exhibited an optimal balance of reactivity and enantioselectivity; high conversion and up to 93% ee, the highest yet reported with any group 4 metal, was observed.⁸

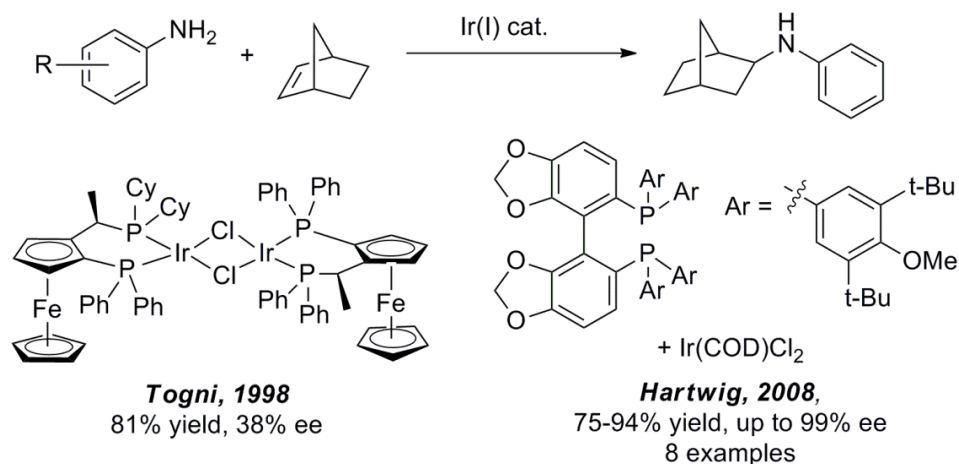
Figure 1.1. Enantioselective intramolecular hydroamination with Zr(IV) complexes.



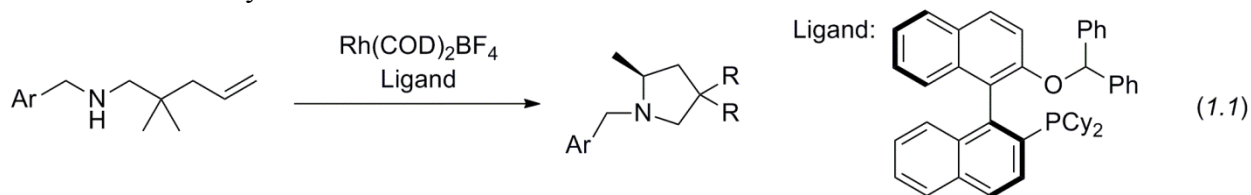
In addition to early metals like zirconium, a number of examples using late metals such as Pd, Rh, Ir and Au have been reported for asymmetric olefin hydroamination.⁹⁻¹¹ However, while asymmetric methods utilizing late transition metal catalysts tend to be more functional group, air and moisture tolerant, they can be less active than their early transition metal or lanthanide counterparts. Indeed, the earliest examples of late-metal hydroamination required the use of strained or activated olefins. In 1997, Togni and coworkers developed the first late metal enantioselective hydroamination reaction of norbornene with aryl amines in the presence of iridium(I) bisphosphine complexes (Figure 1.2).¹² Interestingly, fluoride was required in the reaction to obtain the desired product in high yield and selectivity. Using 2,2'-

bis(diphenylphosphino)-1,1'-binaphthyl (BINAP) as the ligand on iridium(I), enantioselectivity as high as 95% was observed. More recently, Zhou and Hartwig extended the scope of this reaction using DTBM-SEGPHOS as the phosphine ligand.¹³ A variety of aryl amines were used to add across norbornene in excellent enantioselectivity (91-99% ee, Figure 1.2).

Figure 1.2. Iridium(I)-mediated enantioselective hydroamination.

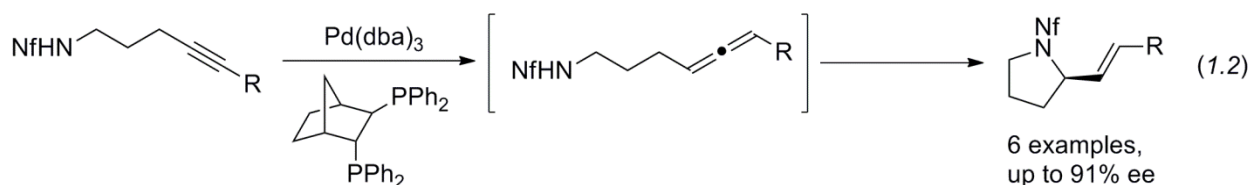


In 2010, Buchwald and coworkers reported the first enantioselective rhodium(I)-catalyzed alkene hydroamination with benzyl amines (eq 1.1).¹⁴ They employed a dicyclohexyl[1,1'-binaphthalen]-2-yl)phosphine (Cy-MOP) derivative as the chiral ligand for the intramolecular reaction at 70 °C. The authors noted that the protecting group on nitrogen had a pronounced effect on the selectivity and reactivity of the transformation and that the rate of cyclization was significantly reduced when an unprotected primary amine was used. Despite these drawbacks, the reaction exhibited good functional group tolerance, and moderate to excellent selectivity for 14 different substrates.



A number of enantioselective palladium(II)-mediated transformations have also been reported.^{15,16} In particular, palladium(II) has been used extensively in the intermolecular hydroamination of vinyl arenes and dienes¹⁵ with primary aryl amines.^{16a} BINAP and a number of its derivatives have been used as the phosphine ligand for palladium and only Markovnikov products are typically observed from this process. While the analogous racemic reaction with secondary amines has been well investigated, only one secondary amine has been used for enantioselective addition.^{16b} Additionally, intramolecular cyclizations onto an alkyne electrophile mediated by palladium(II) catalysts can generate chiral pyrrolidines, instead of dihydropyrrole products. Thus, a method for enantioselective alkyne hydroamination has been reported (eq 1.2).¹⁷ Alkyne insertion followed by β -hydride elimination generates an allene

intermediate and subsequent cyclization of this intermediate proceeds with moderate to good enantioselectivity.

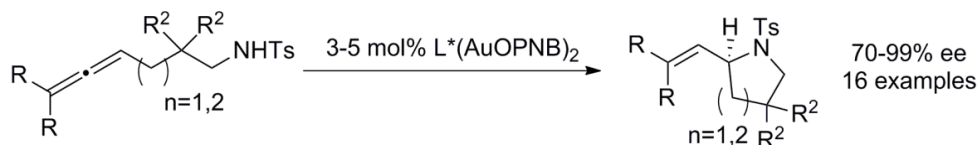


As olefin activation is a known pathway for transition metal-catalyzed hydroamination, gold(I) complexes have become attractive alternatives to other late transition metal catalysts. In recent years, gold(I) complexes have been broadly used in carbon-carbon multiple bond activation due to the ability of gold(I) to act as a potent π -acid.¹⁸ Gold(I) catalysis has been applied to the Conia-ene reaction,¹⁹ allene and alkyne cycloadditions,²⁰ hydroamination,²¹ hydroalkoxylation,²² and hydroarylation²³ to name a few. The stability of gold(I) catalysts to air, moisture, and a variety of functional groups renders gold catalysis a practical and mild method for bench top synthesis.²⁴ In particular, enantioselective gold(I) catalyzed methods provide an alternative^{18c} to asymmetric methods involving air sensitive group(IV) or lanthanide complexes.

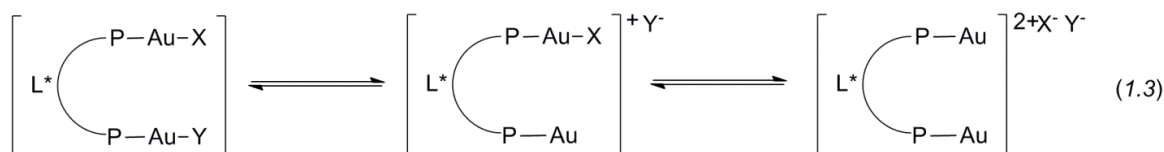
The development of asymmetric gold(I)-catalyzed methods, however, is challenging because mononuclear gold(I) complexes such as Ph_3PAuCl adopt linear geometries, which places ligands 180° from one another.²⁵ This, combined with the average gold-carbon and gold-phosphorus bond lengths means that any chiral information stored in a chiral phosphine ligand is more than 4 Å away from the active site, rendering transfer of chiral information difficult.

One solution to this problem is the implementation of a dinuclear gold complex (eq 1.3). In this case, a second gold(I) center or a second counterion can provide an additional point of interaction with the reactive site. Although the precise nature of this secondary interaction is not well-understood, dinuclear gold(I) complexes have been applied to a variety of asymmetric transformations with good selectivity.²⁶ In 2007, Lalonde et al reported the first enantioselective allene hydroamination catalyzed by dinuclear gold(I) complexes (Table 1.1).^{21a} A variety of substrates were cyclized with good to excellent selectivity at low to moderate temperatures, without exclusion of air or moisture. Interestingly, the transformation demonstrated a profound dependence on the counterion employed. For instance, the dicationic gold complex generated with 2 equivalents of AgBF_4 showed much lower enantioselectivity than the monocationic complex generated from only 1 equivalent of AgBF_4 . These experiments are consistent with the hypothesis that the second gold(I) center and its associated counterion play a major role in enantio-induction (eq 1.3). The optimized reaction conditions employed bis-gold(I)-benzoate complexes.

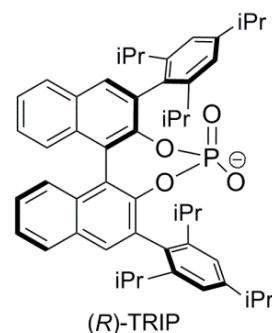
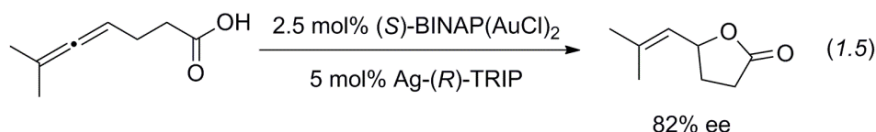
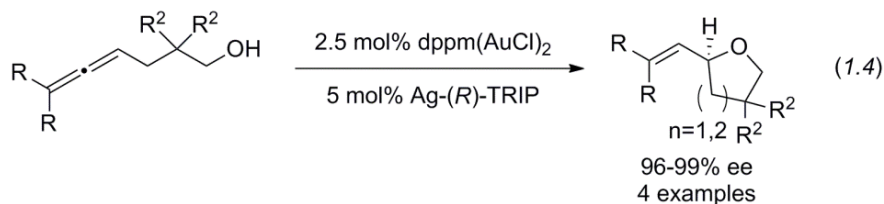
Table 1.1. Dependence of enantioselective hydroamination on the amount of silver salt used.



Catalyst	Conversion	%ee
3 mol% (<i>R</i>)-xylBINAP(AuCl) ₂ + 6 mol% AgBF ₄	82	1
3 mol% (<i>R</i>)-xylBINAP(AuCl) ₂ + 3 mol% AgBF ₄	81	51



In addition to dinuclear complexes, chirality can also be conferred by a chiral counterion aligned closely to the cationic gold center (eq 1.4).²² These approaches have been used independently and in conjunction (eq 1.5) to effect the asymmetric addition of N- and O-nucleophiles to mono- and tri-substituted allenes in high yield and selectivity.¹⁴ Tetrasubstituted allenes, however, are unreactive under any of the reaction conditions reported.

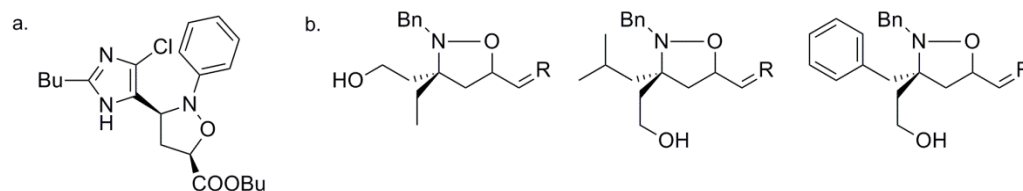


Following these investigations, we were interested in extending the scope of the nucleophile in the allene hydroamination reaction. In particular, we were interested in developing a method for the hydroamination of allenes with N-O and N-N nucleophiles to form isoxazolidines and pyrrazolidines. We hypothesized that the presence of the additional α -heteroatom in the hydroxylamine may lead to novel reactivity unobserved for amine nucleophiles. Isoxazolidines are traditionally synthesized by the 1,3-dipolar cycloaddition of nitro compounds with alkenes^{27,28} and a hydroamination approach for the formation of these heterocycles would be complementary to previous reports. Furthermore, while many enantioselective intramolecular cyclizations have been reported, the intermolecular variant of this transformation is far less

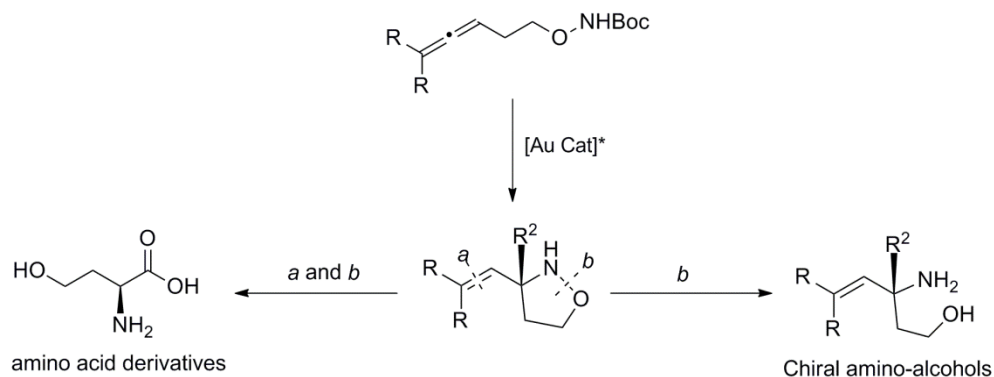
common with gold(I). Thus, we wanted to develop a mild yet general method for this reaction that could be used for both the inter- and intramolecular asymmetric transformations.

Amine and alkoxy amine-containing heterocycles are privileged motifs commonly found in many pharmaceutical, bio-active, and industrial compounds. For instance, enantioenriched isoxazolidines are found in many antifungal and antibacterial agents such as 2-(phenyl)-3-(2-butyl-4-chloro-1*H*-imidazolyl)-5-butylate isoxazolidine (Figure 1.3, a)¹⁵ and have been used to probe the activation domains of various transcriptional factors by Mapp (Figure 1.3, b).¹⁶ These heterocycles also serve as precursors to chiral amino alcohols and amino acid derivatives (Scheme 1.1) following N-O bond cleavage. Thus, the development of catalytic and versatile methods for their preparation is very relevant to synthetic organic chemistry and pharmaceutical research. Enantioselective hydroamination of allenes with N-O nucleophiles is a direct and efficient method for the synthesis of such heterocycles and its derivatives.

Figure 1.3. Biologically active isoxazolidines.



Scheme 1. Derivatization of isoxazolidines to amino-alcohols and amino acids.

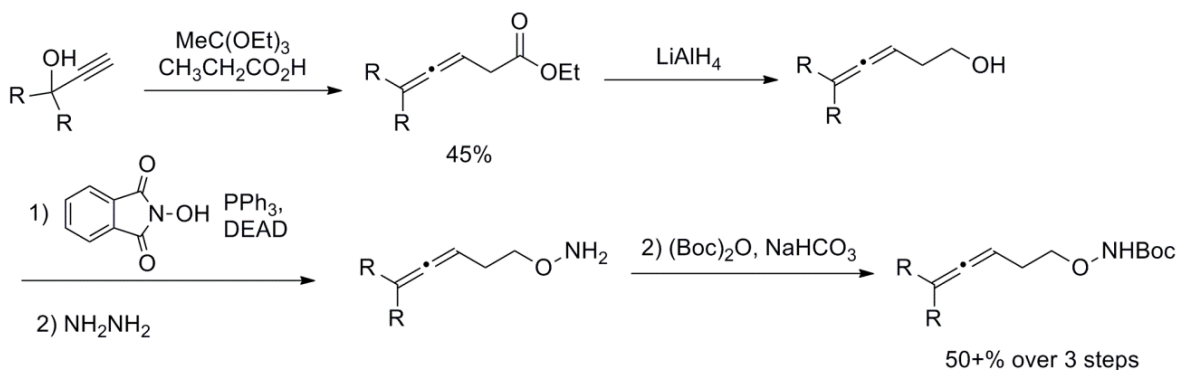


Results:

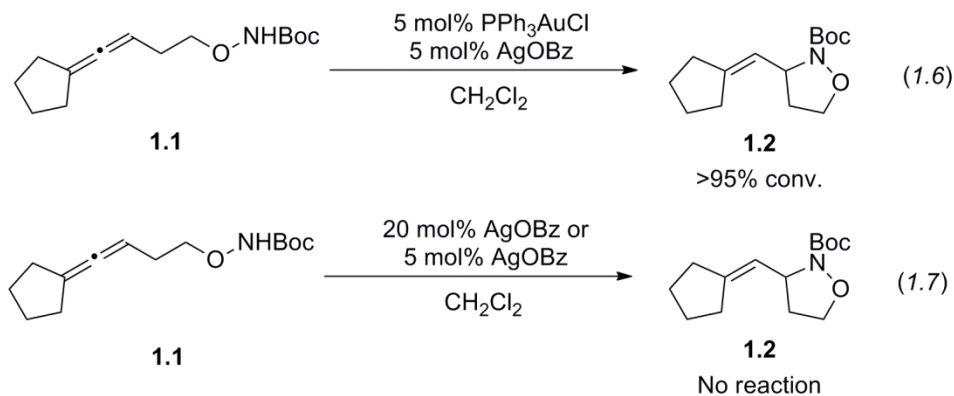
Intramolecular Hydroamination with N-O and N-N Nucleophiles

We began our studies by preparing hydroxylamine-allene substrates for intramolecular cyclization. A variety of allene-hydroxylamines could be prepared in good yield via the Johnson Orthoester Claisen Rearrangement (Scheme 1.2). Mitsunobu reaction of the corresponding allenic alcohol after ester reduction and deprotection of the phthalimide with hydrazine provides the unprotected amino alcohol substrate. We were concerned that unprotected hydroxylamines would chelate strongly to a cationic gold(I) center and hinder catalysis; thus, we chose to protect the hydroxylamines with a carbamate group, which could be readily removed after cyclization.

Scheme 1.2. Synthesis of allene-aminoalcohol substrates, beginning with Claisen Rearrangement to generate the allene fragment.

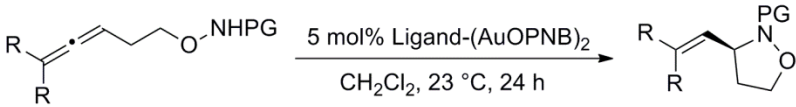


When we treated a standard substrate **1.1** with 5 mol% Ph_3PAuCl and AgOBz , we observed the hydroamination product in quantitative conversion after 24 h at room temperature (eq 7). After 24 h, no particulates or aggregates were observed in the reaction solution, suggesting that the cyclization was indeed catalyzed by a homogeneous gold(I) catalyst rather than by heterogeneous gold nanoparticles. Furthermore, no reaction was observed if p-nitrobenzoic acid or AgOPNB are used alone, suggesting that the observed reaction is indeed mediated by gold(I). A related racemic cyclization was reported by Winter and Krause in 2009.³¹

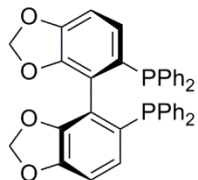


We chose to explore the enantioselective reaction with dinuclear gold catalysts, using *para*-nitrobenzoate (OPNB) as the counterion, as this system exhibited high enantioselectivity in the hydroamination of allenes with amines.^{13a} Initial ligand screens revealed that **1** could indeed be cyclized using 5% of a variety of dinuclear gold(I) bisphosphines. Reaction with isolable (*R*)-BINAP(AuOPNB)₂ catalyst proceeded with good conversion and enantioselectivity (Table 1.1, entry 3). Increasing steric bulk of the phosphine ligand from H-BINAP to Xyl-BINAP (entry 5) provided an addition boost in selectivity and the product could be isolated in good yield and 92% ee (entry 3). While the Cbz-protected substrate was unreactive under these conditions, the unprotected hydroxylamine substrate was readily cyclized, though with much lower enantioselectivity.

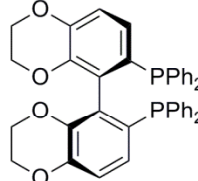
Table 1.2. Initial ligand screens of (AuOPNB)₂ complexes.



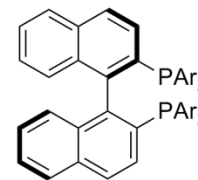
Entry	PG	Ligand ^a	Conversion ^b	%ee
1	Boc	(<i>R</i>)-SEGPPOS	>98%	61%
2	Boc	(<i>R</i>)-SYNPHOS	>98%	81%
3	Boc	(<i>R</i>)-BINAP	>98%	84%
4	Boc	(<i>R</i>)-tol-BINAP	>98%	88%
5	Boc	(<i>R</i>)-xyl-BINAP	>98%	93%
6	H	(<i>R</i>)-xyl-BINAP	>98%	10%
7	Cbz	(<i>R</i>)-xyl-BINAP	8%	N/A



(*R*)-SEGPPOS



(*R*)-SYNPHOS



BINAP framework

^aLigand-(AuOPNB)₂ complexes isolated and used directly for reaction. ^bDetermined by ¹H NMR

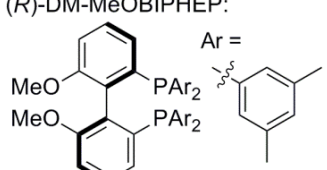
These encouraging results prompted our examination of the generality and scope of this reaction (Table 1.3). The allene terminus can be substituted with both cyclic and acyclic alkyl substituents to yield a variety of enantioenriched isoxazolidines in good yield. Substitution was well-tolerated at any position along the allene backbone, though dimethyl substitution at the 2-position near the nucleophile resulted in a significant decrease in enantioselectivity to 63% (entry 4). Cyclization to form a six-membered N-O heterocycle was also achieved, though this reaction required elevated temperatures and prolonged reaction times in MeNO₂ to obtain high yield. Interestingly, the selectivity of the reaction is not significantly affected by higher reaction temperatures, as the enantioselectivity of the cyclization was decreased by only 2% following a 20 °C increase in temperature (entry 3 and 4).

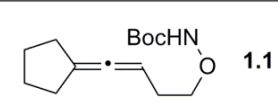
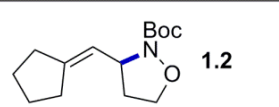
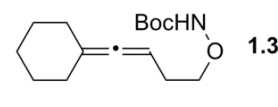
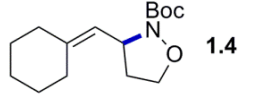
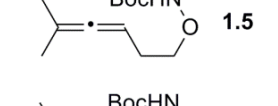
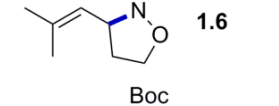
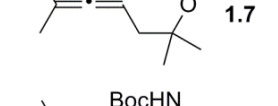
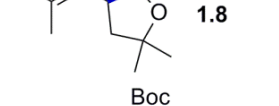
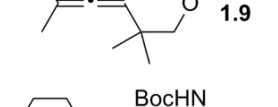
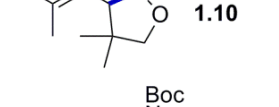
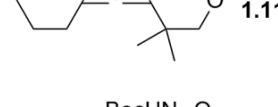
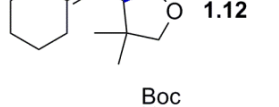
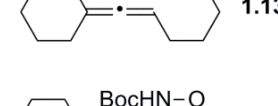

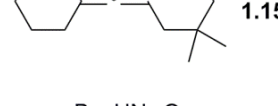
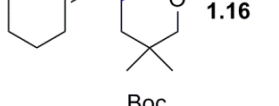
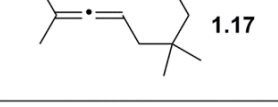
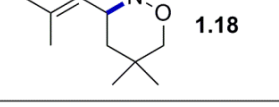
However, while BINAP(AuOPNB)₂ derived complexes proved to be reliable catalysts for the hydroamination of trisubstituted allenes, they were completely unreactive toward terminally

unsubstituted allene **1.19**. However, in this case, the catalyst generated *in situ* from PPh_3AuCl and BINOL derived silver salt (Ag-TRIP) in benzene could provide the desired product (**1.20**) in good conversion and excellent enantioselectivity after 48 h (eq. 1.8).

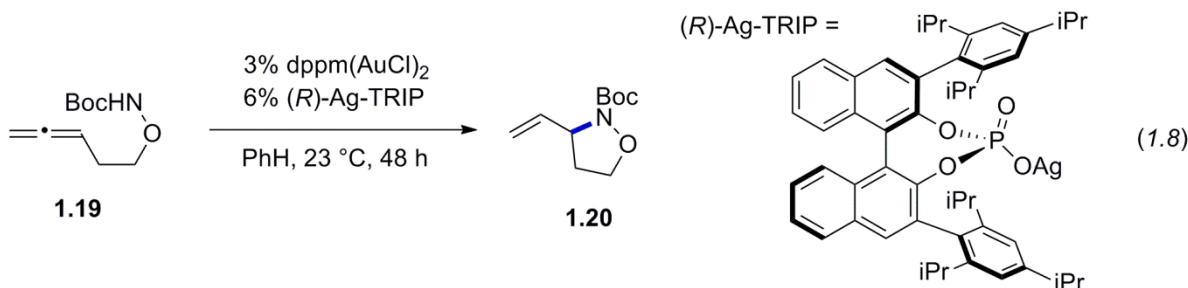
Figure 1.3. Scope of gold(I) catalyzed hydroamination of allenes with N-O nucleophiles to form 5- and 6-membered rings.

(R)-DM-MeOBIPHEP:



Entry	Substrate	Product	Ligand	Temp (°C)	% Yield ^b	%ee ^c
1	 1.1	 1.2	(R)-Xyl-BINAP	23	99	91
2	 1.3	 1.4	(R)-Xyl-BINAP	23	93	92
3	 1.5	 1.6	(R)-Xyl-BINAP	23	91	98
4	 1.7	 1.8	(R)-DM-MeOBIPHEP	50	94	63
5	 1.9	 1.10	(R)-DM-MeOBIPHEP	50	73	99
6	 1.11	 1.12	(R)-Xyl-BINAP	50	78	99
7	 1.13	 1.14	(R)-Xyl-BINAP	65	63	89
8	 1.15	 1.16	(R)-Xyl-BINAP	50	82	89
9	 1.17	 1.18	(R)-Xyl-BINAP	50	85	89

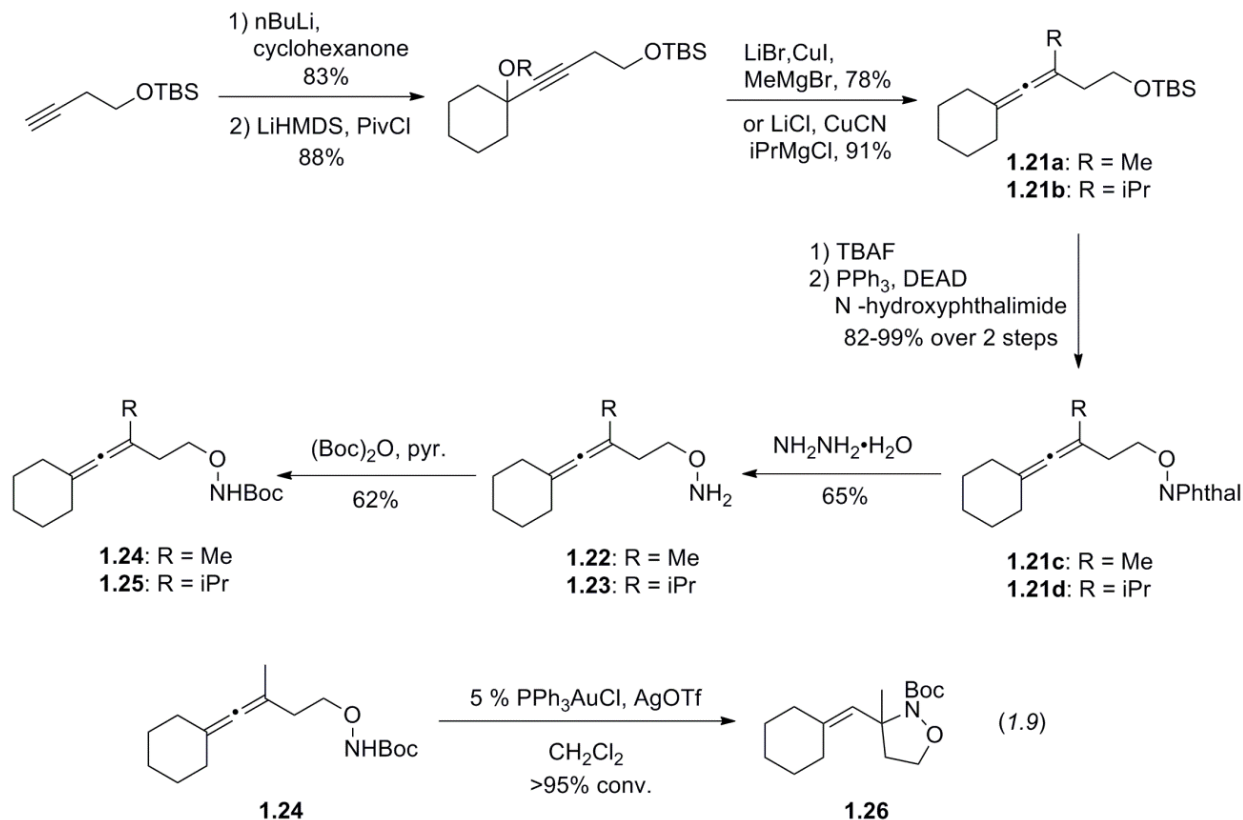
^a CH_2Cl_2 used for all reactions at room temperature and MeNO_2 used for reactions above 40 °C. ^b Isolated yield after column chromatography. ^c Enantioselectivity determined by chiral HPLC



Following these results, we explored the asymmetric cyclization reaction with substrates containing tetrasubstituted allene functions. This class of substrates was particularly interesting to us, as intramolecular hydroamination would yield heterocycles containing a quaternary amine center (Scheme 4). However, substitution leaves the internal olefin very sterically encumbered and less accessible to the gold(I) center. In fact, tetrasubstituted allenes are unreactive to gold(I) catalysts in the intramolecular hydroamination reaction with tosyl amine nucleophiles.³² However, we hypothesized that the increase in nucleophilicity of the amine nucleophile due to the presence of an α -heteroatom may in part compensate for the lack of reactivity of these hindered allenes.

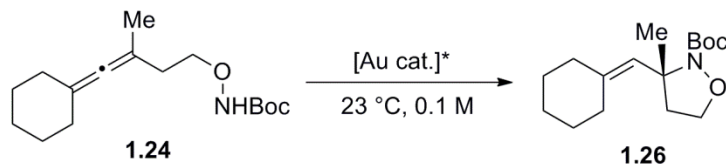
Tetrasubstituted allenes were prepared by reaction of propargyl pivalates with cuprate reagents. To our surprise, cyclization of **1.24** could indeed be performed by a racemic gold(I) catalyst in good conversion at room temperature (eq 1.9).

Scheme 1.3. Representative preparation of tetrasubstituted allene substrates.

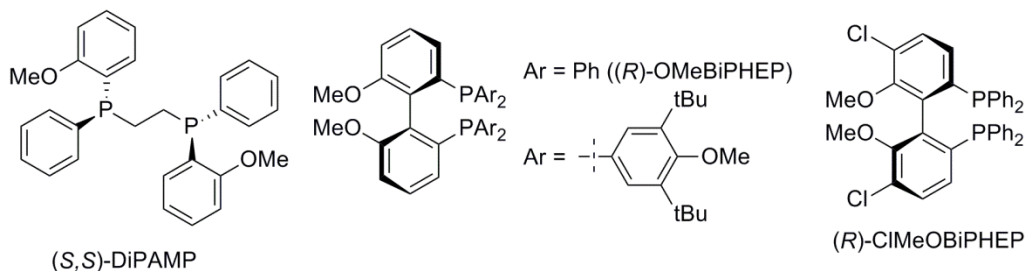


Initial optimization of commercially available ligands showed that less sterically demanding ligands such as MeOBiPHEP gave higher conversion and selectivity than bulkier ligands such as DTBM-MeOBiPHEP (Table 1.4, entry 5 and 6). Unfortunately, the xylyl-BINAP(AuOPNB)₂ catalyst which had proved very effective for the hydroamination of trisubstituted allenes was less effective with substrate **1.24** and **1.25**. Additionally, changing the electronics of the phosphine also seemed to have little effect on the reaction. For example, ClMeOBiPHEP(AuOPNB)₂, MeOBiPHEP(AuOPNB)₂, and SegPhos(AuOPNB)₂, all catalyzed the reaction with similar enantioselectivity. As optimization of the chiral ligand could not provide the desired product in high enantioselectivity, we turned our efforts to using a chiral anion approach for enantioinduction. When one enantiomer of Ag-TRIP was employed in the presence of dppm(AuCl)₂, we observed only 5% ee (entry 7). We hypothesized that pairing Ag-TRIP with a chiral ligand could lead to an enhancement in selectivity, as the chiral anion and the chiral ligand would enforce one another's stereo-bias. However, using (*R*)- or (*S*)-Ag-TRIP with (*S,S*)-DiPAMP(AuCl)₂ failed to promote the desired transformation in good conversion (entries 8 and 9). The enantiomeric excess in the small amounts of products isolated was minimal.

Table 1.4. Ligand and anion optimization for hydroamination of **1.24**.



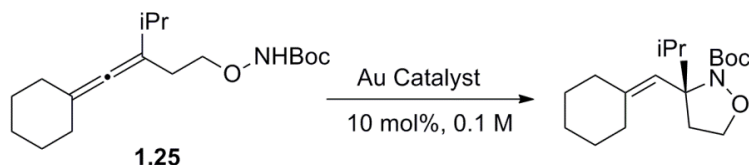
Entry	Catalyst ^a	Solvent	Time (h)	% Conv. ^b	%ee ^c
1	(<i>R</i>)-Xyl-BINAP-(AuOPNB) ₂	CH ₂ Cl ₂	24	50	17
2	(<i>R</i>)-SEGPLHOS(AuOPNB) ₂	CH ₂ Cl ₂	40	61	20
3	(<i>R</i>)-SYNPHOS(AuOPNB) ₂	CH ₂ Cl ₂	40	82	13
4	(<i>R</i>)-ClMeOBiPHEP(AuOPNB) ₂	CH ₂ Cl ₂	40	>95	25
5	(<i>R</i>)-OMeBiPHEP(AuOPNB) ₂	CH ₂ Cl ₂	40	85	30
6	(<i>R</i>)-OMe(DTBM)BiPHEP(AuOPNB) ₂	CH ₂ Cl ₂	40	30	19
7	dppm(AuCl) ₂ + (<i>R</i>)-Ag-TRIP	PhH	24	45	5
8	(<i>S,S</i>)-DiPAMP(AuCl) ₂ + (<i>R</i>)-Ag-TRIP	PhH	48	10	-9
9	(<i>S,S</i>)-DiPAMP(AuCl) ₂ + (<i>R</i>)-Ag-TRIP	PhH	48	10	-13



^a 5% catalyst was used in entries 1-6. For entries 7-9, 3% Au cat and 6% Ag-TRIP was used. ^b Conversion determined by NMR. ^c Enantioselectivity determined by chiral HPLC

We reasoned that one explanation for the poor selectivity of the reaction is the similarity in steric size of the methyl substituent and methylene linker of the allene. Thus, we believed that increasing the size of the alkyl substituent could allow the catalyst to better differentiate between the two enantiomeric transition states. However, increasing the size of the substituent on the internal position of the allene to an isopropyl group (**1.25**) led to minimal reactivity in the cyclization reaction (Table 1.5) even when the reaction mixture was heated to 60 °C for 48 h with 10% catalyst loading.

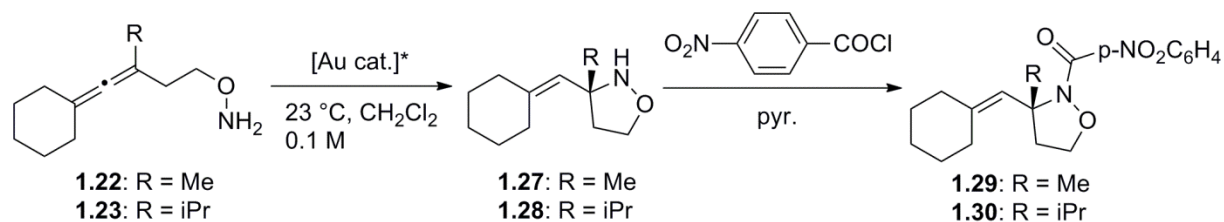
Table 1.5. Enantioselective hydroamination reactions of **1.25**.



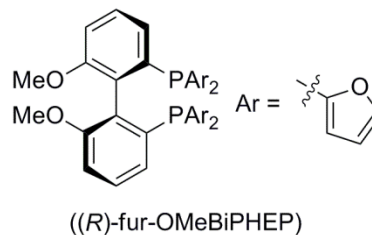
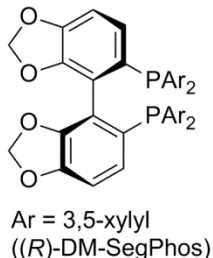
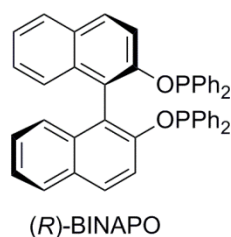
Entry	Catalyst	Solvent	Temp (°C)	Time (h)	Conv (%)
1	(R)-Xyl-BINAP(AuOPNB) ₂	MeNO ₂	24	24	0
2	(R)-Xyl-BINAP(AuOPNB) ₂	MeNO ₂	60	48	<5
3	(R)-MeOBiPHEP(AuOPNB) ₂	CH ₂ Cl ₂	60	48	<5

The low reactivity of the tetrasubstituted allene substrates toward sterically demanding gold complexes or bulky anions limited the number of asymmetric catalysts that could be used. Thus we posited that the reaction would be improved if we decreased the steric bulk surrounding the hydroxylamine nucleophile. As the smallest nucleophile possible is the deprotected amine, we prepared both **1.22** and **1.23** as substrates for cyclization. We observed quantitative conversion to the desired product in 24 h with PPh₃AuCl and AgOTf for **1.22** and **1.23** (Table 1.6). These substrates also demonstrated improved reactivity toward asymmetric gold(I) catalysis (entry 2-17). However, because **1.27** and **1.28** lacked suitable chromophores for enantioresolution using chiral HPLC, they were further derivatized to **1.29** and **1.30** by addition to 4-nitrobenzoyl chloride. The resulting compounds have exhibited up to 49% ee at highly substituted stereogenic centers.

Table 1.6. Ligand optimization for substrates **1.27** and **1.28**.



Entry	Substrate	Catalyst ^a	Time (h)	Prod	% Conv. ^b	%ee ^c
1	1.22	PPh ₃ AuCl + AgOTf	24	23	>95	--
2	1.22	(<i>R</i>)-MeOBiPHEP(AuOPNB) ₂	24	23	>95	49
3	1.22	(<i>R</i>)-ClMeOBiPHEP(AuOPNB) ₂	24	23	>95	31
4	1.22	(<i>R</i>)-DTBM-MeOBiPHEP(AuOPNB) ₂	24	23	90	0
5	1.22	(<i>R</i>)-SEGPHOS(AuOPNB) ₂	24	23	>95	32
6	1.22	(<i>R</i>)-xyl-BINAP(AuOPNB) ₂	24	23	>95	32
7	1.22	(<i>R</i>)-SYNPHOS(AuOPNB) ₂	24	23	>95	47
8	1.23	(<i>R</i>)-MeOBiPHEP(AuOPNB) ₂	48	24	14	36
9	1.23	(<i>R</i>)-furyl-MeOBiPHEP(AuOPNB) ₂	24	24	35	14
10	1.23	(<i>R</i>)-BINAPO(AuOPNB) ₂	24	24	>95	0
11	1.23	(<i>R</i>)-SEGPHOS(AuOPNB) ₂	24	24	66	28
12	1.23	(<i>R</i>)-SYNPHOS(AuOPNB) ₂	24	24	80	38
13	1.23	(<i>R</i>)-DM-SEGPHOS(AuOPNB) ₂	48	24	<5	--
14	1.23	(<i>S,S</i>)-DiPAMP(AuCl) ₂ + (<i>S</i>)-Ag-TRIP	24	23	84	3
15	1.23	(<i>S,S</i>)-DiPAMP(AuCl) ₂ + (<i>R</i>)-Ag-TRIP	24	23	65	-7



^a 5% catalyst was used in entries 1-13. For entries 15,16, 3% (*S,S*)-DiPAMP(AuCl)₂ and 6% B was used. ^b Conversion determined by NMR. ^c Enantioselectivity determined by chiral HPLC.

Despite the decrease in bulk surrounding the nucleophile, steric interactions still seem to be most important in determining both the conversion and the selectivity of the reaction. Bulkier

ligands such as DM-SegPhos and DTBM-MeOBiPHEP decreased both the conversion and selectivity of the reaction (Table 1.7, entry 2, 4, 12, and 14) and (*R*)-MeO-BiPHEP(AuOPNB)₂ once again proved to be most effective in the asymmetric reactions. Adopting the chiral counterion with a chiral ligand also did not increase the selectivity of the cyclization.

Further optimization of the reaction conditions revealed that the reaction is sensitive to the solvent employed. Using our best catalyst MeOBiPHEP(AuOPNB)₂, we observed the highest enantioselectivity when chlorinated solvents such as CH₂Cl₂ and DCE (49% and 44% ee, respectively) were employed. Very non-polar solvents like benzene substantially reduced the conversion observed.

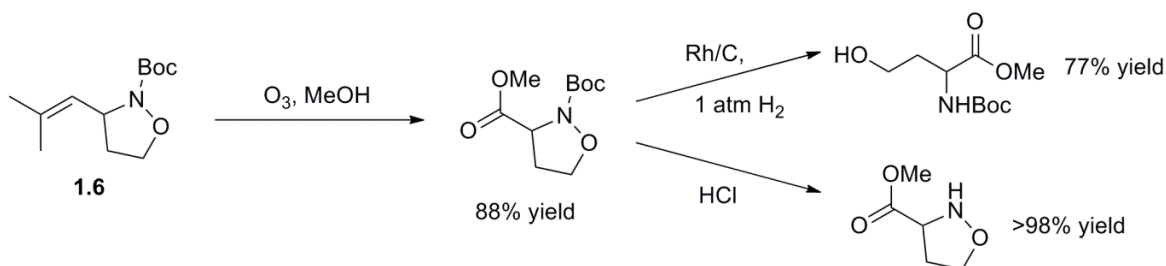
Table 1.7. Solvent screen for substrate **1.22**.

Entry	Solvent	% Conv. ^a	%ee ^b
1	MeNO ₂	>95	8
2	DCE	>95	44
3	PhH	28	3
4	PhF	>95	1
5	MeCN	>95	15
6	1,4-Dioxane	90	9

^a Conversion determined by NMR. ^b Enantioselectivity determined by chiral HPLC

To demonstrate the utility of our hydroamination method, we were able to derivatize the isoxazolidine products from the cyclization (Scheme 1.4). In particular, **1.6** could be ozonized in the presence of methanol to provide the methyl ester isoxazolidine. Hydrogenation of the N-O bond provided the methyl ester of homo serine in high yield. The Boc protecting group on nitrogen is also readily cleaved under acidic conditions to provide the free isoxazolidine.

Scheme 1.4. Functionalization of isoxazolidine products.



Next we turned to allene hydroamination with hydrazine (N-N) nucleophiles. We began with substrate **1.30**, as we hypothesized that a protecting group on the internal nitrogen would limit the number of nucleophilic sites on the substrate. Gratifyingly, this provided the desired product in high yield after 15 h at 50 °C, though the enantioselectivity of the reaction was low. However, placing a second protecting group on the primary nitrogen provided a significant boost in enantioselectivity. After examining a variety of protecting groups, we found placing a 2-mesitylsulfonyl group (Mts) on the terminal amine allowed the desired reaction to proceed in 80% ee. After examining a small panel of phosphine ligands, we found that (*R*)-DTBM-Segphos(AuOPNB)₂ catalyzed the reaction of **1.31** to 78% yield and 97% ee. Using these optimized conditions, we were able to perform the cyclization of three hydrazine substrates in good yield and excellent enantioselectivity (Table 1.8).

Table 1.8. Hydroamination with hydrazine substrates.

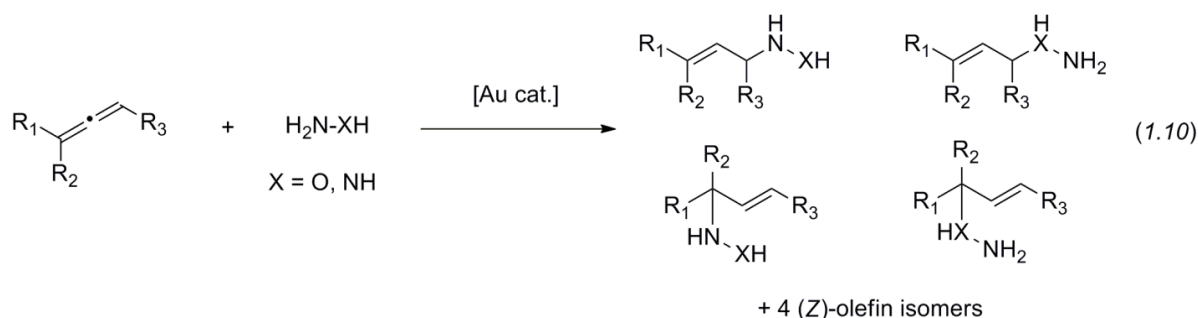
Substrate	Product	Ligand	% Yield ^a	%ee ^b
PG = H, R = (CH ₂) ₅		(<i>R</i>)-Xyl-BINAP	46	5
PG = Boc R = (CH ₂) ₅		(<i>R</i>)-Xyl-BINAP	>98	70
PG = Mts (1.31) R = (CH ₂) ₅	(1.32)	(<i>R</i>)-Xyl-BINAP	>98	80
PG = Mts (1.31) R = (CH ₂) ₅	(1.32)	(<i>R</i>)-DTBM-SEGPHOS	78	97
PG = Mts (1.33) R = (CH ₂) ₄	(1.34)	(<i>R</i>)-DTBM-SEGPHOS	90	83
PG = Mts (1.35) R = Me	(1.36)	(<i>R</i>)-DTBM-SEGPHOS	98	99

^a Isolated yields reported. ^b %ee determined by chiral HPLC

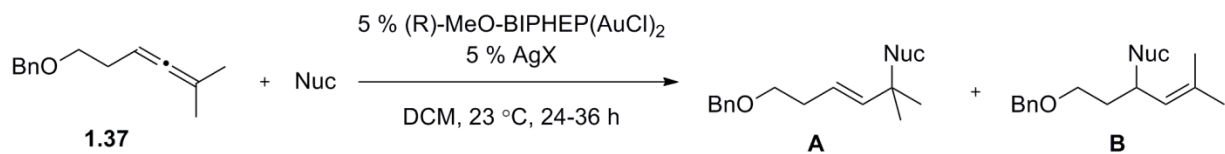
Intermolecular Hydroamination with N-O and N-N Nucleophiles

Following our progress in developing a method for intramolecular enantioselective hydroamination with N-O and N-N nucleophiles, we wanted to develop a similar procedure for the intermolecular transformation. As we have demonstrated previously, the N-X bond in hydroxyl-amine and hydrazine nucleophiles can be readily hydrogenated and we hypothesized that an intermolecular hydroamination with these nucleophiles could provide a more general and facile method of obtaining simple unprotected allylic amines. However, the intermolecular hydroamination reaction with N-X type nucleophiles is challenging for a number of reasons. First, if a trisubstituted allene is used as the olefin partner, two regioisomeric products can result from nucleophilic addition to either terminus of the allene. If an achiral tertiary allene is used, then only addition to the mono-substituted end of the allene would yield a chiral product. Second, if a chiral tertiary allene or a 1,3-disubstituted allene is used, the allylic amine product formed can be either *cis* or *trans* with respect to the olefin. Lastly, if a nucleophile such as H₂NNHBoc or HONHBoc is used, both heteroatoms can add into the allene. Thus, there are several products that can arise from combinations of these possibilities (eq 1.10) and the ability to form one product selectively is important for establishing a synthetically useful method.

To minimize the number of possible products, we began by preparing an achiral tri-



substituted allene substrate for reaction with a variety of hydroxylamines and hydrazines. As we were interested in developing an enantioselective reaction, we performed our substrate screening with MeO-BiPHEP (see Table 1.4 for ligand structure), a relatively small yet representative chiral bisphosphine. Treating substrate **1.37** with HONHBoc nucleophile in the presence of MeO-BiPHEP(AuX)₂ (where AuX is generated *in situ* from halide abstraction with a silver salt) at room temperature unfortunately gave both the hydroamination and hydroalkoxylation products or no observable conversion to product (Table 1.9, entry 1-5). However, protection of the free hydroxyl with a benzyl group eliminated any observable reactivity (entry 6-8). Moving to N-N nucleophile, we saw that the methyl carbazate nucleophile provided only one major hydroamination product, though this was the achiral product (entry 9-13). Unfortunately, neither the dimethyl hydrazine-1,2-dicarboxylate (MocHNNHMoc) nor free hydrazine nucleophile was reactive under the conditions examined (entry 14 and 15, respectively).

Table 1.9. Intermolecular hydroamination of a trisubstituted allene.

Entry	Nucleophile	AgX	% Conv. to A	% Conv. to B
1	NHBoc-OH	AgOTf	(A + B + hydroalkoxylation products) < 5 %	
2	NHBoc-OH	AgBF ₄	(A + B + hydroalkoxylation products) < 5 %	
3	NHBoc-OH	AgSbF ₆	(A + B + hydroalkoxylation products) < 5 %	
4	NHBoc-OH	NaBARF ₂₄	0	0
5	NHBoc-OH	AgNTf ₂	(A + B + hydroalkoxylation products) < 5 %	
6	NHMoc-OBn	AgOTf	0	0
7	NHMoc-OBn	AgBF ₄	0	0
8	NHMoc-OBn	AgNTf ₂	0	0
9	NH ₂ NHMoc	AgOTf	30%	<5%
10	NH ₂ NHMoc	AgBF ₄	39%	<5%
11	NH ₂ NHMoc	AgSbF ₆	33%	<5%
12	NH ₂ NHMoc	AgNTf ₂	60% (at 40 °C in DCE)	<5%
13	NH ₂ NHMoc	AgOTs	25%	<5%
14	(NHMoc) ₂	AgNTf ₂	0	0
15	NH ₂ NH ₂ •H ₂ O	AgNTf ₂	0	0

Moc = Methyl carbamate

As we could not find conditions for hydroamination of **1.36** in which a chiral product is formed in moderate conversion, we turned to a C₂-symmetric allene **1.37** for study. As **1.37** is inherently chiral, high conversion (>50%) of this substrate to product requires a dynamic kinetic resolution process in which the gold complex is able to racemize the starting material in addition to catalyzing the hydroamination process. Gold(I) complexes have been known to racemize allenes at room temperature,³³ and we hypothesized that a dynamic resolution may be possible. When we treated **1.37** with a variety of nucleophiles at 40 °C in the presence of MeO-BIPHEP(AuCl)₂ and AgNTf₂ we found that both methyl carbamate and BnONHMoc yielded the corresponding hydroamination products. In particular, the reaction of **1.37** with methyl carbamate showed promising levels of enantioselectivity. Thus, we chose this allene and nucleophile combination for optimization.

Table 1.10. Hydroamination of C₂-symmetric allene with a variety of nucleophiles.

Nucleophile	Time	Conversion	% ee
(NHMoc) ₂	36 h	0	--
NH ₂ NHMoc	36 h	52%	12%
NH ₂ NCbz	52 h	0	--
BnO-NHMoc	36 h	72%	0%
NH ₂ NH(SO ₂ Mes)	48 h	<5%	--
(NHTs) ₂	48 h	<5%	--

Table 1.11. Optimization of ligand and counterion.

Entry	Ligand	AgX	Conversion	%ee
1	MeO-BIPHEP	AgNTf ₂	52%	12%
2	DTBM-MeO-BIPHEP	AgNTf ₂	20%	2%
3	Cl-MeO-BIPHEP	AgNTf ₂	30%	5%
4	DTBM-SEGPPOS	AgNTf ₂	42%	57%
5	tol-BINAP(AuCl) ₂	AgNTf ₂	37%	-5%
6	dppm-(AuCl) ₂	(R)- Ag-TRIP	0	--
7	DTBM-SEGPPOS	AgBF ₄	20%	43%
8	DTBM-SEGPPOS	AgSbF ₆	32%	57%
9	DTBM-SEGPPOS	AgOTf	20%	37%
10	DTBM-SEGPPOS	AgOTs	<5%	--
11	DTBM-SEGPPOS	AgPNB	0	--
12	DTBM-SEGPPOS	AgTFA	0	--

We examined a number of parameters for optimization, including phosphine ligand, counterion, reaction solvent and equivalents of nucleophile employed. From these studies, we determined that (*R*)-DTBM-Segphos was the best ligand for the reaction and catalyzed the transformation with 57% ee (Table 1.11, entry 1-6). Furthermore, an examination of silver salts revealed that both NTf₂⁻ and SbF₆⁻ were good counterions for the gold(I) complex and afforded the desired product in appreciable yield and modest enantioselectivity (entry, 4, 8). Unfortunately, the *p*-nitrobenzoate complex we previously used for the intramolecular hydroamination was completely unreactive for the intermolecular transformation (entry 10). When we examined the effect of the number of equivalents of silver salt and nucleophile used, we saw that a 1:1 ratio of gold complex to silver salt was optimal (Table 1.11). This trend was previously observed in the intramolecular allene hydroamination with tosyl-amine. Indeed, isolation of the (*R*)-DTBM-SEGPHOS(AuNTf₂)₂ complex and addition of this complex as a solid to the reaction of **1.38** actually decreased the enantioselectivity of the reaction by 8%. Additionally, we obtained another small boost in selectivity when we increased the number of equivalents of nucleophile to 4.0. A solvent screen revealed that while MeNO₂ and DCE were both acceptable solvents for the reaction, reaction in DCE afforded higher enantioselectivity while reaction in MeNO₂ provided higher conversion.

Table 1.11. Optimization of amount of silver salt, equivalents of nucleophile, and solvent used for reaction.

Reaction scheme: **1.38** (allene) + 5 % (*R*)-DTBM-SEGPHOS(AuCl)₂, X % AgNTf₂, X equiv NH₂NHMoc, Solvent, 40 °C, 48 h → **1.39** (hydroamination product).

Entry	% AgNTf	Equiv. of Nuc	Solvent	Conversion	%ee
1	10 mol% ^a	2.0	DCE	42%	57%
2	10 mol%	2.0	DCE	61%	49%
3	5 mol%	2.0	DCE	25%	67%
4	5 mol%	1.0	DCE	18%	62%
5	5 mol%	4.0	DCE	21%	70%
6	5 mol%	4.0	MeNO ₂	61%	50%
7	5 mol%	4.0	PhF	<5%	--
8	5 mol%	4.0	Dioxane	<10%	--

^a Isolated complex (*R*)-DTBM-SEGPHOS(AuNTf₂)₂ used directly.

In all of our attempts at optimizing the intermolecular reaction, we saw that enantioselectivity was often inversely correlated with conversion to product. This prompted us to consider whether the reaction was a truly dynamic process and whether the gold(I) complex was really racemizing the starting allene **1.38** more rapidly than the allene was converted to product. Thus we monitored the reaction of **1.38** over 56 h by removed aliquots at various time points during the course of reaction (Table 1.12). As the reaction progressed, the enantioselectivity of the product **1.39** noticeably decreased while the starting material **1.38** became increasingly enantio-enriched. If the gold(I) complex is completely unable to racemize **1.38** and we assume that each enantiomer of **1.39** can arise from only one enantiomer of **1.38**, we would expect **1.38** to have approximately 35% ee at 30% conversion with 65% ee in **1.39**. As the enantiomeric excess of **1.38** observed was smaller than the value predicted for a completely adynamic process, we reasoned that the rate of allene isomerization must be competitive with the rate of product formation. As the concentration of the more reactive enantiomer of **1.38** was depleted during the reaction, the overall rate of the hydroamination also decreased. This trend may in part account for the modest conversion observed through multiple rounds of optimization.

Table 1.12. Monitoring enantiomeric excess of **1.38** and **1.39** through the course of reaction.

Reaction scheme: **1.38** (a chiral allene with two phenyl groups) reacts with (R)-DTBM-Segphos(AuCl)₂, AgNTf₂, NH₂NHMoc, and DCE to form **1.39** (a chiral amine where the allene has been hydroaminated).

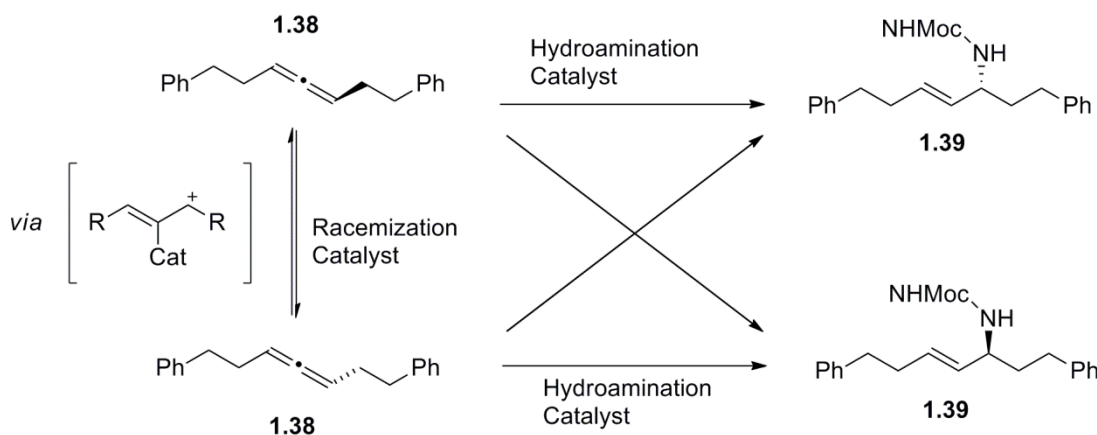
Entry	Time (h)	% Conv.	% ee 1.38	%ee 1.39
1	0	0%	0	-
2	12	10%	7	68
3	24	18%	12	67
4	36	27%	15	64
5	56	35%	24	62

In conclusion, we have developed a method for the intramolecular enantioselective hydroamination of N-N and N-O nucleophiles. While unprotected hydroxylamines and hydrazines demonstrate good reactivity, protection of the amine greatly increases the enantioselectivity of the transformation. With our optimized conditions, we have been able to perform the cyclization of a variety of substrates to form isoxazolidines, tetrahydrooxazines, and pyrrazolidine products in good to excellent enantioselectivity. Furthermore, we were able to use two different tetrasubstituted allenes for cyclization, yielding products bearing quaternary amine centers. We have also examined the intermolecular hydroamination of allenes with C₂-symmetric allenes and methyl carbazate nucleophile. While the reaction proceeds with promising levels of enantioselectivity and conversion, the inability of the gold(I) cation to rapidly racemize the chiral allene substrate prevents the development of a truly kinetic dynamic process for this transformation.

Future Directions

Increasing the rate of racemization of C₂-symmetric allenes like **1.38** could allow us to obtain the intermolecular hydroamination product in higher enantioselectivity and yield. The triflimide counterion used for reaction is mildly coordinating. If instead we employed a counterion like SbF₆⁻, we may be able to generate a gold complex with more cationic character. This should lead to faster allene racemization. A second approach could be to use an additional catalyst capable of rapidly racemizing **1.38**, without catalyzing the hydroamination reaction. For instance, silver triflimide does not catalyze the intermolecular hydroamination, but may still be a competent catalyst for allene racemization (Scheme 1.5).

Scheme 1.5. Kinetic dynamic resolution of **1.39**, where a second catalyst can be employed for racemization.



Computational studies by our group suggest that allene racemization likely occurs through a planar vinyl-gold(I) cation (see Chapter 2 for a complete discussion of computational studies). Thus, electron-withdrawing ligands on gold(I) should promote formation of this achiral intermediate or transition state and increase the rate of racemization. However, this approach maybe complicated by the fact that nucleophilic addition also proceeds rapidly to these types of carbocationic intermediates. To amplify the difference between the rate of racemization versus the rate of hydroamination, a less nucleophilic amine or hydrazine (such as *t*butyl carbazate) may be more suitable. Lastly, the rate of racemization of tri-substituted allenes is much higher than that for di-substituted allenes. Indeed, Widenhoefer calculates that the free energy of activation of allenes like **1.38** is greater than 17.4 kcal/mol. Thus, switching to a chiral trisubstituted allene should also facilitate development of a dynamic kinetic resolution for intermolecular hydroamination.

Experimental

General Reagent and Analytical Information.

All reagents and solvents were obtained from commercial suppliers and used without further purification, unless otherwise specified. All air-sensitive reactions were carried out in dried glassware and solvent, under positive N₂ pressure using syringe and cannula techniques. Glassware was dried at 160 °C overnight or flame dried under vacuum immediately prior to use. Dry tetrahydrofuran was passed through a column of activated alumina. Following workup procedures, organic layer was concentrated under reduced pressure with a rotary evaporator. All flash chromatography was performed on Merck 60 silica gel (32-63 μm). Thin-layer chromatography (TLC) analysis was performed using Merck silica gel 60 F254 TLC plates, and visualized by staining with I₂, UV, anisaldehyde, and/or permanganate. Silver *p*-nitrobenzoate was prepared according to the method of Rubottom.²³ Chiral gold(I) chloride complexes, phosphinegold(I)-bis-*p*-nitrobenzoate complexes and (*S*)-AgTRIP were prepared according to procedures previously described by our group.^{21a,22} Allenic alcohols were prepared by the method described by Widenhoefer.^{22b} Substrate **1.38** and product **1.39** are further discussed in Chapter 2 of this thesis and are fully characterized in Chapter 2, experimental.

¹H and ¹³C NMR spectra were recorded with Bruker DRX-500, AV-500, AVB-400, AVQ-400, and AV-300 spectrometers and chemical shifts are reported in ppm, relative to CHCl₃ (7.26 ppm for ¹H, and 77.23 ppm for ¹³C), unless otherwise noted. Enantiomeric excess was determined on a Shimadzu VP Series Chiral HPLC, using the Chiral PAK AD-H or Regis Technologies WHELK-O columns, eluting with a flowrate of 1 mL/min. Mass spectral and analytical data were obtained via the Micro-Mass/Analytical Facility operated by the College of Chemistry, University of California, Berkeley.

General procedure for the preparation of BocHN-OR hydroxylamine substrates

The corresponding alcohol was added to a stirring solution of PPh₃ and DEAD in THF (0.15 M in alcohol). The reaction mixture was stirred at 0 °C for 30 min before *N*-hydroxyphthalimide was added in one portion. The solution turned dark orange immediately upon addition. The reaction mixture was stirred at room temperature for 6 h, after which time, the reaction mixture was concentrated to afford a thick yellow oil. The crude oil was passed through a silica pad, eluting with 1:9 EtOAc:hexanes. The solution was concentrated and the crude product was redissolved in CH₂Cl₂ (15 mL) and NH₂NH₂·H₂O (2.0 equiv) was added dropwise. The mixture was stirred overnight at room temperature and white precipitants were removed by filtration. Concentration of the organics afforded the deprotected hydroxylamine as a pale yellow oil. The oil was dissolved in 1:4 THF:H₂O (10 mL) and NaHCO₃ (1.5 equiv) and di-*tert*-butyl dicarbonate (1.2 equiv) was added. The biphasic solution was stirred vigorously at room temperature for 5 h, before it was diluted with Et₂O and extracted with brine (10 mL). The organic layer was dried with Na₂SO₄ and concentrated to provide the crude product, which was subsequently chromatographed on SiO₂ to afford the purified substrate.

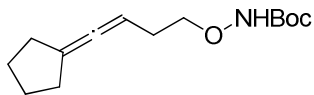
General procedure for the preparation of MtsHN-NBoc-R substrates:

To a solution of homo-allenic alcohol (1 equiv) and triethylamine (1.5 equiv) in CH_2Cl_2 (1 M) at 0 °C was added methane sulfonyl chloride (1.2 equiv). The solution was stirred at 0 °C for 30 min or until TLC showed complete conversion. The solution was poured onto a 1:1 mixture of sat. aq. NaHCO_3 and brine, and extracted with CH_2Cl_2 (3 times). The combined organics were washed with a 1:1 mixture of sat. aq. NaHCO_3 and brine, dried (MgSO_4) and concentrated. To a suspension of NaH (1.1 equiv) in dry DMF (1 M) was added a solution of N-(*tert*-butoxycarbonylamino)phthalimide (1.0 equiv) in dry DMF (1 M) at 0 °C. The mixture was stirred at 23 °C until gas evolution ceased. The solution was cooled to 0 °C before a solution of the crude mesylate in dry DMF (1 M) was transferred via cannula. The resulting solution was stirred at 80 °C overnight, before the mixture was quenched on sat. aq. NH_4Cl , and extracted with Et_2O (4 times). The combined organics were washed with water (4 times), dried (MgSO_4) and concentrated. The crude oil was purified by column chromatography (0-5% EtOAc/Hex). A solution of the homoallenic hydrazine in CH_2Cl_2 (0.6 M) at 0 °C was treated with hydrazine (1 equiv, 60% in water). The solution was stirred at 23 °C for 4 h during which time a white precipitate formed. The mixture was filtered, washed with CH_2Cl_2 (3 times), dried (Na_2SO_4) and concentrated. To solution of the crude hydrazine (1 equiv), and triethylamine (1.5 equiv) in CH_2Cl_2 (0.5 M) was added mesitylene chloride (1.2 equiv) and dimethylaminopyridine (DMAP) (0.1 equiv). The solution was diluted with sat. aq. NaHCO_3 , extracted with CH_2Cl_2 (3 times), dried with MgSO_4 and concentrated. Purification by column chromatography yielded the desired hydrazine substrates.

General procedure for Au(I)-catalyzed hydroamination

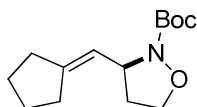
A solution of the gold(I) chloride complex and the silver salt in the specified solvent was sonicated for 3 min and passed through a micropipette filter fiber to remove AgCl precipitates. The resulting solution was added directly to a reaction vessel containing the substrate. The reaction mixture was protected from ambient light with tin foil and stirred at the indicated temperature, for 15 or 48 h. The crude reaction mixture was passed through a silica pad, eluting with 1:1 hexanes: EtOAc to remove gold salts and then purified by flash chromatography on SiO_2 afford the cyclized product.

Hydroamination with hydroxyl amine substrates:

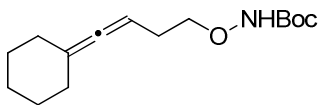


Tert-butyl 4-cyclopentylidenebut-3-enyloxycarbamate (1.1). Following general procedure for substrate synthesis a solution of 2-(4-cyclopentylidenebut-3-enyloxy)isoindoline-1,3-dione, (0.80 g, 2.81 mmol) in CH_2Cl_2 (25 mL) and $\text{NH}_2\text{NH}_2 \cdot \text{H}_2\text{O}$ (0.17 mL, 3.37 mmol) was added. The reaction precipitates were removed by filtration. The organic layer was concentrated to afford a clear oil (0.40 g) which was used without further purification. The oil (0.40 g) was dissolved in CH_2Cl_2 and pyridine (0.30 mL, 3.66 mmol) and di-*tert*-butyl dicarbonate (0.72 mL, 3.13 mmol) was added. The reaction mixture was diluted with CH_2Cl_2 (50 mL) and extracted with NH_4Cl

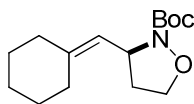
(60 mL). The organic layer was dried with MgSO_4 and concentrated and the crude oil was purified by flash chromatography, eluting with 1:24 EtOAc:hexanes to provide a clear oil (0.40 g, 1.58 mmol, 51% yield overall). ^1H NMR (400 MHz): δ 1.48 (s, 9 H), 1.63-1.67 (m, 4 H), 2.28-2.33 (m, 6 H), 3.89 (t, 2 H, $J = 6.8$ Hz), 5.03-5.08 (m, 1 H), 7.12 (br s, 1 H) ppm. ^{13}C NMR (400 MHz): δ 27.0, 28.1, 28.2, 31.2, 76.0, 81.6, 87.0, 104.2, 156.9, 197.7 ppm. HRMS (FAB) calculated for $[\text{C}_{14}\text{H}_{23}\text{O}_3\text{N}]^+$: m/z 253.1678, found 253.1672.



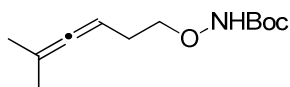
tert-Butyl 3-(cyclopentylidenemethyl)isoxazolidine-2-carboxylate (1.2). Following general procedure for hydroamination, **1.1** (18.5 mg, 73.0 μmol), (R)-xylyl-BINAP(AuOPNB)₂ (5.3 mg, 3.65 μmol), and CH_2Cl_2 (0.75 mL) was added and the mixture was stirred at room temperature for 24 h. The crude mixture was purified by chromatography, eluting with 1:25 EtOAc:hexanes to afford **2** as a clear oil (16.3 mg, 64.2 μmol , 88% yield). ^1H NMR (500 MHz): δ 1.48 (s, 9 H), 1.62-1.66 (m, 2 H), 1.67-1.71 (m, 2 H), 1.95-2.02 (m, 1 H), 2.17-2.33 (m, 3 H), 2.43-2.49 (m, 2 H), 3.75 (q, 1 H, $J = 8.0$ Hz), 4.07 (dt, 1 H, $J = 4.0, 8.0$ Hz), 4.73 (dt, 1 H, $J = 5.0, 8.5$ Hz), 5.31 (dt, 1 H, $J = 9, 2.5$ Hz) ppm. ^{13}C NMR (500 MHz): δ 26.1, 26.3, 28.2, 28.6, 33.6, 35.8, 58.5, 68.7, 81.6, 120.4, 145.9, 157.4 ppm. HRMS (FAB) calculated for $[\text{C}_{14}\text{H}_{23}\text{O}_3\text{N}]^+$: m/z 253.1678, found 253.1682.



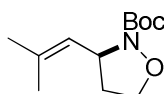
tert-Butyl 4-cyclohexylidenebut-3-enyloxycarbamate (1.3). Following the general procedure for hydroxylamine substrate synthesis, PPh_3 (0.85 g, 3.16 mmol) in THF (15 mL), DEAD (1.44 mL, 3.16 mmol), 4-cyclohexylidenebut-3-en-1-ol (0.40 g, 2.63 mmol) and *N*-hydroxyphthalimide (0.52 g, 3.12 mmol) was used. After 6 h, the reaction mixture was concentrated to afford a thick yellow oil. The crude oil was passed through a silica pad to afford the crude product a white solid (0.72 g). The solids (0.68 g) were redissolved in 15 mL CH_2Cl_2 and $\text{NH}_2\text{NH}_2 \cdot \text{H}_2\text{O}$ was added dropwise. The mixture was stirred overnight at room temperature and precipitants were removed by filtration. The unprotected hydroxylamine as a pale yellow oil (0.38 g). The oil (0.27 g) was dissolved in 1:4 THF: H_2O (5 mL) and NaHCO_3 (0.19 g, 2.56 mmol) and di-tert-butyl dicarbonate was added. The reaction was diluted with Et_2O (40 mL) and extracted with brine (20 mL). The organic layer was dried with Na_2SO_4 , concentrated and purified via flash chromatography, eluting with 1:24 EtOAc:hexanes to afford the desired product as a clear oil (0.45 g, 1.68 mmol, 92% yield overall). ^1H NMR (400 MHz): δ 1.48 (s, 9H), 1.55-1.60 (m, 6 H), 2.07-2.09 (m, 4 H), 2.30 (q, 2 H, $J = 6.8$ Hz), 3.89 (t, 2 H, $J = 6.8$ Hz), 4.93-4.97 (m, 1 H), 7.12 (br s, 1 H) ppm. ^{13}C NMR (400 MHz): δ 26.1, 27.4, 28.1, 28.2, 31.6, 76.0, 81.6, 84.3, 103.0, 156.90, 199.0 ppm. HRMS (FAB) calculated for $[\text{C}_{15}\text{H}_{25}\text{O}_3\text{N}]^+$: m/z 267.1834, found 267.1827.



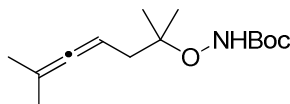
tert-Butyl 3-(cyclohexylidenemethyl)isoxazolidine-2-carboxylate (1.4). Following general procedure for hydroamination, **1.3** (53.4 mg, 0.20 mmol), (S)-xylyl-BINAP(AuOPNB)₂ (8.8 mg, 0.006 mmol) and 0.4 mL CH₂Cl₂ were combined and stirred for 24 h at room temperature. The crude oil was purified via flash chromatography, eluting with 1:24 EtOAc:hexanes to afford a white solid (49.7 mg, 0.183 mmol, 93% yield). ¹H NMR (400 MHz): δ 1.48 (s, 9 H), 1.53-1.67 (m, 6 H), 1.91-2.00 (m, 1 H), 2.07 (t, 2 H, *J* = 2.8 Hz), 2.23 (t, 2 H, *J* = 2.8 Hz), 2.41-2.49 (m, 2 H), 4.74 (q, 1 H, *J* = 8.0 Hz), 4.08 (sextet, 1 H, *J* = 4.0 Hz), 4.87-4.93 (m, 1 H), 5.14 (d, 1 H, *J* = 8.8 Hz) ppm. ¹³C NMR (400 MHz): δ 26.7, 27.7, 28.3, 28.3, 29.0, 36.6, 36.8, 56.3, 68.7, 81.7, 122.2, 141.8, 157.4 ppm. HRMS (FAB) calculated for [C₁₅H₂₅O₃N]⁺: *m/z* 267.1834, found 267.1827.



tert-butyl 5-methylhexa-3,4-dienyloxycarbamate (1.5). The crude mixture was purified by flash column chromatography (0-10% EtOAc/Hexanes) to afford **1.5** as a clear oil. ¹H NMR (400 MHz): δ 7.13 (s, 1H), 4.99 (m, 1H), 3.93 (t, *J* = 7.0 Hz, 2H), 2.33 (q, *J* = 6.9 Hz, 2H), 1.72 (s, 3H), 1.71 (s, 3H), 1.53 (s, 9H). ¹³C NMR (150 MHz): δ 202.4, 156.9, 95.6, 84.5, 81.6, 76.0, 28.2, 27.9, 20.6 ppm. HRMS (FAB) calc'd for [C₁₂H₂₁O₃NNa]⁺: *m/z* 250.1414, found 250.1409.

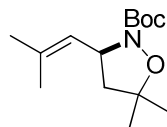


tert-butyl 3-(2-methylprop-1-enyl)isoxazolidine-2-carboxylate (1.6). Following general procedure for hydroamination, allene **1.15** (159 mg, 700 μmol), (*R*)-xylyl-BINAP(AuOPNB)₂ (30 mg, 21 μmol), and CH₂Cl₂ (1.4 mL) was added and the mixture was stirred at room temperature for 24 h. The crude mixture was purified by column chromatography (5-12.5% EtOAc/hexanes) to afford **11** as a clear oil (145 mg, 91% yield, 93% ee): ¹H NMR (600 MHz): δ 5.18 (dd, *J* = 9.1, 0.9 Hz, 1H), 4.83 (td, *J* = 8.7, 5.1 Hz, 1H), 4.09-4.05 (m, 1H), 3.74 (q, *J* = 8.0 Hz, 1H), 2.45 (dtd, *J* = 11.8, 7.9, 4.0 Hz, 1H), 1.95 (dtd, *J* = 12.4, 8.1, 4.6 Hz, 1H), 1.72 (s, 3H), 1.70 (s, 3H), 1.46 (s, 9H) ppm. ¹³C NMR (150 MHz): δ 157.3, 134.0, 125.2, 81.6, 68.7, 57.1, 36.1, 28.2, 25.6, 17.9 ppm. HRMS (FAB) calc'd for [C₁₂H₂₁O₃NNa]⁺: *m/z* 250.1414, found 250.1409. HPLC Regis Technologies Whelk-O 1 column (98:2 hexanes:ethanol; 1 mL/min) tR 11.9 min (minor), 12.6 min (major): 93% ee.

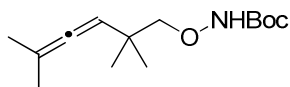


tert-Butyl 2,6-dimethylhepta-4,5-dien-2-yloxycarbamate (1.7). The crude oil was purified by column chromatography (3:97 EtOAc:hexanes) to yield **1.7** as a clear oil (0.45 g, 1.76 mmol,

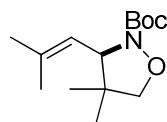
10% yield overall). ^1H NMR (500 MHz): δ 6.70 (br s, 1H), 4.94 (m, 1H), 2.18 (d, 2H, $J = 7.5$ Hz), 1.67 (d, 6H, $J = 3.0$ Hz), 1.47 (s, 9H), 1.22 (s, 6H), ppm. ^{13}C NMR (125 MHz): δ 203.5, 157.5, 94.3, 84.2, 82.9, 81.3, 39.3, 28.2, 23.9, 20.5 ppm. HRMS (ESI) calc'd for $[\text{C}_{14}\text{H}_{25}\text{O}_3\text{N}+\text{Na}]^+$: m/z 278.1727, found 278.1727.



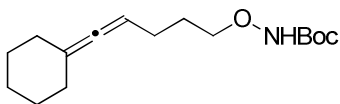
tert-butyl 5,5-dimethyl-3-(2-methylprop-1-enyl)isoxazolidine-2-carboxylate (1.8). Following the general procedure, **1.7** (50.0 mg, 196 μmol), (R)-DM-MeOBIPHEP (AuOPNB)₂ (13.9 mg, 9.8 μmol), and MeNO_2 (0.65 mL) were combined and stirred at 50 $^\circ\text{C}$ for 24 h. The crude mixture was purified by column chromatography (1:99 EtOAc: CH_2Cl_2) to yield a clear oil (46.7 mg, 94% yield, 63% ee). ^1H NMR (400 MHz): δ 5.21 (d, 1H, $J = 7.6$ Hz), 4.89 (dd, 1H, $J = 7.6$, 8.4 Hz), 2.28 (dd, 1H, $J = 8.4$, 12.4 Hz), 1.77-1.74 (m, 1H), 1.74-1.70, (m, 6H), 1.48 (s, 9H), 1.39 (s, 3H), 1.19 (s, 3H) ppm. ^{13}C NMR (125MHz): δ 157.5, 133.3, 125.6, 83.2, 81.0, 57.7, 48.0, 28.3, 25.6, 25.4, 24.8, 17.9 ppm. HPLC Regis Technologies WHELK-O1 column (99:1 hexanes: isopropanol; 1 mL/min): tR 20.4 min (major), 27.8 min (minor). HRMS (ESI) calc'd for $[\text{C}_{14}\text{H}_{25}\text{O}_3\text{N}+\text{Na}]^+$: m/z 278.1727, found 278.1727.



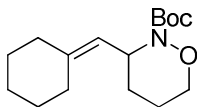
tert-Butyl 2,2,5-trimethylhexa-3,4-dienyloxycarbamate (1.9). The crude oil was purified by flash chromatography, eluting with 1:24 EtOAc: hexanes to provide **1.9** as a clear oil (0.38 g, 1.48 mmol, 8% yield overall). ^1H NMR (500 MHz): δ 1.04 (s, 6 H), 1.48 (s, 9 H), 1.68 (d, 6 H, $J = 3.0$ Hz), 3.63 (s, 2 H), 4.95 (m, 1 H), 7.16 (brs, 1 H) ppm. ^{13}C NMR (500 MHz): δ 20.7, 25.1, 28.2, 35.9, 81.5, 85.8, 96.7, 97.2, 156.7, 200.1 ppm. HRMS (ESI) calc'd for $\text{C}_{14}\text{H}_{23}\text{O}_3\text{N}+\text{Na}]^+$: m/z 278.1727, found 278.1726.



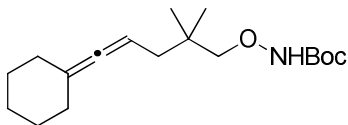
tert-butyl 4,4-dimethyl-3-(2-methylprop-1-enyl)isoxazolidine-2-carboxylate (1.10). Following general procedure for hydroamination, **1.9** (30.4 mg, 127 μmol), (R)-DM-MeOBIPHEP (AuOPNB)₂ (9.0 mg, 6.3 μmol), and MeNO_2 (1.2 mL) were combined and stirred at 50 $^\circ\text{C}$ for 24 h. The crude mixture was purified by column chromatography (1:99 EtOAc:DCM) to yield white crystals (22.2 mg, 73 % yield, 99% ee). ^1H NMR (500 MHz): δ 5.09 (d, 1H, $J = 8.0$ Hz), 4.31 (d, 1H, $J = 8.0$ Hz), 3.71 (d, 1H, $J = 7.5$ Hz), 3.65 (d, 1H, $J = 7.5$ Hz), 1.77 (s, 3H), 1.71 (s, 3H), 1.47 (s, 9H), 1.02 (s, 3H), 0.89 (s, 3H) ppm. ^{13}C NMR (125 MHz): δ 156.8, 135.2, 121.4, 81.2, 79.9, 66.6, 46.3, 28.2, 25.9, 24.6, 21.1, 18.0 ppm. HPLC Chiralpak OD-H (99:1 hexanes:isopropanol; 1 mL/min) tR 10.7 min (major), 13.2 min (minor). HRMS (ESI) calc'd for $[\text{C}_{14}\text{H}_{25}\text{O}_3\text{N}+\text{Na}]^+$: m/z 278.1727, found 278.1726.



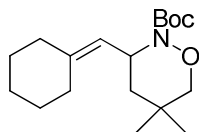
tert-Butyl 5-cyclohexylidenepent-4-enyloxycarbamate (1.13). Following the general procedure for substrate synthesis, PPh_3 (2.86 g, 10.7 mmol), DEAD (4.84 mL, 10.7 mmol) in THF (25 mL), hexa-4,5-dien-1-ol (1.61 g, 9.7 mmol) and *N*-hydroxyphthalimide (1.74 g, 10.7 mmol) was used. The solution became deep orange upon addition of hydroxyphthalimide, but turned pale yellow as it is stirred at room temperature for 6 hr. The crude oil was passed through a silica pad, eluting with 1:4 hexanes: EtOAc (300 mL) to remove triphenyl phosphine oxide and to give the crude product as a white solid (2.48 g). The crude solid (1.50 g, 4.82 mmol) was used without further purification and was redissolved CH_2Cl_2 (25 mL) and $\text{NH}_2\text{NH}_2 \cdot \text{H}_2\text{O}$ (0.47 mL, 9.64 mmol) was added. At the end of reaction, the precipitants were removed by filtration. The organic layer was concentrated to afford a clear oil (0.87 g). The oil (0.54 g) dissolved in THF (3 mL), H_2O (12 mL) and reacted with NaHCO_3 (0.35 g, 4.17 mmol) and di-*tert*-butyl dicarbonate (0.78 g, 3.58 mmol). The crude mixture was diluted with Et_2O (100 mL) and extracted with saturated NH_4Cl (60 mL). The crude oil was purified by flash chromatography, eluting with 1:24 EtOAc: hexanes to provide **1.13** as a clear oil (0.57 g, 2.03 mmol, 68% yield overall). ^1H NMR (400 MHz): δ 1.48 (s, 9 H), 1.50-1.63 (m, 6 H), 1.69-1.76 (q, 2 H, $J = 6.8$ Hz), 2.01-2.09 (m, 6 H), 3.86-3.89 (t, 2 H, $J = 6.8$ Hz), 4.96-4.99 (m, 1 H), 7.10 (br s, 1 H) ppm. ^{13}C NMR (400 MHz): δ 25.4, 26.1, 27.2, 27.4, 28.2, 31.7, 76.2, 87.9, 96.7, 103.1, 156.9, 176.0, 198.3 ppm. HRMS (EI) calculated for $[\text{C}_{16}\text{H}_{27}\text{O}_3\text{N} + \text{Na}]^+$: m/z 304.1883, found 304.1890.



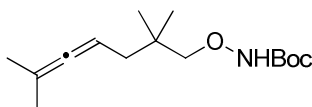
tert-Butyl 3-(cyclohexylidenemethyl)morpholine-2-carboxylate (1.14). Following general procedure for hydroamination, **1.13** (25.0 mg, 88.8 μmol), (R)-xylyl-BINAP(AuOPNB)₂ (6.5 mg, 4.45 μmol), and MeNO_2 (0.3 mL) were combined and stirred at 65 $^\circ\text{C}$ for 24 h. Conversion (>95%) was determined by ^1H NMR analysis of the crude mixture. The crude mixture was purified by chromatography, eluting with CH_2Cl_2 to provide a white solid (15.4 mg, 55 μmol , 62% yield). ^1H NMR (500 MHz): δ 1.47 (s, 9 H), 1.47-1.66 (m, 8 H), 1.92 (m, 1 H), 2.02-2.21 (m, 5 H), 3.88 (dt, 1 H, $J = 2, 12.5$ Hz), 4.07 (dd, 1 H, $J = 10.8, 4.0$ Hz), 4.87 (t, 1 H, $J = 6.4$ Hz), 5.69 (d, 1 H, $J = 8.8$ Hz) ppm. ^{13}C NMR (500 MHz): δ 20.4, 26.7, 27.8, 28.3, 28.5, 29.2, 36.9, 71.6, 81.0, 117.8, 154.9, 142.1 ppm. HRMS (FAB) calculated for $[\text{C}_{16}\text{H}_{27}\text{O}_3\text{N}]^+$: m/z 281.1991, found 281.1983.



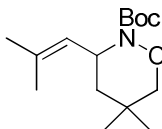
tert-Butyl 5-cyclohexylidene-2,2-dimethylpent-4-enyloxycarbamate (1.15). Following general procedure for substrate synthesis, 5-cyclohexylidene-2,2-dimethylpent-4-en-1-ol was used with PPh_3 , DEAD, and *N*-hydroxyphthalimide. The crude product from the Mitsunobu reaction was treated with $\text{NH}_2\text{NH}_2 \cdot \text{H}_2\text{O}$ in CH_2Cl_2 . Boc-protection was carried out with NaHCO_3 and di-tert-butyl dicarbonate in THF and H_2O . The crude oil was purified by column chromatography (1:49 EtOAc:hexanes) to yield **20** as a clear oil (0.866 g, 2.8 mmol, 33% yield overall). ^1H NMR (400 MHz): δ 7.10 (br s, 1H), 4.92 (m, 1H), 3.61 (s, 2H), 2.10-2.07 (m, 4H), 1.95 (d, 2H, $J = 7.6$ Hz), 1.62-1.56 (m, 2H), 1.55-1.48 (m, 2H), 1.48 (s, 9H), 0.94 (s, 6H) ppm. ^{13}C NMR (100 MHz): δ 200.2, 156.9, 101.0, 85.2, 84.4, 81.5, 39.8, 34.9, 31.7, 28.3, 27.4, 26.2, 24.1 ppm. HRMS (ESI) calc'd for $[\text{C}_{18}\text{H}_{31}\text{O}_3\text{N} + \text{Na}]^+$: m/z 332.2196 found 332.2197.



tert-Butyl 2,2,6-trimethylhepta-4,5-dienyloxycarbamate (1.16). The crude oil was purified by column chromatography (1:24 EtOAc:hexanes) to yield **1.16** as a clear oil (0.87 g, 3.2 mmol, 41% yield overall). ^1H NMR (500 MHz): δ 7.11 (br s, 1H), 0.93 (s, 6H), 4.90 (m, 1H), 3.16 (s, 2H), 1.93 (d, 2H, $J = 8.0$ Hz), 1.66 (d, 6H, $J = 2.5$ Hz), 1.48 (s, 9H) ppm. ^{13}C NMR (125 MHz): δ 203.4, 93.5, 85.1, 84.4, 81.4, 39.4, 34.8, 28.2, 24.1, 20.1 ppm. HRMS (ESI) calc'd for $[\text{C}_{15}\text{H}_{27}\text{O}_3\text{N} + \text{Na}]^+$: m/z 292.1883 found 292.1884.

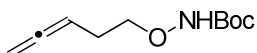


tert-Butyl 2,2,6-trimethylhepta-4,5-dienyloxycarbamate (1.17). The crude oil was purified by column chromatography (1:24 EtOAc:hexanes) to yield **1.17** as a clear oil (0.87 g, 3.2 mmol, 41% yield overall). ^1H NMR (500 MHz): δ 7.11 (br s, 1H), 0.93 (s, 6H), 4.90 (m, 1H), 3.16 (s, 2H), 1.93 (d, 2H, $J = 8.0$ Hz), 1.66 (d, 6H, $J = 2.5$ Hz), 1.48 (s, 9H) ppm. ^{13}C NMR (125 MHz): δ 203.4, 93.5, 85.1, 84.4, 81.4, 39.4, 34.8, 28.2, 24.1, 20.1 ppm. HRMS (ESI) calc'd for $[\text{C}_{15}\text{H}_{27}\text{O}_3\text{N} + \text{Na}]^+$: m/z 292.1883 found 292.1884.

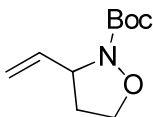


tert-Butyl 5,5-dimethyl-3-(2-methylprop-1-enyl)morpholine-2-carboxylate (1.18). Following general procedure for hydroamination, **1.17** (50.0 mg, 162 μmol), (*R*)-xylyl-BINAP(AuOPNB) $_2$ (11.8 mg, 8.9 μmol), and MeNO_2 (0.53 mL) were combined and stirred at 50 $^\circ\text{C}$ for 24 h. The crude mixture was purified by column chromatography (1:99 EtOAc: CH_2Cl_2) to yield white

solids (39.5 mg, 128 μ mol, 79% yield, 89% ee). ^1H NMR (500 MHz): δ 5.60 (d, 1H, J = 8.4 Hz), 4.78 (m, 1H), 3.63 (d, 1H, J = 11.2 Hz), 3.58 (d, 1H, J = 11.2 Hz), 1.75 (m, 1H), 1.71 (s, 3H), 1.50 (m, 1H), 1.64 (s, 3H), 1.47 (s, 9H), 1.10 (s, 3H), 0.86 (s, 3H) ppm. ^{13}C NMR (125 MHz): δ 155.0, 132.3, 124.1, 81.1, 81.0, 52.7, 40.9, 29.6, 28.3, 27.5, 26.5, 25.5, 17.8 ppm. HPLC Regis Technologies Whelk-O 1 column (98:2 hexanes:ethanol; 1 mL/min) tR 14.7 min (minor), 20.3 min (major): 89% ee; HRMS (ESI) calc'd for $[\text{C}_{15}\text{H}_{27}\text{O}_3\text{N}+\text{Na}]^+$: m/z 292.1883 found 292.1884.

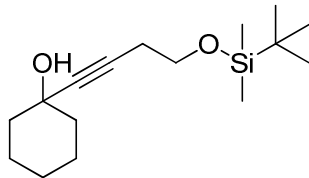


***tert*-Butyl penta-3,4-dienyloxycarbamate (1.19).** Following the general procedure for hydroxylamine substrate synthesis, PPh_3 (1.06 g, 3.92 mmol), DEAD (1.78 mL, 3.92 mmol), penta-3,4-dien-1-ol (0.30 g, 3.57 mmol) and *N*-hydroxyphthalimide (0.64 g, 3.92 mmol) was used. Removal of solvent afforded the crude product as a thick yellow oil. The oil was passed through a silica pad, eluting with 1:4 hexanes: EtOAc (300 mL) to remove triphenylphosphine oxide and give the crude product as a white solid (0.63 g). The solid was redissolved CH_2Cl_2 (15 mL) and reacted with $\text{NH}_2\text{NH}_2 \cdot \text{H}_2\text{O}$ (0.27 mL, 5.50 mmol). Upon reaction completion, the precipitants were removed by filtration. The organic layer was concentrated to afford a clear oil (0.27 g). The oil was dissolved in THF (1 mL) and H_2O (4 mL) and treated with NaHCO_3 (0.28 g, 3.30 mmol) and di-*tert*-butyl dicarbonate (0.66 g, 3.02 mmol). After 2 h, the reaction was diluted with Et_2O (40 mL) and extracted with saturated NH_4Cl (20 mL). The crude oil was purified by flash chromatography, eluting with 1:24 EtOAc:hexanes to provide **7** as a clear oil (0.46 g, 2.31 mmol, 65% yield over 3 steps). ^1H NMR (400 MHz): δ 1.48 (s, 9 H), 2.32-2.38 (m, 2 H), 3.90-3.94 (t, 2 H, J = 6.8 Hz), 4.69-4.72 (m, 2 H), 5.17 (quintet, 1 H, J = 6.8 Hz) ppm. ^{13}C NMR (400 MHz): δ 27.1, 28.2, 75.2, 75.7, 81.8, 86.1, 157.0, 209.0 ppm. HRMS (EI) calculated for $[\text{C}_{10}\text{H}_{17}\text{O}_1\text{N}_1-\text{C}_4\text{H}_9+\text{H}]^+$: m/z 143.0582, found 143.0588.

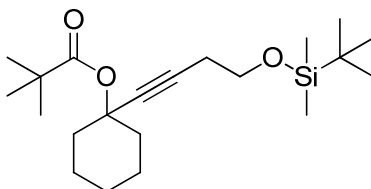


***tert*-Butyl 3-vinylisoxazolidine-2-carboxylate (1.20).** Following general procedure for hydroamination, $\text{dppm}(\text{AuCl})_2$ (1.9 mg, 2.26 μ mol), (*S*)-Ag-TRIP (3.9 mg, 4.52 μ mol), **1.19** (15.0 mg, 75.0 μ mol), and benzene (0.75 mL) were combined and stirred at room temperature for 48 h. The crude product was purified via flash chromatography eluting with 1:24 EtOAc:hexanes to afford a clear oil (9.4 mg, 48.0 μ mol, 64% yield). ^1H NMR (500 MHz): δ 1.49 (s, 9 H), 2.04-2.11 (m, 1 H), 2.44-2.50 (m, 1 H), 3.76-3.81 (m, 1 H), 4.05-4.09 (m, 1 H), 4.57-4.61, 5.13 (d, 1 H, J = 10.0 Hz), 5.27 (d, 1 H, J = 18.5 Hz), 5.82 (m, 1 H) ppm. ^{13}C NMR (500 MHz): δ 28.3, 35.2, 60.2, 68.6, 81.9, 115.6, 137.4, 157.1 ppm. HRMS (EI) calculated for $[\text{C}_{10}\text{H}_{17}\text{O}_1\text{N}_1-\text{C}_4\text{H}_9\text{O}_1]^+$: m/z 126.0555, found 126.0552.

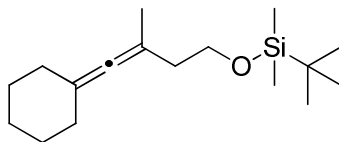
Synthesis of tetra-substituted allenes:



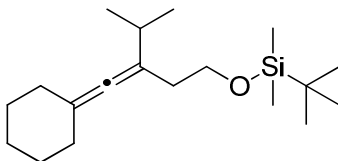
1-(4-(*tert*-Butyldimethylsilyloxy)but-1-ynyl)cyclohexanol. To a solution of (but-3-ynoxy)(*tert*-butyl)dimethylsilane (4.00 g, 21.7 mmol) in anhydrous THF (42 mL) was added 11.9 mL (23.9 mmol) of *n*-BuLi at -78 °C under N₂. The solution was stirred for 60 min at -78 °C. Next, a solution of cyclohexanone (2.47 mL, 23.9 mmol) in THF (3 mL) was added and the mixture was allowed to warm to room temperature over 2 h. The reaction mixture was quenched by dropwise addition of saturated NH₄Cl (20 mL). The mixture was transferred to a separatory funnel and Et₂O (40 mL) was added. The layers were separated and the aqueous layer was washed with two portions of Et₂O (40 mL each). The organic layer was combined, dried with Na₂SO₄, and concentrated. The oil was purified by chromatography on SiO₂, eluting with 1:15 EtOAc:hexanes to afford **12** (5.08 g, 18.0 mmol, 83% yield) as a clear oil. ¹H NMR (400 MHz): δ 0.08 (s, 6 H), 0.90 (s, 9 H), 1.27-1.33 (m, 2 H), 1.42-1.69 (m, 8 H), 2.40-2.45 (t, 2 H, *J* = 9.6 Hz), 3.68-3.72 (t, 2 H, *J* = 9.6) ppm. The ¹H NMR data matched the spectroscopic data reported in literature.³⁷



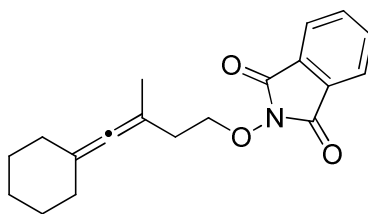
1-(4-(*Isopropyl*dimethylsilyloxy)but-1-ynyl)cyclohexyl pivalate. To a solution of 1-(4-(*tert*-Butyldimethylsilyloxy)but-1-ynyl)cyclohexanol (3.00 g, 10.6 mmol) in anhydrous THF (25 mL) at 0 °C under N₂ was added LiHMDS (1.78 g, 10.6 mmol) in one portion. The solution was stirred at 0 °C for 15 min and pivaloyl chloride (1.31 mL, 10.6 mmol) was added. The mixture was allowed to warm to room temperature over 1 h and quenched with saturated NH₄Cl (20 mL). The mixture was transferred to a separatory funnel and extracted with Et₂O (100 mL). The organic layer was dried with MgSO₄ and concentrated. The oil was purified by chromatography on SiO₂, eluting with 1:24 EtOAc:hexanes to afford the pivalate (3.40 g, 9.33 mmol, 88% yield) as a clear oil. ¹H NMR (400 MHz): δ 0.06 (s, 6 H), 0.89 (s, 9 H), 1.19 (s, 9 H), 1.40-1.43 (m, 2 H), 1.53-1.69 (m, 4 H), 1.91-1.95 (m, 4 H), 2.41-2.46 (t, 2 H, *J* = 9.6 Hz), δ 3.67-3.72 (t, 2 H, *J* = 9.6 Hz). The ¹H NMR data matched the spectroscopic data reported in literature.³⁷



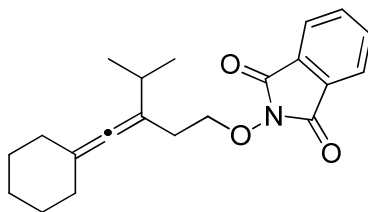
tert-Butyl(4-cyclohexylidene-3-methylbut-3-enyloxy)dimethylsilane (1.21a). A flame dried flask was charged with anhydrous CuI (3.43 g, 18.0 mmol), LiBr (1.57 g, 18.0 mmol), and THF (40 mL). The solution was cooled to 0 °C and MeMgBr (6.75 mL, 18.0 mmol) was added. The mixture was stirred for 25 min and a solution of 1-(4-(Isopropyldimethylsilyloxy)but-1-ynyl)cyclohexyl pivalate (1.1 g, 3.0 mmol) in THF (5 mL) was added dropwise over 5 min. The solution was warmed to room temperature over 4 h and quenched by the addition of 40 mL of 1:4 NH₄OH and NH₄Cl solution. The mixture was extracted twice with Et₂O (50 mL each) and the organic layer was dried with Na₂SO₄ and concentrated. The crude oil was purified by chromatography on SiO₂, eluting with hexanes to give a pale yellow oil (0.62 g, 2.33 mmol, 78% yield). ¹H NMR (400 MHz): δ 0.06 (s, 6 H), 0.90 (s, 9 H), 1.43-1.55 (m, 4 H), 1.57-1.65 (m, 2 H), 2.02-2.05 (m, 4 H), 2.12-2.16 (t, 2 H, *J* = 9.6 Hz), 3.65-3.69 (t, 2 H, *J* = 9.6 Hz) ppm. ¹³C NMR (400 MHz) δ -5.3, 18.4, 20.1, 26.0, 26.3, 27.8, 32.1, 37.7, 62.4, 93.4, 101.7, 195.6 ppm. HRMS (EI) calculated for [C₁₇H₃₂O₁Si₁-C₄H₉]⁺: *m/z* 223.1518, found 223.1519.



tert-Butyl(3-(cyclohexylidenemethylene)-4-methylpentyloxy)dimethylsilane (1.21b). A flame-dried flask was charged with anhydrous LiCl (0.84 g, 19.9 mmol) and CuCN (0.89 g, 9.93 mmol) and dry THF (75 mL). The solution was stirred at -78 °C for 5 min, and iPrMgCl (10.9 mL, 19.9 mmol) was added dropwise. The solution was warmed slowly to -35 °C over 1 h. Then a solution of 1-(4-(Isopropyldimethylsilyloxy)but-1-ynyl)cyclohexyl pivalate (0.910 g, 2.48 mmol) in THF (5 mL) was added and the entire mixture was warmed slowly to room temperature. The reaction mixture was stirred for a total of 4 hours and quenched by the dropwise addition of 1:4 NH₄OH: NH₄Cl. The mixture was transferred to a separatory funnel and extracted with Et₂O (100 mL). The organic layer was washed with NH₄Cl (20 mL), then dried with Na₂SO₄ and concentrated. The crude mixture was purified by flash chromatography on SiO₂, eluting with hexanes to afford a pale yellow oil (0.66 g, 2.25 mmol, 91% yield). ¹H NMR (400 MHz): δ 0.06 (s, 6 H), 0.90 (s, 9 H), 0.97 (d, 6 H, *J* = 6.8 Hz), 1.50-1.59 (m, 6 H), 2.02-2.09 (m, 5 H), 2.15-2.18 (t, 2 H, *J* = 7.6 Hz), 3.63-3.67 (t, 2 H, *J* = 7.6 Hz) ppm. ¹³C NMR (400 MHz): δ -5.3, 18.4, 21.9, 25.8, 26.0, 27.9, 31.6, 32.3, 34.4, 62.9, 104.4, 104.7, 194.0 ppm. HRMS (EI) calculated for [C₁₉H₃₆O₁Si₁-C₄H₉]⁺: *m/z* 251.1831, found 251.1825.

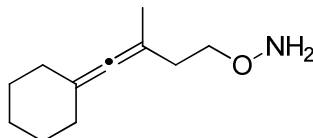


2-(4-Cyclohexylidene-3-methylbut-3-enyloxy)isoindoline-1,3-dione (1.21c). A solution of **1.21a** (0.62 g, 2.33 mmol) in THF (15 mL) was cooled to 0 °C and TBAF (2.56 mL, 2.56 mmol) was added. The reaction mixture was warmed to room temperature and stirred for 2 hr. Saturated NH₄Cl (40 mL) was added and mixture was extracted with Et₂O (50 mL). The organic layer was dried with Na₂SO₄ and concentrated to yield 4-cyclohexylidene-3-methylbut-3-en-1-ol as a pale yellow oil (0.43 g). The crude oil was redissolved in dry THF (5 mL) and the solution was added to a prestirred mixture of PPh₃ (0.766 g, 2.84 mmol) and DEAD (1.3 mL, 2.84 mmol) in dry THF (20 mL) at 0 °C. The reaction mixture was stirred at 0 °C for 30 min before *N*-hydroxyphthalimide (0.464 g, 2.84 mmol) was added in one portion. The solution became deep red immediately upon addition of hydroxyphthalimide but turned clear as it is stirred at room temperature for 2 h. The reaction mixture was concentrated slowly under reduced pressure and the crude mixture was purified via flash chromatography on SiO₂, eluting with 3:47 EtOAc:hexanes to afford a white solid (0.64 g, 2.06 mmol, 82% yield over 2 steps). ¹H NMR (400 MHz): δ 1.46-1.56 (m, 6 H), 1.72 (s, 3 H), 2.03-2.06 (m, 4 H), 2.44 (t, 2 H, *J* = 7.6 Hz), 4.27 (t, 2 H, *J* = 7.6 Hz). ¹³C NMR (400 MHz) δ 20.3, 26.2, 27.7, 31.9, 32.5, 77.1, 92.1, 103.1, 123.5, 129.0, 134.4, 163.7, 195.2 ppm. HRMS (FAB) calculated for [C₁₆H₂₆O₃N+H]⁺: *m/z* 312.1600, found 312.1604.

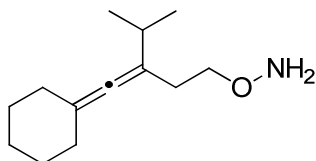


2-(3-(Cyclohexylidenemethylene)-4-methylpentyloxy)isoindoline-1,3-dione (1.21d). A solution of **1.21b** (0.66 g, 2.25 mmol) in THF (20 mL) was cooled to 0 °C and TBAF (2.48 mL, 2.48 mmol) was added. The reaction mixture was warmed to room temperature and stirred for 5 hr. Saturated NH₄Cl (40 mL) was added and the mixture was extracted with Et₂O (50 mL). The organic layer was dried with Na₂SO₄ and concentrated to yield a pale yellow oil. The oil was redissolved in dry THF (5 mL) and then added to a prestirred solution of PPh₃ (1.49 g, 5.55 mmol) and DEAD (2.4 mL, 5.55 mmol) in dry THF (15 mL), at 0 °C. The solution was stirred at 0 °C for 45 min before *N*-hydroxyphthalimide (0.91 g, 5.55 mmol) was added in one portion. The reaction mixture turned deep red immediately upon hydroxyphthalimide addition. The reaction mixture was stirred at room temperature for 6 h, until the reaction mixture was pale yellow. The solution was concentrated to a viscous oil, which was purified via flash chromatography on SiO₂, eluting with 1:9 EtOAc:hexanes to afford white solids (0.74 g, 2.20 mmol, 99% yield). ¹H NMR (400 MHz): δ 0.93 (d, 6 H, *J* = 6.8 Hz), 1.43-1.64 (m, 6 H), 1.97-

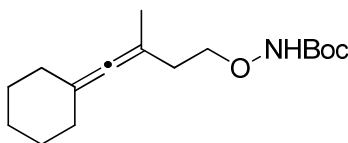
2.12 (m, 5 H), 2.45 (t, 2 H, $J = 7.6$ Hz), 4.23 (t, 2 H, $t = 7.6$ Hz), 7.76 (m, 2 H), 7.82 (m, 2 H) ppm. ^{13}C NMR (400 MHz): δ 21.9, 26.2, 27.8, 29.4, 31.8, 32.1, 77.6, 103.4, 105.9, 123.5, 129.0, 134.4, 163.7, 193.6 ppm. HRMS (FAB) calculated for $[\text{C}_{21}\text{H}_{25}\text{N}_1\text{O}_3]^+$: m/z 339.1834, found 339.1840.



O-(4-cyclohexylidene-3-methylbut-3-enyl)hydroxylamine (1.22). 2-(4-Cyclohexylidene-3-methylbut-3-enyloxy)isoindoline-1,3-dione (**1.21c**) (0.64 g, 2.06 mmol) was dissolved in CH_2Cl_2 (10 mL) and $\text{NH}_2\text{NH}_2 \cdot \text{H}_2\text{O}$ (0.20 mL, 4.11 mmol) was added to the solution. The reaction mixture was stirred at room temperature for 16 h, and white precipitants appear. The reaction mixture was filtered and concentrated. The crude mixture was purified via flash chromatography on SiO_2 , eluting with 1:9 EtOAc:hexanes to afford a clear oil (0.24 g, 65% yield). ^1H NMR (400 MHz): δ 1.49-1.59 (m, 6 H), 1.68 (s, 3 H), 2.05-2.08 (m, 4 H), 2.20 (t, 2 H, $J = 7.2$ Hz), 3.75 (t, 2 H, $J = 7.2$ Hz), 5.36 (br s, 2 H) ppm. ^{13}C NMR (400 MHz): δ 20.1, 26.3, 27.8, 32.0, 33.0, 74.4, 93.2, 102.1, 195.5 ppm. HRMS (EI) calculated for $[\text{C}_{11}\text{H}_{19}\text{O}_1\text{N}+\text{H}]^+$: m/z 182.1539, found 182.1545.

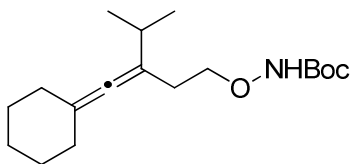


O-(3-(cyclohexylidenemethylene)-4-methylpentyl)hydroxylamine (1.23). To a solution of **1.23** (0.74 g, 2.20 mmol) in CH_2Cl_2 (20 mL), $\text{NH}_2\text{NH}_2 \cdot \text{H}_2\text{O}$ (0.25 mL, 4.4 mmol) was added. The reaction mixture was stirred overnight and white precipitants were observed. The reaction mixture was filtered and concentrated. The crude oil was purified by flash chromatography on SiO_2 , eluting with 2:23 EtOAc:hexanes to provide a clear oil (0.46 g, 2.20 mmol, 99% yield). ^1H NMR (400 MHz): δ 0.99 (d, 6 H, $J = 6.4$ Hz), 1.49-1.65 (m, 6 H), 2.06-2.08 (m, 5 H), 2.22 (t, 2 H, $J = 7.2$ Hz), 3.72 (t, 2 H, $J = 7.2$ Hz) 5.35 (br s, 2 H) ppm. ^{13}C NMR (400 MHz): δ 21.9, 26.3, 27.9, 29.8, 31.6, 32.2, 75.0, 104.5, 104.9, 193.9 ppm. HRMS (EI) calculated for $[\text{C}_{13}\text{H}_{23}\text{ON}+\text{H}]^+$: m/z 210.1852, found 210.1859

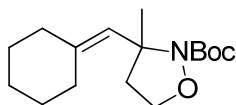


tert-Butyl 4-cyclohexylidene-3-methylbut-3-enyloxycarbamate (1.24). To a solution of **1.22** (0.24 g, 1.32 mmol) in CH_2Cl_2 (10 mL), pyridine (0.15 mL, 1.83 mmol) and di-tert-butyl dicarbonate (0.34 g, 1.56 mmol) were added. The reaction mixture was stirred room temperature for 5 h, before brine (30 mL) was added and the organic layer was extracted with two portions of CH_2Cl_2 (30 mL each). The organic layer was dried, concentrated, and purified by flash

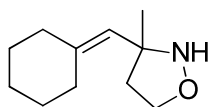
chromatography, eluting with 2:23 EtOAc:hexanes to afford a clear oil (0.23 g, 0.82 mmol, 62% yield). ^1H NMR (400 MHz): δ 1.48 (s, 9 H), 1.48-1.59 (m, 6 H), 1.67 (s, 3 H), 2.03-2.06 (m, 4 H), 2.25 (t, 2 H, $J = 7.2$ Hz), 3.91 (t, 2 H, $J = 7.2$ Hz), 7.11 (br s, 1 H) ppm. ^{13}C NMR (400 MHz): δ 20.1, 26.2, 27.7, 28.2, 31.9, 32.5, 75.0, 81.5, 102.4, 156.9, 195.4 ppm. HRMS (EI) calculated for $[\text{C}_{16}\text{H}_{27}\text{O}_3\text{N}+\text{Na}]^+$: m/z 304.1883, found 304.1893.



tert-Butyl 3-(cyclohexylidenemethylene)-4-methylpentylloxycarbamate (1.25). To a solution of **1.23** (0.42 g, 2.01 mmol) in H_2O (4 mL) and THF (1 mL), NaHCO_3 (0.20 g, 2.41 mmol) and di-tert-butyl dicarbonate (0.48 g, 2.21 mmol) were added. The reaction mixture was stirred at room temperature for 4 h. Saturated NaHCO_3 (10 mL) was added, the mixture was transferred to a separatory funnel, and the organic layer was extracted twice with Et_2O (30 mL each). The organic layer was dried, concentrated, then purified by flash chromatography on SiO_2 , eluting with 1:24 EtOAc:hexanes, to afford a clear oil (0.62 g, 1.81 mmol, 90% yield). ^1H NMR (400 MHz): δ 0.98 (d, 6 H, $J = 6.8$ Hz), 1.48 (s, 9 H), 1.50-1.64 (m, 6 H), 2.00-2.09 (m, 5 H), 2.27 (t, 2 H, $J = 7.6$ Hz), 3.90 (t, 2 H, $J = 7.2$ Hz), 7.08 (br s, 1 H) ppm. ^{13}C NMR (400 MHz): δ 21.9, 26.3, 27.9, 29.4, 31.7, 32.2, 75.7, 81.6, 104.2, 105.2, 156.9, 193.9 ppm. HRMS (EI) calculated for $[\text{C}_{18}\text{H}_{31}\text{O}_3\text{N}+\text{Na}]^+$: m/z 332.2202, found 332.2206.

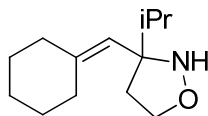


tert-Butyl 3-(cyclohexylidenemethyl)-3-methylisoxazolidine-2-carboxylate (1.26). Following general procedure for hydroamination, **1.22** (15.0 mg, 53.3 μmol), (R)-MeO-BIPHEP (AuOPNB) $_2$ (3.9 mg, 3.0 μmol) and CH_2Cl_2 (0.6 mL) were combined and stirred for 48 h. Conversion (85%) was determined by crude NMR. The reaction mixture was purified by chromatography, eluting with 1:19 EtOAc:hexanes to afford a clear oil (12.7 mg, 45.3 μmol , 85% yield). ^1H NMR (400 MHz): δ 1.48 (s, 9 H), 1.49-1.65 (m, 6 H), 2.04-2.05 (m, 2 H), 2.20-2.22 (m, 2 H), 2.30-2.35 (m, 1 H), 2.48-2.54 (m, 1 H), 3.98 (q, 1 H, $J = 6.0$ Hz), 4.02-4.06 (m, 1 H), 5.43 (s, 1 H) ppm. ^{13}C NMR (400 MHz): δ 26.4, 27.2, 27.4, 28.4, 28.6, 29.5, 37.6, 45.5, 63.2, 66.4, 80.9, 126.5, 141.1, 152.7 ppm. HRMS (EI) calculated for $[\text{C}_{16}\text{H}_{27}\text{O}_3\text{N}+\text{Na}]^+$: m/z 304.1883, found 304.1893.

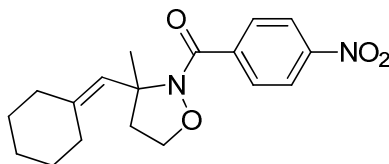


3-(Cyclohexylidenemethyl)-3-methylisoxazolidine (1.27). Following general procedure for hydroamination, **1.22** (13.0 mg, 70.6 μmol), (R)-MeO-BIPHEP(AuOPNB) $_2$ (3.9 mg, 3.53 μmol) and CH_2Cl_2 (0.7 mL) were combined and stirred for 48 h. Conversion (>95%) was determined by crude NMR. The reaction mixture was purified by chromatography, eluting with 1:9 EtOAc:hexanes to afford a clear oil (10.0 mg, 55.2 μmol , 79% yield). ^1H NMR (400 MHz): δ

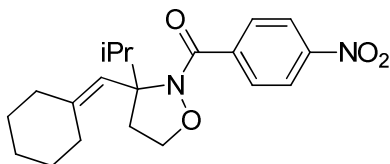
1.32 (s, 9 H), 1.45-1.54 (m, 6 H), 1.99-2.11 (m, 2 H), 2.11-2.23 (m, 2 H), 2.23-2.35 (m, 2 H), 3.83 (q, 1 H, $J = 6.4$ Hz), 4.02 (q, 1 H, $J = 6.4$ Hz), 5.35 (s, 1 H) ppm. ^{13}C NMR (400 MHz): 26.1, 26.4, 27.8, 28.7, 30.6, 37.5, 44.3, 64.1, 70.4, 124.8, 143.8 ppm. HRMS (EI) calculated for $[\text{C}_{11}\text{H}_{19}\text{O}_1\text{N}+\text{H}]^+$: m/z 182.1539, found 182.1545.



3-(Cyclohexylidenemethyl)-3-isopropylisoxazolidine (1.28). Following general procedure for hydroamination, **1.23** (15.0 mg, 71.7 μmol), (*R*)-SegPhos(AuOPNB) $_2$ (4.5 mg, 3.58 μmol) and CH_2Cl_2 (0.5 mL) were combined and stirred at room temperature for 24 h. Conversion (66%) was determined by crude NMR. The crude mixture was purified via chromatography, eluting with 1:24 THF:hexanes to provide a clear oil (10 mg, 47.3 μmol , 66% yield). ^1H NMR (400 MHz): δ 0.94 (d, 6 H, $J = 6.8$ Hz), 1.52-1.55 (m, 6 H), 1.90 (quintet, 1 H, $J = 6.8$ Hz), 1.96-2.04 (m, 1 H), 2.02-2.12 (m, 2 H), 2.29-2.39 (m, 3 H), 3.73 (q, 1 H, $J = 8.0$ Hz), 3.98-4.03 (m, 1 H), 5.23 (s, 1 H) ppm. ^{13}C NMR (400 MHz): δ 18.2, 18.4, 26.4, 27.9, 28.9, 30.8, 36.1, 38.2, 40.0, 70.7, 71.0, 123.4, 143.3 ppm. HRMS (EI) calculated for $[\text{C}_{13}\text{H}_{23}\text{O}_1\text{N}_1-\text{C}_3\text{H}_7]^+$: m/z 166.1232, found 166.1233.



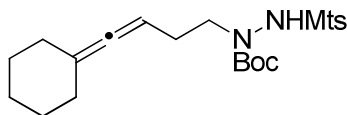
(3-(Cyclohexylidenemethyl)-3-methylisoxazolidin-2-yl) (4-nitrophenyl) methanone (1.29). 3-(Cyclohexylidenemethyl)-3-methylisoxazolidine (**1.27**) (8.0 mg, 44.1 μmol) was dissolved in CH_2Cl_2 (0.5 mL) and pyridine (5.6 μL , 69.0 μmol) and 4-nitrobenzoyl chloride (10.6 mg, 57.4 μmol) were added. The reaction mixture was stirred for 16 h at room temperature and the crude reaction mixture was chromatographed on 1:19 THF:hexanes to afford a pale yellow solid (9.0 mg, 27.3 μmol , 62% yield). ^1H NMR (400 MHz): δ 1.44-1.64 (m, 6 H), 2.12 (s, 3 H), 2.05-2.19 (m, 2 H), 2.16-2.32 (m, 2 H), 2.43-2.49 (m, 1 H), 2.61-2.68 (m, 1 H), 4.04-4.10 (m, 1 H), 4.15-4.20 (m, 1 H), 5.62 (s, 1 H), 7.88 (d, 2 H, $J = 9.2$ Hz), 8.24 (d, 2 H, $J = 9.2$ Hz) ppm. ^{13}C NMR (400 MHz): 26.4, 27.5, 28.6, 29.6, 30.3, 37.5, 45.2, 64.3, 68.4, 123.0, 124.6, 129.6, 141.1, 142.2, 148.7, 160.4. HRMS (EI) calculated for $[\text{C}_{18}\text{H}_{22}\text{O}_4\text{N}_4+\text{H}]^+$: m/z 331.1652, found 331.1658 ppm.



(3-(Cyclohexylidenemethyl)-3-isopropylisoxazolidin-2-yl)(4-nitrophenyl) methanone (1.30). 3-(Cyclohexylidenemethyl)-3-isopropylisoxazolidine (**1.28**) (10.0 mg, 47.7 μmol) was dissolved in CH_2Cl_2 (0.5 mL) and pyridine (5.6 μL , 69.0 μmol) and 4-nitrobenzoyl chloride (10.6 mg, 57.4 μmol) were added. The reaction mixture was stirred for 16 h at room temperature and the crude reaction mixture was chromatographed on 1:19 THF:hexanes to afford a pale yellow solid (15.0

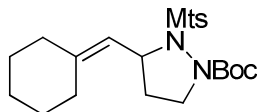
mg, 42.0 mmol, 88% yield). ^1H NMR (400 MHz): δ 0.97 (d, 3 H, J = 6.8 Hz), 1.07 (d, 3 H, J = 6.8 Hz), 1.49-1.63 (m, 6 H), 2.09-2.19 (m, 4 H), 2.40-2.47 (m, 1 H), 2.59-2.65 (m, 1 H), 2.88 (quintet, 1 H, J = 6.8 Hz), 4.04 (q, 1 H, J = 7.6 Hz), 4.17 (dd, 1 H, J = 5.6, 8.0 Hz), 5.66 (s, 1 H), 7.83 (d, 2, J = 8.8 Hz), 8.23 (d, 2 H, J = 8.8 Hz) ppm. ^{13}C NMR (500 MHz): δ 17.6, 18.3, 26.4, 27.4, 28.7, 29.6, 30.4, 33.5, 37.3, 38.3, 68.5, 70.7, 123.0, 125.5, 129.3, 141.5, 142.3, 148.5, 160.2 ppm. HRMS (EI) calculated for $[\text{C}_{20}\text{H}_{26}\text{O}_4\text{N}_2+\text{H}]^+$: m/z 358.1893, found 358.1899.

Hydroamination with hydrazine substrates:



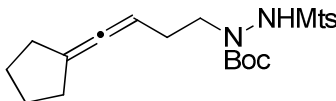
tert-butyl 1-(4-cyclohexylidenebut-3-enyl)-2-(mesitylsulfonyl)hydrazinecarboxylate (1.31).

The crude mixture was purified by flash column chromatography (2-8% EtOAc/hexanes) to afford **1.31** as a clear oil: ^1H NMR (600 MHz): δ 6.93 (s, 2H), 4.94-4.90 (m, 1H), 3.65-3.54 (br s, 2H), 2.63 (s, 3H), 2.35-2.19 (m, 10H), 1.68-1.57 (m, 5H), 1.19 (s, 9H) ppm. ^{13}C NMR (150 MHz): δ 198.1, 142.9, 140.9, 131.7, 104.0, 87.7, 81.9, 31.1, 27.7, 27.0, 23.4, 20.9 ppm. HRMS (ESI) calc'd for $[\text{C}_{24}\text{H}_{36}\text{O}_4\text{N}_2\text{NaS}]^+$: m/z 471.2288, found 471.2287.



tert-butyl 3-(cyclohexylidenemethyl)-2-(mesitylsulfonyl)pyrazolidine-1-carboxylate (1.32).

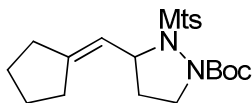
Following general procedure A, allene **1.31** (50 mg, 111 μmol), (*R*)-DTBM-Segphos(AuOPNB)₂ (10.6 mg, 5.6 μmol), and MeNO_2 (0.375 mL) was added and the mixture was stirred at 50 $^\circ\text{C}$ for 15 h. The crude mixture was purified by flash column chromatography (0-9% EtOAc/Hexanes) to afford **1.32** as a clear oil (38 mg, 76% yield, 97% ee). ^1H NMR (400 MHz): δ 6.96 (s, 2H), 5.23 (td, J = 8.2, 3.0 Hz, 1H), 4.87 (d, J = 8.7 Hz, 1H), 4.12-4.06 (m, 1H), 3.64 (ddd, J = 10.8, 9.5, 5.7 Hz, 1H), 2.67 (s, 6H), 2.61-2.52 (m, 1H), 2.46-2.41 (m, 1H), 2.33 (s, 3H), 2.27-2.21 (m, 1H), 2.08 (d, J = 2.0 Hz, 2H), 1.88 (dddd, J = 12.0, 8.9, 5.8, 3.0 Hz, 1H), 1.62-1.52 (m, 6H), 1.13 (s, 9H); ^{13}C NMR (101 MHz): δ 156.9, 144.0, 143.0, 142.1, 131.4, 131.0, 120.1, 81.09, 81.09, 77.27, 77.27, 55.93, 55.93, 47.62, 47.62, 37.0, 33.7, 29.3, 28.5, 27.6, 26.6, 23.1, 21.0. HRMS (ESI) calc'd for $[\text{C}_{24}\text{H}_{36}\text{O}_4\text{N}_2\text{NaS}]^+$: m/z 471.2288, found 471.2282. HPLC Regis technologies Whelk-O 1 column (98:2 hexanes:Ethanol; 1 mL/min) t_R 19.8 min (major), 25.8 min (minor): 97% ee.



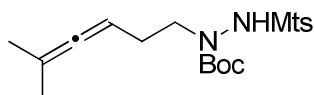
tert-butyl 1-(4-cyclopentylidenebut-3-enyl)-2-(mesitylsulfonyl)hydrazinecarboxylate (1.33).

The crude mixture was purified by flash column chromatography (2-8% EtOAc/hexanes) to afford **8** as a clear oil: ^1H NMR (600 MHz): δ 6.92 (s, 2H), 4.81 (t, J = 6.9 Hz, 1H), 3.61-3.57 (br s, 2H), 2.26 (s, 3H), 2.22 (q, J = 6.9 Hz, 2H), 2.06 (m, 4H), 1.58-1.47 (m, 6H), 1.20 (s, 9H) ppm. ^{13}C NMR (150 MHz): δ 199.2, 142.9, 140.9, 131.7, 102.8, 85.0, 82.0, 31.4, 27.66, 27.61,

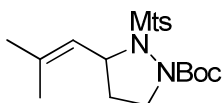
27.4, 26.1, 23.4, 20.9 ppm. HRMS (ESI) calc'd for $[C_{23}H_{34}O_4N_2NaS]^+$: m/z 457.2131, found 457.2126.



tert-butyl 3-(cyclopentylidenemethyl)-2-(mesitylsulfonyl)pyrazolidine-1-carboxylate (1.34). Following general procedure A, allene **1.33** (50 mg, 115 μ mol), (*R*)-DTBM-Segphos(AuOPNB)₂ (10.6 mg, 5.6 μ mol), and MeNO₂ (0.380 mL) was added and the mixture was stirred at 50 °C for 15 h. The crude mixture was purified by flash column chromatography (0-7% EtOAc/Hexanes) to afford **9** as a clear oil (30 mg, 60% yield, 90% ee). ¹H NMR (400 MHz) δ 6.96 (s, 2H), 5.10-5.05 (m, 2H), 4.11-4.05 (m, 1H), 3.62 (ddd, J = 10.8, 9.2, 6.3 Hz, 1H), 2.66 (s, 6H), 2.58-2.51 (m, 2H), 2.33 (s, 3H), 2.28-2.24 (t, 2H, J = 7.6 Hz), 1.91-1.85 (m, 1H), 1.78-1.71 (m, 2H), 1.66 (quintet, J = 6.7 Hz, 3H), 1.13 (s, 9H) ppm. ¹³C NMR (101 MHz): δ 156.8, 147.6, 142.9, 142.1, 131.4, 131.0, 119.0, 81.1, 76.7, 58.3, 47.7, 33.8, 33.3, 29.0, 27.6, 26.38, 26.19, 23.0, 21.0 ppm. HRMS (ESI) calc'd for $[C_{23}H_{34}O_4N_2NaS]^+$: m/z 457.2131, found 457.2132. HPLC Regis Technologies Whelk-O 1 column (98:2 hexanes:isopropanol; 1 mL/min) t_R 18.8 min (major), 24.9 min (minor): 90% ee.



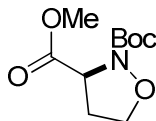
tert-butyl 2-(mesitylsulfonyl)-1-(5-methylhexa-3,4-dienyl)hydrazinecarboxylate (1.35). The crude mixture was purified by flash column chromatography (0-10% EtOAc/hexanes) to afford **6** as a clear oil. ¹H NMR shows a mixture of rotational isomers ¹H NMR (600 MHz): δ 6.93 (s, 2H), 5.04 (m, 0.3H), 4.80 (m, 0.7H), 3.64-3.49 (br s, 2H), 2.63 (s, 6H), 2.27 (s, 3H), 2.21 (q, J = 6.9 Hz, 1.5H), 1.89 (q, J = 7.2 Hz, 0.5H), 1.67 (s, 6H), 1.17 (s, 9H) ppm. ¹³C NMR (150 MHz): δ 202.6, 142.9, 140.9, 131.7, 123.4, 95.4, 85.1, 82.0, 27.67, 27.66, 25.6, 25.0, 23.4, 20.9, 20.5, 17.7 ppm. HRMS (ESI) calc'd for $[C_{21}H_{32}O_4N_2NaS]^+$: m/z 431.1975, found 431.1976.



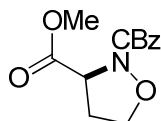
tert-butyl 2-(mesitylsulfonyl)-3-(2-methylprop-1-enyl)pyrazolidine-1-carboxylate (1.36). Following general procedure A, allene **1.35** (15 mg, 34 μ mol), (*R*)-DTBM-Segphos(AuOPNB)₂ (3.2 mg, 1.7 μ mol), and MeNO₂ (0.300 mL) was added and the mixture was stirred at 50 °C for 15 h. The crude mixture was purified by flash column chromatography (0-6% EtOAc/Hexanes) to afford **7** as a clear oil (10 mg, 66% yield, 98% ee): ¹H NMR (600 MHz): δ 6.92 (s, 2H), 5.13 (td, J = 8.2, 3.1 Hz, 1H), 4.91 (d, J = 8.6 Hz, 1H), 4.03 (ddd, J = 10.6, 8.9, 5.8 Hz, 1H), 3.59 (ddd, J = 10.6, 9.6, 5.8 Hz, 1H), 2.62 (s, 6H), 2.55-2.49 (m, 1H), 2.29 (s, 3H), 1.83 (td, J = 6.0, 3.0 Hz, 1H), 1.78 (s, 3H), 1.70 (s, 3H), 1.09 (s, 9H) ppm. ¹³C NMR (100 MHz): δ 156.8, 142.9, 142.1, 135.9, 131.4, 130.9, 123.5, 81.0, 56.8, 47.6, 33.5, 27.5, 25.6, 22.9, 20.9, 18.3 ppm. HRMS (ESI) calc'd for $[C_{21}H_{32}O_4N_2NaS]^+$: m/z 431.1975, found 431.1978. HPLC Regis Technologies

Whelk-O 1 column (99:1 Hex:isopropanol; 1 mL/min) t_R 20.2min (major), 26.8 min (minor): 98% ee.

Determination of absolute stereochemistry:



2-*tert*-butyl 3-methyl isoxazolidine-2,3-dicarboxylate. To a solution of isoxazolidine **1.5** (100 mg, 0.238 mmol) in CH₂Cl₂ (2.4 mL) was added a solution of NaOH in MeOH (1.2 mL, 3.06 mmol, 2.5 M). The resulting mixture was cooled to -78 °C and O₃ was bubbled through continuously. After approximately 10 min the initially pale yellow solution took on the characteristic blue color of ozone and a yellow precipitate was observed. The reaction mixture was diluted with H₂O (4 mL) and Et₂O (4 mL) and warmed to rt. The aqueous layer was extracted with Et₂O (4 x 20 mL), the combined organic extracts were washed with brine (10 mL), dried over MgSO₄, filtered, and concentrated. The crude mixture was purified by flash column chromatography (20-30% EtOAc/hexanes) to afford the desired product as a clear oil (70 mg, 0.3 mmol, 68% yield, 93% ee). ¹H NMR (600 MHz): δ 4.71 (dd, *J* = 9.4, 4.8 Hz, 1H), 4.13 (td, *J* = 7.9, 4.4 Hz, 1H), 3.80 (q, *J* = 7.9 Hz, 1H), 3.77 (s, 3H), 2.60 (dddd, *J* = 12.3, 9.3, 7.6, 4.5 Hz, 1H), 2.47 (dtd, *J* = 12.5, 7.9, 4.7 Hz, 1H), 1.47 (s, 9H) ppm. ¹³C NMR (150 MHz): δ 171.2, 156.0, 82.7, 68.4, 59.5, 52.6, 32.8, 28.1 ppm. HRMS (FAB) calc'd for [C₁₀H₁₇O₅N]⁺: *m/z* 231.1107, found 231.1109. HPLC Chiralpak AS column (90:10 hexanes:isopropanol, 1 mL/min) t_R 8.1 min (minor), 9.4 min (major): 93% ee.



(*S*)-methyl-2-benzoyloxycarbonyl-3-isoxazolidinecarboxylate. Trifluoroacetic acid (0.25 mL) was added to a solution of 2-*tert*-butyl 3-methyl isoxazolidine-2,3-dicarboxylate (25 mg, 0.11 mmol) in CH₂Cl₂ cooled to 0 °C. The resulting mixture was stirred at 0 °C for 40 min before concentrating to a yellow oil. The oily residue was dissolved in THF (0.2 mL), then, water (0.2 mL), and sodium carbonate (30 mg, 0.275 mmol 2.5 equiv) were added. The solution was cooled to 0 °C and benzyl chloroformate (20 uL, 0.13 mmol, 1.2 equiv) was added. The solution was stirred at 0 °C for 30 min, poured onto sat. aq. NaHCO₃ (10 mL), extracted with EtOAc (3 x 10 mL), dried (MgSO₄) and concentrated to yield an oily residue. The crude mixture was purified by flash column chromatography (25-40% EtOAc/hexanes) to afford the desired product as a clear oil (24 mg, 0.09 mmol, 82% yield): ¹H NMR (600 MHz): δ 7.38-7.30 (m, 5H), 5.21 (m, 2H), 4.78 (dd, *J* = 9.4, 4.9 Hz, 1H), 4.16 (td, *J* = 7.9, 4.3 Hz, 1H), 3.82 (q, *J* = 7.8 Hz, 1H), 2.65-2.60 (m, 1H), 2.50 (dtd, *J* = 12.4, 8.1, 4.6 Hz, 1H) ppm. ¹³C NMR (150 MHz): δ 170.8, 156.8, 135.5, 128.54, 128.39, 128.26, 68.9, 68.4, 59.5, 52.7, 32.9 ppm. [α]_D = -91.1 (c = 1.0, CHCl₃) (lit. -97.8 (c = 1.5, CHCl₃). Spectral data are consistent with previously published literature values,^x and the stereochemistry of other isoxazolidine products are assigned by analogy.

References

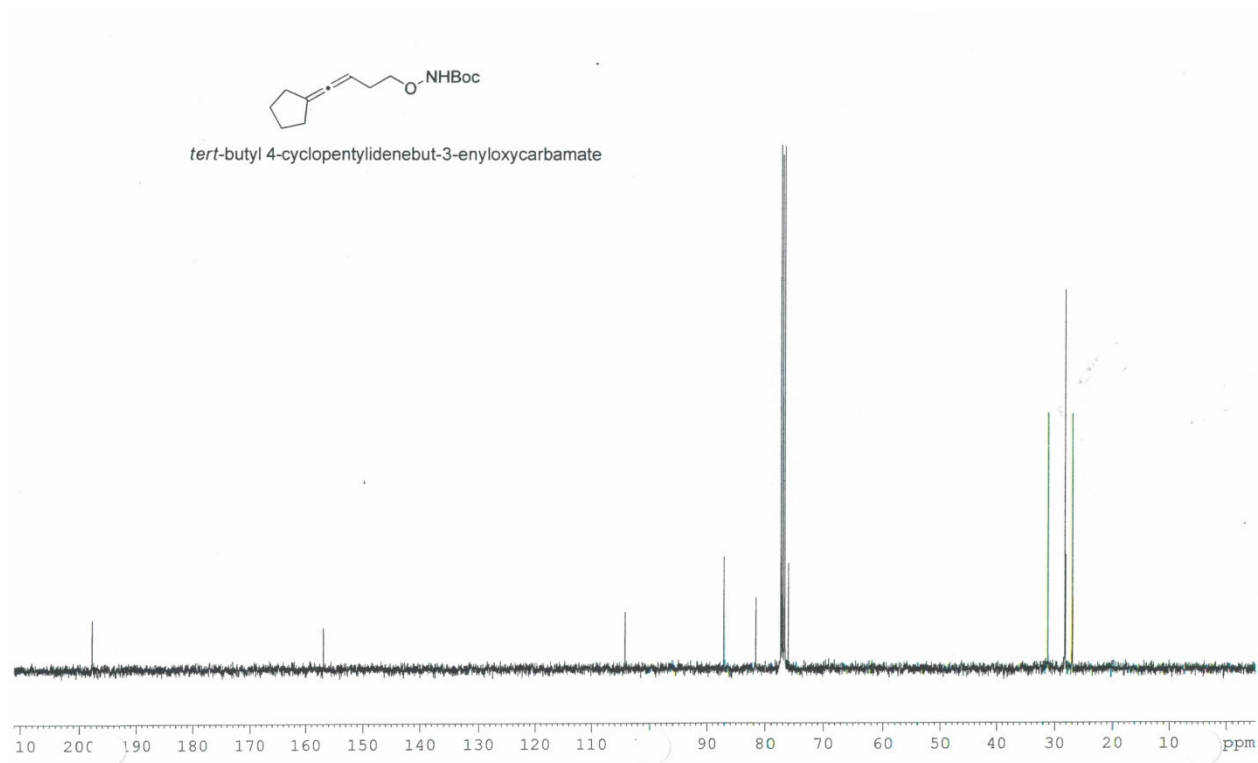
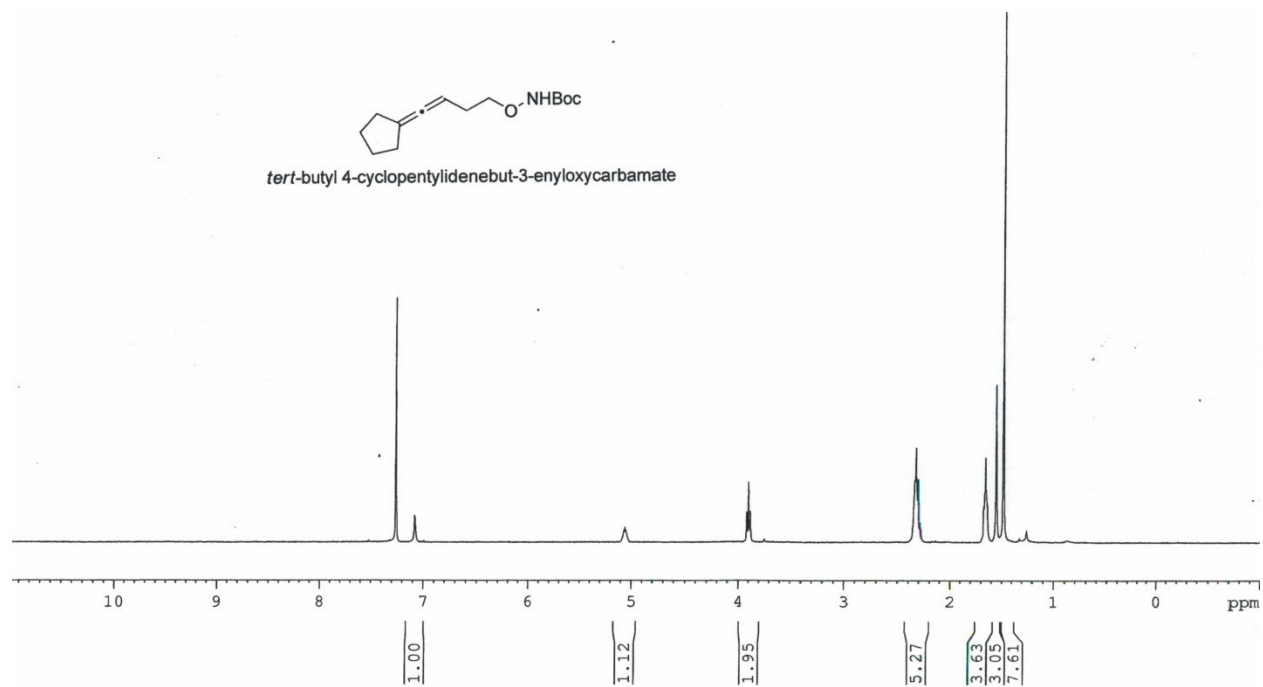
- (1) (a) Muller, T. E.; Beller, M. *J. Chem. Soc.* **1998**, 4, 583. (b) Müller, T. E.; Beller, M. *Chem. Rev.* **1998**, 2, 675.
- (2) Muller, T. E.; Hultzs, K. C.; Yus, M.; Foubelo, F.; Tada, M. *Chem. Rev.* **2008**, 108, 3795.
- (3) Coulson, D. R. *Tetrahedron Lett.* **1971**, 12, 429.
- (4) Hultzs, K. C., *Adv. Synth. Catal.*, **2005**, 347, 367.
- (5) Watson, D. A.; Chiu, M.; Bergman, R.G. *Organometallics* **2006**, 25, 4731.
- (6) Bexrud, J. A.; Beard, J. D.; Leitch, D. C.; Schafer, L. L. *Angew. Chem. Int. Ed.* **2007**, 46, 354.
- (7) Gott, A. L.; Clarke, A. J.; Clarkson, G. J.; Scott, P. *Chem. Commun.* **2008**, 1422.
- (8) Manna, K.; Xu, S.; Sadow, A. D. *Angew. Chem. Int. Ed.* **2011**, 50, 1865.
- (9) Hartwig, J. F. *Pure Appl. Chem.* **2004**, 3, 507.
- (10) Hesp, K. D.; Stradiotto, M. *Chem. Cat. Chem.* **2010**, 2, 1192.
- (11) Zhang, J.; Guang, C.; He, C. *J. Am. Chem. Soc.*, **2006**, 128, 1798.
- (12) Dorta, R.; Egli, P.; Zurcher, F.; Togni, A. *J. Am. Chem. Soc.* **1997**, 119, 10857.
- (13) Zhou, J.; Hartwig, J. F. *J. Am. Chem. Soc.* **2008**, 130, 12220.
- (14) Shen, X.; Buchwald, S. L. *Angew. Chem. Int. Ed.* **2010**, 49, 564.
- (15) Lober, O.; Kawatsura, M.; Hartwig, J. F. *J. Am. Chem. Soc.* **2001**, 123, 4366.
- (16) (a) Kawatsura, M.; Hartwig, J. F. *J. Am. Chem. Soc.* **2000**, 122, 9546. (b) Utsunomiya, M.; Hartwig, J. F. *J. Am. Chem. Soc.* **2003**, 125, 14286.
- (17) Lutete, L. M.; Kadota, I.; Yamamoto, Y. *J. Am. Chem. Soc.* **2004**, 126, 1622.
- (18) (a) Gorin, D. J.; Sherry, B. D.; Toste, F. D. *Chem. Rev.* **2008**, 108, 3351. (b) Hashmi, A. S. K.; Gutchings, G. J. *Angew. Chem. Int. Ed.* **2006**, 45, 7896. (c) Widenhoefer, R., A. *Chem. Eur. Journal*, **2008**, 14, 5382.
- (19) Kennedy-Smith, J. J.; Staben, S. T.; Toste, F. D. *J. Am. Chem. Soc.* **2004**, 126, 4526.
- (20) (a) Mauleon, P.; Zeldin, R. M.; Gonzalez, A.Z.; Toste, F. D. *J. Am. Chem. Soc.* **2009**, 131, 6348. (b) Luzung, M. R.; Mauleon, P.; Toste, F. D. *J. Am. Chem. Soc.* **2007**, 129, 12402.
- (21) (a) LaLonde, R. L.; Sherry, B. D.; Kang, E. J.; Toste, F. D. *J. Am. Chem. Soc.* **2007**, 129, 2452. (b) Zhang, Z.; Bender, C. F.; Widenhoefer, R. A. *J. Am. Chem. Soc.* **2007**, 129, 4148.
- (22) Hamilton, G. L.; Kang, E. J.; Mba, M.; Toste, F. D. *Science* **2007**, 317, 496.
- (23) Liu, C.; Widenhoefer, R. A. *Org. Lett.*, **2007**, 9, 1935.
- (24) Gorin, D.J.; Toste, F. D. *Nature* **2007**, 446, 395.

- (25) Grandberg, K. I.; Dyadchenko, V. P. *J. Organomet. Chem.*, **1994**, 474, 1.
- (26) Sengupta, S.; Shi, X. *Chem. Cat. Chem.*, **2010**, 2, 609.
- (27) Jen, W. S.; Wiener, J. J. M.; MacMillan, D. W. C. *J. Am. Chem. Soc.*, **2001**, 122, 9874.
- (28) Gothelkf, K.; Jorgensen, K. *Org. Lett.*, **1994**, 59, 5687.
- (29) Sadashiva, M. P.; Mallesha, H.; Karunakara Murthy, K.; and Rangappa, K. S. *Bioorg. Med. Chem.* **2005**, 7, 1811.
- (30) Buhrlage, S.J; Brennan, B. B.; Minter, A. R; Mapp, A. K. *J. Am. Chem. Soc.* **2005**, 36, 12456.
- (31) Winter, C.; Krause, N. *Angew. Chem. Int. Ed.* **2009**, 48, 6339.
- (32) Lalonde, R. K.; Toste, F. D. unpublished work.
- (33) Rubottom, G. M.; Mott, R. C.; Henrik D. Juve, J., *J. Org. Chem.* **1981**, 46, 2717.
- (34) Sherry, B. D.; Toste, F. D. *J. Am. Chem. Soc.* **2004**, 126, 15978.
- (35) Wang, Z. J.; Benitez, D.; Tkatchouk, E.; Goddard, W. A.; Toste, F. D. *J. Am. Chem. Soc.* **2010**, 132, 13064
- (36) Brown, T. M.; Sugie, A.; Leed, M. G. D.; Widenhoefer, R. A. *Chem. Euro. J.* **2012**, ASAP. DOI: 10.1002/chem.201103289.
- (37) Zhurnal, O. K. U.S. Patent 75722, **1967**.

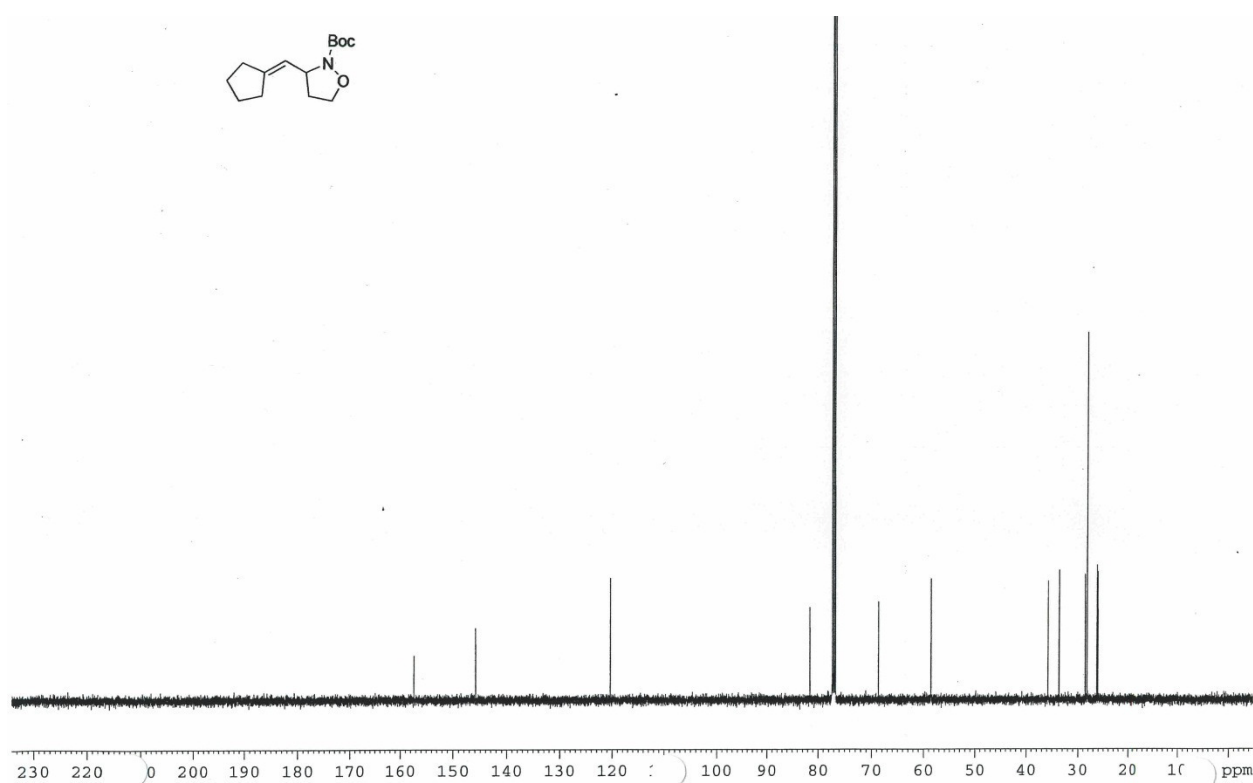
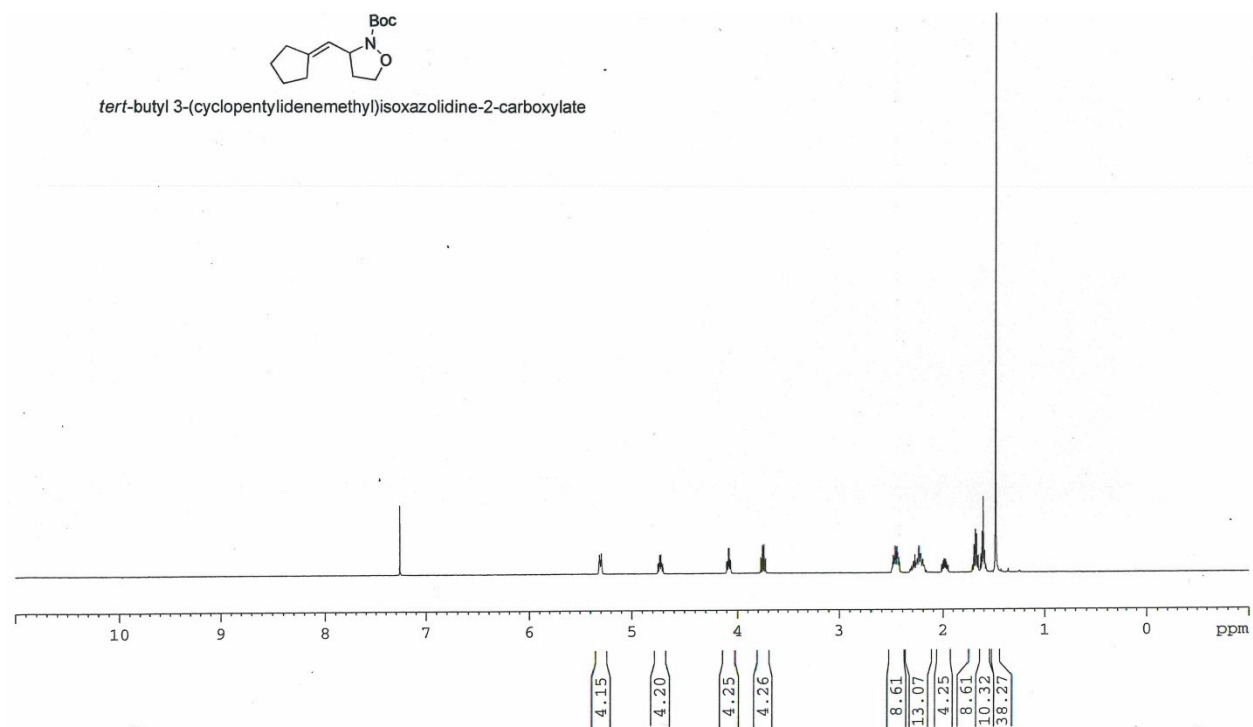
Appendix 1A

NMR Spectra

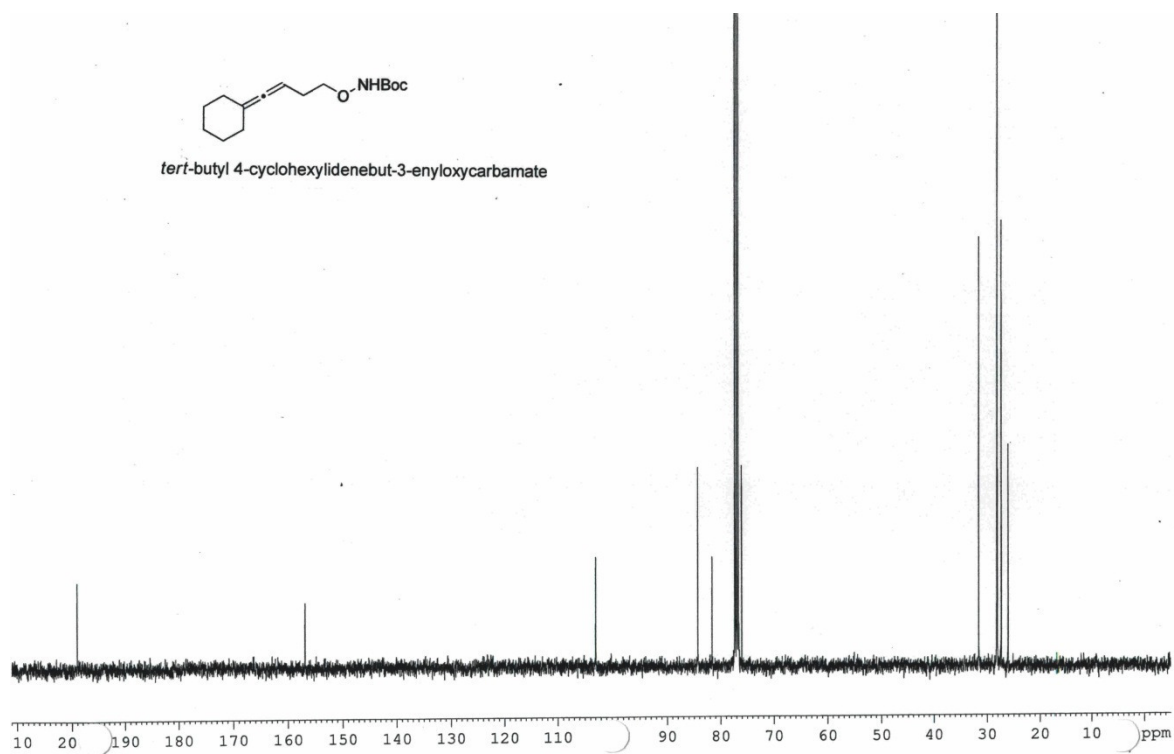
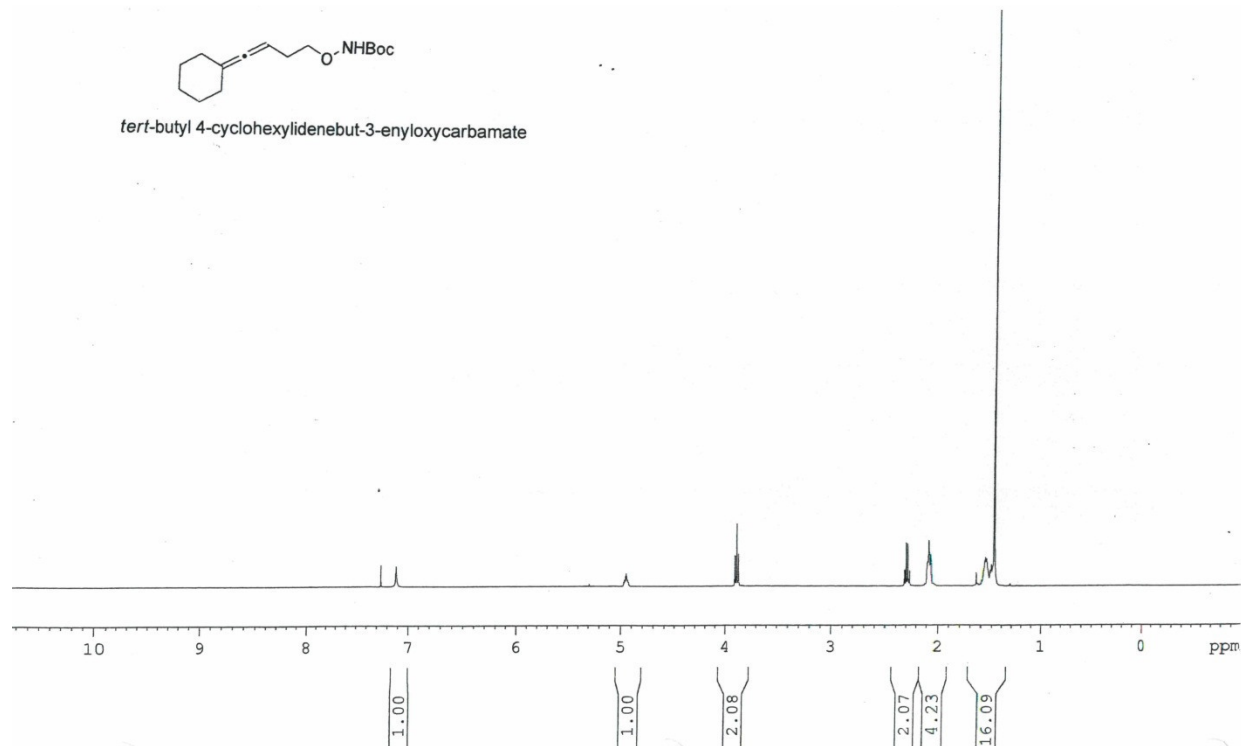
Allene 1.1



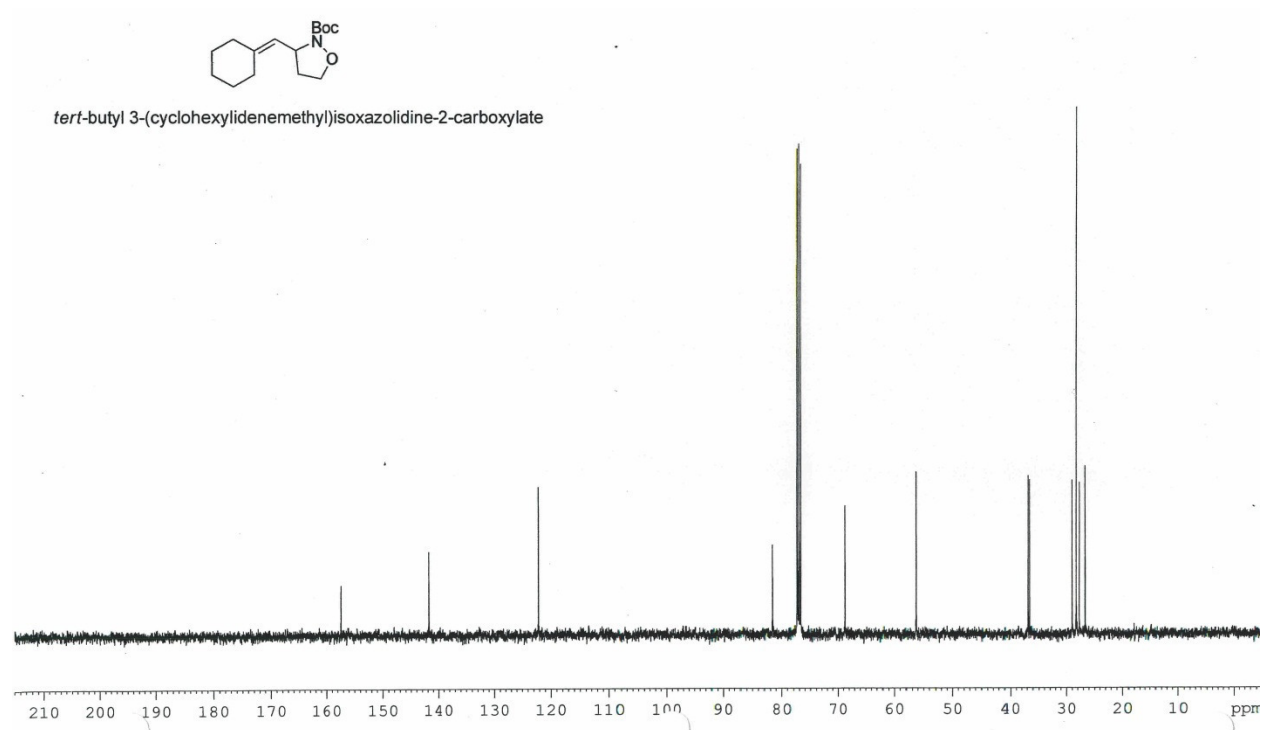
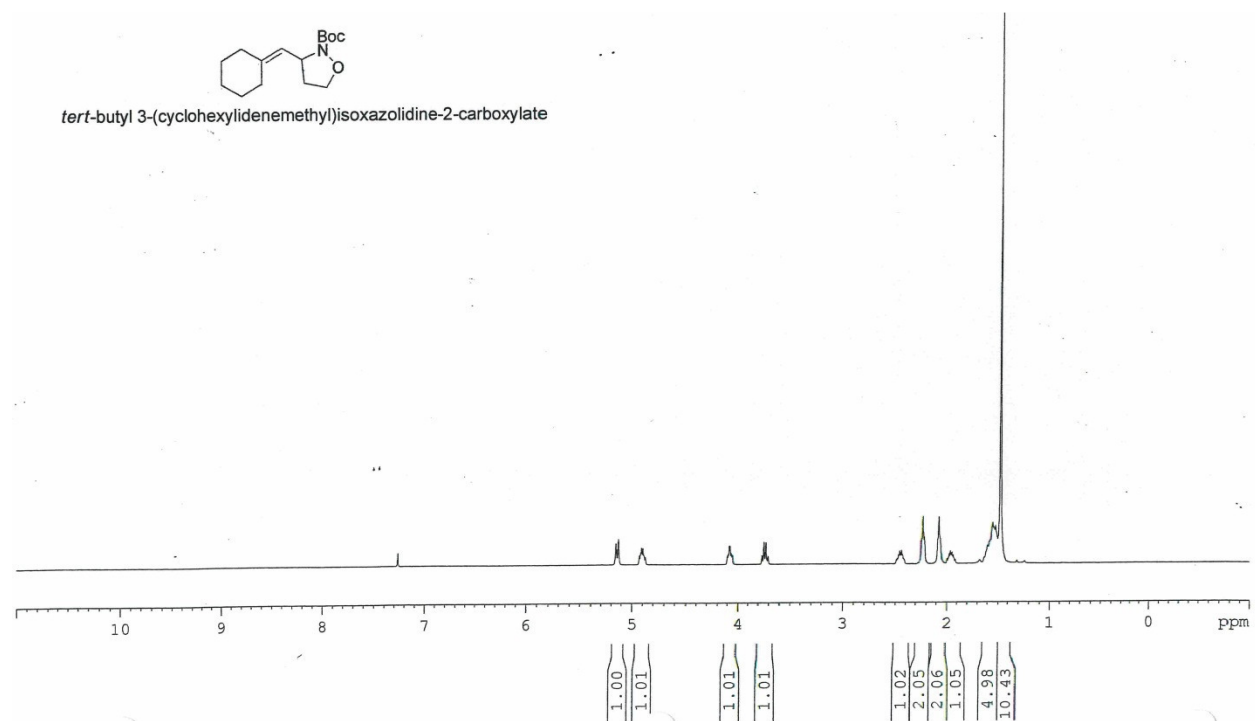
Product **1.2**



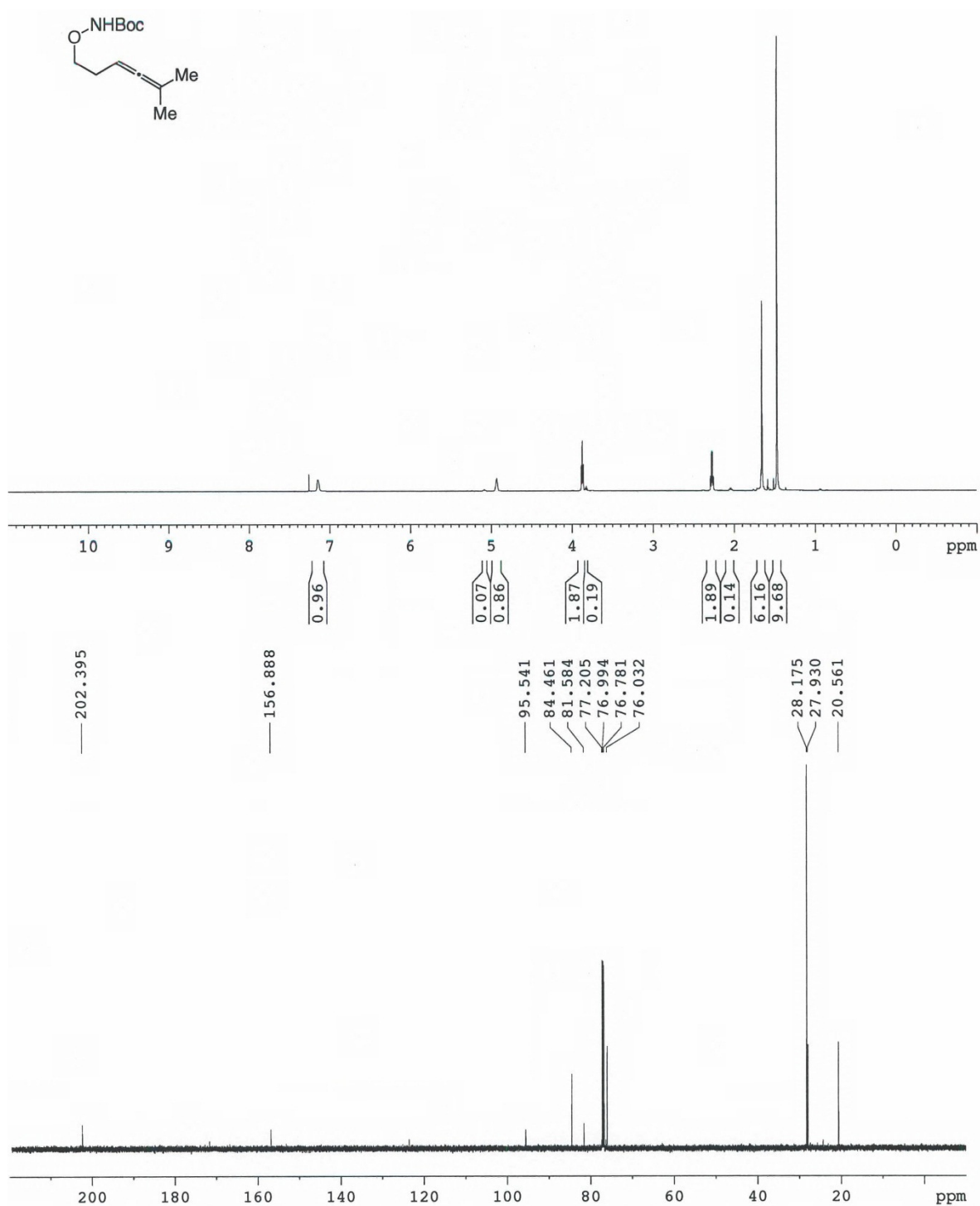
Allene 1.3



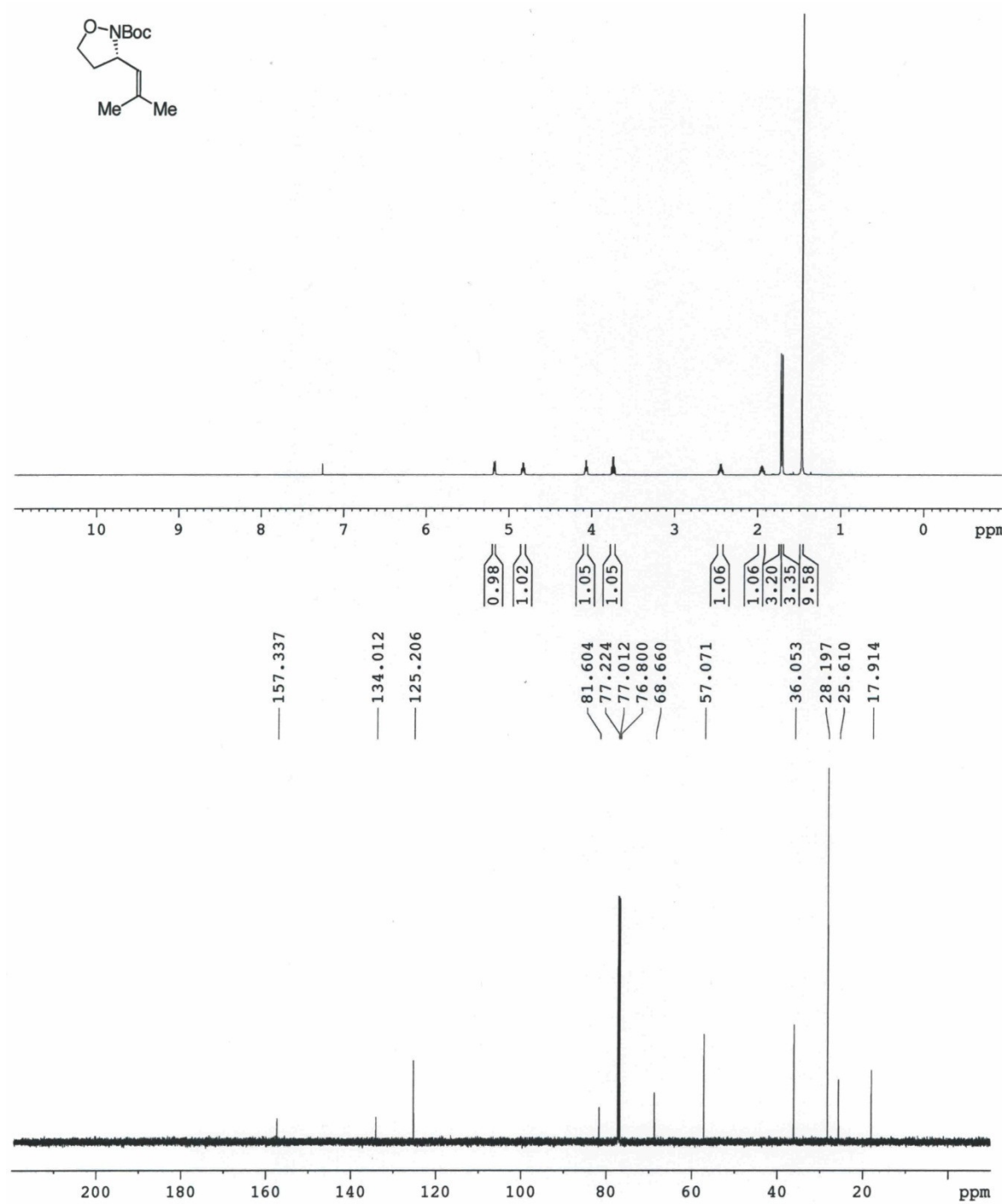
Product 1.4



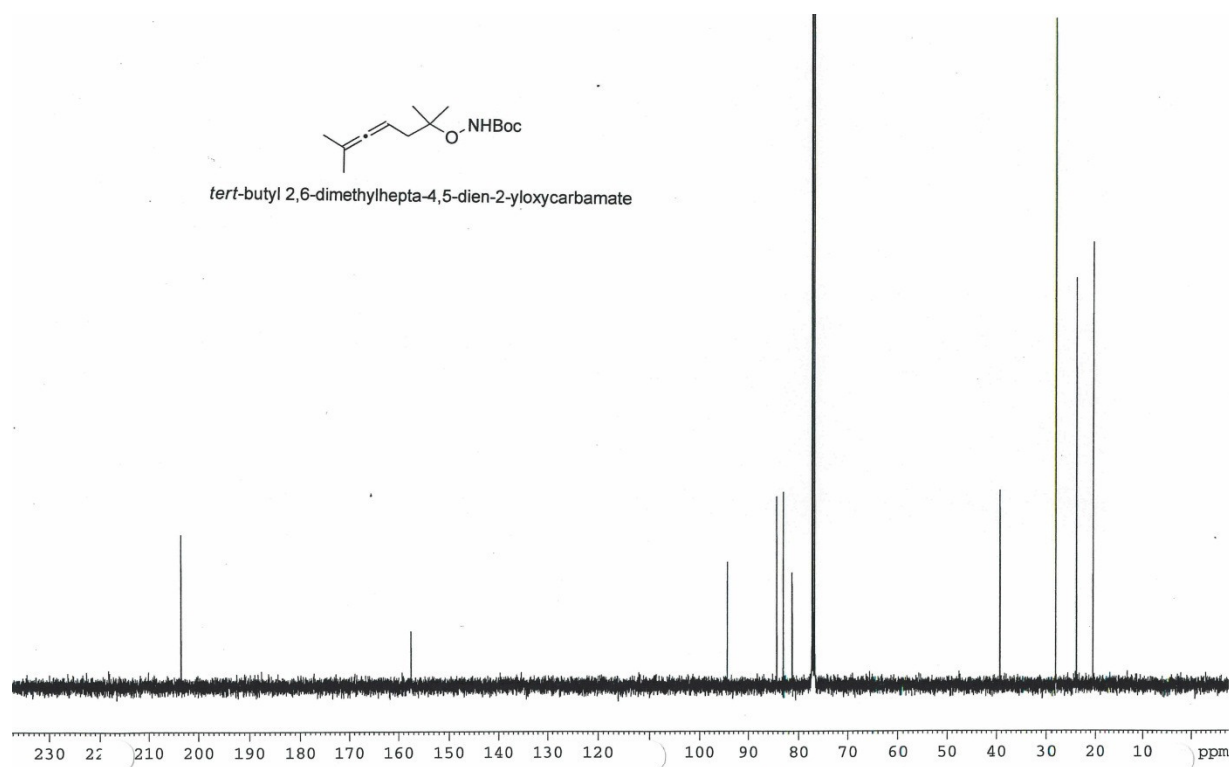
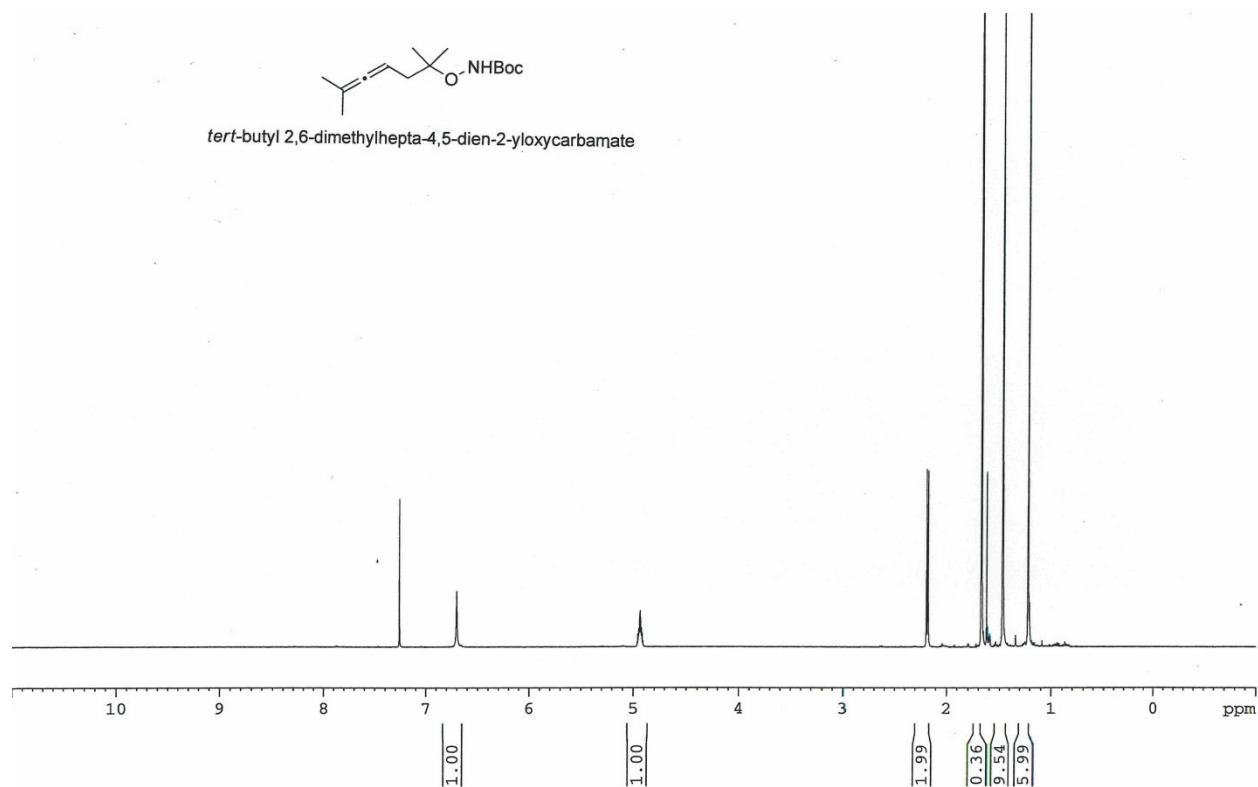
Allene **1.5**



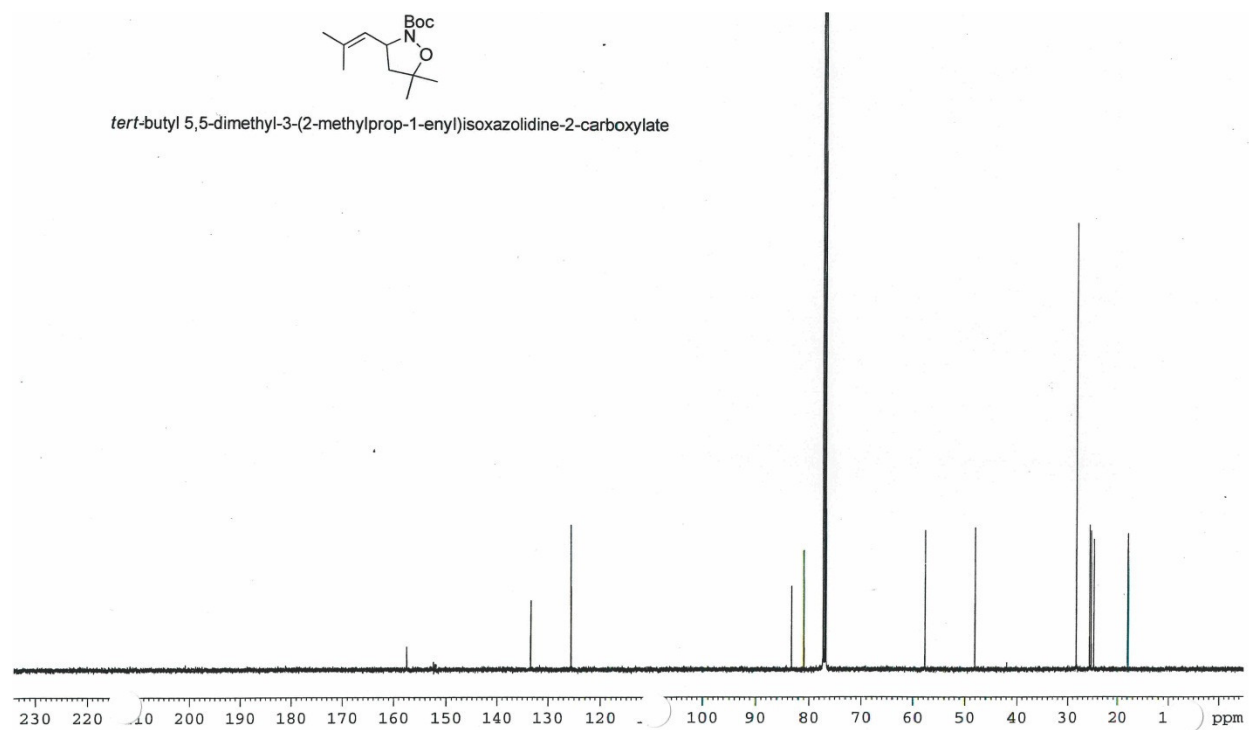
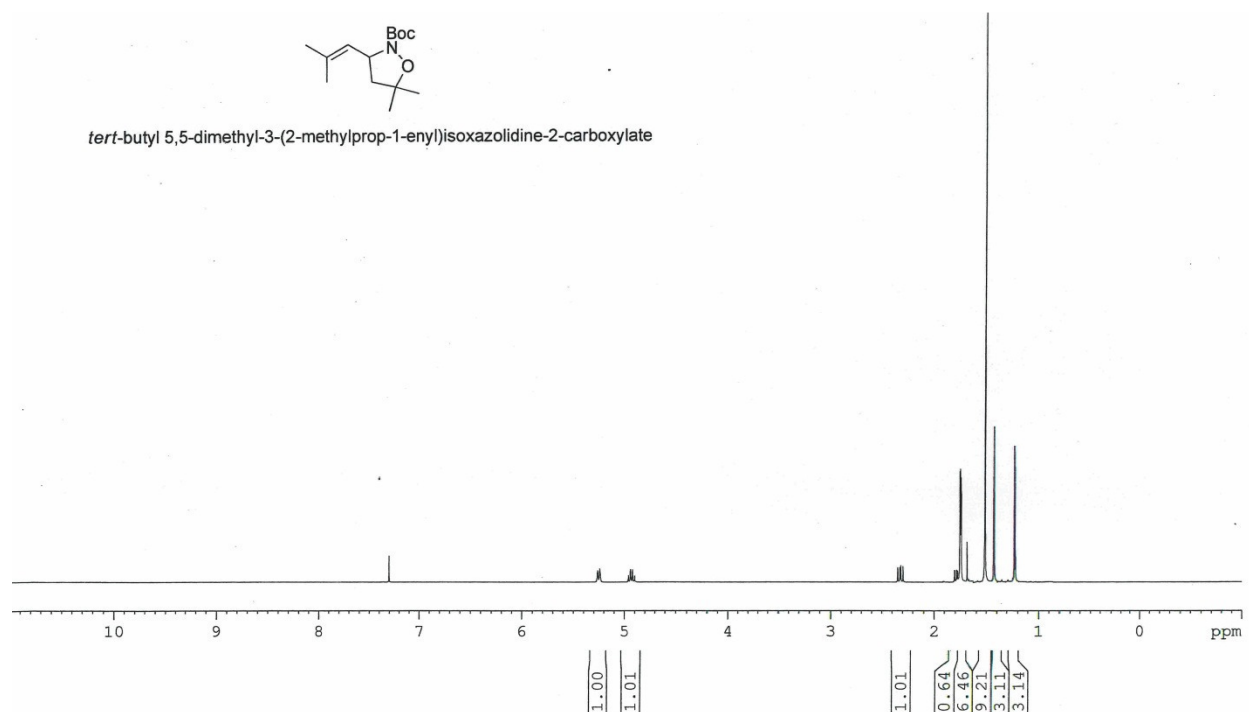
Product **1.6**



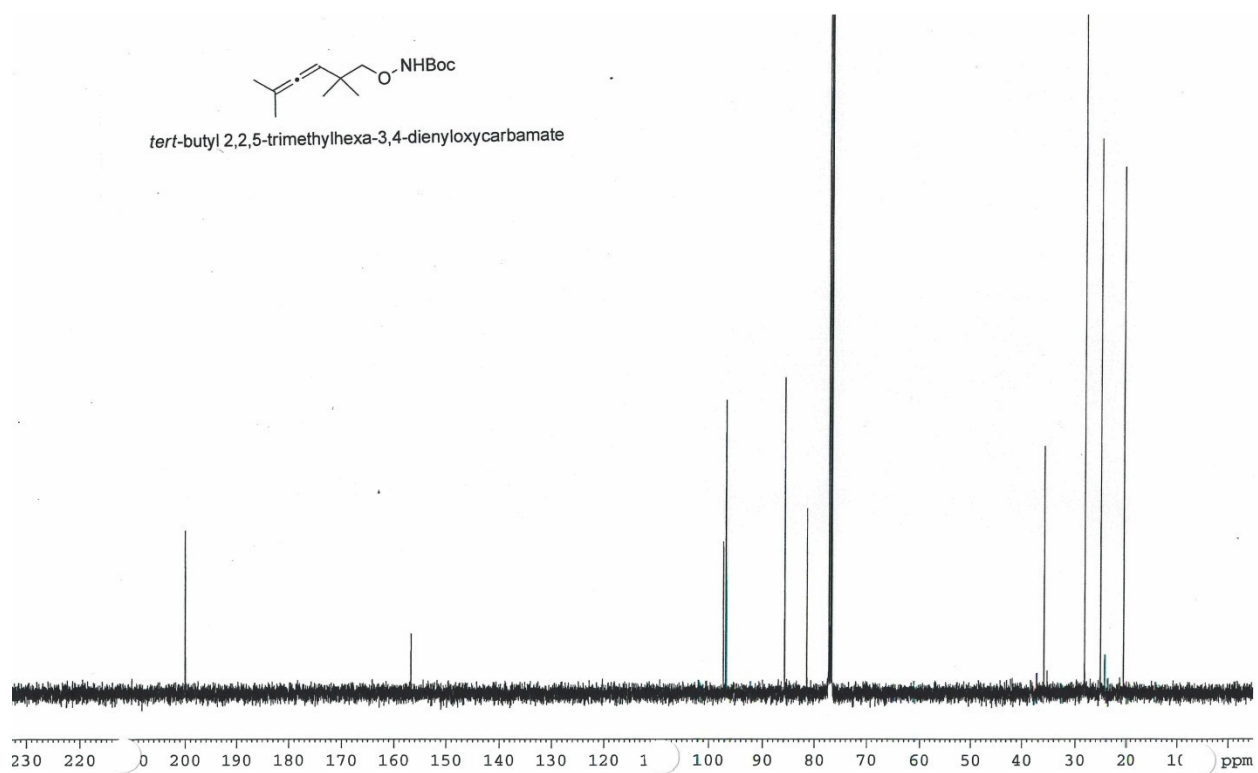
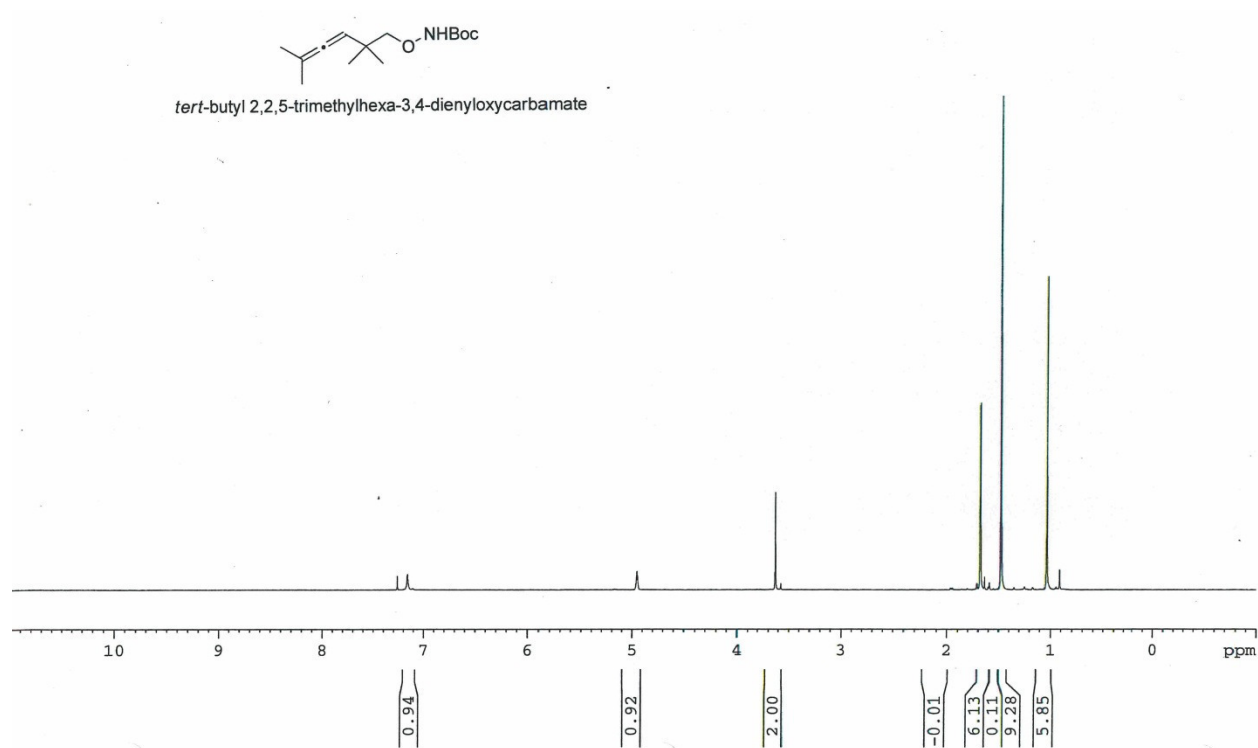
Allene 1.7



Product **1.8**



Allene **1.9**



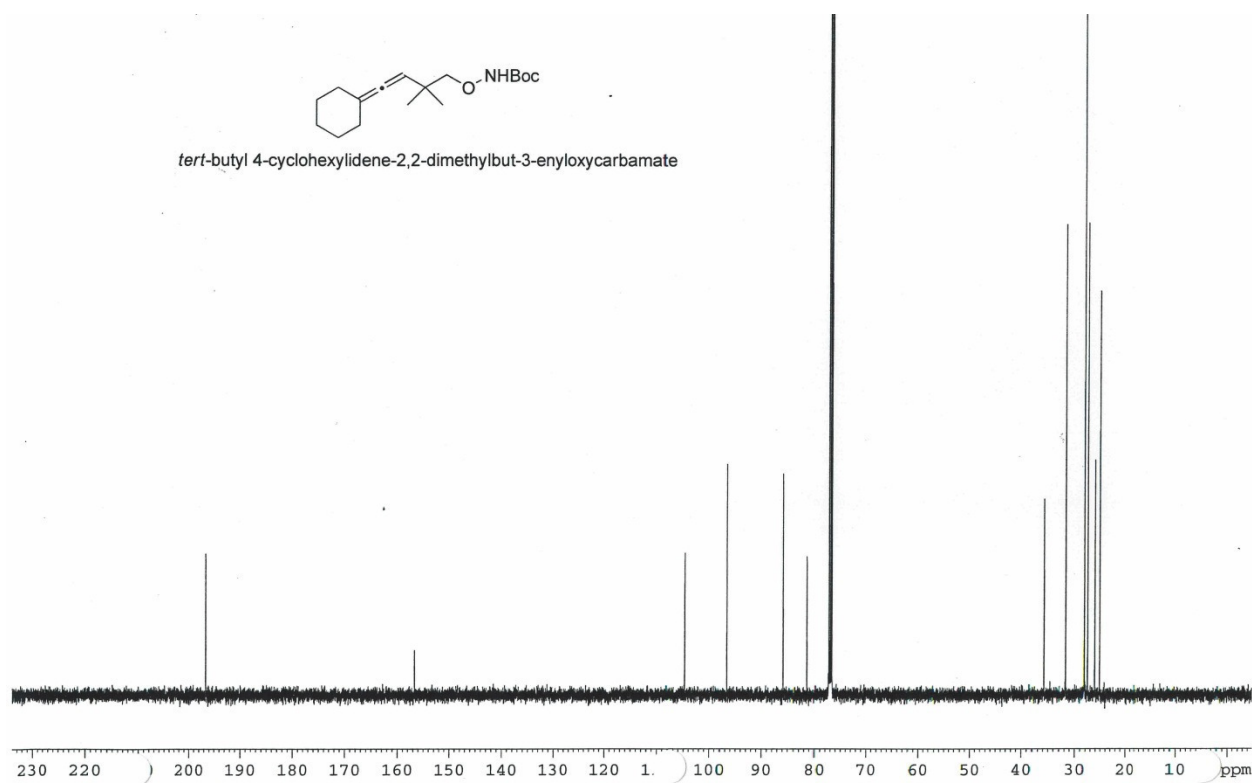
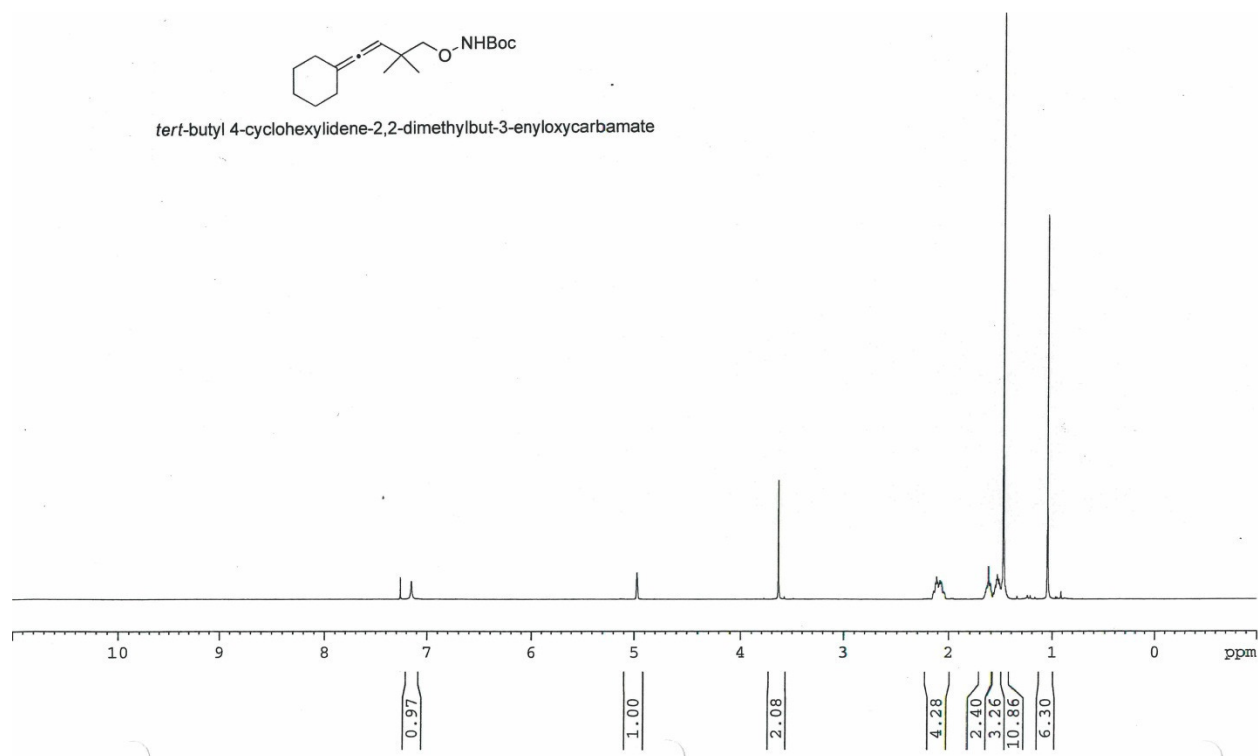
CC(C)=CC1(C)COC(=N1)C(C)(C)C(C)(C)C(C)(C)C(C)C(=O)O

tert-butyl 4,4-dimethyl-3-(2-methylprop-1-enyl)isoxazolidine-2-carboxylate

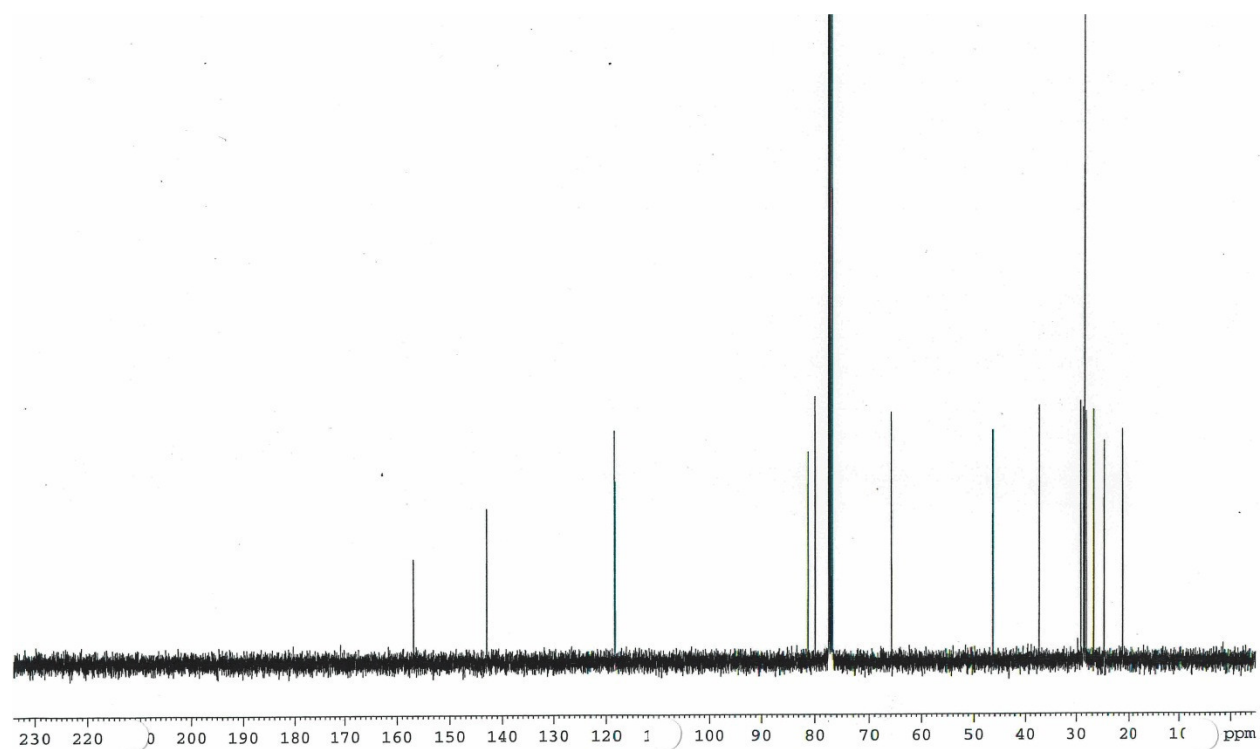
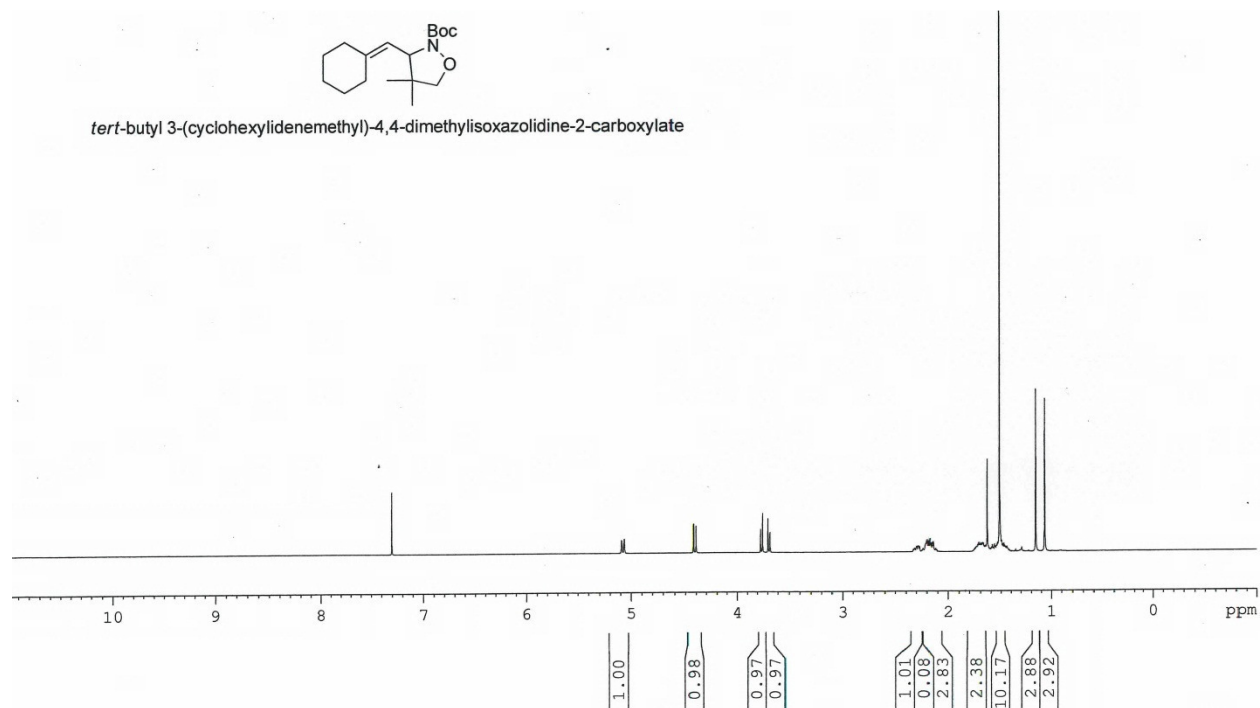
1.00 0.99 2.06 3.04 3.34 3.31 3.17 3.17



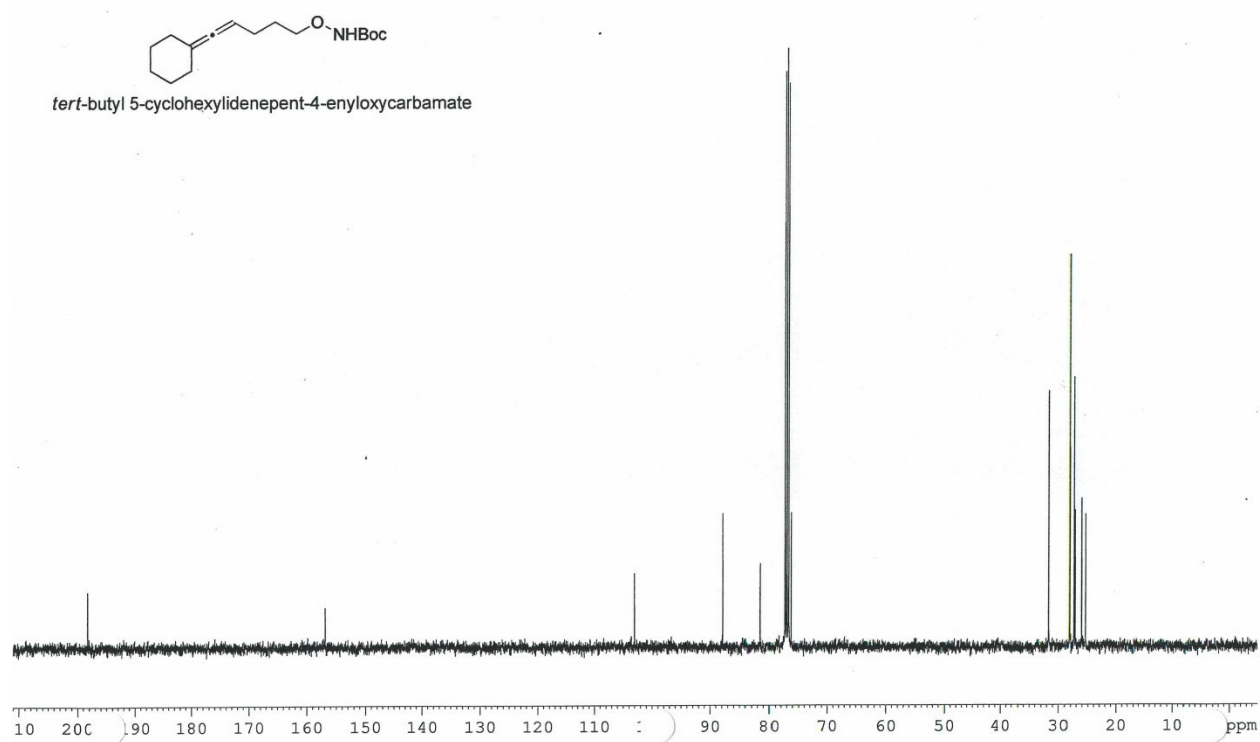
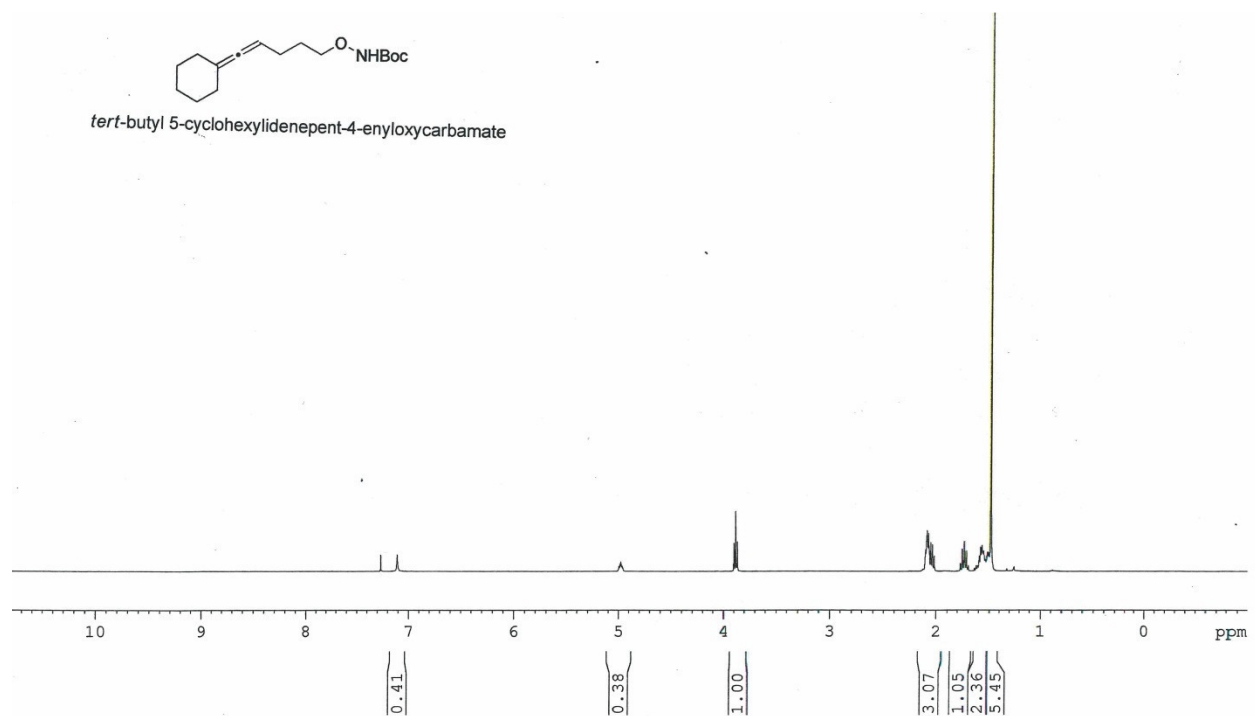
Allene **1.11**



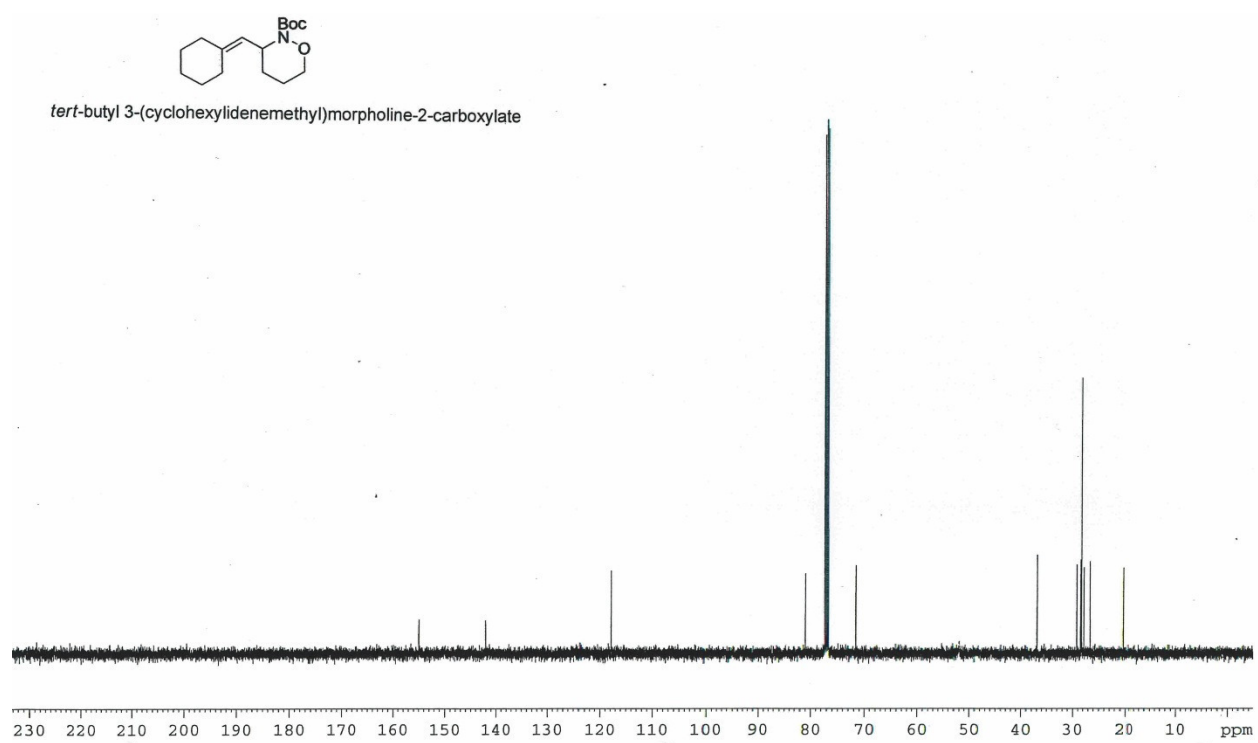
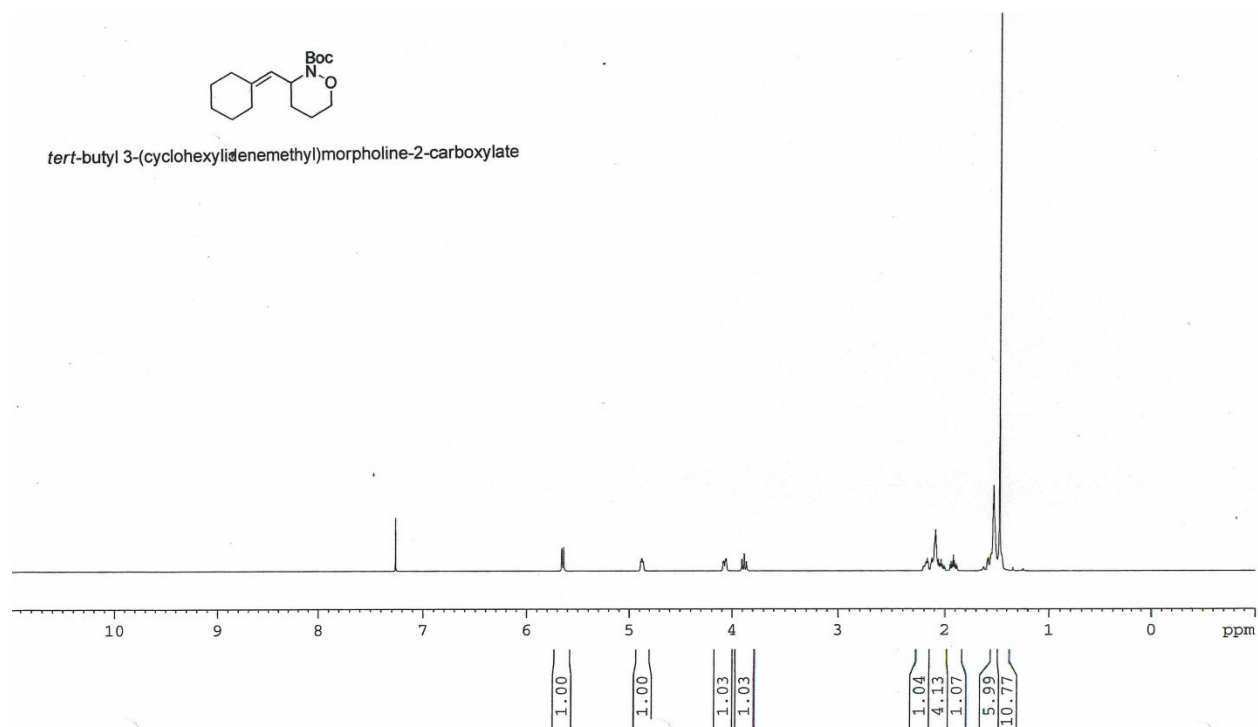
Product **1.12**



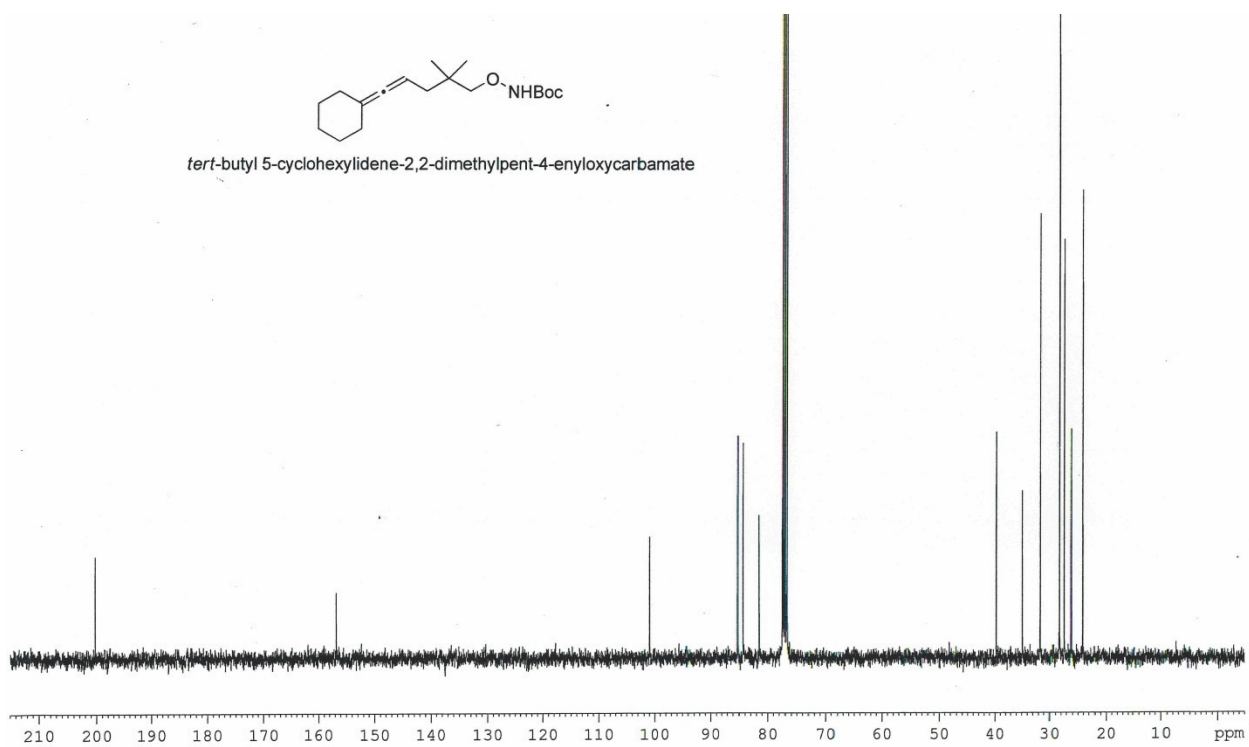
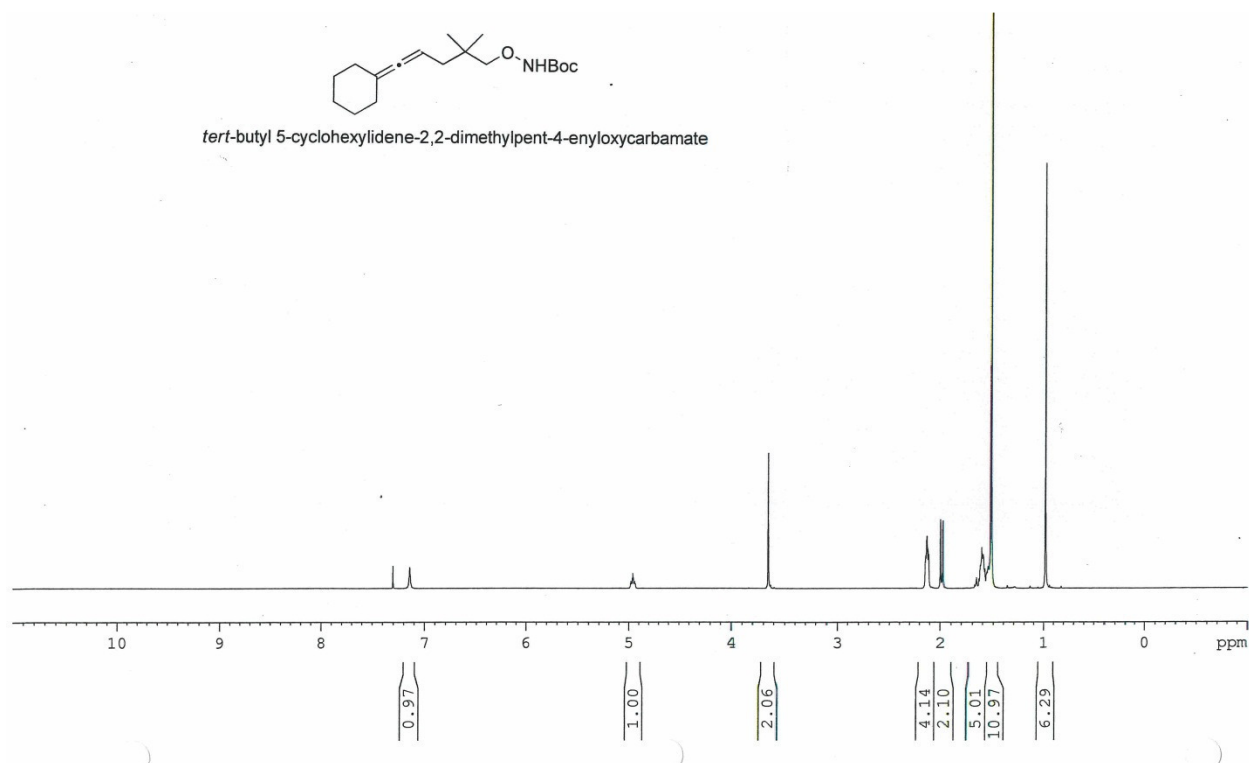
Allene **1.13**



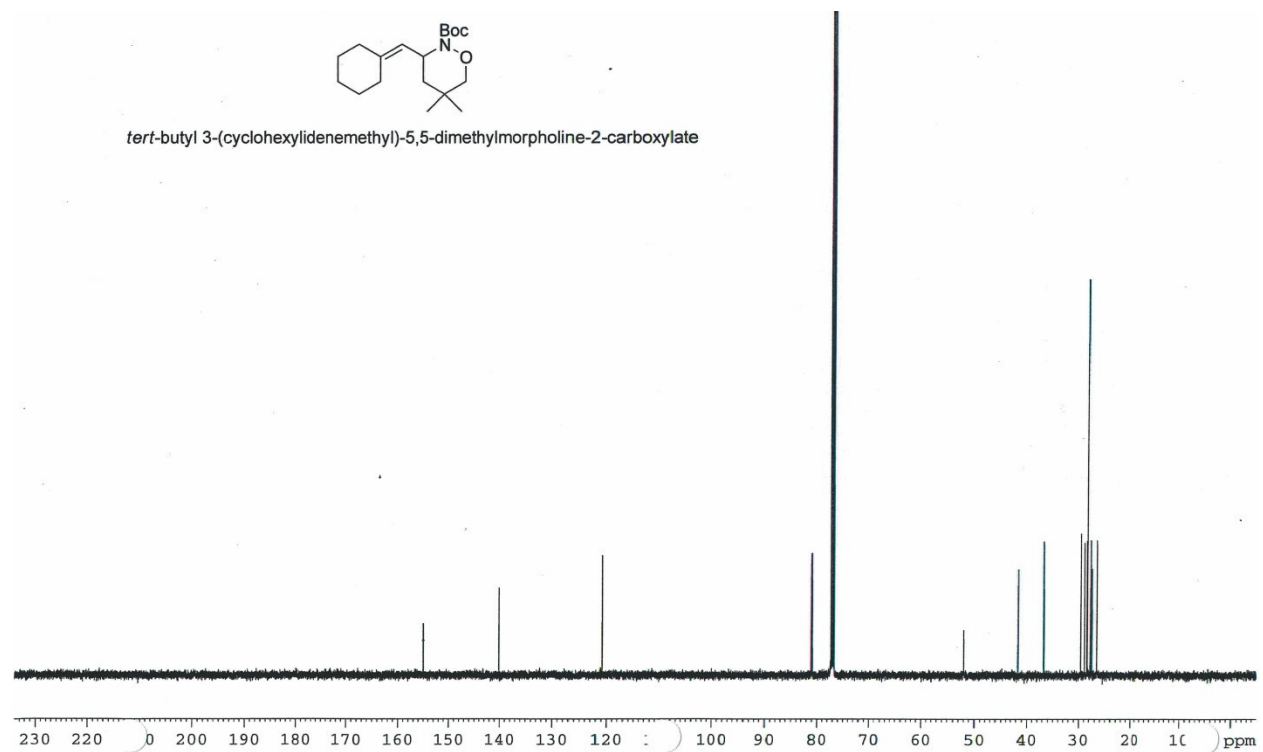
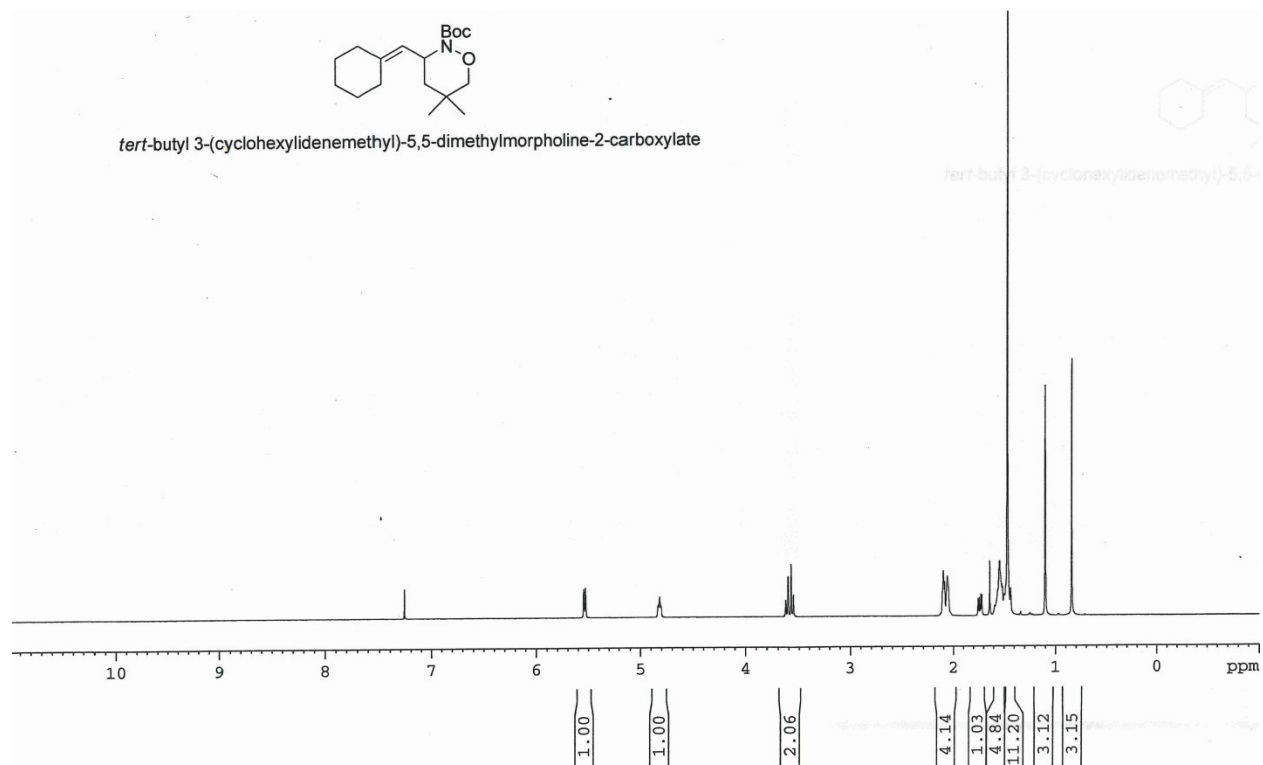
Product **1.14**



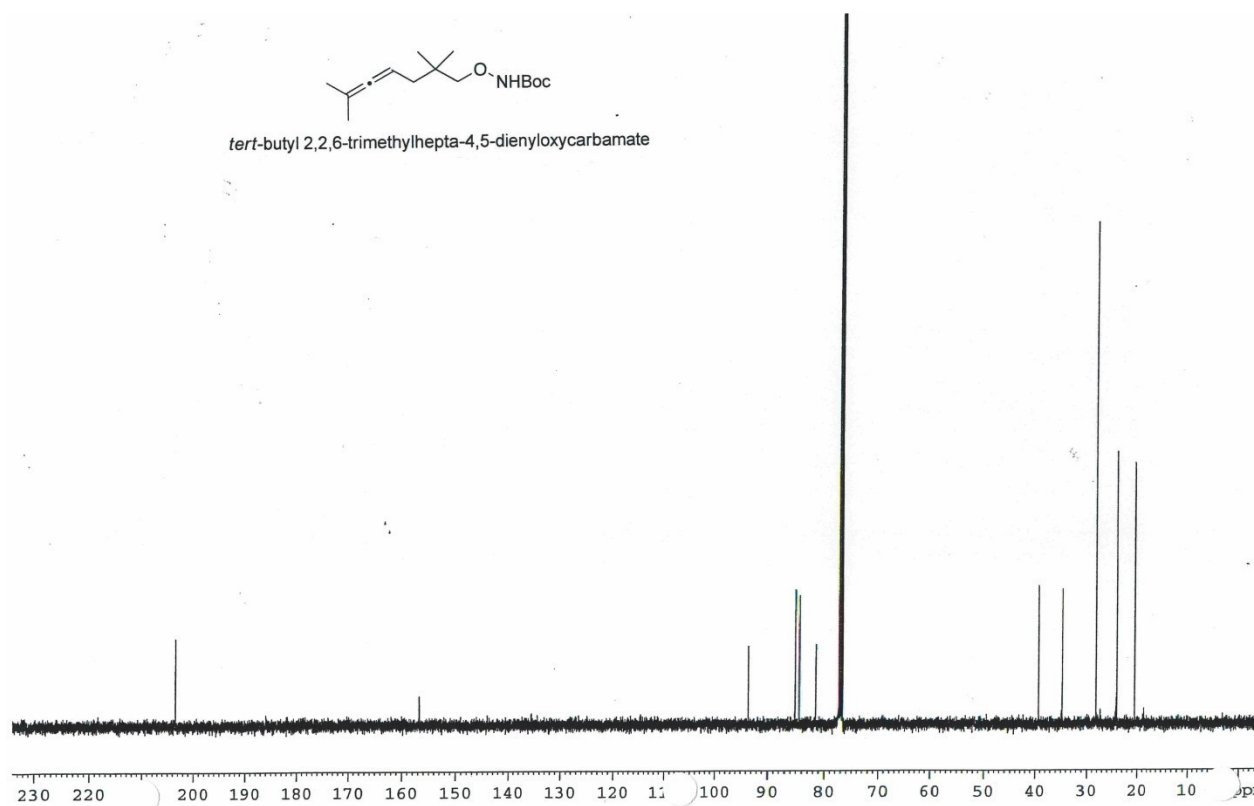
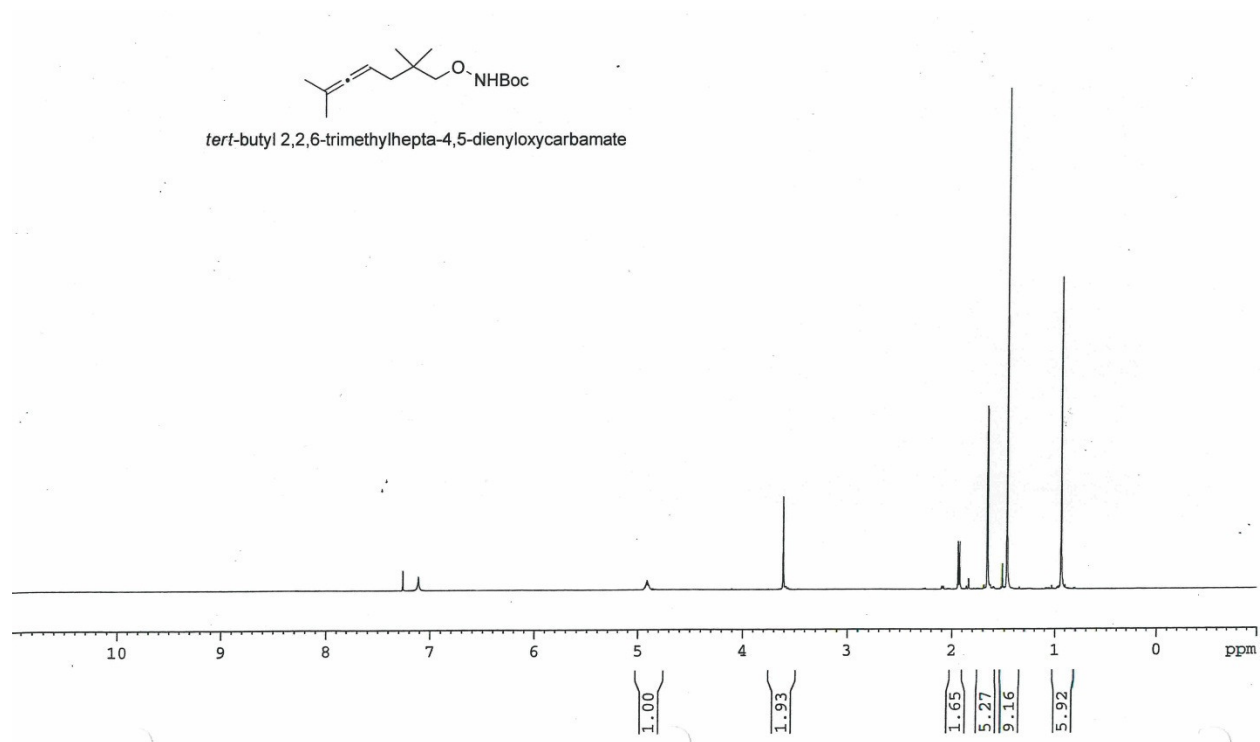
Allene **1.15**



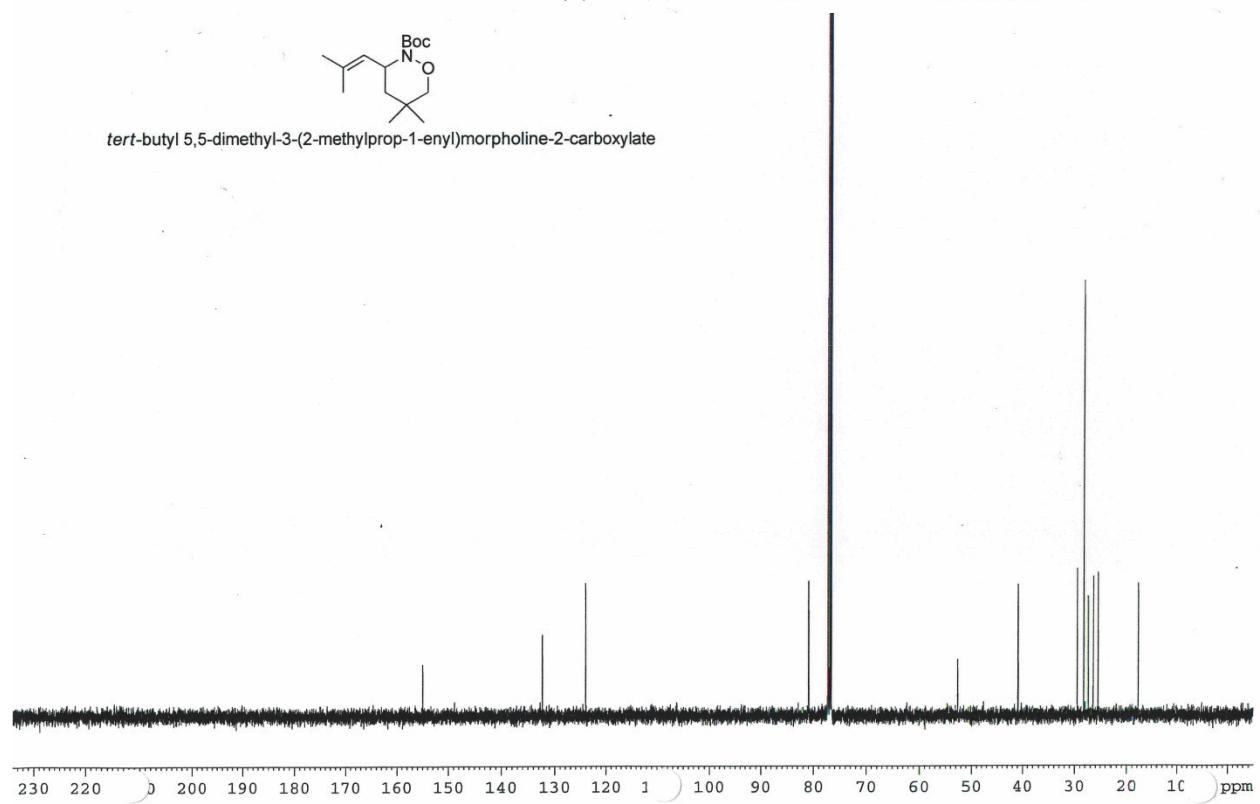
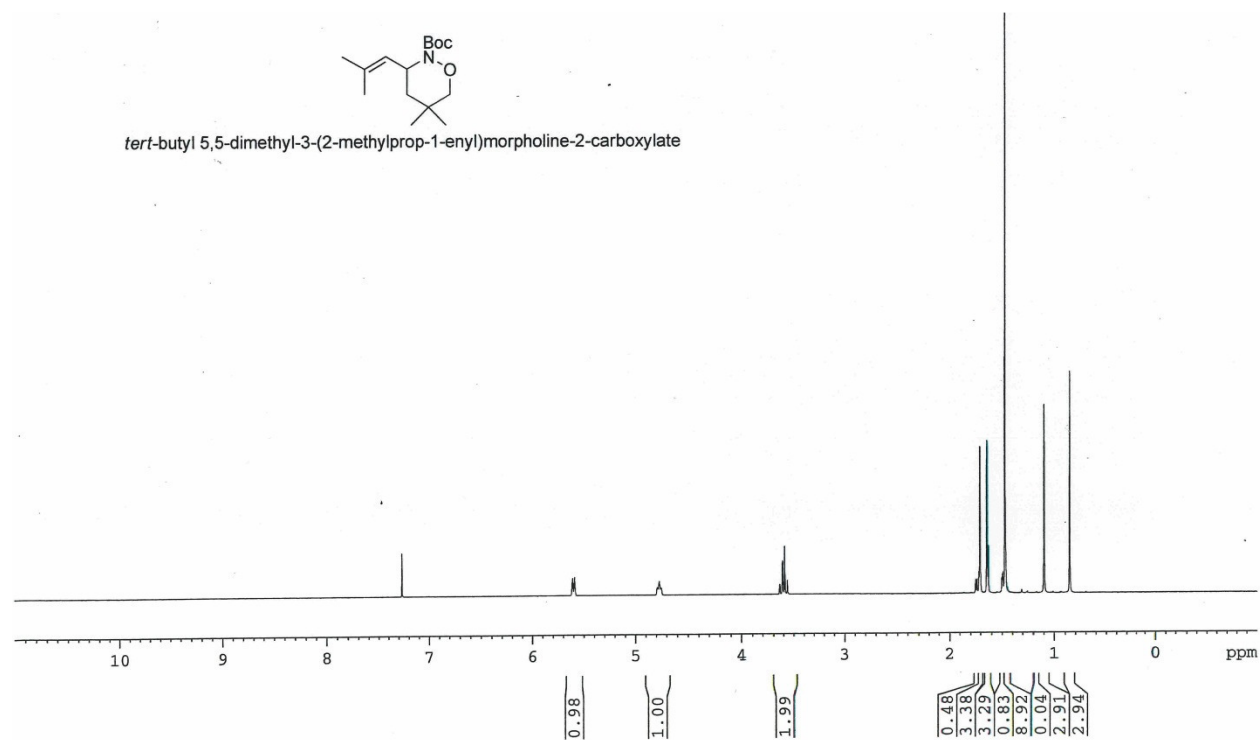
Product **1.16**



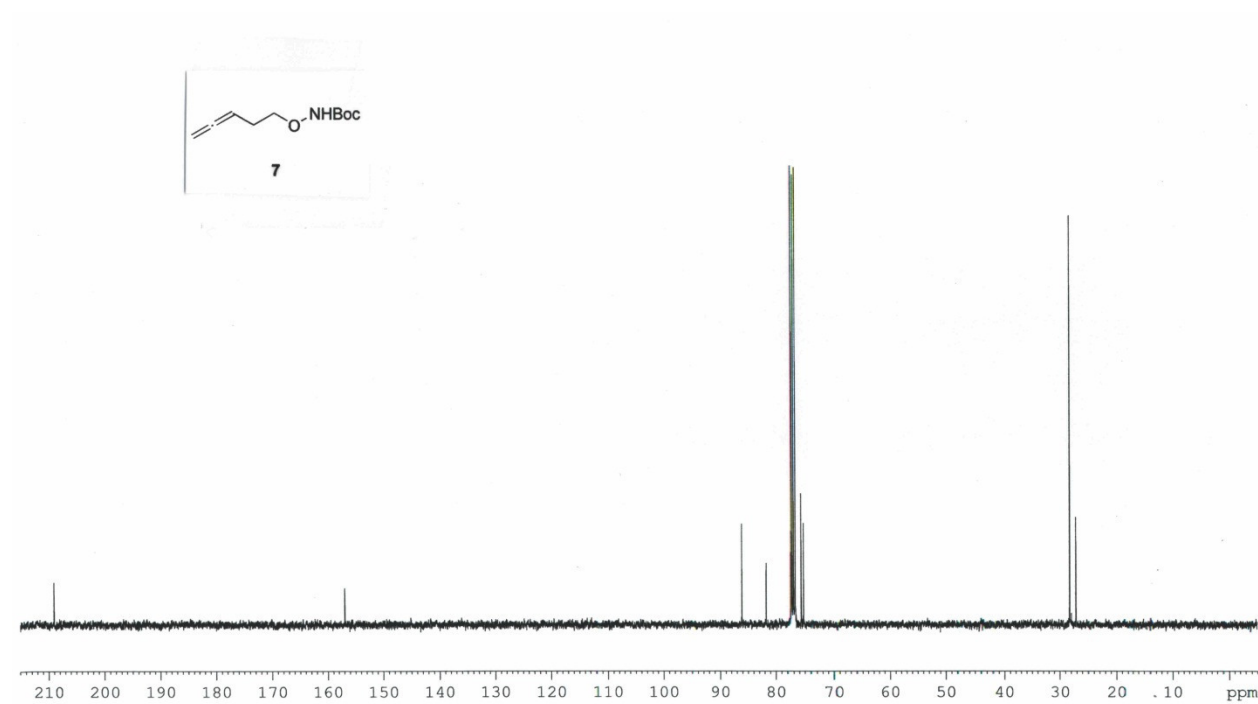
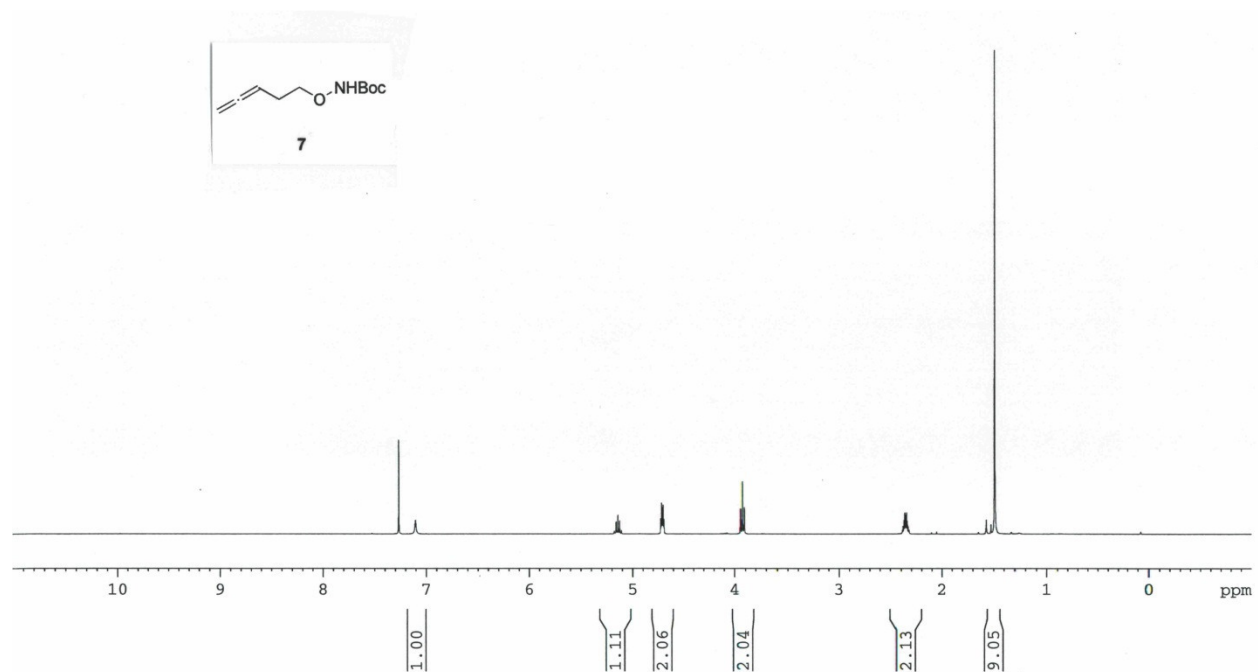
Allene **1.17**



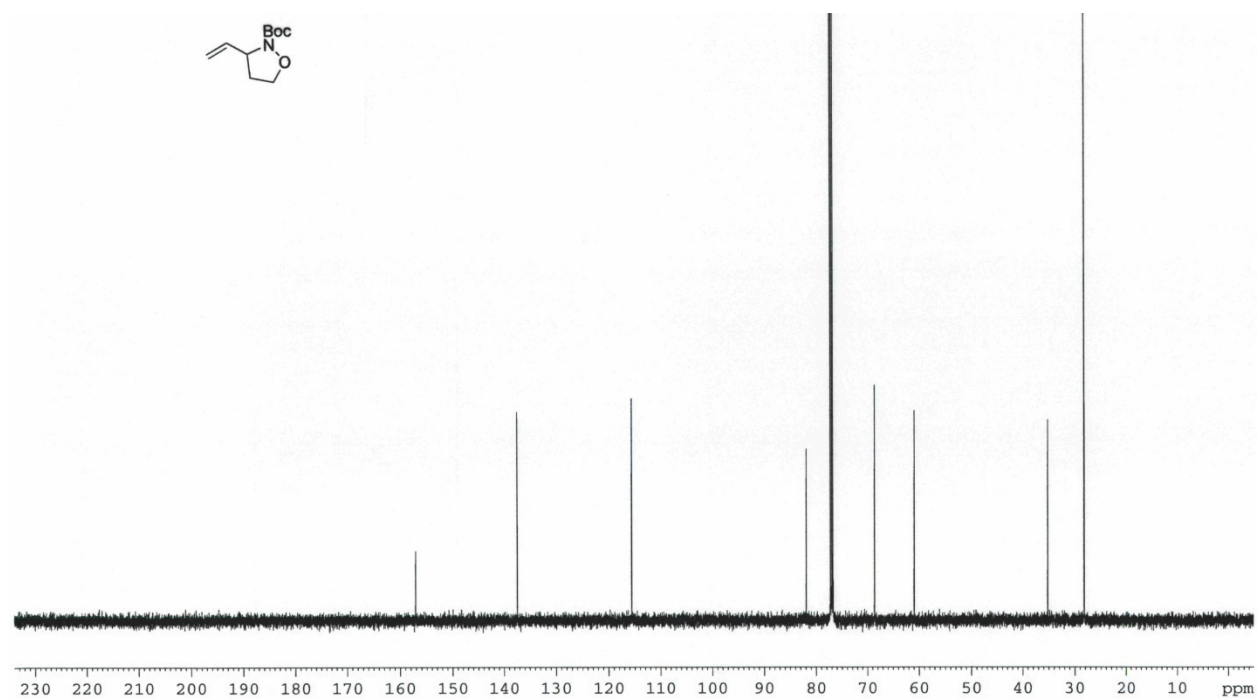
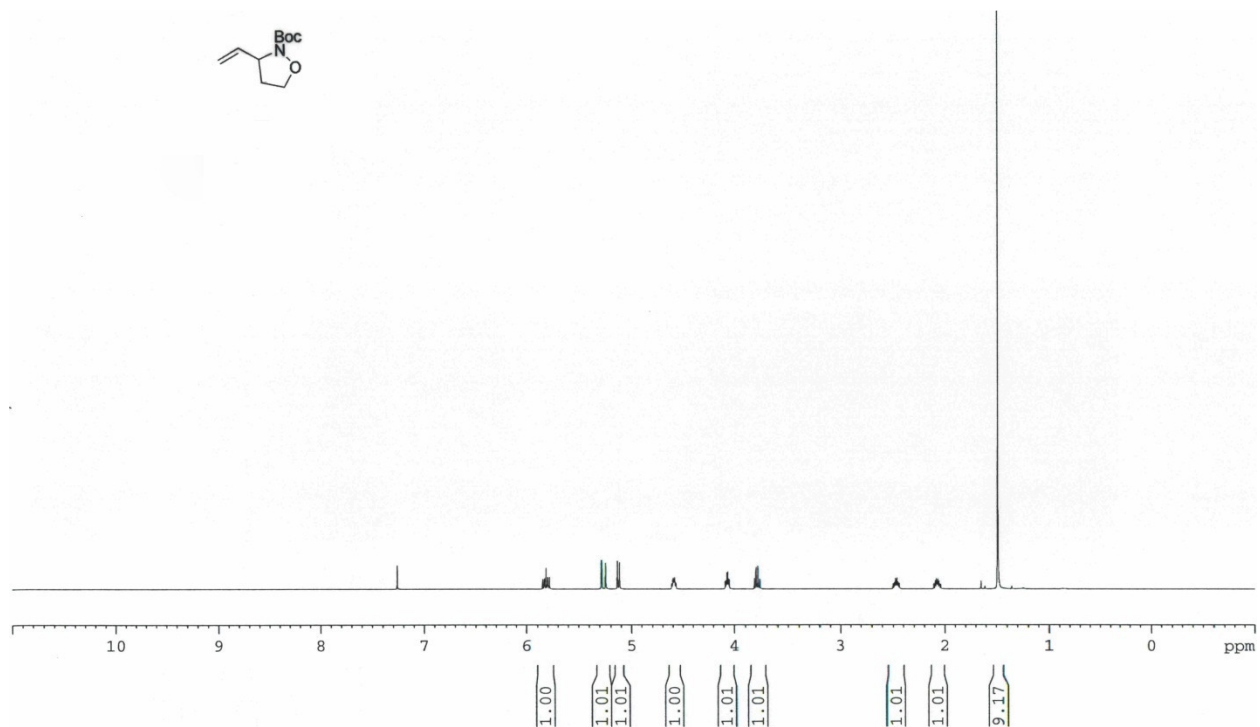
Product **1.18**



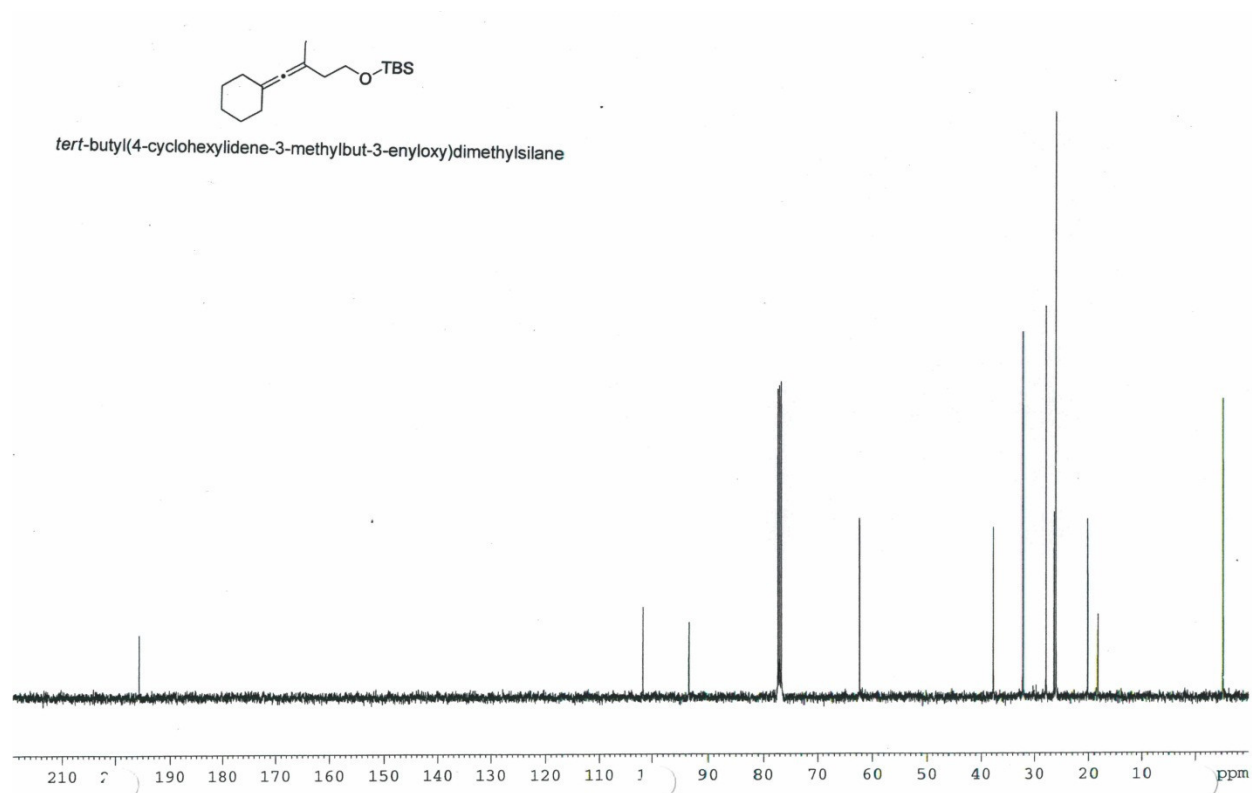
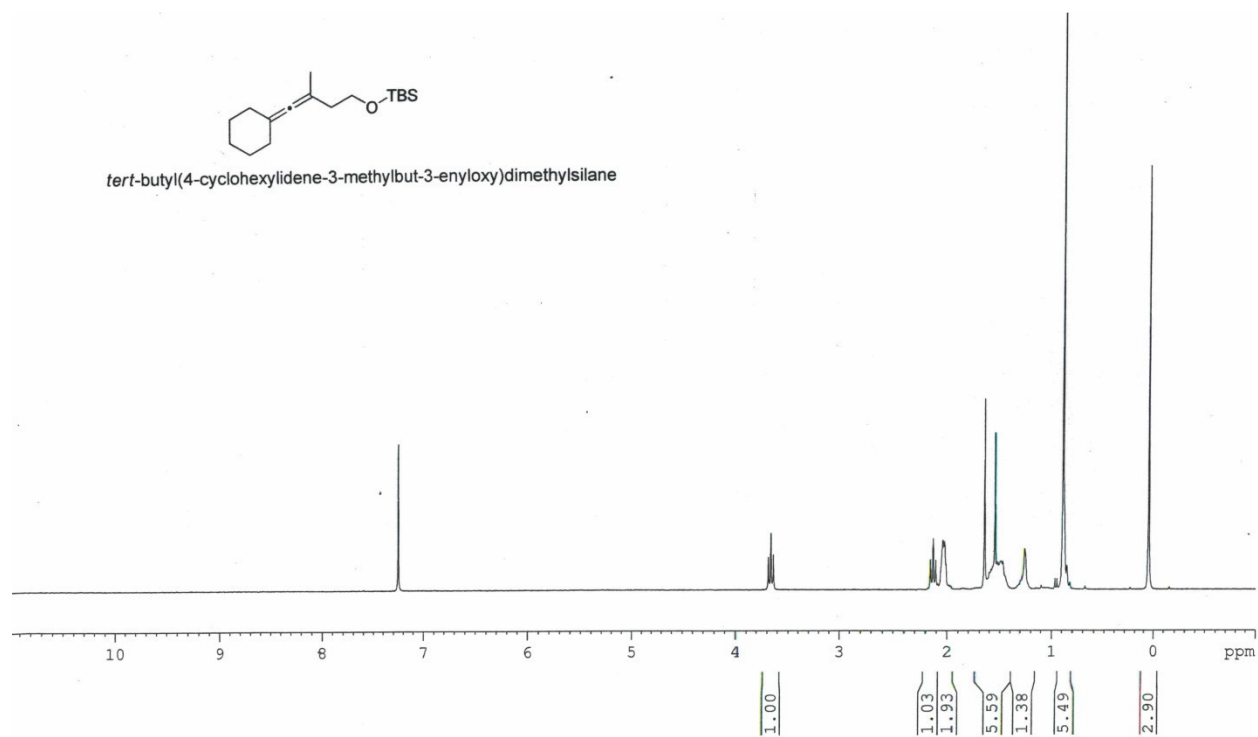
Allene **1.19**



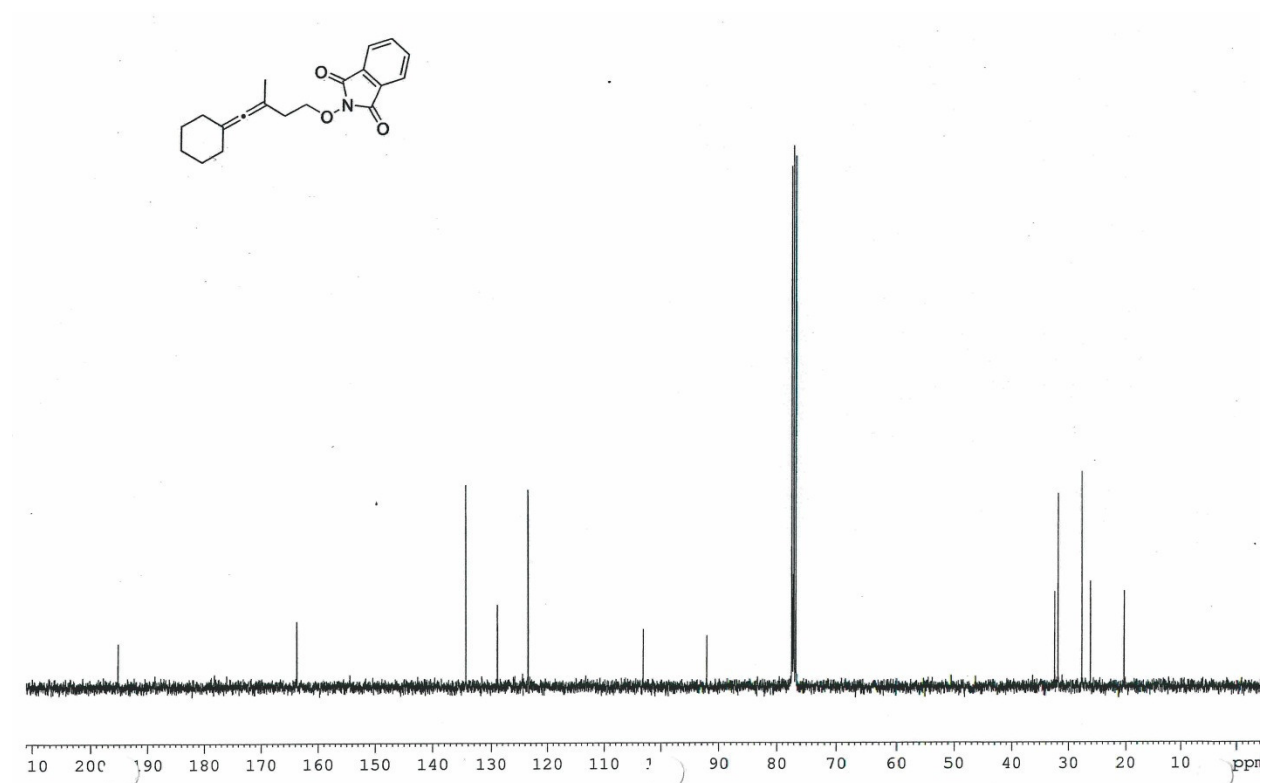
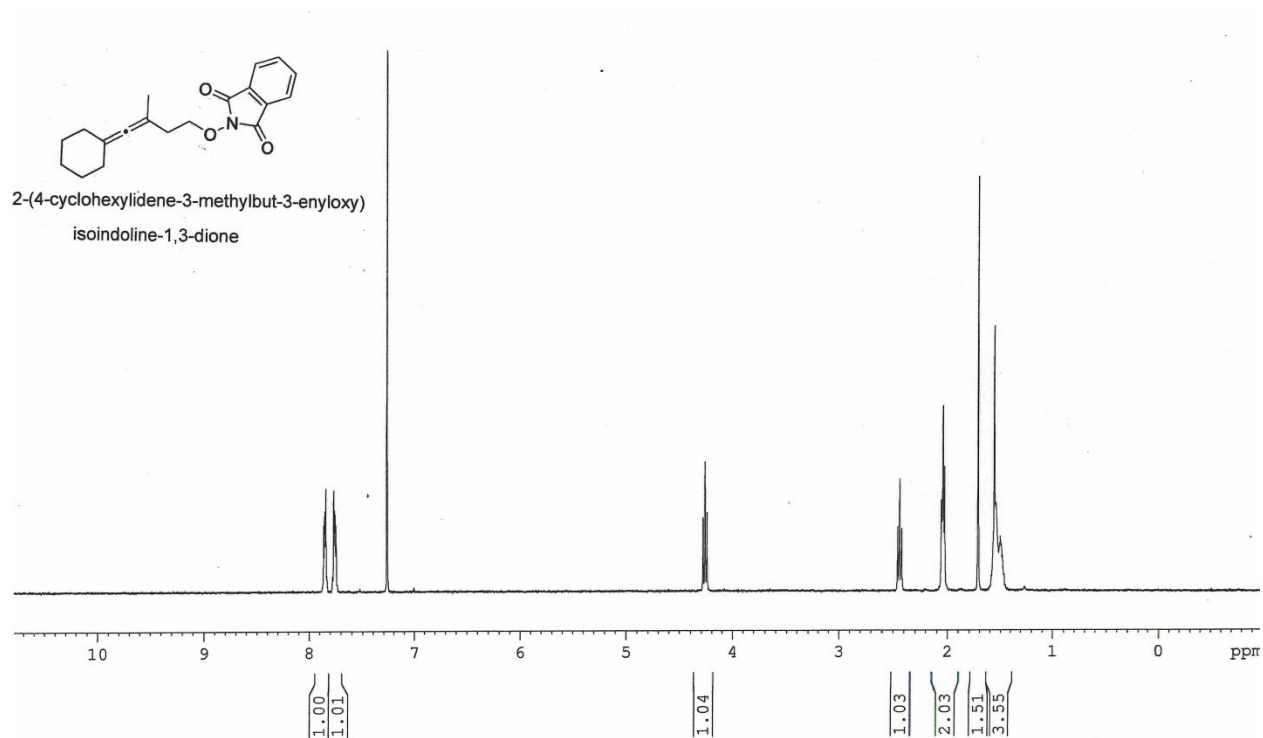
Product **1.20**



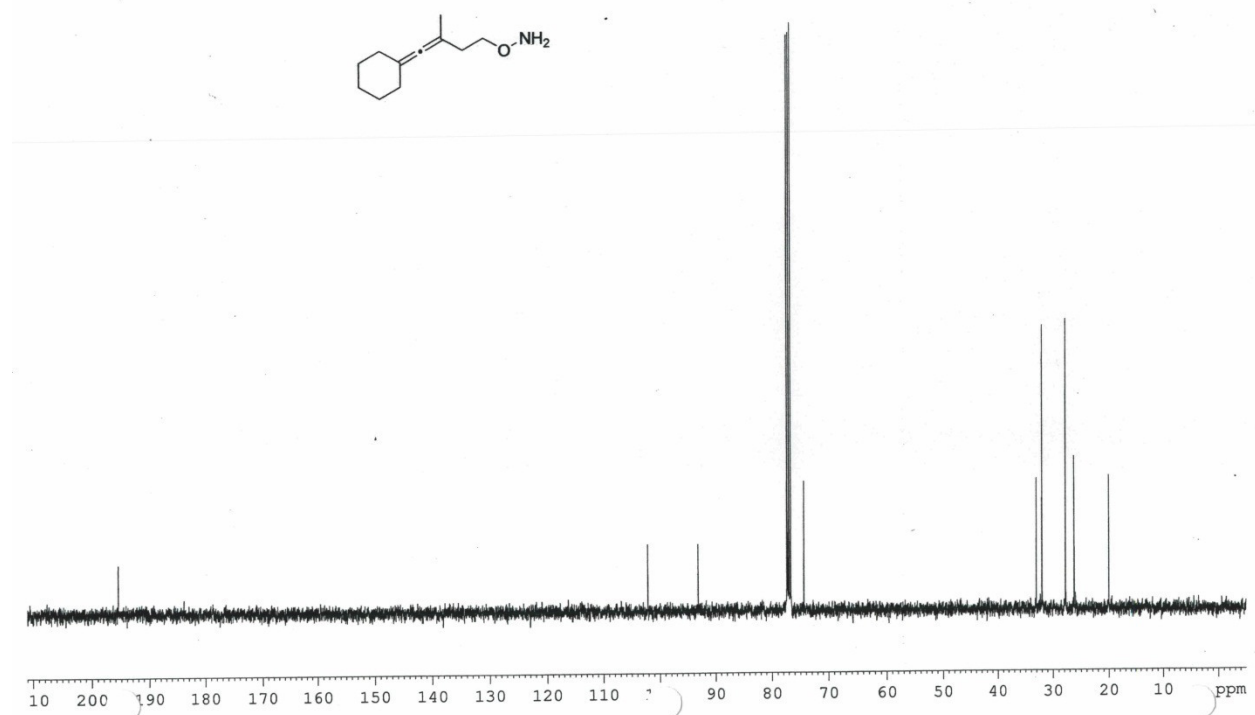
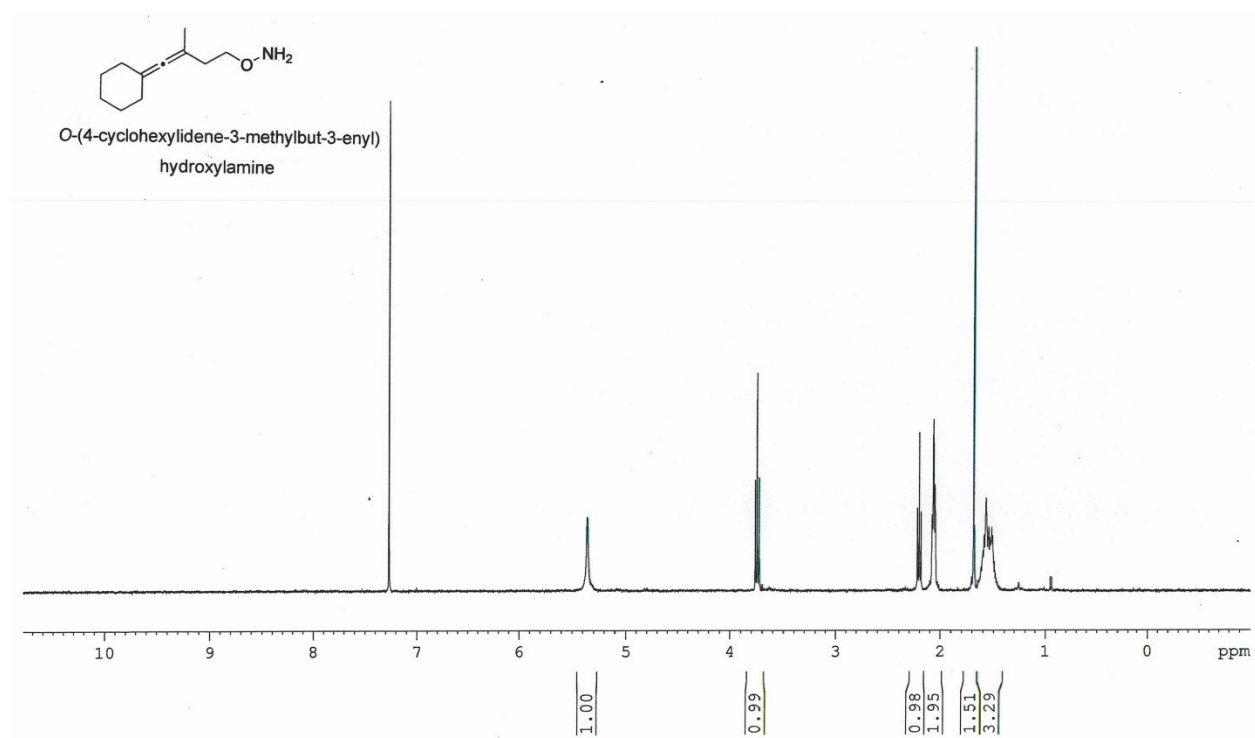
Allene **1.21a**



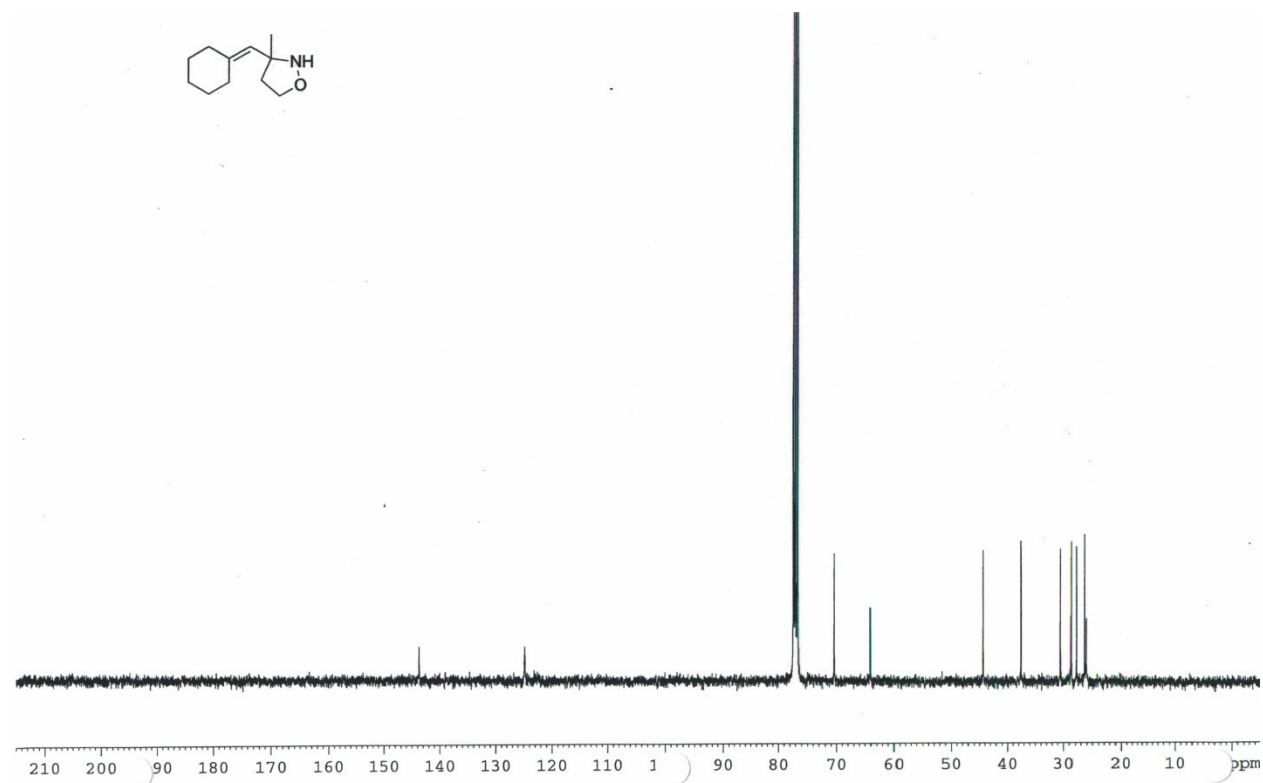
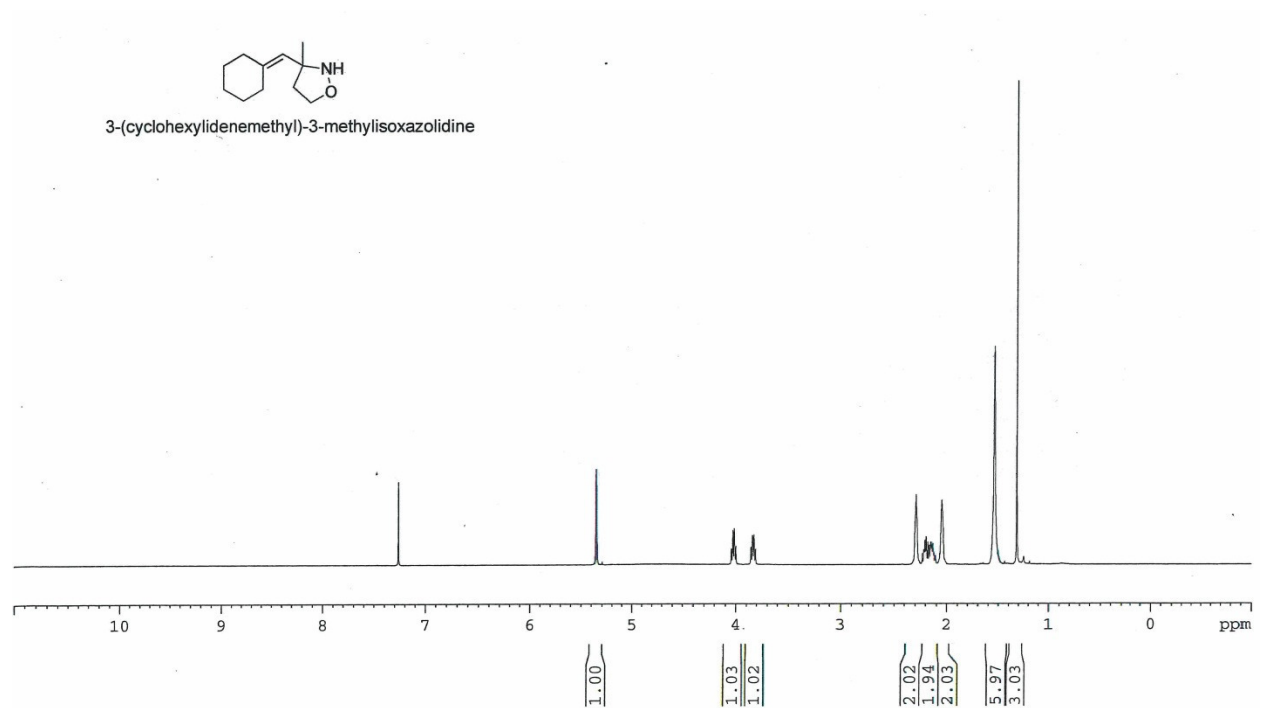
Allene **1.21c**



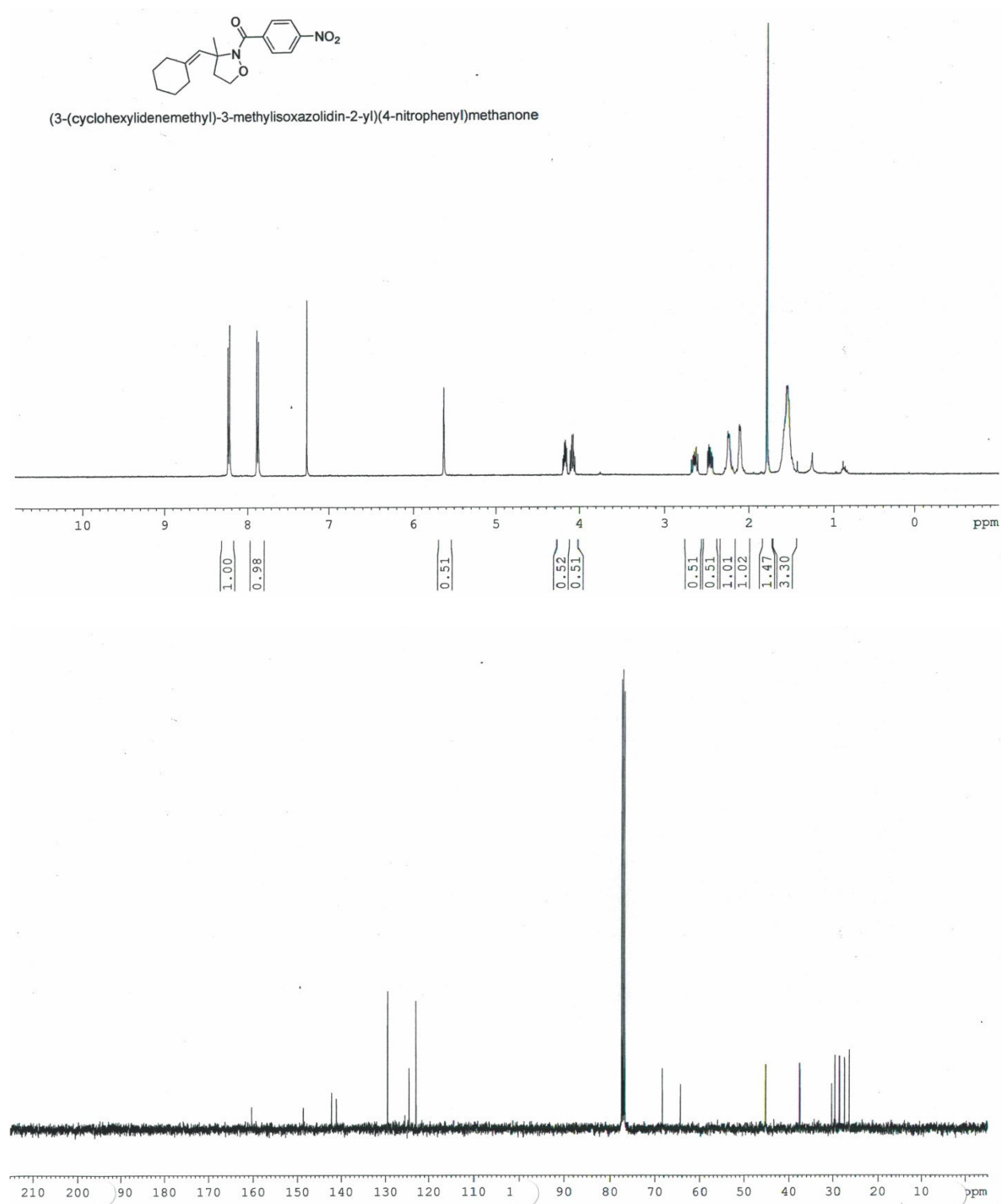
Allene **1.22**



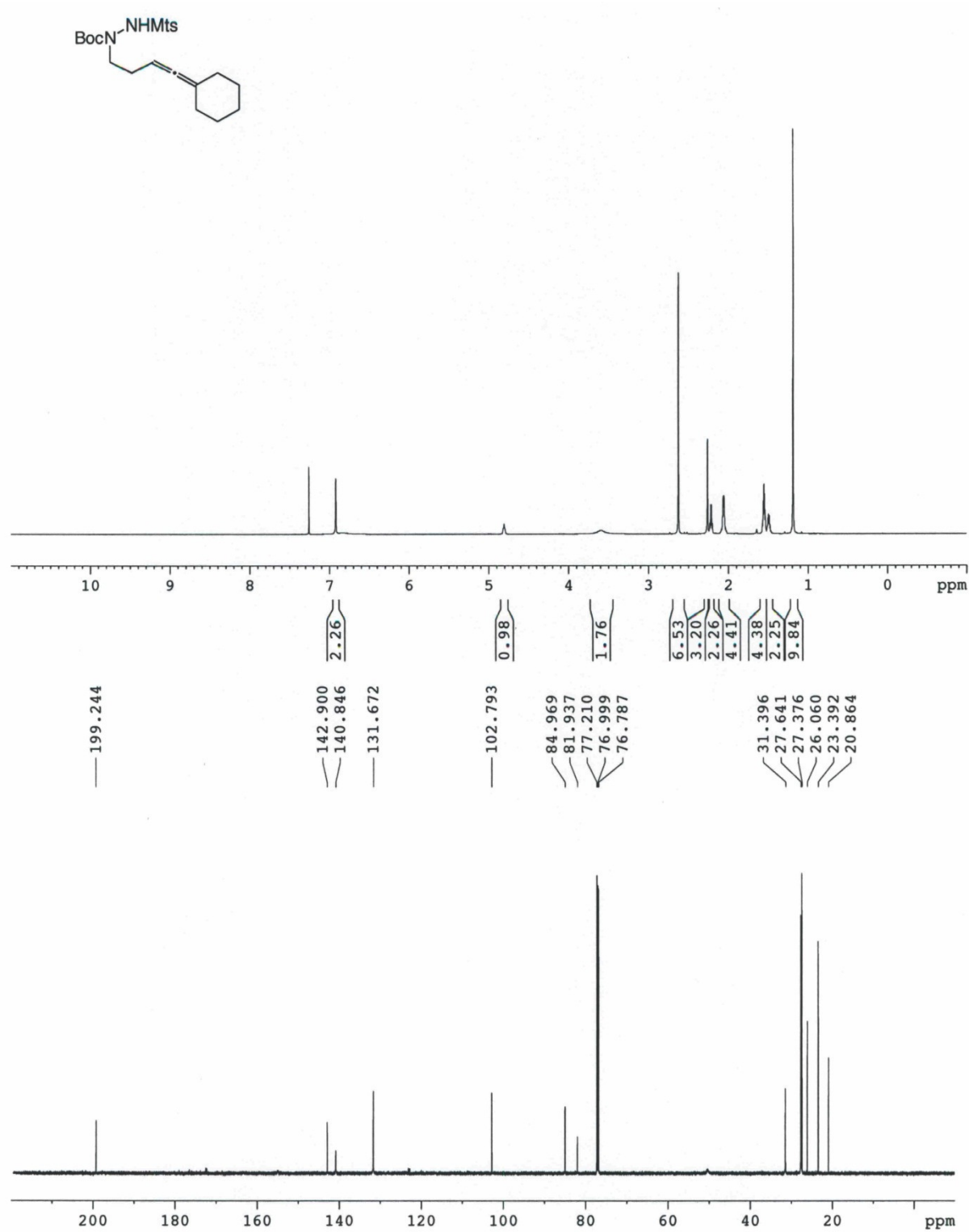
Product **1.27**



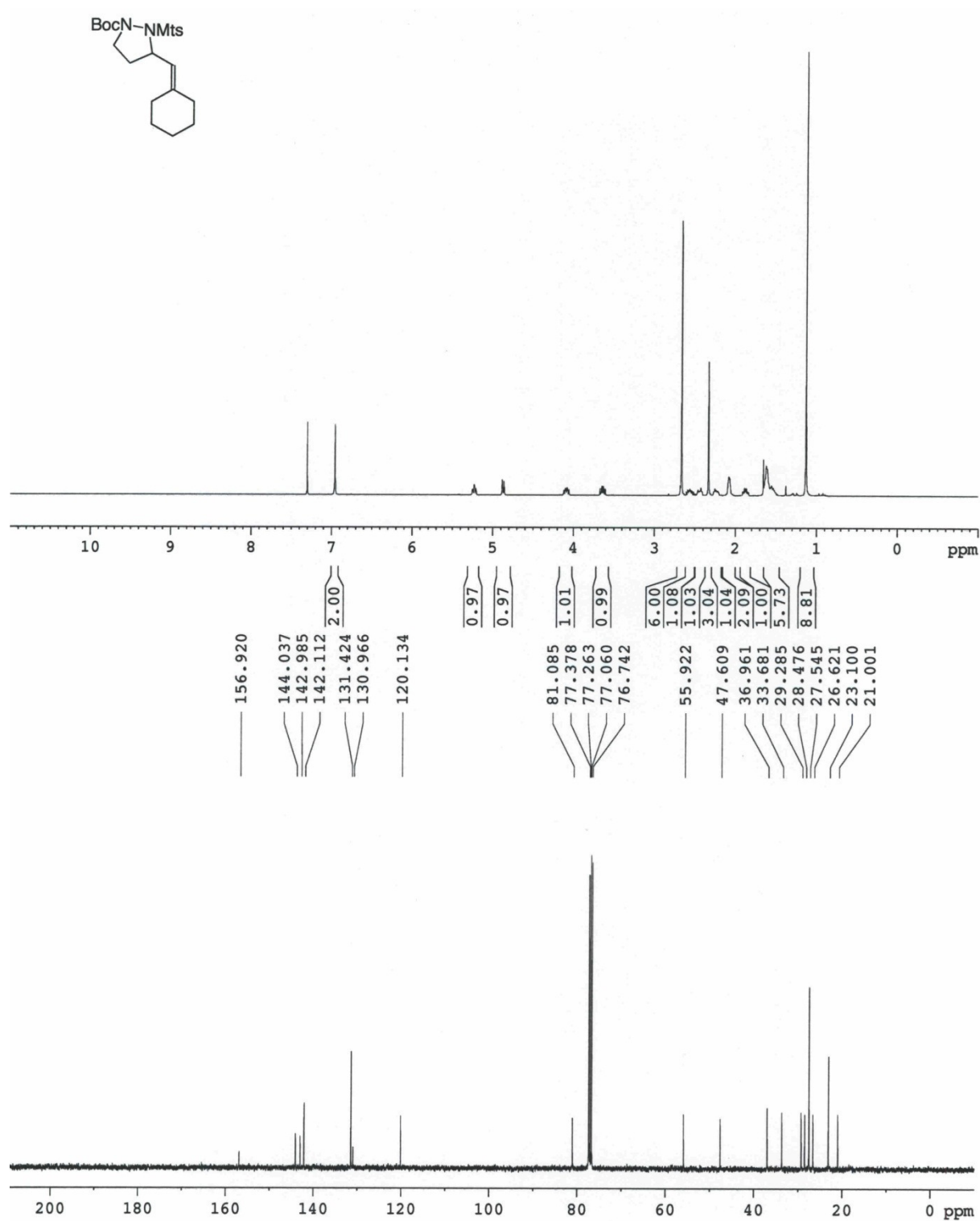
Product **1.29**



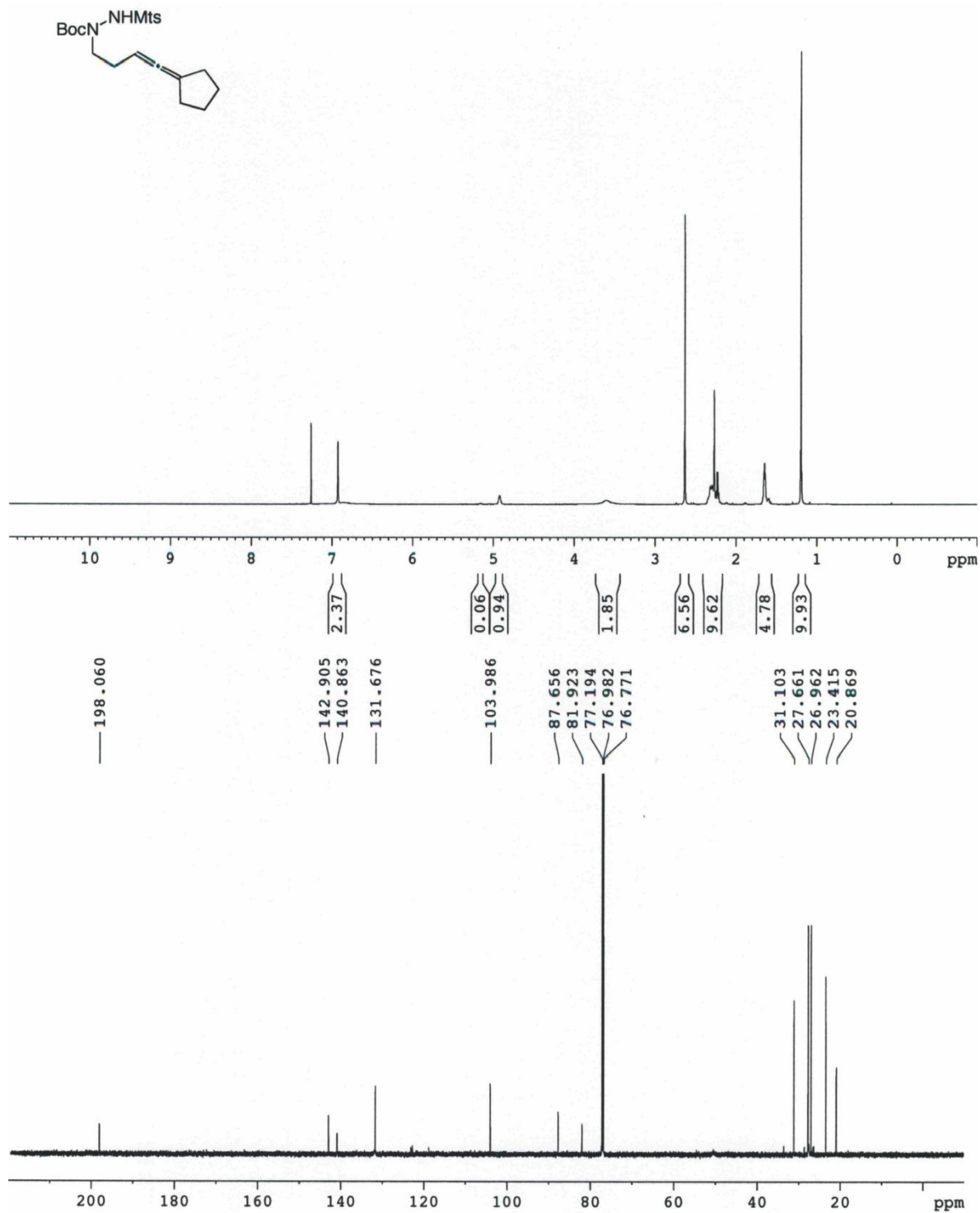
Allene **1.31**



Product **1.32**



Allene **1.33**

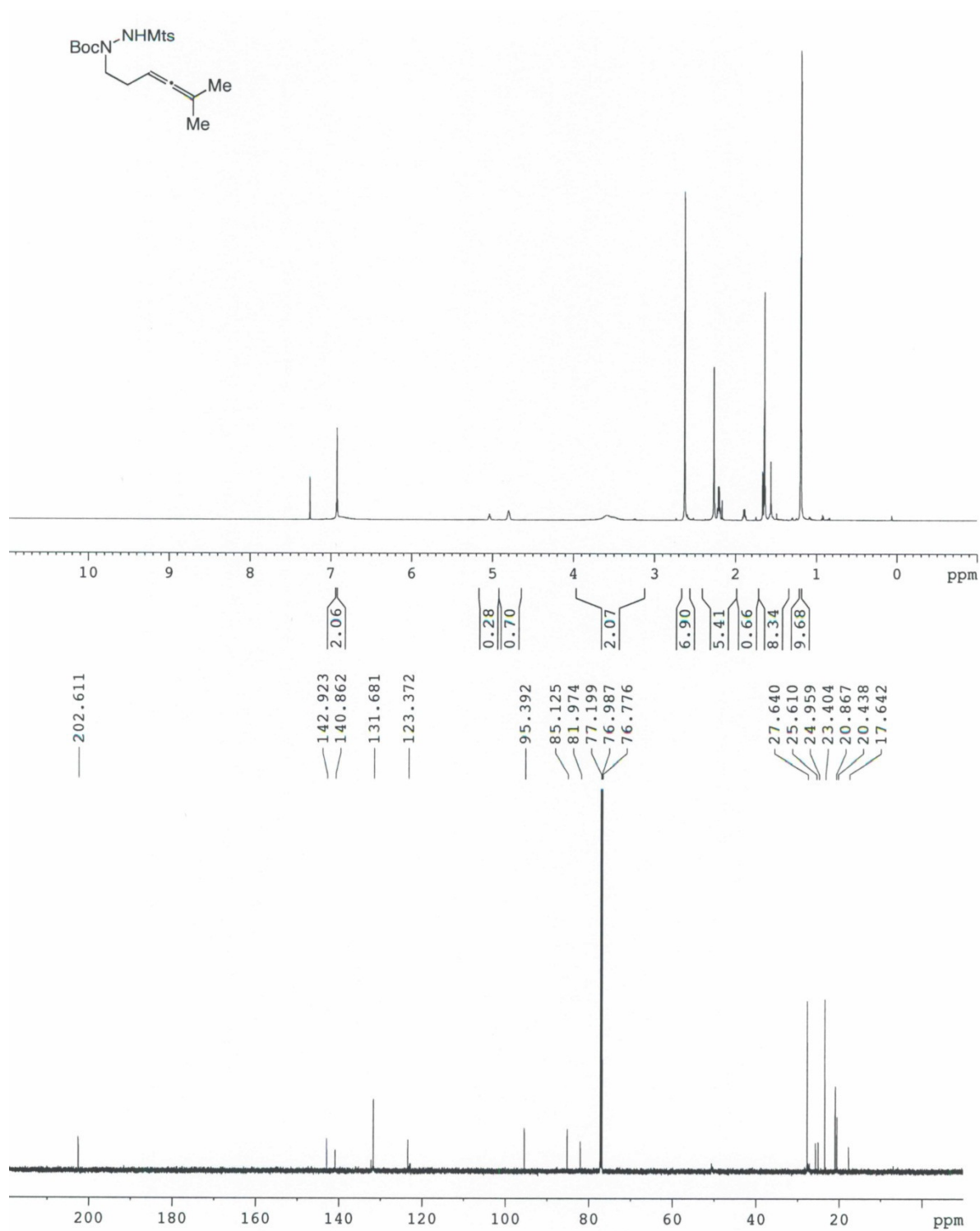


Chemical structure of BocN-NMts is shown. The structure is a bicyclic compound with a BocN group and an NMts group.

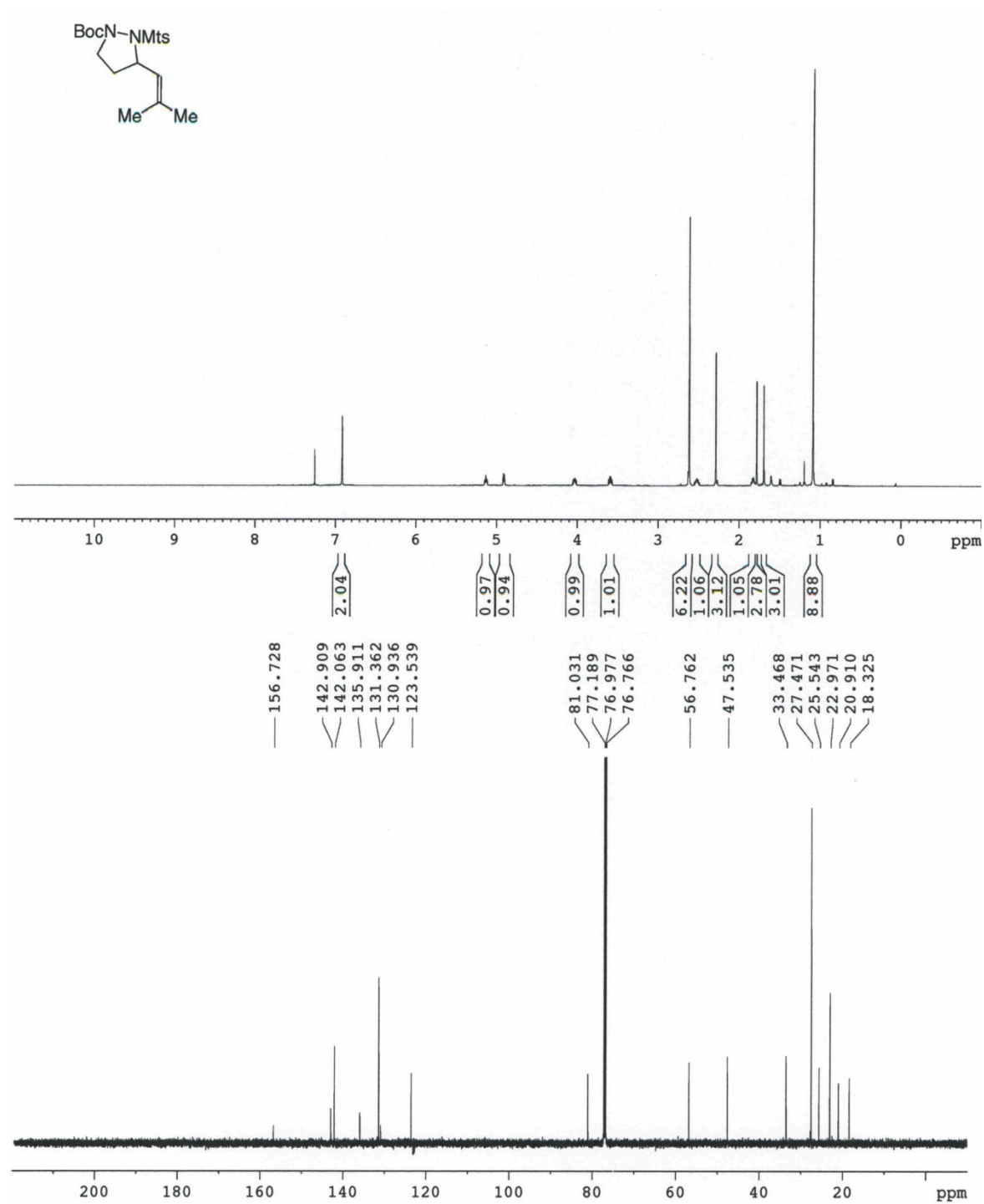
¹H NMR spectrum (400 MHz, CDCl₃) is shown. The x-axis is labeled ppm and ranges from 0 to 10. The spectrum shows several peaks, including a large peak at approximately 1.2 ppm, a peak at approximately 2.1 ppm, and a peak at approximately 7.1 ppm. Integration values are provided for several peaks: 1.96, 1.00, 1.00, 5.97, 2.12, 3.65, 2.33, 1.05, 2.03, 2.69, 8.88, 26.367, 26.170, 23.027, and 20.975.

¹³C NMR spectrum (100 MHz, CDCl₃) is shown. The x-axis is labeled ppm and ranges from 0 to 200. The spectrum shows several peaks, including a large peak at approximately 77 ppm, and peaks at approximately 156.828, 147.569, 142.936, 142.095, 131.423, 131.025, 118.949, 81.114, 77.366, 77.048, 76.730, 58.307, 47.691, 33.752, 33.258, 29.034, 27.557, 26.367, 26.170, 23.027, and 20.975 ppm.

Allene **1.35**

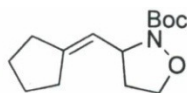


Product **1.36**



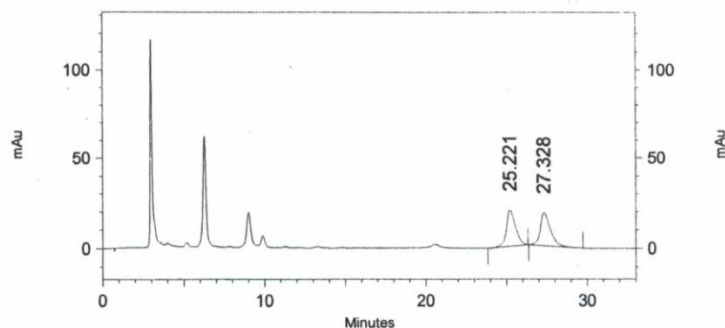
Appendix 1B

HPLC Data



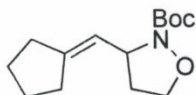
C:\EZStart\Projects\Default\Data\jwang\jwII-136mba_WH9802IP_30min.metBeach3-10-2009 2-43-31 PM.dat Method:
C:\EZStart\Projects\Default\Method\jwang\WHELK\mba_WH9802IP_30min.met
Injection volume: 5 uL

Description: {Data Description}



2: 225 nm, 4 nm Results

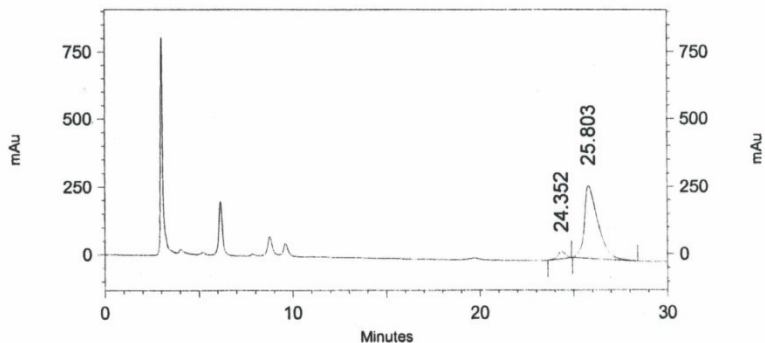
Retention Time	Area	Area Percent
25.221	775408	49.716
27.328	784262	50.284



Enantioenriched

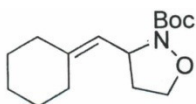
C:\EZStart\Projects\Default\Data\jwang\jwI-082a_mba_WH9802IP_30min.met11-14-2007 2-48-47 PM.dat Method:
C:\EZStart\Projects\Default\Method\jwang\WHELK\mba_WH9802IP_30min.met
Injection volume: 10 uL

Description: {Data Description}



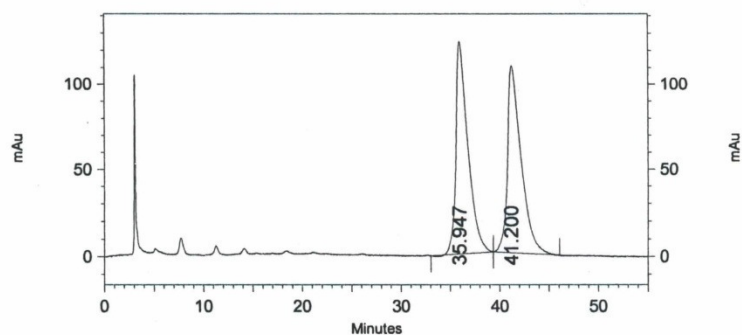
1: 215 nm, 4 nm Results

Retention Time	Area	Area Percent
24.352	731567	5.102
25.803	13608485	94.898



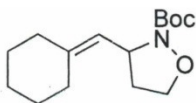
C:\EZStart\Projects\Default\Data\jwang\jwII-135mba_WH9901IP_55min.met9-30-20
 08 7-36-03 PM Method:
 C:\EZStart\Projects\Default\Method\jwang\WHELK\mba_WH9901IP_55min.met
 Injection volume: 12 uL

Description: {Data Description}



1: 215 nm, 4 nm Results

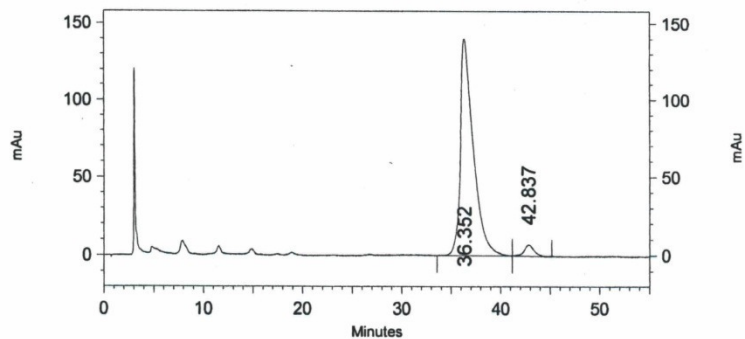
Retention Time	Area	Area Percent
35.947	10388168	50.017
41.200	10381180	49.983



Enantioenriched

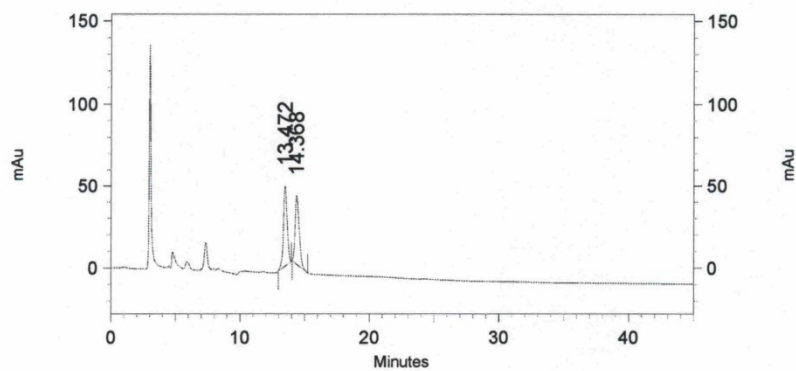
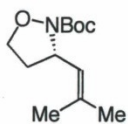
C:\EZStart\Projects\Default\Data\jwang\jwII-026mba_WH9901IP_55min.met9-30-20
 08 8-33-06 PM Method:
 C:\EZStart\Projects\Default\Method\jwang\WHELK\mba_WH9901IP_55min.met
 Injection volume: 12 uL

Description: {Data Description}



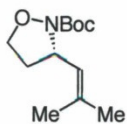
1: 215 nm, 4 nm Results

Retention Time	Area	Area Percent
36.352	12670548	96.251
42.837	493511	3.749

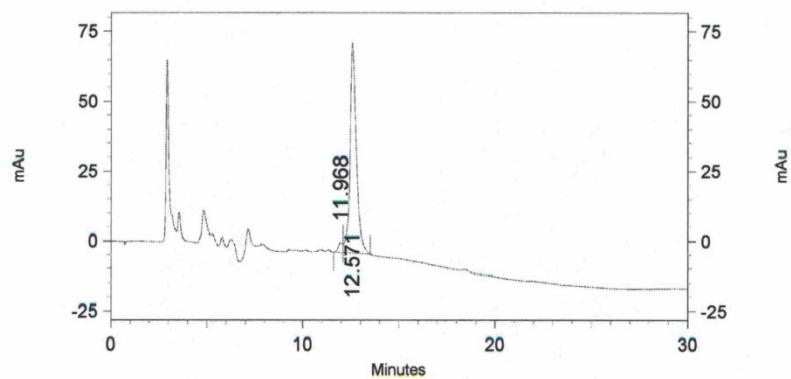


1: 230 nm, 4 nm Results

Retention Time	Area	Area Percent
13.472	967163	51.293
14.368	918412	48.707

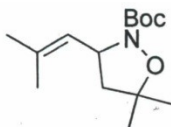


Enantioenriched



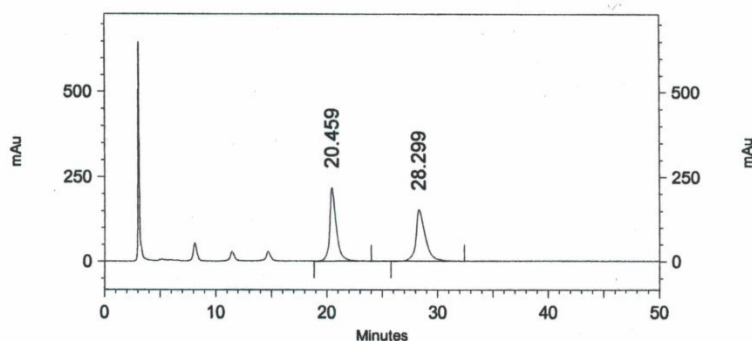
1: 230 nm, 4 nm Results

Retention Time	Area	Area Percent
11.968	54402	3.058
12.571	1724371	96.942



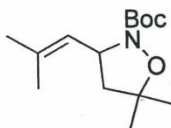
C:\EZStart\Projects\Default\Data\jwang\jwII-128ImbaWH9901IP_50.metBeach8-28-2008 4-05-54 AM.dat Method:
C:\EZStart\Projects\Default\Method\jwang\WHELK\mba_WH9901IP_50min.met
Injection volume: 12 uL

Description: {Data Description}



1: 210 nm, 4 nm Results

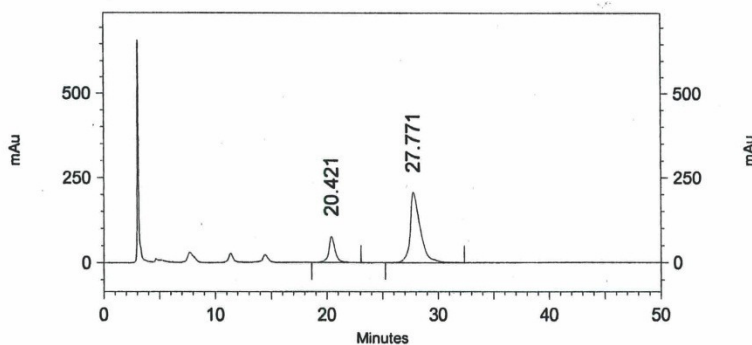
Retention Time	Area	Area Percent
20.459	8979888	50.103
28.299	8942811	49.897



Enantioenriched

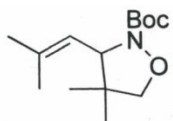
C:\EZStart\Projects\Default\Data\jwang\jwII-128IImbaWH9901IP_50.metBeach8-28-2008 4-57-55 AM.dat Method:
C:\EZStart\Projects\Default\Method\jwang\WHELK\mba_WH9901IP_50min.met
Injection volume: 12 uL

Description: {Data Description}



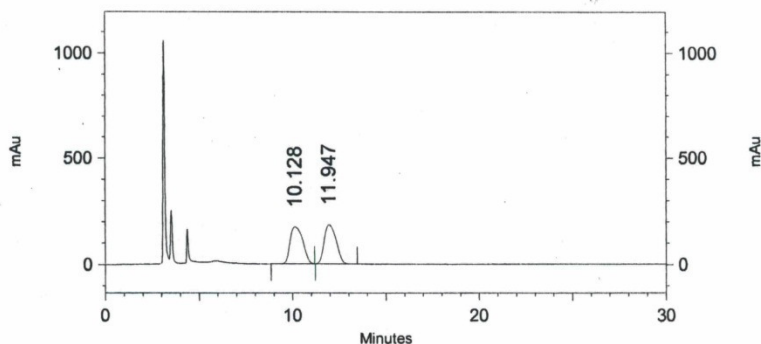
1: 210 nm, 4 nm Results

Retention Time	Area	Area Percent
20.421	2972227	18.647
27.771	12966830	81.353



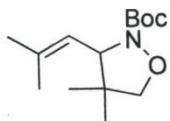
C:\EZStart\Projects\Default\Data\jwang\jwII-104jw_OD9901IP_30min.metBeach8-4
 -2008 11-48-53 PM.dat Method:
 C:\EZStart\Projects\Default\Method\jwang\OD\jw_OD9901IP_30min.met
 Injection volume: 12 uL

Description: {Data Description}



1: 215 nm, 4 nm Results

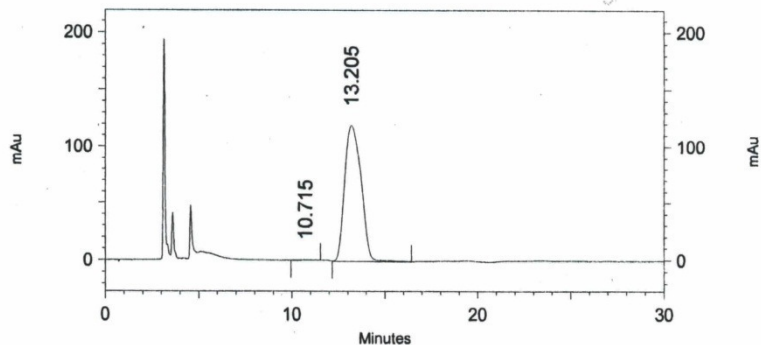
Retention Time	Area	Area Percent
10.128	8082455	50.225
11.947	8010048	49.775



Enantioenriched

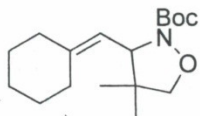
C:\EZStart\Projects\Default\Data\jwang\jwII-107IIjw_OD9901IP_30min.metBeach8
 -6-2008 12-00-42 AM.dat Method:
 C:\EZStart\Projects\Default\Method\jwang\OD\jw_OD9901IP_30min.met
 Injection volume: 12 uL

Description: {Data Description}



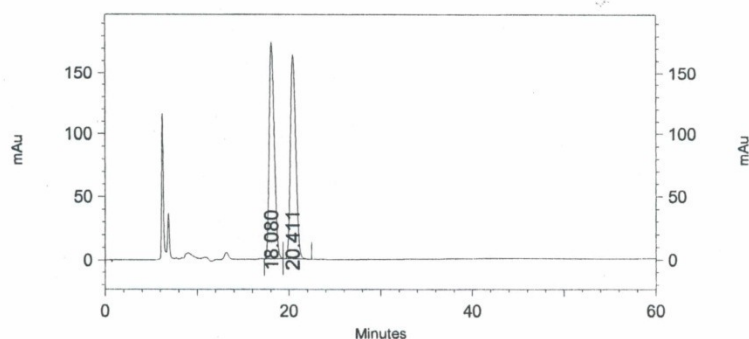
1: 215 nm, 4 nm Results

Retention Time	Area	Area Percent
10.715	8206	0.111
13.205	7366305	99.889



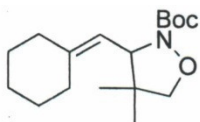
C:\EZStart\Projects\Default\Data\jwang\jwII-127Ijw_OD9901IP_pt5flow_60min.m
 tBeach3-10-2009 7-06-44 PM.dat Method:
 C:\EZStart\Projects\Default\Method\jwang\OD\jw_OD9901IP_pt5flow_60min.met
 Injection volume: 5 uL

Description: {Data Description}



1: 215 nm, 4 nm Results

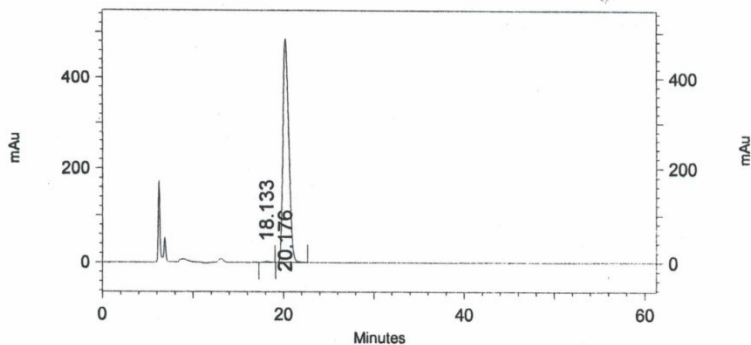
Retention Time	Area	Area Percent
18.080	6693043	49.943
20.411	6708405	50.057



Enantioenriched

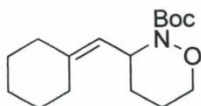
C:\EZStart\Projects\Default\Data\jwang\jwII-127IIjw_OD9901IP_pt5flow_60min.m
 etBeach3-10-2009 6-03-21 PM.dat Method:
 C:\EZStart\Projects\Default\Method\jwang\OD\jw_OD9901IP_pt5flow_60min.met
 Injection volume: 10 uL

Description: {Data Description}



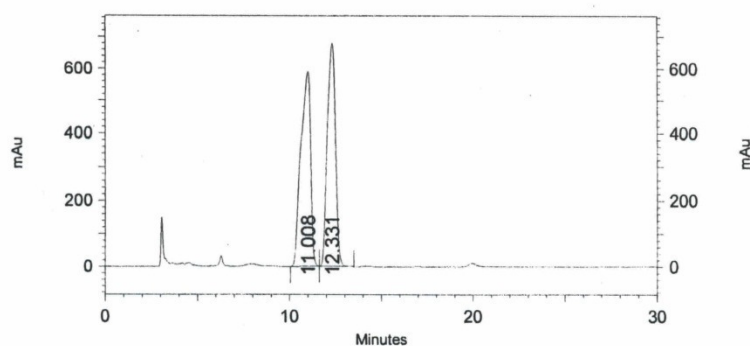
1: 215 nm, 4 nm Results

Retention Time	Area	Area Percent
18.133	81468	0.375
20.176	21654103	99.625



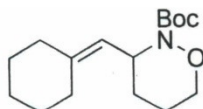
C:\EZStart\Projects\Default\Data\jwang\jwI-089ajw_AD9901IP_30min.met11-26-20
 07 3-18-11 PM.dat Method:
 C:\EZStart\Projects\Default\Method\jwang\AD\mba_AD9901IP_30min.met
 Injection volume: 15 uL

Description: {Data Description}



1: 215 nm, 4 nm Results

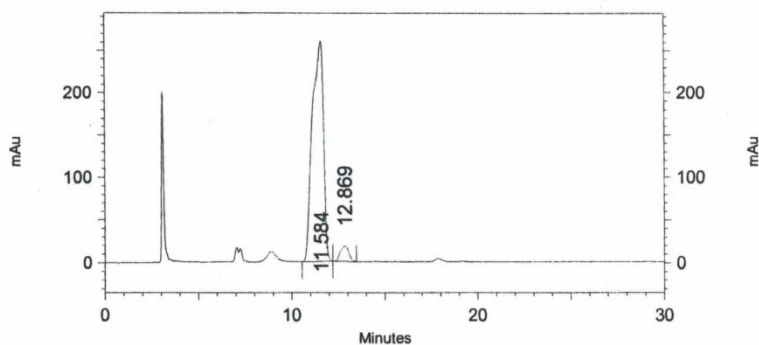
Retention Time	Area	Area Percent
11.008	21668065	50.786
12.331	20997449	49.214



Enantioenriched

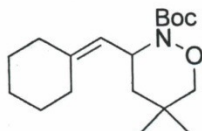
C:\EZStart\Projects\Default\Data\jwang\jwI-103Imba_AD9901IP_30min.met1-13-20
 08 5-16-04 PM.dat Method:
 C:\EZStart\Projects\Default\Method\jwang\AD\mba_AD9901IP_30min.met
 Injection volume: 12 uL

Description: {Data Description}



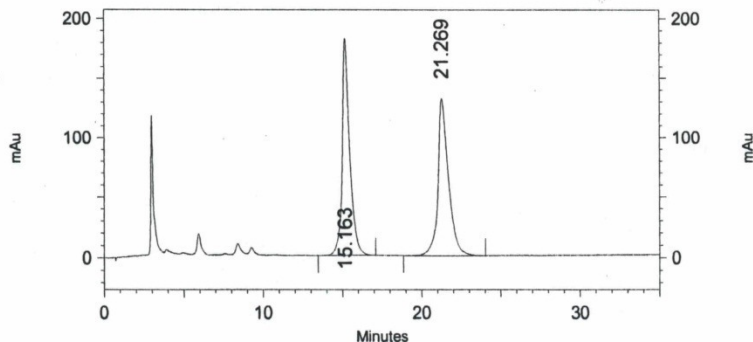
1: 218 nm, 4 nm Results

Retention Time	Area	Area Percent
11.584	10827943	95.106
12.869	557150	4.894



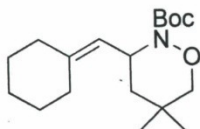
C:\EZStart\Projects\Default\Data\jwang\jwII-087mba_WH9802IP_30min.metBeach7-10-2008 12-44-52 PM.dat Method:
C:\EZStart\Projects\Default\Method\jwang\WHELK\mba_WH9802IP_30min.met
Injection volume: 12 uL

Description: {Data Description}



1: 215 nm, 4 nm Results

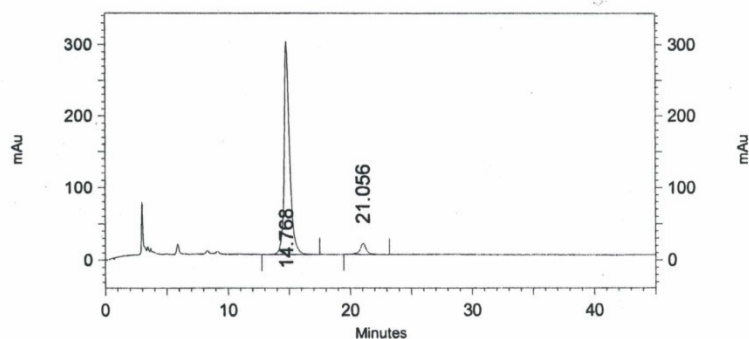
Retention Time	Area	Area Percent
15.163	5935301	49.432
21.269	6071757	50.568



Enantioenriched

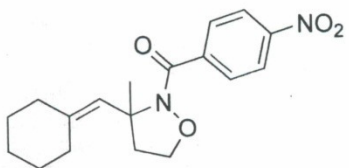
C:\EZStart\Projects\Default\Data\jwang\jwII-088Imba_WH9802IP_45min.metBeach7-11-2008 8-41-38 PM.dat Method:
C:\EZStart\Projects\Default\Method\jwang\WHELK\mba_WH9802IP_45min.met
Injection volume: 12 uL

Description: {Data Description}



1: 215 nm, 4 nm Results

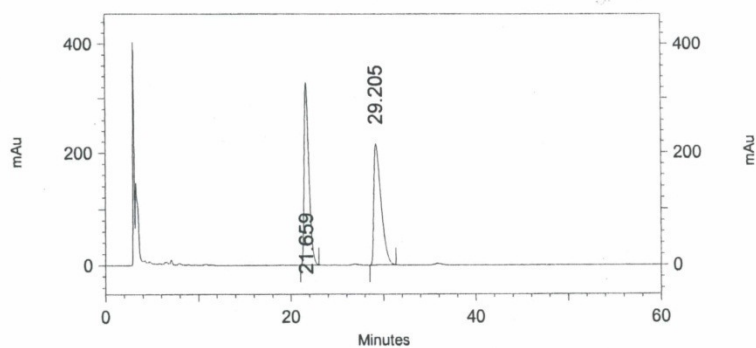
Retention Time	Area	Area Percent
14.768	9201314	94.666
21.056	518409	5.334



205Ijw_AD9505IP_60min.met4-5-2008

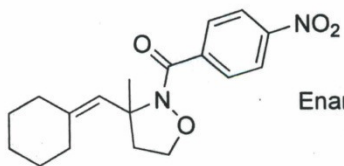
AD\jw_AD9505IP_60min.met

escription: {Data Description}



1: 230 nm, 4 nm Results

Retention Time	Area	Area Percent
21.659	11592778	49.963
29.205	11610167	50.037

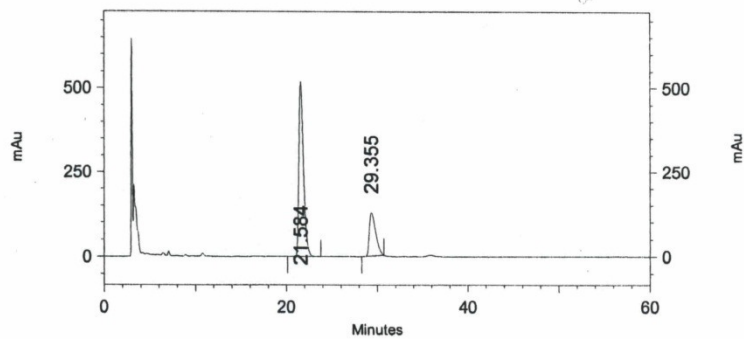


Enantioenriched

AD9505IP_60min.met4-5-200

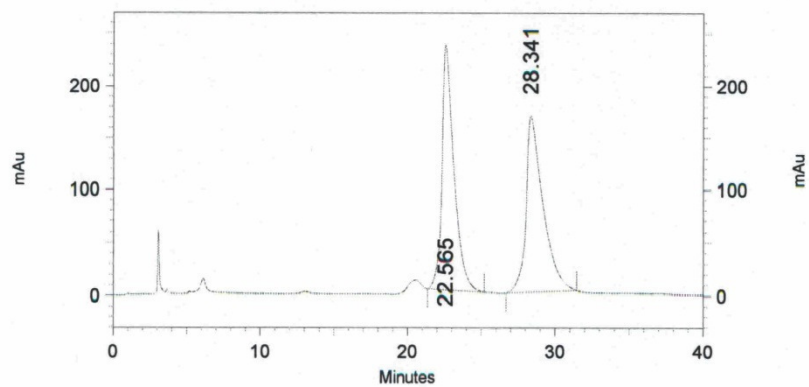
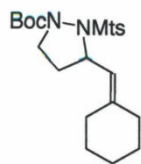
05IP_60min.met

Description: {Data Description}



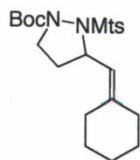
1: 225 nm, 4 nm Results

Retention Time	Area	Area Percent
21.584	18252687	74.762
29.355	6161768	25.238

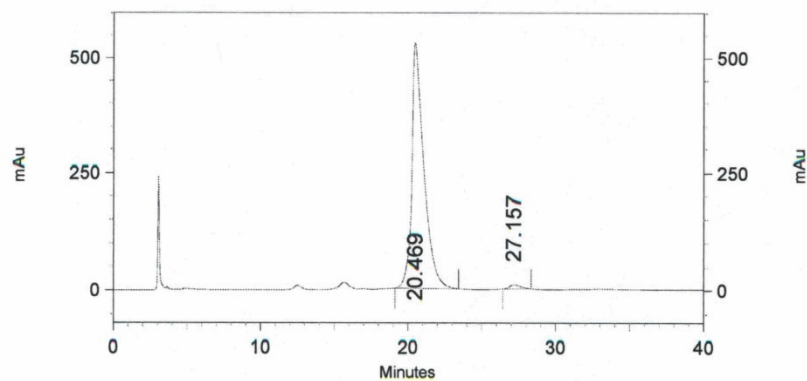


1: 230 nm, 4 nm Results

Retention Time	Area	Area Percent
22.565	13150309	49.588
28.341	13368955	50.412

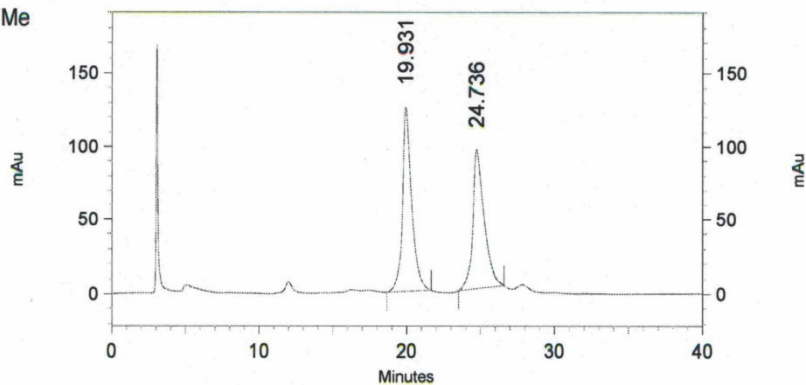


Enantioenriched



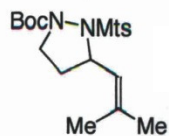
1: 230 nm, 4 nm Results

Retention Time	Area	Area Percent
20.469	29776859	98.393
27.157	486388	1.607

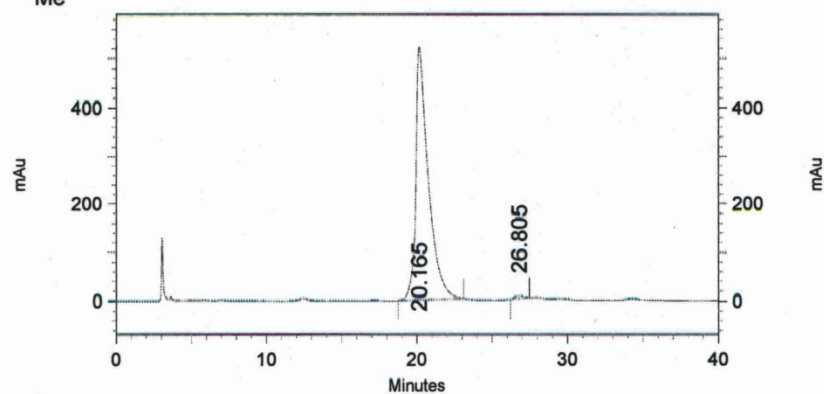


1: 230 nm, 4 nm Results

Retention Time	Area	Area Percent
19.931	5398688	51.840
24.736	5015495	48.160



Enantioenriched



1: 230 nm, 4 nm Results

Retention Time	Area	Area Percent
20.165	30024208	99.179
26.805	248513	0.821

Chapter 2:

Mechanistic Studies of Gold(I)-Catalyzed Hydroamination of Allenes and Dienes

A portion of this work has been published in Wang, Z. J.; Benitez, D.; Tkatchouk, E.; Goddard, W. A.; Toste, F. D. “Mechanistic Study of Gold(I)-Catalyzed Intermolecular Hydroamination of Allenes” *J. Am. Chem. Soc.* **2010**, *132*, 13064-13071¹ and Kanno, O.; Kuriyama, W.; Wang, Z. J.; Toste, F. D. “Regio- and Enantioselective Hydroamination of Dienes by Gold(I)/Menthol Cooperative Catalysis” *Angew. Chem. Int. Ed.* **2011**, *42* 9919-9922.

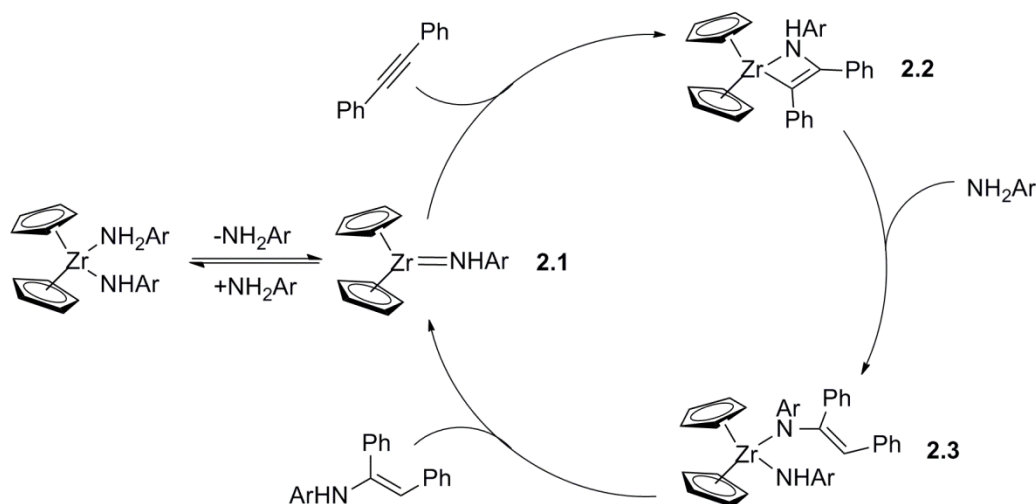
¹ Dr. Diego Benitez and Ekaterina Tkatchouk performed the computational studies of intermolecular allene hydroamination. ² Dr. Osamu Kanno and Wataru Kuriyama performed the initial reaction discovery, catalyst optimization and substrate scope studies for diene hydroamination.

Introduction

Many methods for hydroamination using transition metal complexes incorporating group 4, 9, 10, 11 metals have emerged.¹ The product selectivities observed and conditions required in these reactions are as diverse as the mechanisms by which catalysis proceeds.² As hydroamination requires the addition of an amine across a carbon-carbon multiple bond, catalysts can accelerate the reaction by either binding to the amine to form a more activated nucleophile, or coordinating to the π -bond to form a better electrophile. Transition metal catalysts can undergo both of these pathways, depending on the metal center used. For instance, while early transition metals like titanium react readily with the amine to form reactive amido and imido-complexes,³ late metals like Pt(II) favor pi-bond activation pathways.⁴ In addition to transition metals, alkali metals and lanthanides have also been used in hydroamination; the mechanism of these processes are also distinct⁵ but will not be discussed here.

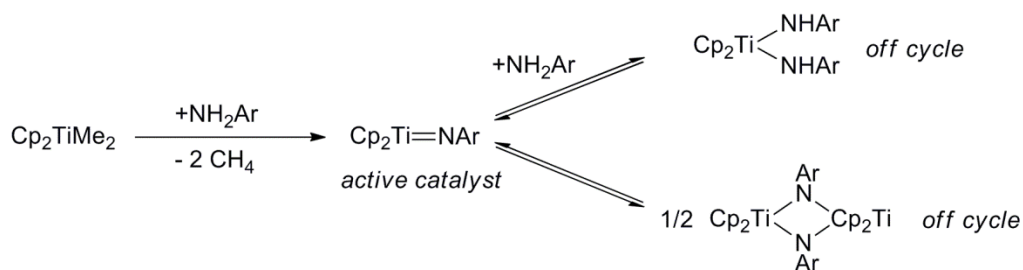
The mechanism of catalytic intermolecular hydroamination has been studied for a number of transition metal catalysts. In particular, both Bergman and Doye have reported detailed mechanistic investigations of zirconium and titanium-mediated hydroamination.^{6,7} The precatalyst in these reactions is a titanium or zirconium bisamide complex, which can enter the catalytic cycle as the metal-imido (**2.1**) after loss of an amine (Figure 2.1). Formation of the metal-imido complex is reversible and amine competes with alkyne for reaction with **2.1**. Addition of **2.1** across an alkyne forms an aza-metallocyclobutane (**2.2**), which can then be protonated by another amine to provide complex **2.3**. Extrusion of the product then reforms **2.1**. Kinetic analysis of catalytic intermolecular alkyne hydroamination by $\text{Cp}_2\text{Zr}(\text{NHAr})_2$ showed first order dependence in catalyst, inverse first order dependence in amine, and first order dependence in alkyne, consistent with reversible formation of the metal-imido complex **2.1**. Interestingly, the rate of reaction is enhanced using bulkier amines, as release of strain with loss of amine drives formation of **2.1**.

Figure 2.1. Mechanism of zirconium-bisamide catalyzed intermolecular hydroamination of alkynes.



Kinetic analysis of related reactions catalyzed by titanium complexes reveals that a similar mechanism is operative. Remarkably, the titanium-imido complexes are isolable and can be used for allene hydroamination at moderate temperatures.. The reaction is selective for amine addition to the C₂ position of allene. DFT calculations performed on this and related systems show that formation of the aza-metallacycle is rate limiting for allene and alkyne but that protonation of the metallacycle by amine is rate limiting with ethylene.⁸ Doye and Pohlki have also posited that a dimeric titanium complex may be in equilibrium with the active imido species (Scheme 2.1).⁷

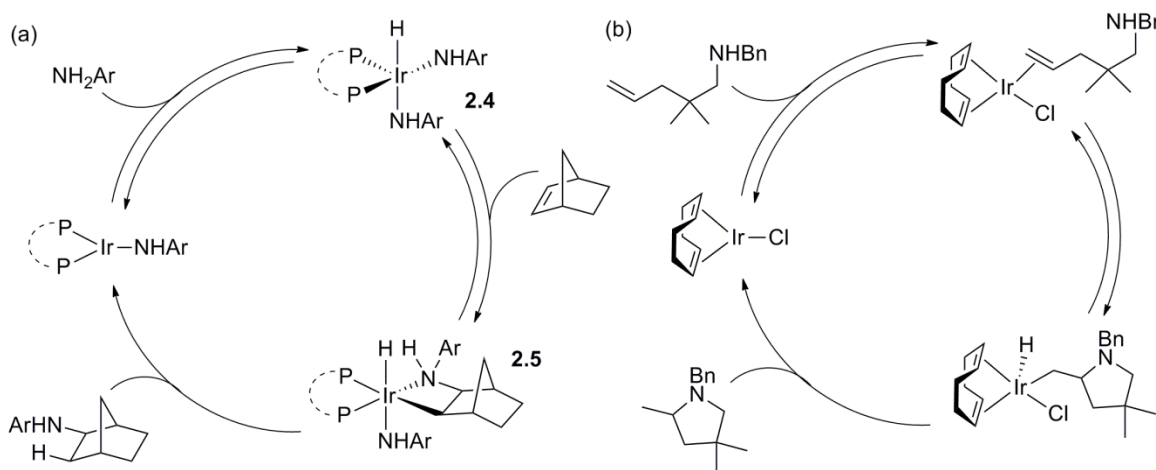
Scheme 2.1. Titanium(IV)-imido complex in equilibrium with the bisamido-complex and a Ti(IV)-dimer.



In recent years, a number of group 9 rhodium and iridium complexes have also been used in regio- and enantioselective hydroamination of olefins.⁹ In particular, progress has been made toward general methods for enantioselective hydroamination and Anti-Markovnikov-selective addition to terminal olefins. The mechanism of norbornene hydroamination with aniline in the presence of stoichiometric iridium was first studied by Milstein and coworkers¹⁰ and a similar reaction pathway was proposed for the enantioselective catalytic reaction developed years later by Hartwig (Figure 2.2a).¹¹ Activation of the nucleophile occurs via oxidative addition across the N-H bond to form iridium-bisamido complex **2.4**. Olefin insertion into the amido bond provides complex **2.5**, which then undergoes C-H reductive elimination to provide the desired product with concomitant regeneration of the active catalyst. Interestingly, both first order and saturation kinetics can be observed for norbornene, suggesting that the rate determining step can change depending on the concentration of this substrate. However, if a simple aliphatic olefin is used, first order kinetics in the alkene substrate is always observed and reductive elimination is predicted to be the rate limiting step. A similar mechanism has been proposed for Rh(I)-mediated hydroamination.¹²

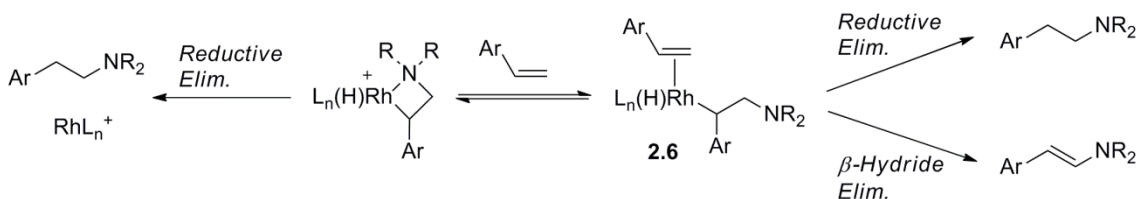
Recently, a second mechanism for this reaction has been presented based on computational studies. Stradiotto and coworkers have proposed that when the iridium center is too electron poor to undergo oxidative addition, olefin coordination may occur first (Figure 2.2b).¹³ In this case, addition of the amine to the olefin followed by formation of an Ir(III)-hydride generates the analogous intermediate previously proposed. Reductive elimination is again predicted to be the rate-limiting step.

Figure 2.2. Mechanisms proposed for Ir(I)-catalyzed hydroamination (a) for electron rich complexes, as determined by Hartwig and (b) for electron-deficient complexes, as reported by Stradiotto.



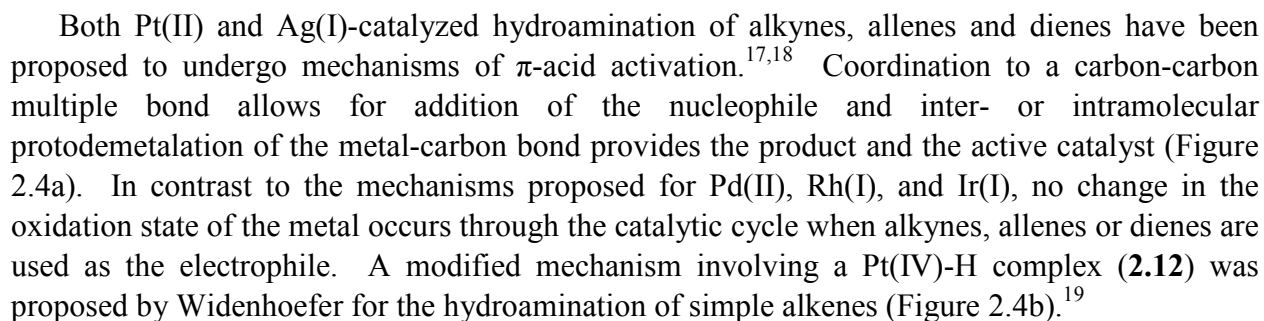
Interestingly, in the hydroamination of styrene or linear olefins, β -hydride elimination can compete with C-H reductive elimination and both hydroamination and oxidative amination products can be observed (Scheme 2.2).¹³ The rhodium dihydride complex formed as a result of β -hydride elimination can hydrogenate an equivalent of styrene to ethyl benzene to regenerate the Rh(I)-catalyst. However, β -hydride elimination is proposed to proceed through alkene-complex **2.6**, and indeed higher concentrations of alkene seem to favor formation of the enamine product over the amine product. By modulating the substrate concentrations, Hartwig and coworkers were able to observe divergent selectivity for the two products in the Rh(I) catalyzed hydroamination of styrenes.¹⁴

Scheme 2.2. Competing pathways for formation of amine and enamine products in Rh(I)-catalyzed hydroamination.



A number of group 10 and 11 metals readily catalyze hydroamination reactions and a variety of methods have been developed using Pd(II), Pt(II), Ag(I), and Au(I)-complexes.¹⁵ In general, these metals favor mechanisms involving activation of the olefin for nucleophilic addition. For instance, the active catalyst in the Pd(II) hydroamination of vinyl arenes has been determined to be a palladium-hydride complex **2.7** (Figure 2.3).¹⁶ Olefin insertion into the Pd-H bond generates a η^3 -phenethyl complex **2.8**. The enantiopure (*S*)-Pd-phenethyl-(*R*)-BINAP complex was isolated and nucleophilic addition to this complex proceeds with inversion, suggesting external nucleophilic attack. Dissociation of the product and proton transfer regenerates **2.7**.

Figure 2.3. Pd(II)-catalyzed hydroamination, proceeding through Pd-H complex.



The figure displays two catalytic cycles for the hydroamination of alkenes using Pt(II) complexes.

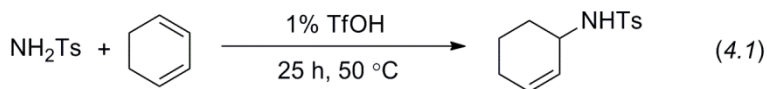
a) Catalytic cycle for the hydroamination of an alkene (R-CH=CH₂) with an amine (RHN-CH₂-CH=CH-R¹). The cycle involves the following steps:

- Initial complex:** A Pt(II) complex with two phosphine ligands (P) and two chloride ligands (Cl).
- Alkene coordination:** The alkene coordinates to the Pt center, forming a π-allyl complex.
- Amine coordination:** The amine coordinates to the Pt center, forming a Pt(IV) complex.
- Product release:** The product, an alkylamine, is released, regenerating the initial Pt(II) complex.

b) Catalytic cycle for the hydroamination of an alkene (R-CH=CH₂) with an amine (RHN-CH₂-CH=CH-R¹). The cycle involves the following steps:

- Initial complex:** A Pt(II) complex with two phosphine ligands (P) and two chloride ligands (Cl).
- Alkene coordination:** The alkene coordinates to the Pt center, forming a π-allyl complex.
- Amine coordination:** The amine coordinates to the Pt center, forming a Pt(IV) complex.
- Product release:** The product, an alkylamine, is released, regenerating the initial Pt(II) complex.

In 2006, Hartwig and coworkers performed a direct comparison of hydroamination and hydroalkoxylation by metal triflates of Cu(II), Ag(I), Au(I), and Fe(III) with the analogous transformation by HOTf at moderate temperatures.²⁰ Interestingly, the reactions catalyzed by metal triflates proceeded at similar rates and selectivities with that catalyzed by triflic acid (eq. 4.1). These results called into question whether hydroamination with metal triflates were catalyzed by the metal complex or trace amounts of triflic acid. Furthermore, a similar study of Pt(II) catalyzed hydroarylation showed that the hydroarylation reaction was also likely to be mediated by acid rather than metal.²¹

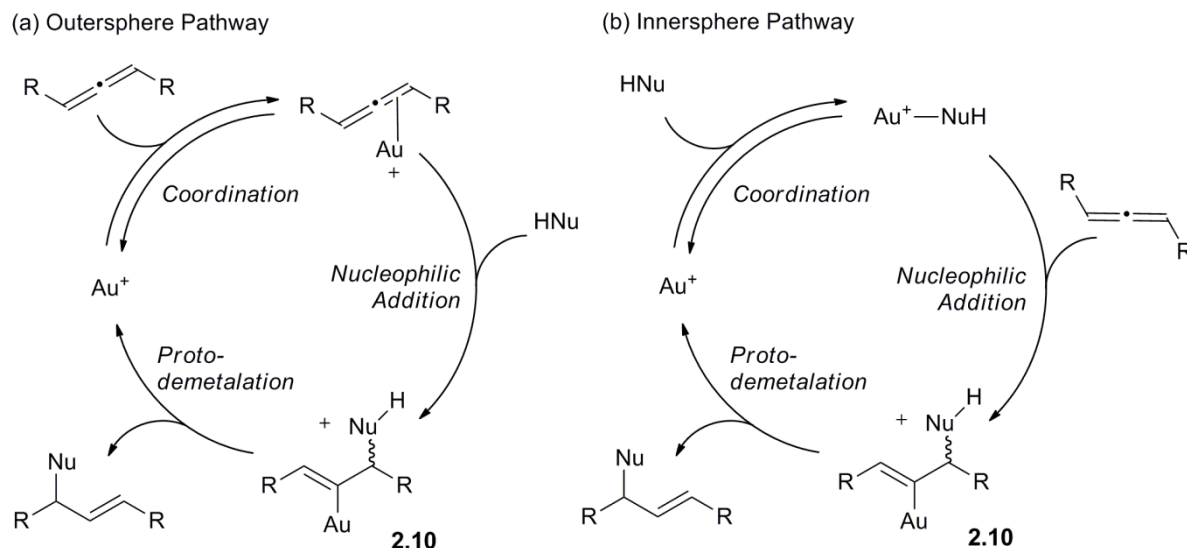


In recent years, a number of racemic and enantioselective gold(I) mediated hydroamination, hydroarylation and hydroalkoxylation reactions have emerged.²² The stability of gold(I) complexes to air and moisture renders gold catalysis a practical and mild method for bench top synthesis.²³ However, the mechanism of this important class of reactions is only beginning to be explored. While multiple mechanisms for the hydroamination, hydroalkoxylation and hydroarylation of allenes have been proposed, few studies regarding the nature of the active catalyst, the rate limiting step of the reaction, and the role of allene and nucleophile in the transformation have been performed.²⁴⁻²⁷

While experimental observations in gold(III)-catalyzed hydroamination and hydroalkoxylation reactions suggest that these reactions proceed through an inner sphere mechanism,²⁸ both inner sphere and outer sphere mechanisms for nucleophilic addition to allenes promoted by gold(I) complexes have been proposed (Figure 2.5).^{29, 30} In the outer sphere mechanism the cationic gold(I) complex acts as a π -acid to induce addition of the nucleophile across the C-C π -bond. Protodemetalation of the vinyl gold intermediate then regenerates the gold(I) catalyst (Figure 2.5a). In the inner sphere mechanism, a gold(I)-amine or gold(I)-amido complex is formed and addition of the nucleophile across an olefin in an intermolecular fashion, or via a tri-coordinate gold-olefin-amine complex can form vinyl gold complex **2.10** (Figure 2.5b). Bertrand has reported isolation of a catalytically competent N-heterocyclic carbene gold(I)-amine complex for allene hydroamination.³⁰ These results suggest that gold(I)-amines may indeed participate in the catalytic cycle.

In both mechanisms, monomeric cationic gold(I) complexes are proposed to be the catalytically relevant species. However, the “aurophilicity” of gold(I)^{23,31,32} and the number of reported transformations featuring dinuclear complexes in gold(I) catalysis suggest that a dimeric gold(I) complex may be involved in the catalytic cycle. Furthermore, Gagné has described the isolation of a vinyl-gold dimer from allene hydroarylation reaction,²⁷ suggesting that dinuclear gold(I) complexes should also be considered as potential intermediates. Thus, a kinetic study of this class of reactions is needed to determine the role of each reagent in the catalytic cycle and the composition of the rate limiting transition state.

Figure 2.5. Outer sphere and inner sphere mechanisms proposed for the hydroamination of allenes with gold(I) catalysts.



Part of the challenge of performing detailed kinetic studies of gold(I) catalyzed hydroamination reactions is that many of the most active catalysts employed are generated *in situ* from gold(I) trimers or the gold chloride and the corresponding silver salt, making it difficult to determine the precise concentration of catalyst employed.^{33,34} In 2009, we reported the intramolecular hydroamination reaction of allenes with hydrazine nucleophiles catalyzed by an isolable gold(I) complexes at room temperature.³⁵ We hypothesized that an intermolecular variant of this transformation could provide a valuable platform for a systematic study of the mechanism of the reaction. To distinguish between the inner- and outer sphere mechanisms, and to discover the stoichiometry of gold catalyst in the rate-determining transition state, a detailed study was performed to determine: (1) the order of the reaction in each reagent (2) the resting state of the catalyst, the nature of other intermediates within the catalytic cycle (3) the effect of electronics of the catalyst on the rate of reaction and (4) the reversibility of the reaction.

While many transformations for the gold-mediated addition of nucleophiles to alkynes and allenes, far fewer examples of hydroamination or hydroalkoxylation of dienes and simple olefins have been reported. Recently, we have also developed a method for the enantioselective intramolecular hydroamination of dienes.³⁶ Remarkably, this reaction proceeded to high conversion only in the presence of alcohol solvent or a protic additive like menthol. Furthermore, the addition of alcohol completely reverses the product regioselectivity observed. These experimental observations suggest that the two related hydroamination reactions may actually proceed via different mechanisms and a kinetic study of both systems is needed to elucidate the subtle differences. Lastly, determining the role of the alcohol additive in the reaction may extend the utility of such additives to other gold(I)-catalyzed transformations.

Results

Hydroamination of allenes

We began our studies with 1,7-diphenylhepta-3,4-diene (**1.38**), because the symmetry of the substrate greatly simplified the number of chemically distinct environments in which the gold(I) catalyst could coordinate. Recently, $\text{Ph}_3\text{PAuNTf}_2$ has been effectively used in the activation of carbon-carbon multiple bonds³⁷ and we hypothesized that this isolable complex would be a reliable Au^+ source for mechanistic analysis. We found that **1.38** underwent the desired reaction with 2.5 equiv of methyl carbazate and 9 mol% $\text{Ph}_3\text{PAuNTf}_2$ in MeNO_2 at 45 °C, providing the hydroamination products in a 5:1 *trans:cis* ratio with greater than 95% conversion after 12 h (eq 2.2). The pK_b of methyl carbazates has been determined to be 10.5, rendering acid catalysis unlikely under catalytic conditions. As a control, we performed the hydroamination reaction in the presence of 20 mol% HNTf_2 or 10 mol% AgNTf_2 (eq 4.3 and 4.4, respectively) and saw very little conversion to desired product, suggesting that catalysis is indeed mediated by $\text{Au}(\text{I})$. Monitoring the first 3.25 h of the reaction by ^1H NMR at 45 °C showed that the reaction was remarkably clean and that the total concentration of **1.38** and **1.39** during the course of the reaction was consistent with the concentration of **1.38** at $t = 0$ (Figure 2.6). We were encouraged by these results to further examine the precise role of the $\text{Ph}_3\text{PAuNTf}_2$ in the catalytic cycle.

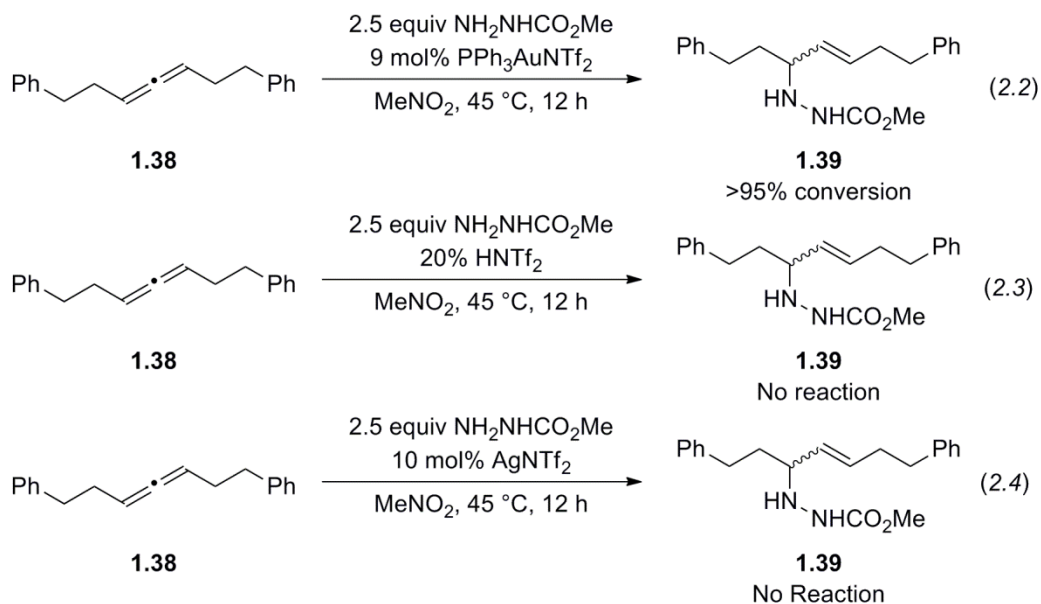
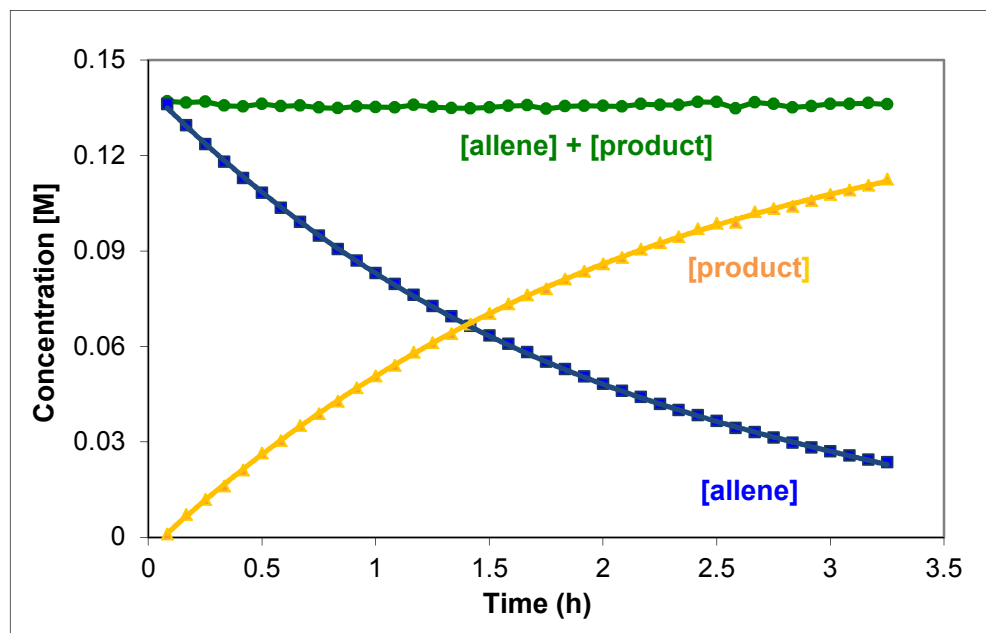


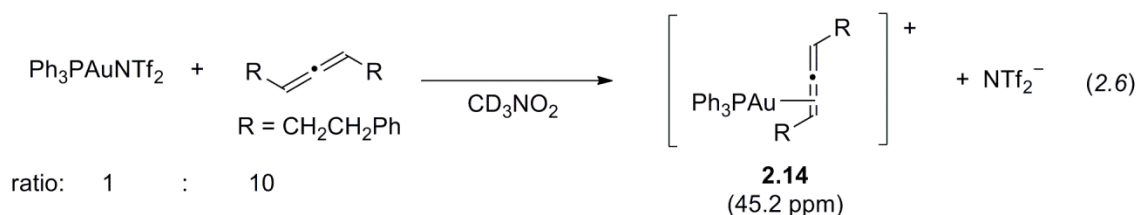
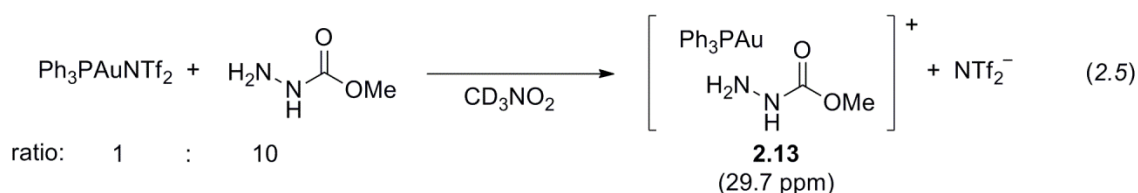
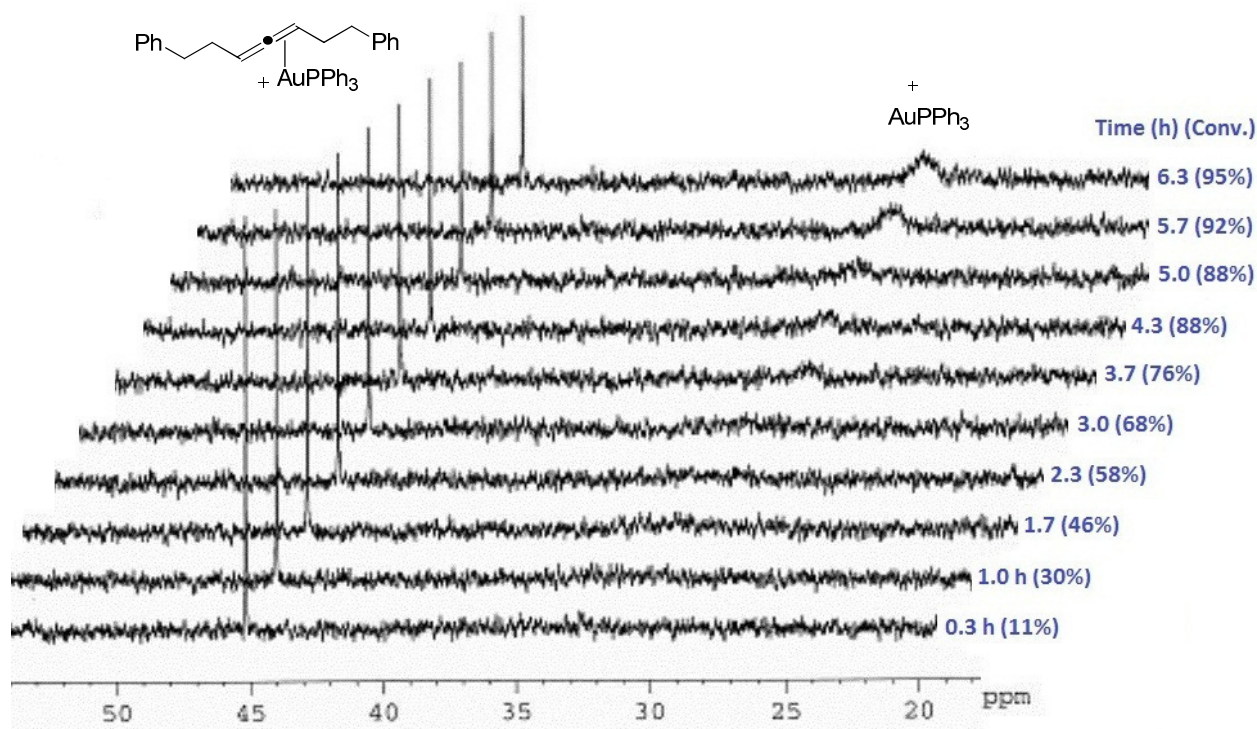
Figure 2.6. Reaction of allene **1.38** with methyl carbazate where ■ = [**1.38**], ▲ = [**1.39**], and ● = [**1.38**] + [**1.39**]. See eq. 2.2 for reference.



Phosphorus NMR methods have been previously used to study gold(I) intermediates and the ^{31}P NMR signal of the phosphine ligand was found to be very sensitive to the electronic environment around the gold center.³⁸ Upon addition of the catalyst to a reaction mixture containing **1.38** and methyl carbazate, the signal corresponding to the $\text{Ph}_3\text{PAuNTf}_2$ ($\delta = 30.3$ ppm) vanished and a new signal at 45.2 ppm was observed. As the reaction progressed and the concentration of **1.38** remaining in solution decreased, a second broad peak at 30 ppm also appeared (Figure 2.7).

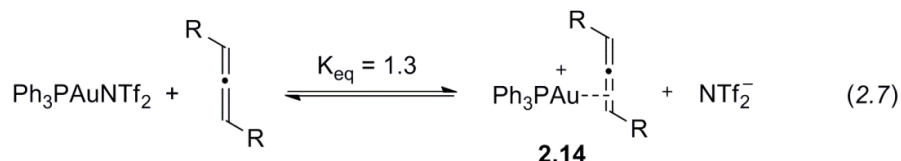
Both gold-amine³⁹ and gold-allene^{40,41} complexes have been previously postulated as intermediates in gold catalyzed reactions. To determine the nature of the compounds comprising the observed peaks at 30 and 45 ppm, we independently prepared two samples containing ($\text{Ph}_3\text{PAuNTf}_2$ and methyl carbazate, in a 1:10 ratio) and ($\text{Ph}_3\text{PAuNTf}_2$ and **1.38**, in a 1:10 ratio) in CD_3NO_2 . The sample containing $\text{Ph}_3\text{PAuNTf}_2$ and methyl carbazate showed a broadened ^{31}P NMR signal at δ 29.7 ppm (eq 2.5), in the same region as the second peak that appeared as catalytic reaction progressed. The second sample containing $\text{Ph}_3\text{PAuNTf}_2$ and **1.38**, however, showed the same ^{31}P NMR signal at 45.2 ppm as was observed in the catalytic reaction (eq 2.6).

Figure 2.7. The hydroamination reaction was monitored by ^{31}P NMR spectroscopy.



The peak at 45.2 ppm is consistent with the ^{31}P NMR shifts of other alkyl- and vinyl- AuPPh_3 species reported in the literature.⁴²⁻⁴⁶ In addition, the same species can be independently generated from a solution of Ph_3PAuCl and AgBF_4 in the presence of **1.38** without additional NTf_2^- . Thus, we hypothesized that this peak corresponded to a Ph_3PAu^+ -allene complex with no coordinated counterion. In the catalytic reaction, this complex is in equilibrium with other cationic gold species, such as Ph_3PAu^+ and Ph_3PAu^+ -carbazate. When the concentration of **1.38** was relatively high at the beginning of the reaction, the equilibrium favored the gold-allene complex. As the reaction progressed, the concentration of **1.38** decreased and the equilibrium shifted such that the other cationic gold species were also observable by NMR. Attempts to isolate complexes **2.13** or **2.14** were unsuccessful.

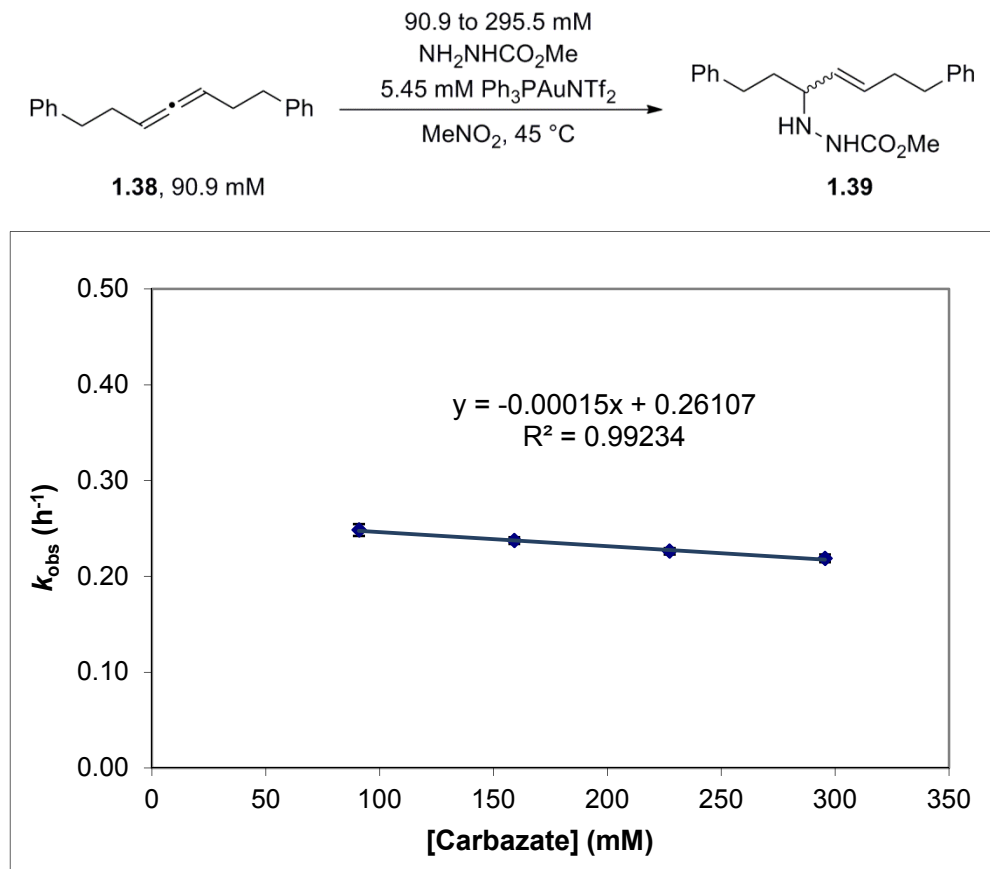
The composition of the cationic gold species observed under catalytic conditions could not be determined as both Ph_3PAu^+ and gold-carbazate complex **2.13** show phosphorus NMR signals around 30 ppm. In the absence of nucleophile, the K_{eq} for the equilibrium between allene **1.38** and $\text{Ph}_3\text{PAuNTf}_2$, and complex **2.14** was found to be 1.32 at 50 °C using ^{31}P NMR with PPh_3 internal standard and sufficient relaxation delay between scans (eq 4.8). This value is within an order of magnitude to the K_{eq} reported for structurally similar gold(I) pi-alkene complexes.⁴⁷



Due to the C_2 symmetry of the allene, two diastereotopic π -gold complexes could theoretically be formed; yet we could not resolve the two complexes by either ^{31}P or ^1H NMR at low temperature (0 to -84 °C). However, computational studies have predicted the barrier for exchange between the two diastereotopic faces of a simple disubstituted alkyl allene to be very low.⁴⁸ In addition, the energy difference between the two π -complexes that could form is calculated to be only 1.0 kcal/mol. Thus, it is likely that under catalytic reaction conditions, this species is two-coordinate cationic gold-allene complex with a fully dissociated counterion, where the gold center is rapidly exchanging between the two faces of the allene.

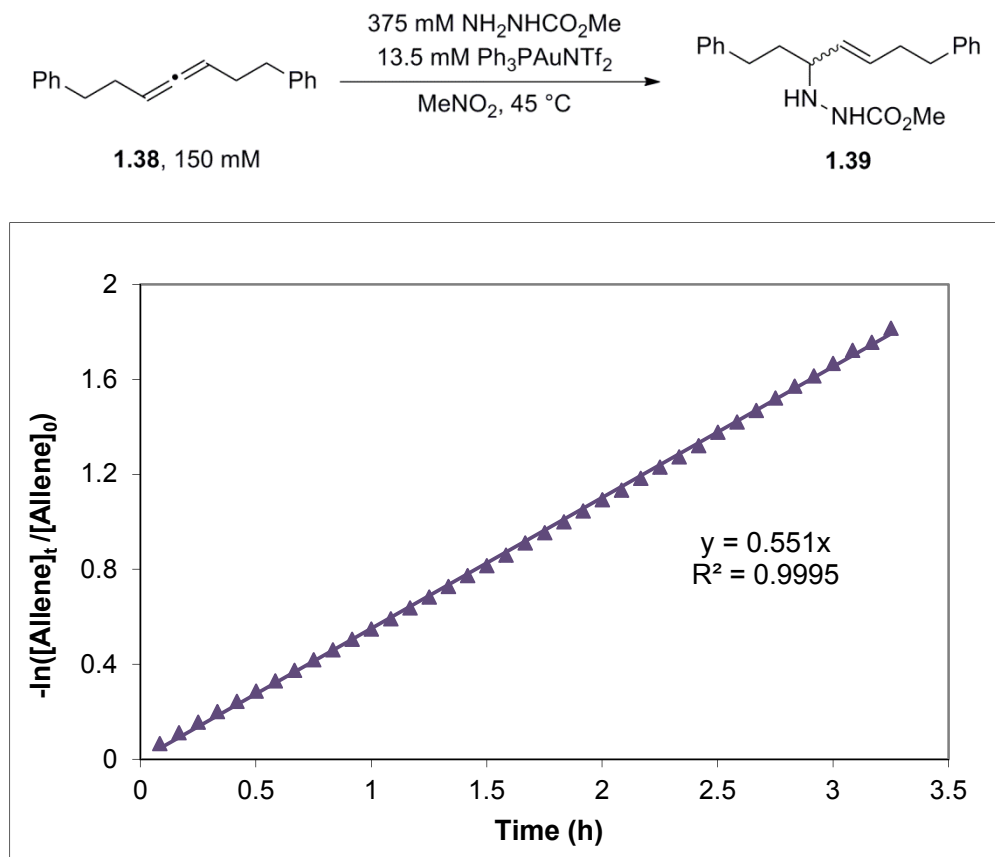
Order in Nucleophile. In order to determine the rate-determining transition state for the catalytic reaction, we sought to establish kinetic order of the reaction in $\text{Ph}_3\text{PAuNTf}_2$, **1.38**, and methyl carbazate. We began our studies by examining the order of the nucleophile by the method of initial rates. The allene **1.38** (90.9 mM) and $\text{Ph}_3\text{PAuNTf}_2$ (5.45 mM) were combined with varying concentrations of methyl carbazate from 90.0 to 295.5 mM in CD_3NO_2 at 45 °C. The reactions were monitored by ^1H NMR and a plot of k_{obs} ,⁴⁹ (as determined by $(\Delta \mathbf{1.39}/\Delta t)/[\mathbf{1.38}]_0$, where $[\mathbf{1.38}]_0 = 90.91$ mM) at each concentration of methyl carbazate provided a straight line with $R^2 = 0.9923$ and a slope of -0.00015 h^{-1} (Figure 2.8). The order in methyl carbazate was verified by a least squares fit to $f(x) = ax^n$, which provided $n = -0.108$ (Supporting Information, Figure S2.3). The small systematic variation observed in rate constants when the concentration of nucleophile is changed is likely due to changes in solvent polarity caused by varying concentration of carbazate, rather than true kinetic order of methyl carbazate in the overall rate law. These results indicate that methyl carbazate is likely not involved in the rate-determining transition state. In contrast, previously proposed mechanisms have implied nucleophilic addition or protodemetalation to be the rate-limiting step in gold(I) catalyzed hydroamination.^{50,51}

Figure 2.8. A plot of k_{obs} versus concentration of methyl carbazate, where k_{obs} was determined by the method of initial rates.



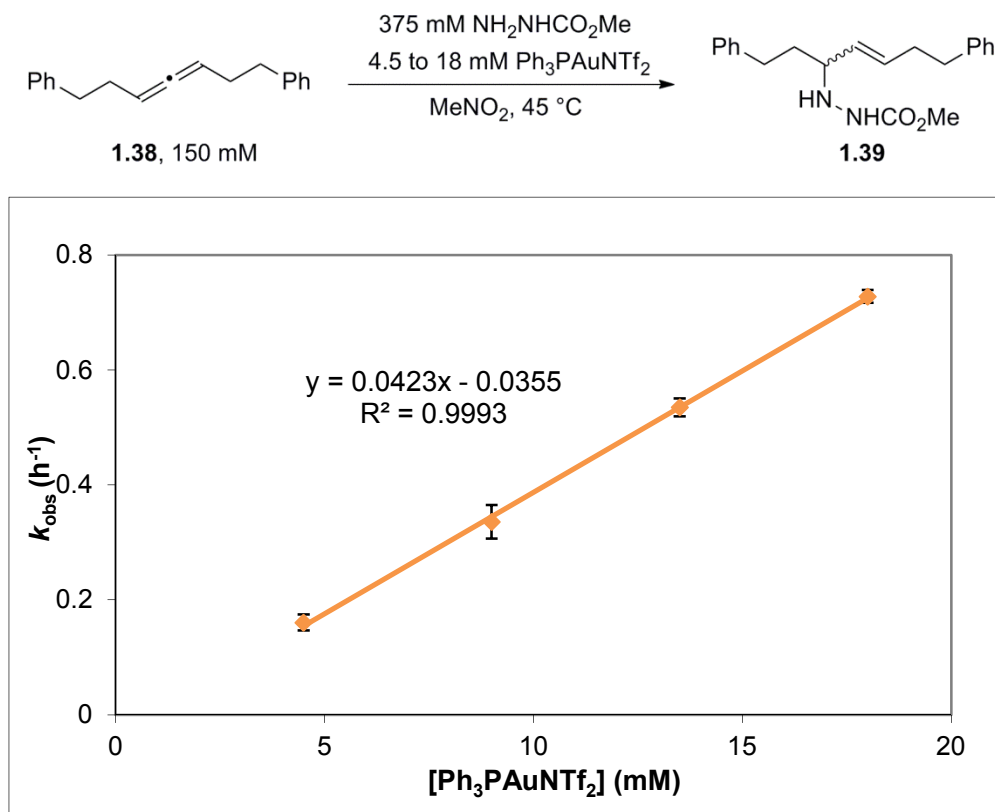
Order in Allene. The order in **1.38** was next determined by monitoring the reaction of **1.38** (150 mM), methyl carbazate (325 mM) and $\text{Ph}_3\text{PAuNTf}_2$ (13.5 mM) in CD_3NO_2 at 45°C (Figure 2.9) by ^1H NMR. The reaction followed pseudo first order kinetics in **1.38** and provided linear plots of $-\ln([\text{Allene}]_t/[\text{Allene}]_0)$ vs. time with $R^2 = 0.9995$. A similar first-order fit is observed at four different catalyst concentrations from 3-12 mol% $\text{Ph}_3\text{PAuNTf}_2$. The pseudo first order rate constants (k_{obs}) measured reflects the rate of formation of both *trans* and *cis* hydroamination products. The first order dependence on **1.38** implies that the allene is involved in the turnover limiting transition state and that there is an equilibrium between the free and gold-bound allene, such that the reaction does not exhibit saturation kinetics in allene.

Figure 2.9. A representative plot of $-\ln[1.38(t)/1.38_0]$ versus time (h) for determination of k_{obs} in the reaction of allene **1.38** with methyl carbazate.



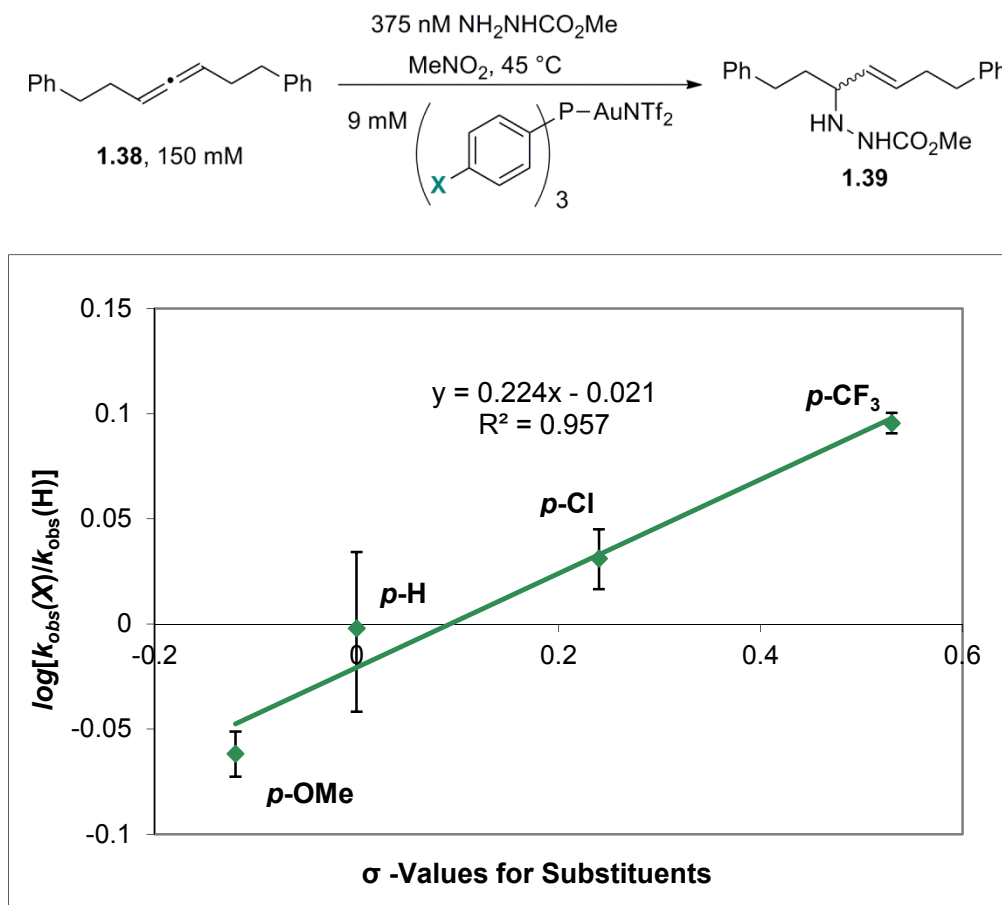
Order in Gold. The order in $\text{Ph}_3\text{PAuNTf}_2$ was examined by measuring the pseudo-first order rate constant, k_{obs} , for the reaction at various catalyst loadings. Allene **1.38** (150 mM) and methyl carbazate (325 mM) were combined with various concentrations of $\text{Ph}_3\text{PAuNTf}_2$ (4.5 to 18 mM) in CD_3NO_2 at 45°C . Plotting the measured k_{obs} of the reaction at a range of catalyst loadings provided a straight line with $R^2 = 0.9993$ (Figure 2.10). This result suggests that the overall reaction is first order in gold and implies that the rate-limiting transition state contains only one gold center.

Figure 2.10. A plot of k_{obs} versus $[\text{Ph}_3\text{PAuNTf}_2]$, using 2.5 equiv methyl carbazate.



Hammett Analysis. The Toste group has previously investigated the ability of ligand electronics to affect the rate of certain pathways in a gold(I) catalyzed process.⁵² Thus, a Hammett study of the reaction was performed to probe the sensitivity of the reaction to changes in the electronic properties of the phosphine ligand in the $\text{Ar}_3\text{PAuNTf}_2$ catalyst. Toward this goal, phosphine gold catalysts bearing substitution in the *para* position were prepared. The reaction of **1.38** (150 mM) and methyl carbazate (325 mM) in the presence of 6 mol % (*p*-X- C_6H_4)₃PAuNTf₂ (X = CF₃, Cl, H, and OMe) in CD_3NO_2 at 45 °C was monitored by ¹H NMR. Plotting $\log[(k_{\text{obs,X}})/(k_{\text{obs,H}})]$ against σ provided a straight line ($R^2 = 0.96$) with $\rho = 0.22$ (Figure 2.11). A positive ρ value is consistent with a decrease in partial positive charge on the phosphine ligand in the transition state. The kinetic order and Hammett analysis of the reaction are consistent with the gold(I) activation of the allene as the rate-limiting transition state in the catalytic cycle.

Figure 2.11. A Hammett plot of k_{obs} for hydroamination of **1.38** in the presence of $\text{Ar}_3\text{PAuNTf}_2$.



Chirality Transfer. We sought to determine whether chirality transfer was possible from the allene to the hydroamination product to determine whether the reaction went through chiral or planar gold intermediates. While trisubstituted allenes are known to racemize rapidly in the presence of gold(I) catalysts,⁵³ good chirality transfer has been observed with some unfunctionalized disubstituted allenes.⁵⁴ In addition, chirality transfer would exclude a planar allyl cation as part of the catalytic cycle, as such a species would lead to complete racemization. Enantioenriched **1.38** (101 mM, 87% ee) was prepared by the method described by Myers⁵⁵ and was subjected to $\text{Ph}_3\text{PAuNTf}_2$ in the absence of nucleophile. Complete racemization was observed after a few hours (eq 2.8). However, when enantioenriched **1.38** was combined with methyl carbazate and $\text{Ph}_3\text{PAuNTf}_2$ at 45 °C, the hydroamination product was formed with chirality transfer. The enantiomeric excess of the major hydroamination product **1.38_{trans}** was determined by chiral HPLC analysis and summarized in Table 2.1.

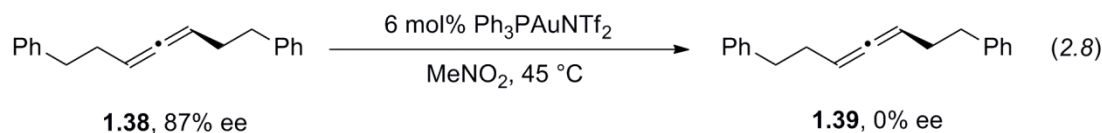


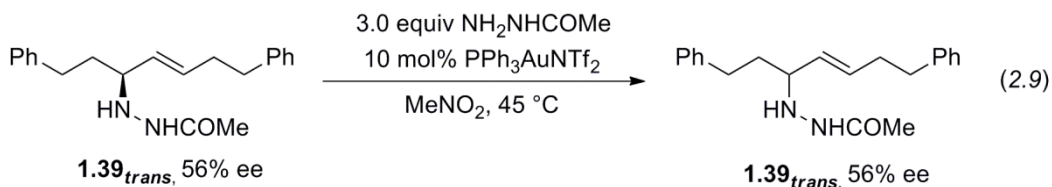
Table 2.1. Chirality transfer from enantioenriched **1.38** to product with varying concentration of methyl carbazate.

Entry	Equiv. of Carbazate	X	Yield (%) of 1.38	ee (%) of 1.38
1	1.0	H	81	28
2	2.0	H	75	48
3	4.0	H	81	56
4	8.0	H	79	56
5	2.0	OMe	69	56
6	2.0	Cl	74	50
7	2.0	CF ₃	85	45

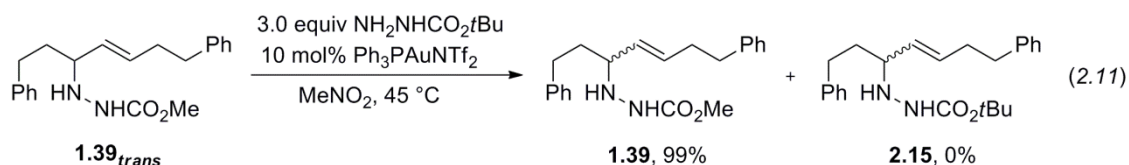
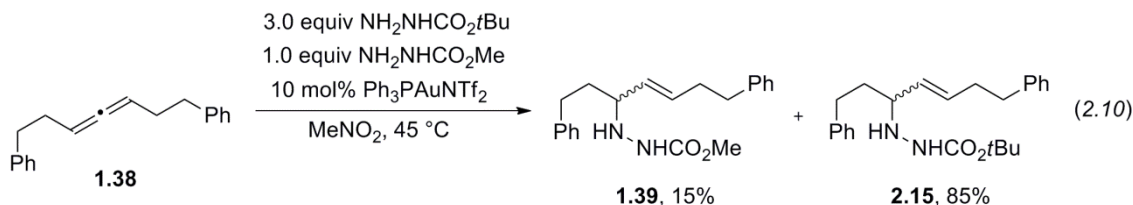
Interestingly, though some chirality transfer was observed at all concentrations of nucleophile, the highest levels of transfer were observed for reactions where greater than 4 equivalents of methyl carbazate was used. This indicates that the reaction cannot be proceeding exclusively through a planar intermediate. In addition, the ability of nucleophile concentration to affect chirality transfer suggests that racemization can occur from the chiral allyl-gold intermediate and this process proceeds at a rate competitive with trapping of the intermediate by methyl carbazate. This is in line with our previous observations that racemic allene will become enantioenriched as the hydroamination reaction progresses in presence of a chiral catalyst like (*R*)-DTBM-Segphos(AuNTf₂)₂ (see Chapter 1). The degree of chirality transfer is also affected by the electronics of the phosphine on the gold complex (Table 2.2). The highest levels of chirality transfer are observed for electron rich ligands like (*p*-MeO-C₆H₄)₃P.

Reversibility of the Reaction. While protodeauration of the gold catalyst is conventionally depicted as an irreversible process in a catalytic reaction, Lee recently reported an example of reversible hydroalkoxylation⁵⁶ in the presence of Ph₃PAuNTf₂. Furthermore, an irreversible reaction under catalytic conditions would allow us to exclude the possibility that the incomplete chirality transfer we observed previously was due to racemization of the product. To probe whether the intermolecular hydroamination reaction is reversible, enantioenriched **1.39** (56% ee)

was subjected to 2 equiv of methyl carbazate and 10 mol % achiral $\text{Ph}_3\text{PAuNTf}_2$. After 6 h, **1.39** was recovered in 56% ee with no erosion of enantiopurity (eq 2.9), supporting an irreversible protodemetalation. However, conservation of enantiomeric excess could also result from a reversible reaction that regenerates an enantioenriched allene-gold intermediate that can then reform **1.39** with good chirality transfer.



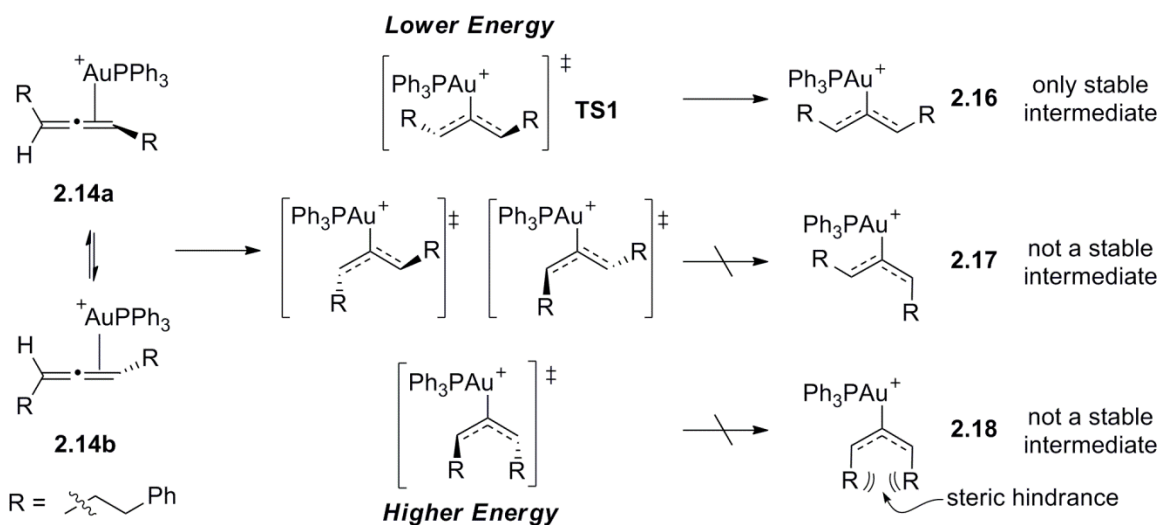
We hypothesized that a crossover experiment with a second hydrazide nucleophile would be able to distinguish between these possibilities. If a chiral allene or gold-allene complex was indeed being reversibly formed, hydroamination products from trapping with both hydrazide nucleophiles should be observed. In a competition experiment with 1 equiv methyl carbazate and 3 equiv *t*-butyl carbazate, both hydroamination products were observed in a 15:85 ratio in >95% conversion (eq 2.10), indicating that formation of **2.15** is kinetically competitive with formation of **1.39**. Thus, if the reaction is reversible and **1.39** is resubjected to catalytic conditions in the presence of 3 equiv of *t*-butyl carbazate, a mixture of **1.39** and **2.15** should be expected. However, heating the reaction to 45 °C for 8 hr produced **1.39** as the sole product (eq 2.11). The lack of detectable amounts of **2.15** indicated that chiral allene or gold-allene intermediates could not be forming reversibly under the reaction conditions.



Computational Studies. To corroborate the kinetic data observed and to gain insight into the nature of the intermediates in the catalytic cycle, we investigated the mechanism for hydroamination of allenes using density functional theory (DFT) with the B3LYP and M06 functionals. We used the experimental observations as a guide for exploring the geometry and potential energy surface for the reaction. We investigated the catalytic reaction of model (*S*)-penta-2,3-diene, methyl carbazate and $\text{Ph}_3\text{PAu(I)}^+$. We calculated the free energy of coordination of the allene to $\text{Ph}_3\text{PAu(I)}^+$ to be -9.2 kcal/mol, in favor of the allene-gold complex **2.14**.⁵⁷ Activation of **2.14** proceeds through transition state **TS1**, which lies 4.9 kcal/mol higher in energy than the planar, cationic gold(I) complex **2.16** (Scheme 2.3). Though the methyl carbazate is included in calculations, the nucleophile itself is not associated with **TS1** or **2.16**.

Widenhoefer has proposed that the activation energy for intermolecular exchange of allenes with gold(I) is low compared to free energy required for allene epimerization, and indeed we found a pre-equilibrium between **2.14a** and **2.14b**.^{48a} Furthermore, Malacria and co-workers reported that the steric hindrance at the allylic positions determines the energies and stabilities of the possible isomeric forms of the planar, cationic gold(I) complex.^{48b} In agreement with their analysis, we find that only intermediate **2.16** is stable. In comparison, intermediates **2.17** and **2.18** are not minima and relax to **2.14a** or **2.14b**.

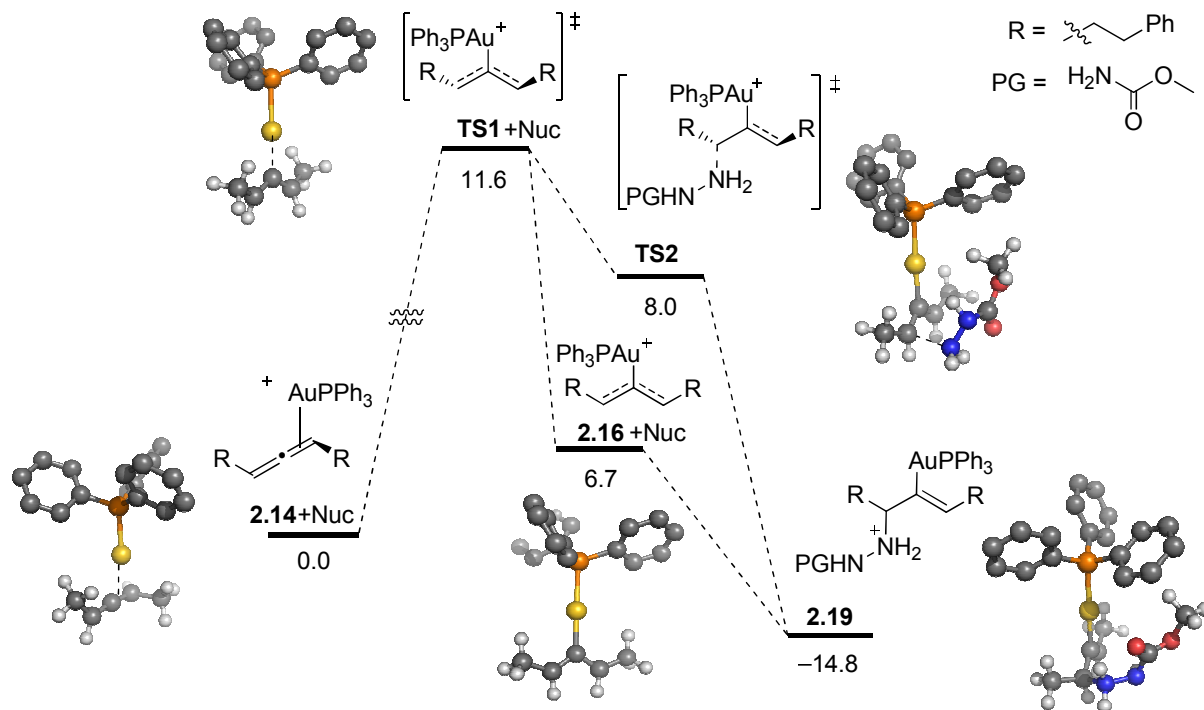
Scheme 2.3. Geometries of (*S*)-penta-2,3-diene and [Ph₃PAu]⁺ as coordination, transition state, and allylic cation complexes.



A partial reaction coordinate diagram from our computational studies is shown in Figure 2.11. As we moved further along the reaction coordinate, a second transition state (**TS2**) involving the addition of methyl carbazate to the allene-gold species was found. We found that transition state **TS1** leads to adjacent transition state **TS2** without an intervening intermediate of with appreciable lifetime. On the basis of our experimental observations and calculations, we propose a *two-step, no intermediate*⁵⁸ process similar to the one described by Nevado for a Au(I) catalyzed cyclization.⁵⁹ The geometry of the allene fragment in **TS1** and **TS2** resembles a bent allene.⁴⁸ Intermediate **2.19** ($\Delta G = -14.8$ kcal/mol) undergoes protodeauration leading to product ($\Delta G = -24.1$ kcal/mol), in agreement with the irreversibility of the reaction.

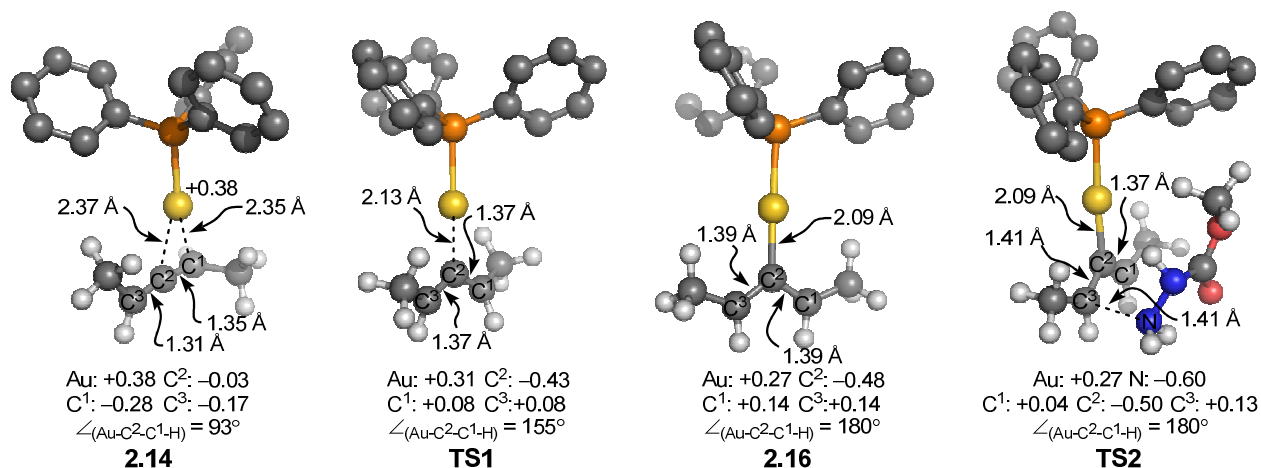
The lifetime of structures in between transition states **TS1** and **TS2** is affected by the relative concentration and reactivity of the nucleophile, and thus relates directly to the magnitude of chirality transfer. The reaction coordinate bifurcates following **TS1**, leading to **TS2** or intermediate **2.16**. At higher nucleophile concentrations, addition of the nucleophile is fast and the *two-step no intermediate* pathway is favored, leading to higher levels of chirality transfer. At lower concentrations of nucleophile, **TS1** leaks to the planar intermediate **2.16** with loss of chirality. The operating reaction mechanism is a continuum between a traditional *two-step* process with loss of chirality and a *two-step no-intermediate* process with retention of the stereochemistry.

Figure 2.12. Partial reaction coordinate diagram for Au(I) catalyzed hydroamination of (*S*)-penta-2,3-diene. Energy values are free energies (ΔG) for the lowest energy isomer at 298 K.



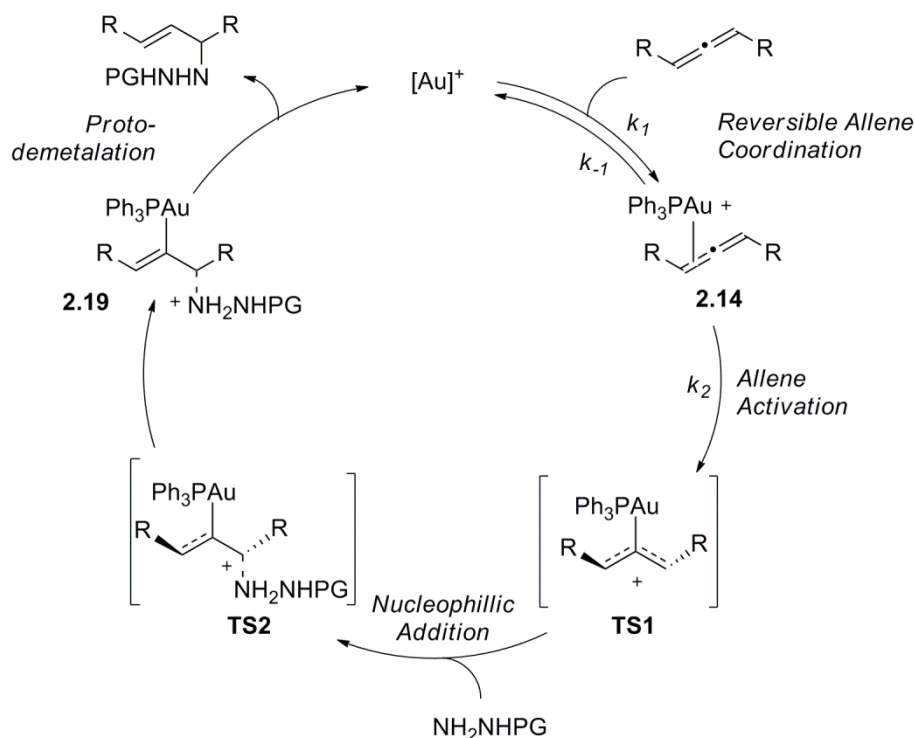
We studied the structural and electronic details of the located transition structures and compared them to those of Au-allene coordinated complex **2.14**. Shown in Figure 2.13 are key metrical parameters and natural charges derived from natural population analyses of the corresponding M06 wavefunction. We find that for **2.14**, the charge on C^3 is the least negative (vs. C^1), while the charge on C^1 is the most negative of the allene carbon atoms.

Figure 2.13. Structural and natural atomic charge of selected complexes.



On the basis of the kinetic, ligand effect, reversibility, chirality transfer, and computational studies performed, we propose mechanism for the gold(I)-catalyzed hydroamination of allenes shown in Figure 2.14. The resting state of the catalyst is consistent with a cationic gold-allene complex in which the gold moiety is rapidly exchanging between the two diastereomeric faces of the C_2 symmetric allene and is in equilibrium with other cationic gold species, denoted $[Au]^+$. As the concentration of allene is depleted through the course of reaction, the concentration of $[Au]^+$ increases. Our computational studies suggest that a bent allene-gold complex is the rate determining transition state (**TS1**) in the catalytic cycle and our kinetic data provide direct experimental support for these calculations. The overall reaction exhibits zeroth order dependence on the concentration of nucleophile, suggesting that nucleophilic addition must occur after the rate-determining step. This observation is in agreement with calculated free energy of **TS2**, which is 3.6 kcal/mol lower than that of **TS1**. In addition, the pseudo first order dependence on the concentration of allene and $Ph_3PAuNTf_2$ suggest that the catalytic species is monomeric and that the ratio of allene to catalyst in the transition state is 1:1. Thus, an inner sphere mechanism where the nucleophile coordinates to the gold center prior to or during allene activation is unlikely, as such a mechanism would exhibit positive order in nucleophile.

Figure 2.14. Proposed mechanism for hydroamination of **1** with $Ph_3PAuNTf_2$.



We have demonstrated that the nucleophilic addition and protodemetalation steps are irreversible under catalytic conditions and occur after the rate limiting transition state. Thus, we posited that our reaction could be modeled using Michaelis-Menten kinetics. The general Michaelis-Menten equation is shown in eq 2.13. Under conditions where the concentration of **1.38** is small relative to K_M and the Michaelis-Menten equation can be reduced to eq 2.14, providing a rate law that is first order in gold and **1.38**. Unfortunately, attempts to increase the concentration of **1.38** to obtain saturation kinetics in **1.38**

were unsuccessful. In particular, using a high concentration of **1.38** (up to 1.0 M) did indeed result in a rate of reaction that is lower than that predicted by eq. 2.14; however, at these concentrations, the volume of **1.38** is significant relative to the amount of MeNO₂ used and we could not rule out that the nonlinear behavior observed was due to changes in solvent polarity rather than true saturation kinetics.

$$\text{rate} = \frac{k_2[\text{Ph}_3\text{PAuNTf}_2][\mathbf{1.38}]}{[\mathbf{1.38}] + K_M} \quad \text{where } K_M = \frac{k_2 + k_{-1}}{k_1} \quad (2.13)$$

$$\text{rate} = \frac{k_2[\text{Ph}_3\text{PAuNTf}_2][\mathbf{1.38}]}{K_M} = k_{\text{obs}}[\text{Ph}_3\text{PAuNTf}_2][\mathbf{1.38}] \quad (2.14)$$

$$\text{where } k_{\text{obs}} = \frac{k_2 k_1}{k_2 + k_{-1}}$$

A Hammett study of the reaction demonstrates that changing the electronics of the Ar₃P ligand noticeably affected the rate of reaction and provides quantitative evidence that gold(I) reactivity can be modulated by ligand electronics. In particular, phosphines with electron-withdrawing *para* substituents increased the rate of the reaction while electron-donating substituents slow the reaction relative to Ph₃PAuNTf₂. This is consistent with a rate-determining transition state that exhibits a reduction in δ⁺ character on the phosphine relative to the ground state. Our proposed transition state allows for the delocalization of positive charge from the Ph₃PAu⁺ onto the allenic fragment, and is hence consistent with the ρ value observed. Furthermore, the inability to regenerate the gold-allene intermediate from the isolated hydroamination products (**1.39**) under catalytic conditions suggests that either one or both the addition or the protodemetalation steps are irreversible.

Hydroamination of Dienes

Although allenes and dienes are olefin isomers, development of enantioselective diene hydroamination methods has proved more challenging.⁵¹ However, this transformation is interesting from a mechanistic perspective due to the number of products possible from a simple intramolecular cyclization. In particular, two different 5 member ring products can be formed from cyclization: a homoallylic pyrrolidine and an allylic pyrrolidine. The relative ratios of these two products is sensitive to reaction conditions and a mechanistic analysis is needed to elucidate how each product is formed.

To develop a model reaction for enantioselective catalysis and kinetic studies, we focused on the reaction of diene **2.20** with catalytic amounts cationic gold(I) complexes. While attempts to catalyze the reaction with triphenylphosphinegold(I) and other mono-cationic gold complexes did not produce appreciable amounts of any cyclic product (Table 2.3, entry 1), we were pleased to find that the combination of (*R*)-DTBM-SEGPHOS(AuCl)₂ and AgBF₄ in dichloromethane gave pyrrolidine **2.21** exclusively in detectable 5% conversion after 24 h (entry 2). After examining a variety of protecting groups on nitrogen, we found that the Mbs (*p*-methoxybenzenesulfonyl) amine (**2.21**) gave a small enhancement in reactivity (entry 3). However, when the solvent was switched to MeOH (entry 4), we saw dramatic increases in reaction rate.

Additionally, when *i*PrOH was used as solvent, both products **2.22a** and **2.22b** were observed, with the major product **2.22a** formed in 92% enantiomeric excess (entry 5). The pronounced rate acceleration and change in product distribution suggested that alcohols are important for controlling the regioselectivity and rate of reaction.

Table 2.3. Initial screen of catalyst, protecting group, and solvent for diene hydroamination.

Entry	PG	Au Cat.	Solvent	Total Conv. (%) ^a	Ratio (2.22b : 2.22a) ^b	2.22b (%ee)	2.22a (%ee) ^c
1	Ts (2.20)	Ph ₃ PAuCl	DCM	trace	--	--	--
2	Ts	(<i>R</i>)-DTBM-SEGPHOS(AuCl) ₂	DCM	5	1 : 0	--	--
3	Mbs (2.21)	(<i>R</i>)-DTBM-SEGPHOS(AuCl) ₂	DCM	18	1 : 0	35	--
4	Mbs	(<i>R</i>)-DTBM-SEGPHOS(AuCl) ₂	MeOH	81	1 : 0.5	2	84
5	Mbs	(<i>R</i>)-DTBM-SEGPHOS(AuCl) ₂	<i>i</i> PrOH	>99	1 : 1.2	11 ^d	92

[a] Conversion was determined by ¹H NMR and HPLC. [b] A very small amount of (*Z*)-**2.22a** was included (1-3%). [c] ee corresponds to that of the (*E*)-isomer. [d] 11% ee was observed for the (*S*)-enantiomer

We next examined the effect of a range of achiral and chiral alcohols additives on the catalytic reaction in DCM. In particular, we hypothesized that a chiral alcohol may “match” the chiral information enforced by (*R*)-DTBM-SEGPHOS and lead to higher levels of selectivity. Gratifyingly, we found that *l*-menthol provided the desired products in quantitative conversion and a 1:9 ratio of **2.21**:**2.22** with excellent enantioselectivity for the major product (95% ee). Furthermore, the amount of menthol used could be reduced to 2.0 equivalents without significant impact on the regio- or enantioselectivity of reaction.

To investigate the mechanism of the hydroamination and to determine the role of gold and *l*-menthol, we monitored the reaction by ¹H NMR. For this purpose, we chose substrate **2.23**, as reaction with this diene reaches high conversion after 12 h and is thus suitable for studies by point kinetics. However, after an exhaustive solvent screen including other chlorinated solvents like DCE and chloroform, only DCM was a suitable solvent for the reaction. As the boiling

point of DCM is close to the reaction temperature, we could not reliably obtain quantitative measurements of rate constant. Furthermore, the reaction was also most selective when the BF_4^- counterion was used, but the (R) -DTBM-SEPHOS(AuBF_4)₂ complex was not isolable and needed to be generated *in situ*. Thus, the concentration of the active catalyst could not be quantitatively determined. However, we hypothesized that a comparative rate study would eliminate systematic error from solvent evaporation and *in situ* generation of the active catalyst.

We examined the reaction of **2.23** under three conditions: (1) with 2.0 equivalents of *l*-menthol as an additive (2) with 2.0 equivalents of *i*PrOH and (3) with no additives simultaneously by ^1H NMR. The reactions all exhibited first order kinetics. As two products can be formed from **2.23**, the overall first order rate constant for consumption of starting material (k_{tot}) is equal to the sum of the rate constants for the formation of each product (k_a and k_b , for formation of **2.24a** and **2.24b** respectively, Figure 2.15, Figure 2.16). Additionally the ratio of rate constants for each product, k_a/k_b , is directly proportional to the concentration of **2.24a** and **2.24b** at all times. Solving the system of equations shown below, would provide the acceleration (i.e., k_{ax}/k_a and k_{bx}/k_b , where x denotes either *i*PrOH or *l*-menthol additive) afforded by both *i*PrOH or *l*-menthol on the rate of formation of each product, relative to the background reaction in the absence of additive.

Figure 2.15. Systems of equations for diene hydroamination to obtain rate acceleration for formation of each product as a result of additive.

$$\begin{array}{l} \frac{k_a}{k_b} = R \quad \text{and} \quad \frac{k_{\text{ax}}}{k_{\text{bx}}} = R_x \\ k_a + k_b = k_{\text{tot}} \quad \text{and} \quad k_{\text{ax}} + k_{\text{bx}} = k_{\text{tot},x} \end{array} \implies \frac{k_{\text{ax}}}{k_a} = \frac{(R+1)k_{\text{tot},x}}{(R_x+1)k_{\text{tot}}} \quad \text{and} \quad \frac{k_{\text{bx}}}{k_b} = \frac{(R^{-1}+1)k_{\text{tot},x}}{(R_x^{-1}+1)k_{\text{tot}}}$$

R = Ratio of rates, no additive

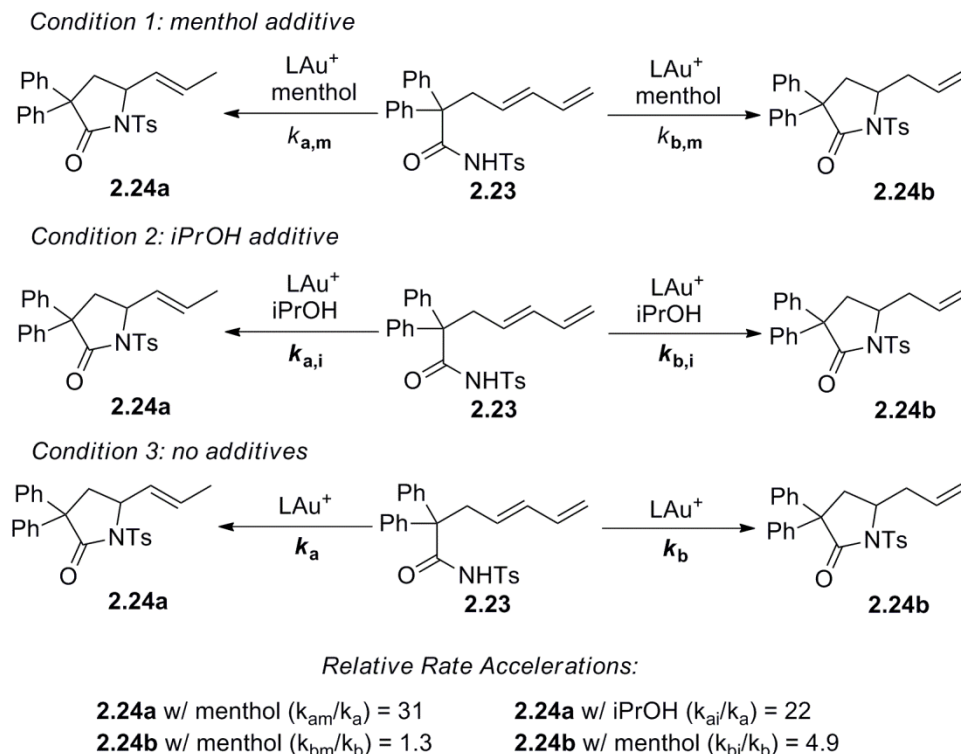
R_x = Ratio of rates, with additive x

k_{tot} = Rate constant for formation of both products, no additive

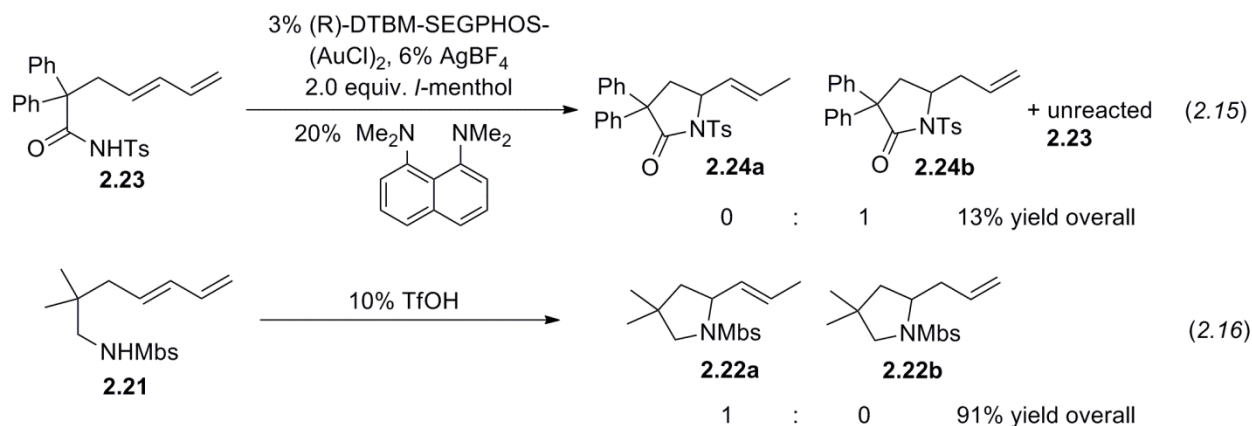
$k_{\text{tot},x}$ = Rate constant for formation of both products, with additive x

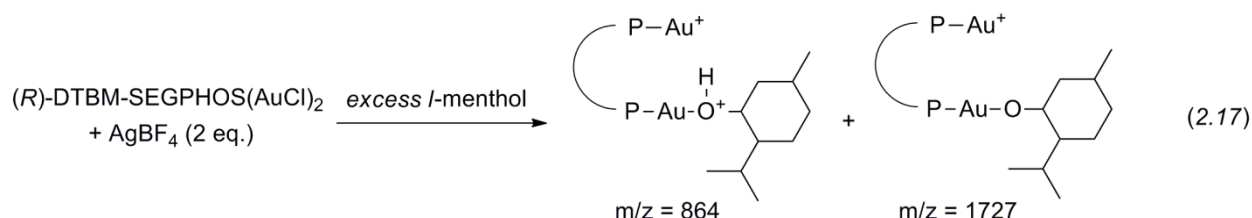
We monitored the three reactions for 14 h or until >98% conversion was reached. Gratifyingly, the ratio of the concentration of **2.24a** and **2.24b** were in general constant through the course of reaction (see experimental section for reaction traces of all three reactions). Interestingly, we found that while *l*-menthol had almost no effect on the rate of formation of **2.24b**, the addition of menthol greatly increased the rate of formation of **2.24a** (Figure 2.16).¹² Isopropanol increased the relative rate of formation of both products, but it enhanced the rate of formation of the allylic product **2.24b** much more dramatically. To ensure that the rate acceleration observed was not due to interconversion of the two products to a thermodynamic distribution, we isolated an authentic sample of **2.24b** and resubjected it to 3% (R) -DTBM-SEPHOS(AuCl)₂, 6% AgBF_4 , and 2.0 equivalents of *l*-menthol overnight at room temperature. Indeed, no equilibration to **2.24a** was observed after 18 h.

Figure 2.16. Relative rate enhancement of *l*-menthol for formation of **2.24a** and **2.24b** under two conditions.



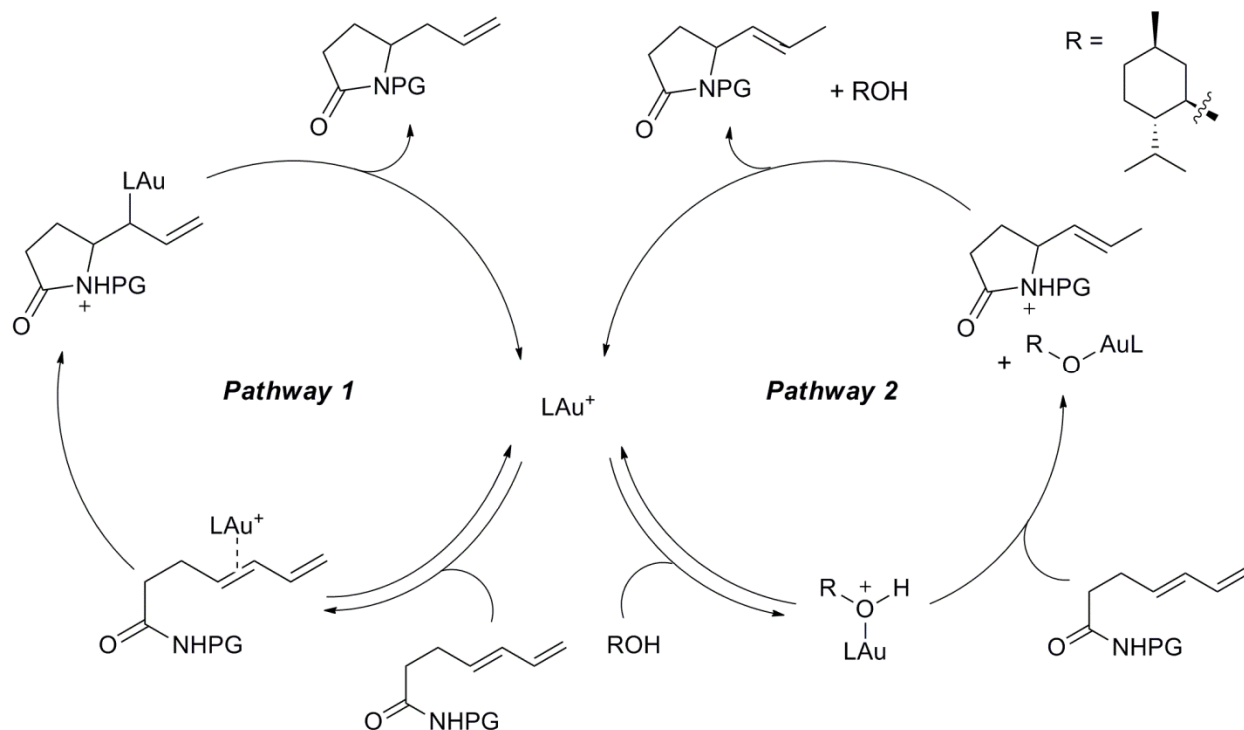
In addition, when 20% of Proton Sponge was added to the reaction of **2.20** with (*R*)-DTBM-SEGP_{HOS}(AuCl)₂ and *l*-menthol, none of the allylic product **2.23** was formed (eq. 2.15) and rate of overall reaction was significantly reduced. However, if a related but acid-stable substrate (**2.21**) was treated with 10 mol% TfOH in the absence of gold(I), the allylic product **2.22a** was formed exclusively (eq. 2.16). Finally, mass spectrometry of a solution of (*R*)-DTBM-SEGP_{HOS}(AuCl)₂ and *l*-menthol showed peaks at *m/z* = 1727 (singly charged ion) and 864 (doubly charged ion), which correspond to a 1:1 complex of (*R*)-DTBM-SEGP_{HOS}(Au)₂²⁺ and *l*-menthol (eq 2.17).





These experiments lead us to believe that the homoallylic and allylic products (i.e., **2.24b** and **2.24a**, respectively) are being formed predominantly *via* two different mechanisms; one that involves traditional coordination, nucleophilic addition and protodemetalation by gold similar to that which has been previously observed for allenes,⁶⁰ and a second proceeding through an “acid-catalyzed” pathway in which the gold complex acts as a Lewis acid by binding to *l*-menthol, increasing its Brønsted acidity. In pathway 1, coordination of gold catalyst to the diene enables intramolecular addition, and protodemetalation frees the gold catalyst. In pathway 2, gold coordinates to *l*-menthol and generates a Brønsted acidic species that then allows for diene protonation and attack of the nucleophile. When a base such as Proton Sponge is added, catalysis via the acid-mediated pathway 2 is inhibited, but pathway 1 is still operative, albeit at a diminished rate. Exclusive formation of allylic product by Brønsted-acid catalysis with TfOH is also consistent with our mechanistic proposal (Figure 2.17), as a strong Brønsted-acid is generated in pathway 2.

Figure 2.17. Two mechanisms, pathway 1 and pathway 2, are proposed to account for formation of **2.24b** and **2.24a**, respectively.



In conclusion, we have reported the first example of intermolecular hydroamination of allenes with a N-N linked nucleophile in the presence of a gold(I) catalyst, $\text{Ph}_3\text{PAuNTf}_2$. This system has allowed us to conduct the first detailed kinetic study of the mechanism of gold(I)-mediated allene activation. Our findings provide experimental evidence that allene activation is the rate-limiting step in gold(I)-catalyzed addition of hydrazide nucleophiles to allenes. Computational studies predict that the reaction examined proceeds via a two-step no-intermediate mechanism and that the second transition state immediately following the rate determining step is not planar, but likely axially chiral. Importantly, the dependence of the degree of chirality transfer on the concentration of the nucleophile suggests that a pathway proceeding through a traditional two-step pathway involving a planar intermediate is also available.

Additionally, we reported the first examples of Lewis acid activated Brønsted acidity in gold(I) catalysis. This novel catalyst system was applied to the formation of pyrrolidine and piperidine adducts through a gold(I)/*l*-menthol-catalyzed enantioselective diene hydroamination. The regioselectivity and enantioselectivity of the reaction can be controlled by the addition of *l*-menthol as a co-catalyst, which we believe acts as a Brønsted acid when coordinated to the gold catalyst and results in the formation of homoallylic rather than allylic pyrrolidines. The 1,3-diene scaffold has access to both mechanistic pathways involved for gold(I) catalysed hydroamination, depending on whether a protic additive is present.

We believe the differences in the mechanism of allene versus diene hydroamination can be attributed to the relative ease of protodemetalation from the vinyl versus allylic gold complex. While the gold intermediate from allene hydroamination is a vinyl-gold specie, the intermediate from diene hydroamination is an allyl-gold complex that protodemetallates much less readily.^{51b} As a result, an alternative mechanistic pathway is dominant when possible for diene hydroamination. The change in mechanism observed is preceded for both early metal and late metal catalyzed reactions. Indeed, while both alkyne and allene hydroamination with Pt(II) proceeds through π -acid catalysis, the analogous reactions with simple alkenes is proposed to go through a high oxidation state Pt(IV)-hydride, due to the difficulty of direct protodemetalation from the Pt(II)-alkyl complex.¹⁹ Furthermore, our own experiments have shown that protodemetalation from an alkyl-gold complex can be challenging, even under strongly acidic conditions. Our mechanistic studies here have important implications for the future development of racemic and enantioselective C-X bond forming reactions *via* addition of a nucleophiles to allenes and dienes promoted by gold(I).

Experimental

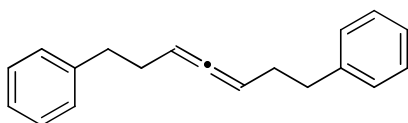
I. General Procedures and Materials

All reagents and solvents were obtained from commercial suppliers and used without further purification, unless otherwise specified. All air-sensitive reactions were carried out in dried glassware and solvent, under positive N₂ pressure using syringe and cannula techniques. Glassware was dried at 160 °C overnight or flame dried under vacuum immediately prior to use. Dry tetrahydrofuran was passed through a column of activated alumina. Following workup procedures, organics were concentrated under reduced pressure with a rotary evaporator. All flash chromatography was performed on Merck 60 silica gel (32-63 μm). Thin-layer chromatography (TLC) analysis was performed using Merck silica gel 60 F254 TLC plates, and visualized by staining with I₂, UV, anisaldehyde, and/or potassium permanganate. Ph₃PAuNTf₂ was prepared by the method described by Gagosz^{37a} and stored at -20 °C, protected from ambient light. Gold(I) chlorides (Ar₃PAuCl) were prepared following the method reported by Lalonde.^{51b}

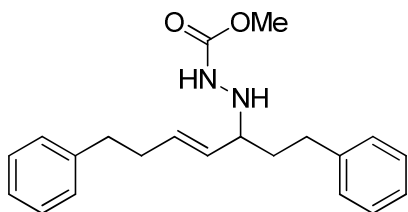
¹H and ¹³C NMR spectra were recorded with Bruker AVQ-400, DRX-500, AV-500 and AV-600 spectrometers and chemical shifts are reported in ppm, relative to residual proton peaks of CDCl₃, CD₂Cl₂ or CD₃NO₂, unless otherwise noted. Deuterated solvents were obtained from Cambridge Isotope Laboratories and used without further purification. Enantiomeric excess was determined on a Shimadzu VP Series Chiral HPLC, using the Chiral PAK OD-H, eluting with a flowrate of 0.5 mL/min. Mass spectral and analytical data were obtained via the Micro-Mass/Analytical Facility operated by the College of Chemistry, University of California, Berkeley.

II. Allene Hydroamination Mechanistic Studies

Synthesis of Starting Materials and Catalysts.



1,7-diphenylhepta-3,4-diene (1.38). To a dried flask containing a solution of Ph₃P (3.43 g, 13.1 mmol) in 40 mL dry THF, DIAD (2.75 mL, 13.1 mmol) was added dropwise under N₂ at 0 °C. The solution was stirred for 10 min at 0 °C before 1,7-diphenylhept-4-yn-3-ol⁶¹ (1.73 g, 6.55 mmol) was added as a solution in 1 mL THF. After 45 min, 2-nitrobenzenesulfonylhydrazide (2.82 g, 13.1 mmol) was added as slurry in 4 mL THF. The reaction was allowed to warm to 23 °C and was stirred for an 8 h, after which the crude reaction mixture was concentrated. The resulting viscous oil was passed through a silica plug, eluting with 300 mL of 12:88 EtOAc:hexanes. The organics were concentrated in vacuo and chromatographed on SiO₂, eluting with 0.5:99.5 EtOAc:hexanes. The allene product was isolated as a clear oil (660 mg, 41% yield). ¹H NMR spectra of the allene matches known spectroscopic data.⁶³

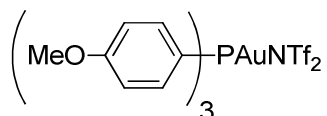


(E)-N'-(1,7-diphenylhept-4-en-3-yl)methyl carbazate (1.39_{trans}). To a solution of 1,7-diphenylhepta-3,4-diene (**1**) (30.0 mg, 0.121 mmol) and methyl carbazate (27.2 mg, 0.302 mmol) in MeNO₂ (0.6 mL), Ph₃PAuNTf₂ (5.37 mg, 0.00726 mmol) was added. The reaction mixture was protected from light, heated to 45 °C and stirred for 12 h. The crude reaction mixture was passed through a silica pad, eluting with 10 mL of 1:1 EtOAc:hexanes. The resulting solution was concentrated and chromatographed on SiO₂, eluting with 1:4 EtOAc:hexanes, to afford the product as a white solid (34 mg, 84%). ¹H NMR (CDCl₃, 600 MHz): δ 1.61-1.66 (m, 1 H), 1.81-1.85 (m, 1 H), 2.40-2.45 (m, 2 H), 2.51-2.63 (m, 2 H), 2.73-2.76 (m, 2 H), 3.36 (br s, 1 H), 3.73 (s, 3 H), 5.20-5.25 (dd, 1 H, *J* = 18, 10.2 Hz), 5.63-5.69 (dt, 1 H, *J* = 18, 8.4 Hz). ³¹C{¹H} NMR (CDCl₃, 100 MHz): δ 31.98, 34.13, 34.65, 35.56, 52.40, 62.87, 125.80, 125.92, 128.34, 128.54, 134.39, 141.54, 141.95, 157.74. HRMS (ESI) calculated for [C₂₁H₂₆O₂N₂+Na]⁺: *m/z* 361.1886, found 361.1883.

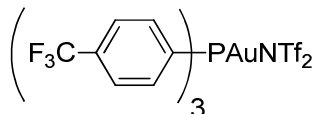


(Z)-N'-(1,7-diphenylhept-4-en-3-yl)methyl carbazate (1.39_{cis}). To a solution of 1,7-diphenylhepta-3,4-diene (**1**) (30.0 mg, 0.121 mmol) and methyl carbazate (27.2 mg, 0.302 mmol) in MeNO₂ (0.6 mL), Ph₃PAuNTf₂ (5.37 mg, 0.00726 mmol) was added. The reaction mixture protected from light, heated to 45 °C and stirred for 12 h. The crude reaction mixture was passed through a silica pad, eluting with 10 mL of 1:1 EtOAc:hexanes. The resulting solution was concentrated and chromatographed on SiO₂, eluting with 1:4 EtOAc:hexanes, to afford the product as a white solid (5.3 mg, 13%). ¹H NMR (CDCl₃, 500 MHz): δ 1.61-1.66 (m, 1 H), 1.81-1.85 (m, 1 H), 2.40-2.45 (m, 2 H), 2.51-2.63 (m, 2 H), 2.73-2.76 (m, 2 H), 3.36 (br s, 1 H), 3.73 (s, 3 H), 5.20-5.25 (dd, 1 H, *J* = 18, 10.2 Hz), 5.63-5.69 (dt, 1 H, *J* = 18, 8.4 Hz). ³¹C{¹H} NMR (CDCl₃, 100 MHz): δ 32.66, 33.41, 34.66, 35.55, 52.99, 62.72, 125.82, 128.28, 128.31, 128.35, 128.52, 132.00, 141.951, 157.74. HRMS (ESI) calculated for [C₂₁H₂₆O₂N₂+Na]⁺: *m/z* 361.1886, found 361.1883.

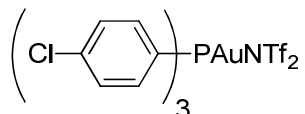
General Procedure for Preparation of Ar₃PAuNTf₂. Gold(I) chloride (1.0 equiv) and AgNTf₂ (1.5 equiv) were combined in CH₂Cl₂. The solution was sonicated for 2 min at room temperature and filtered through a pad of micropipette filter fiber. The solution was concentrated and dried in vacuo to afford the corresponding gold-triflimide catalyst as a solid.



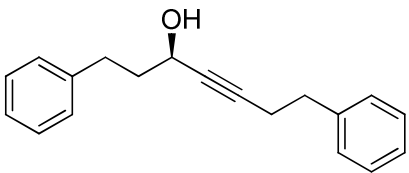
Tris(4-methoxyphenyl)phosphine-gold(I)-triflimide. Following general procedure A, gold chloride (20.0 mg, 0.0342 mmol), AgNTf₂ (19.9 mg, 0.0513 mmol) were combined in 1 mL CH₂Cl₂. The (p-OMe-C₆H₄)₃PAuNTf₂ catalyst was obtained as a white solid (29 mg, 99% yield) and stored at -20 °C, protected from ambient light. ¹H NMR (CD₂Cl₂, 600 MHz): δ 3.87 (s, 9 H), 7.03-7.05 (m, 6 H), 7.41-7.46 (m, 6 H) ppm. ³¹P{¹H} NMR (CD₂Cl₂, 240 MHz): δ 26.13 ppm.



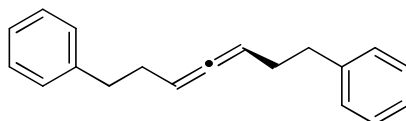
Tris(4-(trifluoromethyl)phenyl)phosphine-gold(I)-triflimide. Following general procedure A, gold chloride (20.0 mg, 0.0286 mmol), AgNTf₂ (16.7 mg, 0.0429 mmol) were combined in 1 mL CH₂Cl₂. The (p-CF₃-C₆H₄)₃PAuNTf₂ catalyst was obtained as a white solid (29 mg, 99% yield) and stored at -20 °C, protected from ambient light. ¹H NMR (CD₂Cl₂, 600 MHz): δ 7.67-7.71 (m, 6 H), 7.86-7.88 (m, 6 H) ppm. ³¹P{¹H} NMR (CD₂Cl₂, 240 MHz): δ 30.33 ppm.



Tris(4-chlorophenyl)phosphine-gold(I)-triflimide. Following general procedure A, gold chloride (15.0 mg, 0.0251 mmol), AgNTf₂ (14.6 mg, 0.0377 mmol) were combined in 1 mL CH₂Cl₂. The (p-Cl-C₆H₄)₃PAuNTf₂ catalyst was obtained as a white solid (29 mg, 99% yield) and stored at -20 °C, protected from ambient light. ¹H NMR (CD₂Cl₂, 600 MHz): δ 7.42-7.47 (m, 6 H), 7.55-7.58 (m, 6 H) ppm. ³¹P{¹H} NMR (CD₂Cl₂, 240 MHz): δ 28.60 ppm.



(R)-1,7-diphenylhept-4-yn-3-ol. To a solution of 1,7-diphenylhept-4-yn-3-one (495 mg, 1.89 mmol) in 20 mL THF at 0 °C under an N₂ atmosphere, a solution of (*S*)-alpine borane (5.67 mmol in THF, Sigma-Aldrich) was added at 0 °C. The reaction was stirred at 23 °C for 20 hours then acetaldehyde (1mL) and aminoethanol (1mL) was added. The resulting solution was stirred for 30 min then diluted with 50 mL Et₂O and extracted with brine (30 mL). The precipitants in the organic solution were removed by filtration and the crude solution was concentrated to a thick oil. The oil was purified by chromatography on SiO₂, eluting with 3:97 EtOAc:hexanes and the desired product was isolated (250 mg, 47% yield).



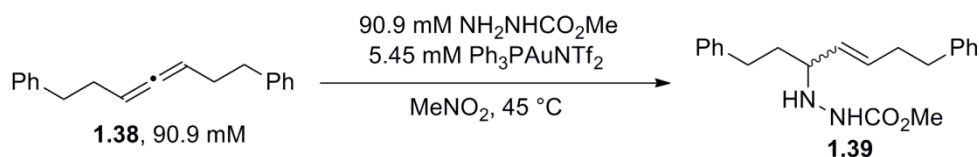
(S)-1,7-diphenylhepta-3,4-diene (1.39). Following the same procedure reported above for the synthesis of the racemic allene, the (S)-1,7-diphenylhepta-3,4-diene could be formed in 87% ee, as determined by chiral HPLC, on Chiral PAK OD-H, eluting with 99.5:0.5 hexanes:*i*PrOH with a flowrate of 0.5 mL/min.

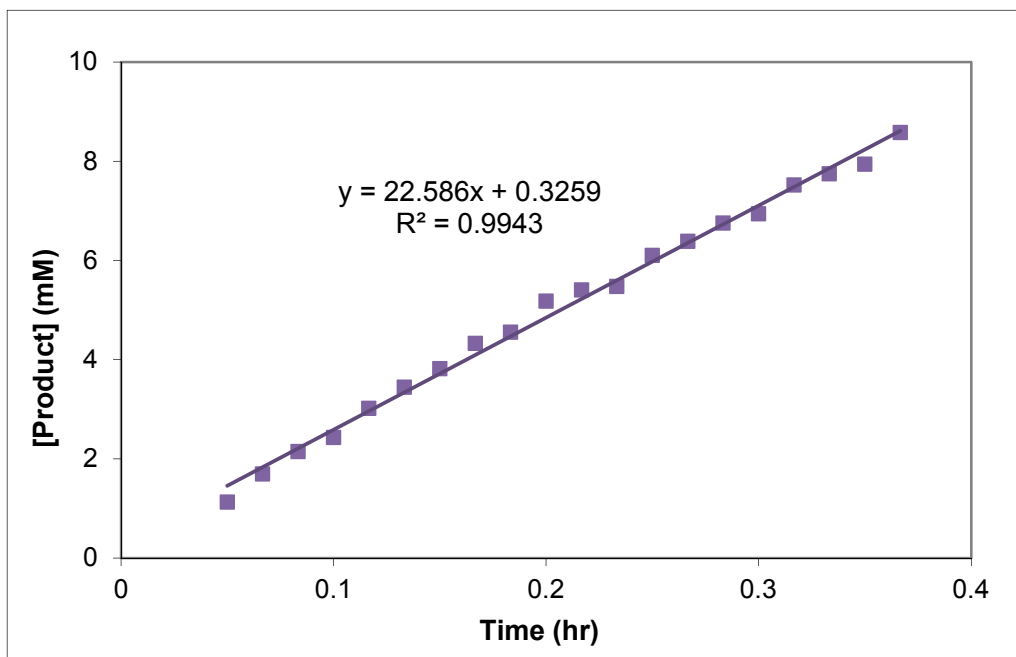
Kinetic Analysis of Formation of 1.39 from 1.38 and Methyl Carbazate.

General Procedure for Kinetic Experiments. Kinetic experiments were performed using NMR techniques on a Bruker AV-600 spectrometer and each reported rate constant represents an individual kinetics experiment. Standard solutions of catalyst were made by weighing the gold(I) complex into a vial and adding deuterated solvent. Stock solutions containing both 1,7-diphenylhepta-3,4-diene (**1.38**) and 1,3,5-tri-*tert*-butylbenzene (internal standard) were prepared similarly. To a J-Young tube protected from light, methyl carbazate, substrate, internal standard, and Au catalyst were added. The reactions were heated to 45 °C and monitored by single pulse ^1H and $^{31}\text{P}\{^1\text{H}\}$ NMR. The concentrations of substrate and product were determined by relative integration to the *t*-butyl peak in the standard. The average rate constants reported reflect an average of three kinetic runs. The observed first order rate constant (k_{obs}) reported reflects $k_{\text{obs}} = (k_{\text{trans}} + k_{\text{cis}})$, where k_{trans} and k_{cis} correspond to the rate of formation for the trans and cis olefin products, respectively.

Order in Nucleophile. The order in nucleophile was determined by the method of initial rates at various concentrations of methyl carbazate. Following the general procedure for kinetics, 0.3 mL of a standard solution of allene (12.4 mg, 50.0 μmol , per aliquot) and 1,3,5-tri-*tert*-butylbenzene (4.11 mg, 0.0167 μmol , per aliquot) in CD_3NO_2 , 0.15 mL of a standard solution of methyl carbazate (4.50 to 14.64 mg, 50.0 to 163 μmol , per aliquot) in CD_3NO_2 and 0.1 mL of a standard solution of $\text{Ph}_3\text{PAuNTf}_2$ (2.22 mg, 3.00 μmol , per aliquot) in CD_3NO_2 were combined. The reaction was heated to 45 °C in probe and was monitored for conversion up to 9% by single pulse ^1H NMR. A representative plot of [**1.39**] (mM) versus time (h) is shown below with slope = $22.6 \pm 0.4 \text{ mM h}^{-1}$ and $R^2=0.9943$ (Figure S2.1).

Figure S2.1. A plot of [Product] versus time at [Nuc] = 90.9 mM, where product = **1.39**.



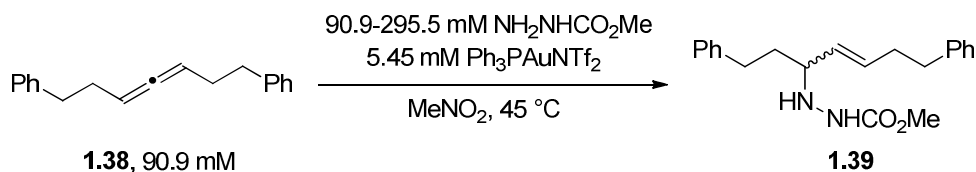


Kinetic data for k_{obs} (where $k_{\text{obs}} \approx (\Delta[\text{product}]/\Delta t)/[\text{allene}]_0$ and $[\text{allene}]_0 = 90.91 \text{ mM}$) at all methyl carbazate concentrations are tabulated in Table S2.1. A plot of the data provided a straight line with $R^2 = 0.9923$ and slope = $-1.47(9) \times 10^{-4} \pm \text{h}^{-1}$, suggesting a zero order dependence on nucleophile (Figure S2.2). A non-linear least squares fit of the data to the equation $f(x) = a(x)^n$ provided $n = -0.1083$ with $R^2 = 0.9835$ (Figure S2.3).

Table S2.1. Measured k_{obs} at 90.9 to 295.5 mM of methyl carbazate.

[Nuc] (mM)	Trial 1 (h ⁻¹)	Trial 2 (h ⁻¹)	Trial 3 (h ⁻¹)	Average (h ⁻¹)
90.91	0.255(18)	0.242(4)	0.248(4)	0.248(7)
159.1	0.240(4)	0.238(3)	0.234(4)	0.237(3)
227.3	0.222(3)	0.229(3)	0.228(3)	0.225(2)
295.5	0.215(4)	0.218(3)	0.223(5)	0.214(1)

Figure S2.2. A plot of k_{obs} at various concentrations of methyl carbazate.



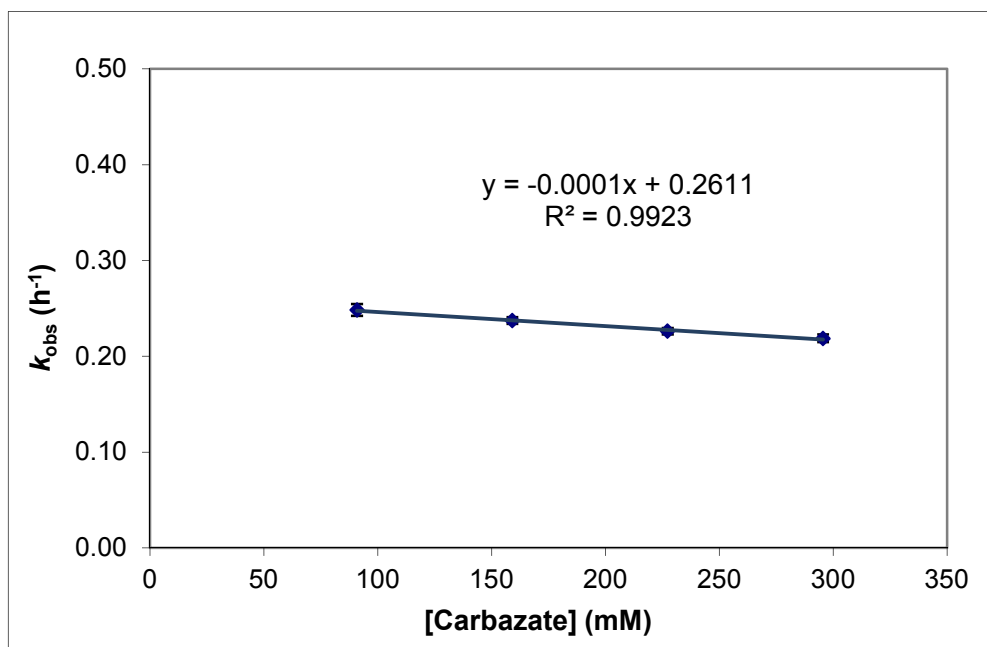
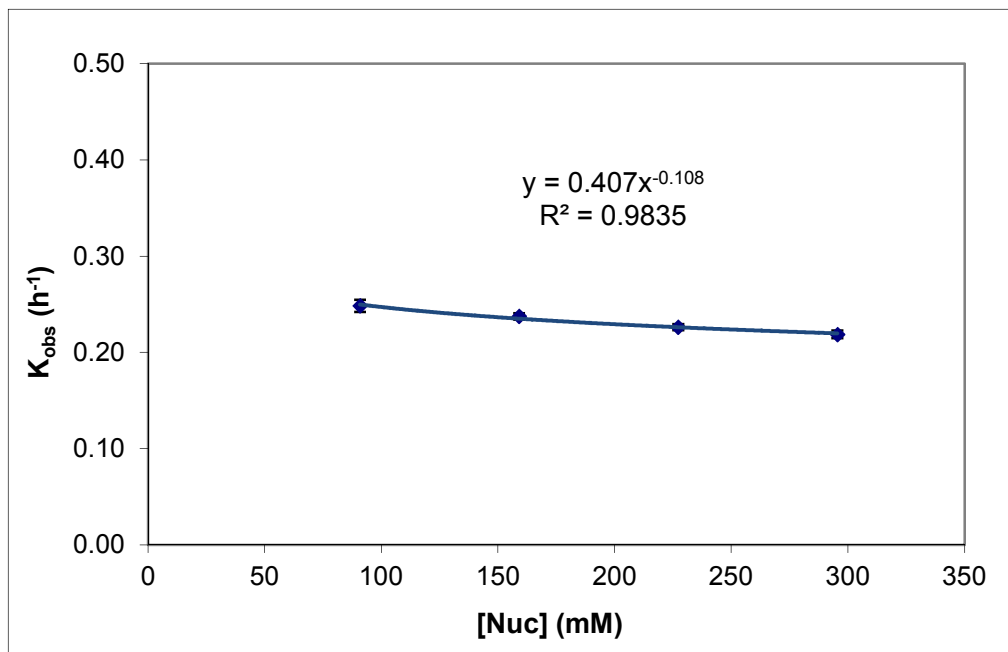


Figure S2.3. Non-linear least squares fit of the data to the equation $f(x) = a(x)^n$.



Order in Allene. The order in $\text{Ph}_3\text{PAuNTf}_2$ was determined by monitoring the rate of disappearance of allene at 3 to 12 mol % catalyst loadings. General procedure for kinetics was used with methyl carbazate (20.3 mg, 225 mmol), 0.4 mL of a standard solution containing (per aliquot) **1.38** (22.4 mg, 90.0 mmol) and 1,3,5-tri-*tert*-butylbenzene (7.40 mg, 30.0 mmol) (internal standard) in CD_3NO_2 , and 0.2 mL of a standard solution containing (per aliquot) $\text{Ph}_3\text{PAuNTf}_2$ (2.00 to 7.98 mg, 2.7 to 10.8 mmol) in CD_3NO_2 . The reactions were heated to 45 °C

and monitored by single pulse ^1H NMR up to 80-85% conversion. Representative plots of $-\ln([\text{allene}]_t/[\text{allene}]_0)$ vs. time at 3, 6, 9 and 12 mol% catalyst loading is shown below (Figure S2.4). While the slope of the lines varies with catalyst loading, the plots are linear at all catalyst concentrations examined. This suggests that the reaction is first order in allene. This was confirmed by fitting the data to a least squares fit to $f(x) = a(x)^n$ (Figure S2.5).

Figure S2.4. Plot of $-\ln([\text{allene}]_t/[\text{allene}]_0)$ versus time (h) where allene = **1.38** at 3-12 mol% catalyst loading.

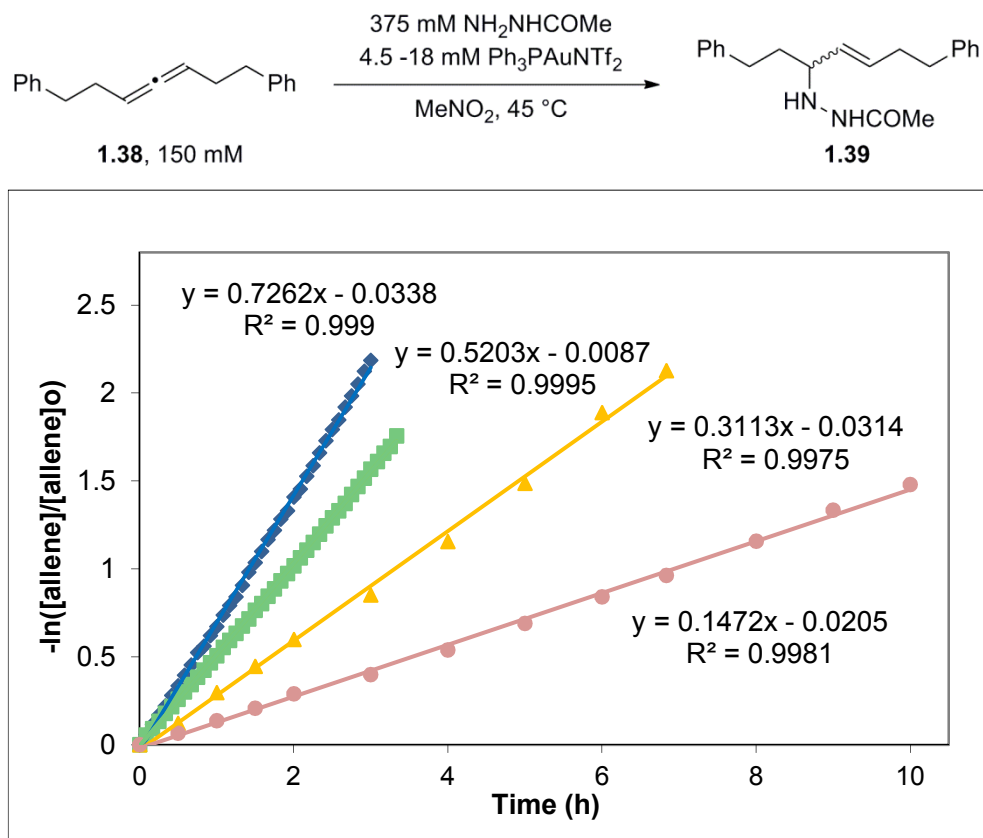
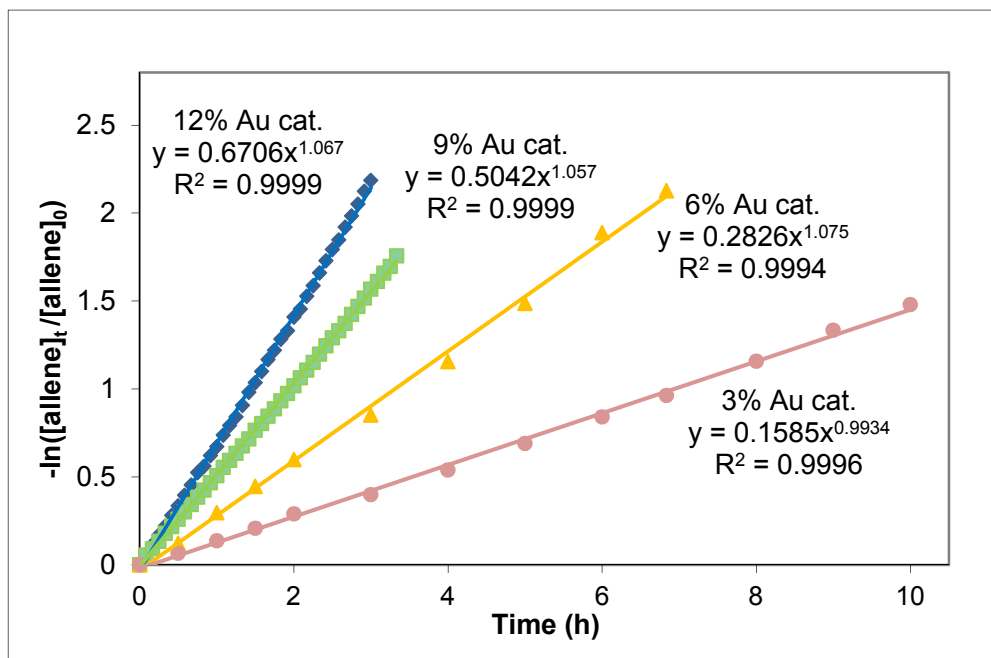


Figure S2.5. Non-linear least squares fit of the kinetics data to $f(x) = a(x)^n$.



Order in Catalyst. Each rate constant (k_{obs}) is obtained from the slope of the $-\ln([allene]_t/[allene]_0)$ versus time plot at 3, 6, 9 and 12 mol% catalyst loading. Three independent kinetic experiments were averaged to obtain an average k_{obs} . The results are tabulated in Table 2.2. A plot of average k_{obs} versus $[Ph_3PAuNTf_2]$ provided a straight line with slope = 0.0423(8), $R^2 = 0.9993$, suggesting a 1st order dependence on $Ph_3PAuNTf_2$ (Figure S2.6). This was confirmed by an non-linear least squares of the data to the equation $f(x) = a(x)^n$ which provided $n = 1.093$, with $R^2 = 0.9997$ (Figure S2.7).

Table 2.2. Measured rate constants at 3 to 12 mol% catalyst loading.

$[PPh_3AuNTf_2]$ (mM)	Trial 1 (h ⁻¹)	Trial 2 (h ⁻¹)	Trial 3 (h ⁻¹)	Average (h ⁻¹)
4.5	0.175(4)	0.147(2)	0.160(2)	0.161(14)
9.0	0.368(11)	0.311(6)	0.328(3)	0.336(29)
13.5	0.534(17)	0.520(2)	0.551(2)	0.535(15)
18.0	0.718(24)	0.726(4)	0.740(4)	0.728(11)

Figure S2.6. Plot of average k_{obs} versus $[\text{Ph}_3\text{PAuNTf}_2]$.

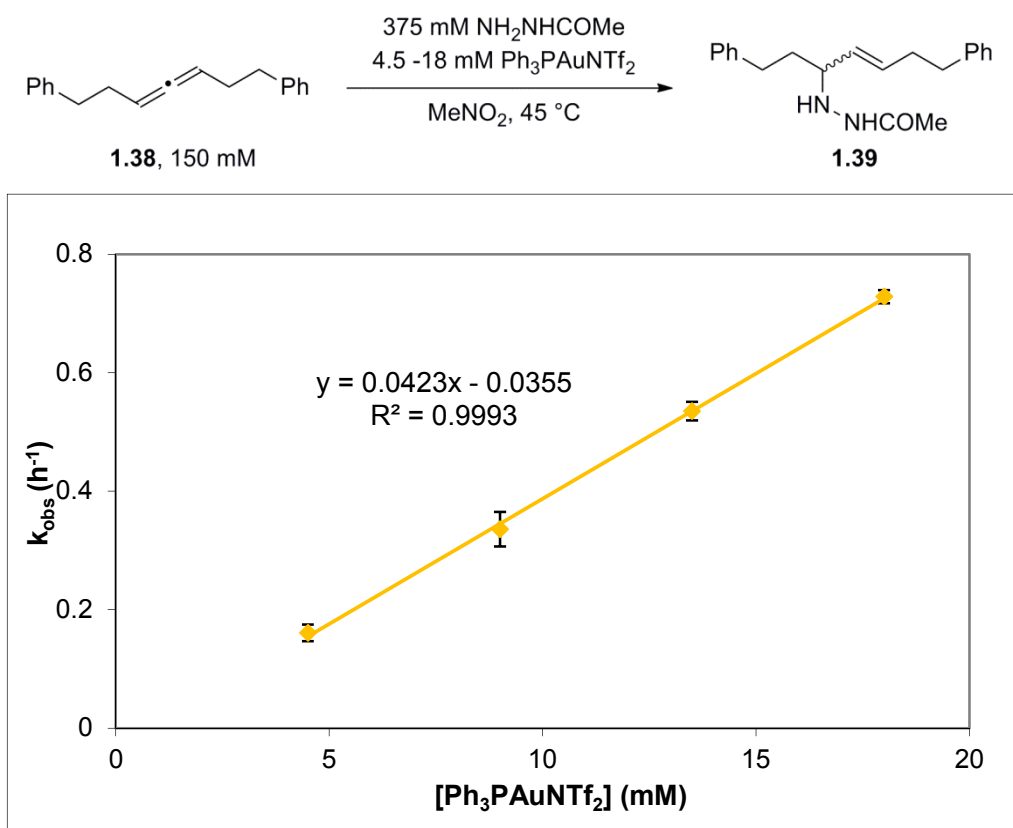
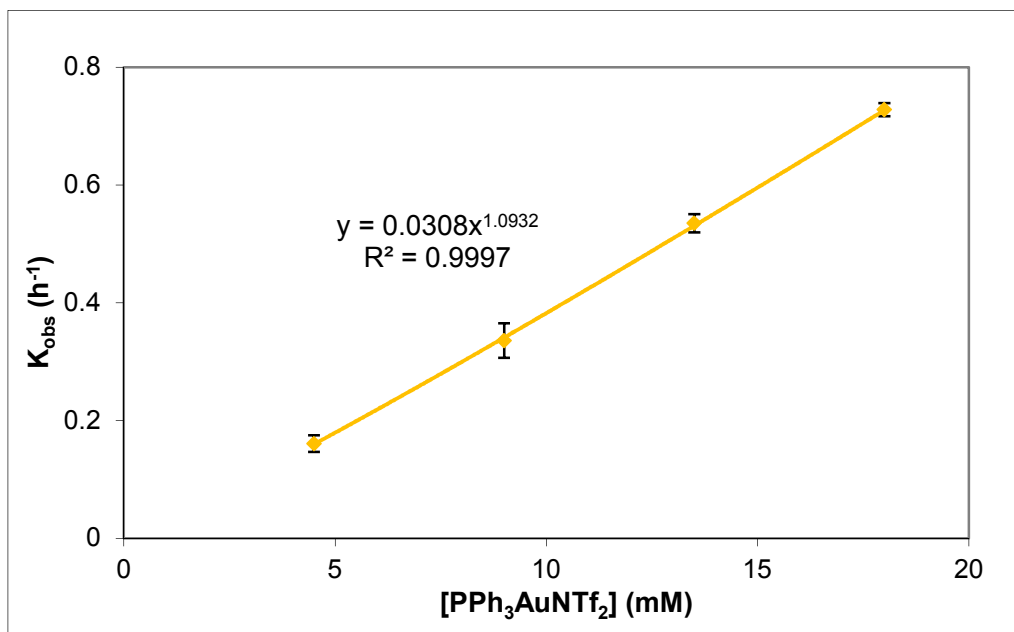


Figure S2.7. Non-linear least squares fit of the kinetic data to the equation $f(x) = a(x)^n$.



Observation of catalyst resting state.

General procedure for kinetics was used with methyl carbazate (27.2 mg, 301.8 μmol), **1.38** (30.0 mg, 120.7 μmol), 1,3,5-tri-*tert*-butylbenzene (internal standard) (9.20 mg, 40.2 μmol), and $\text{Ph}_3\text{PAuNTf}_2$ (4.50 mg, 6.04 μmol) in 600 μL CD_3NO_2 . The catalyst resting state was determined by monitoring ^{31}P NMR at 45 $^\circ\text{C}$. Ten minutes after the addition of $\text{Ph}_3\text{PAuNTf}_2$ to the substrate mixture, the ^{31}P peak corresponding to the parent catalyst vanished and a new peak at $\delta = 45.2$ ppm (44.8 ppm in CD_2Cl_2) was observed. This peak persisted through the entire course of the reaction until the concentration of **1.38** was comparable to the concentration of $\text{Ph}_3\text{PAuNTf}_2$. Figure S2.8 is a ^{31}P NMR of the reaction from 11-95% conversion.

Figure S2.8. Monitoring the catalyst resting state by ^{31}P NMR.

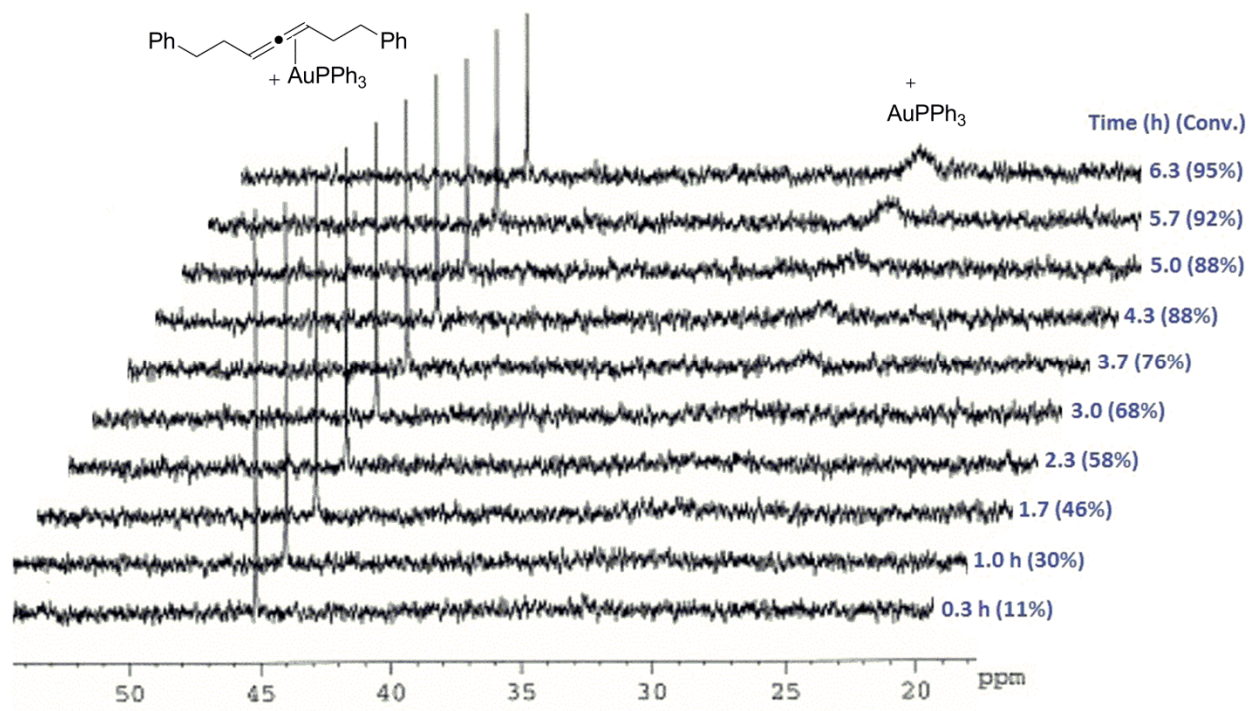


Figure S2.9 and S.210 are ^{31}P NMR spectra of $\text{Ph}_3\text{PAuNTf}_2$ alone and $\text{Ph}_3\text{PAuNTf}_2$ (10 mg, 13.5 μmol) and methyl carbazate (1.2 mg, 13.5 μmol) in a 1:1 ratio in 500 μL , respectively. This solution produced a peak at $\delta = 29.7$ ppm that was distinct from that of the parent catalyst but was not that of the resting state. We assigned this peak as the gold-hydrazide complex, **2.13**. We also considered the coordination of methyl carbazate by the N or O atoms. However, our calculations suggest that the predicted relative nuclear shielding for the methyl carbazate structure is more consistent with an oxygen coordination (calculated $\Delta\delta = 1.2$ ppm, vs. $\Delta\delta = 0.6$ ppm from experiment) than the nitrogen coordination (calculated $\Delta\delta = -4.2$ ppm).

Figure S2.9. Reference spectrum for the parent catalyst, Ph₃PAuNTf₂.

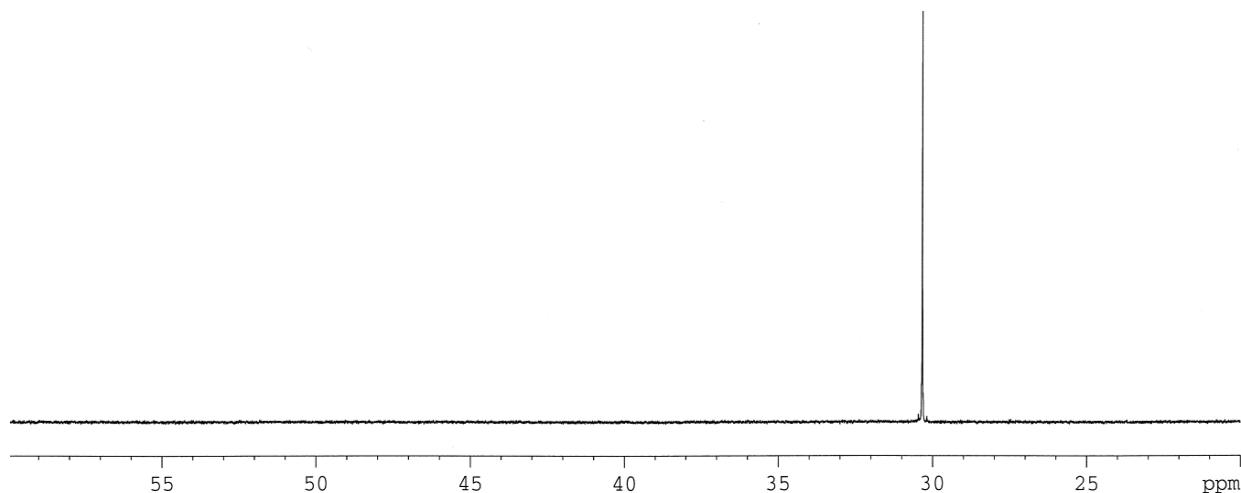


Figure S2.10. Solution of methyl carbazate and Ph₃PAuNTf₂ at 45 °C.

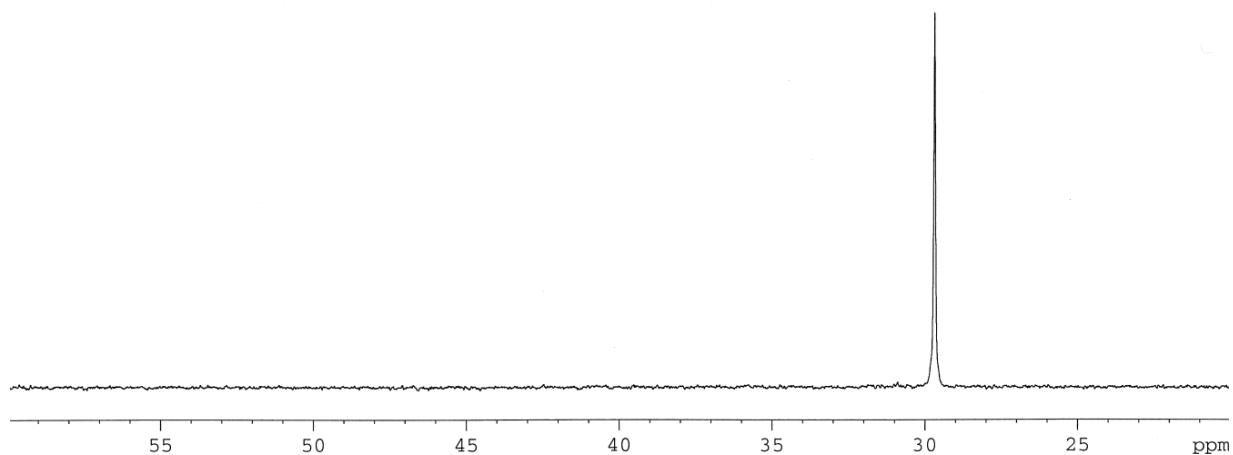
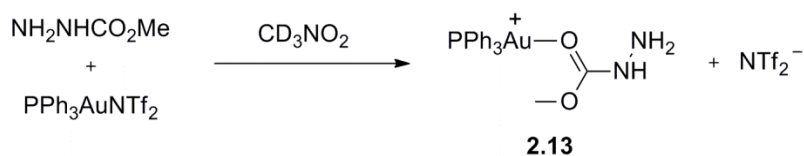
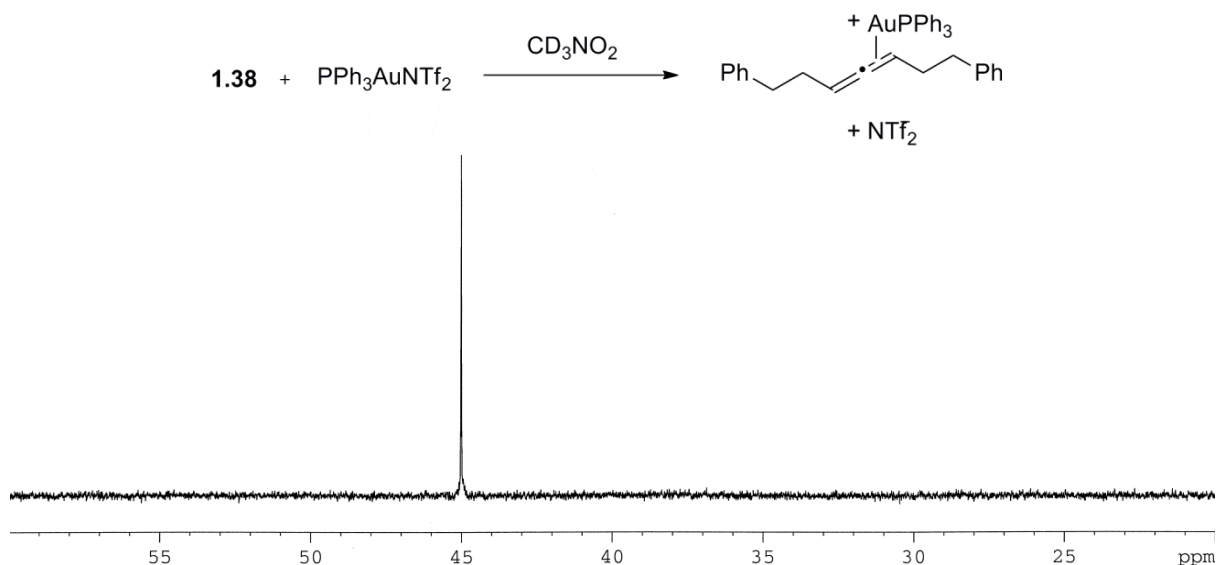


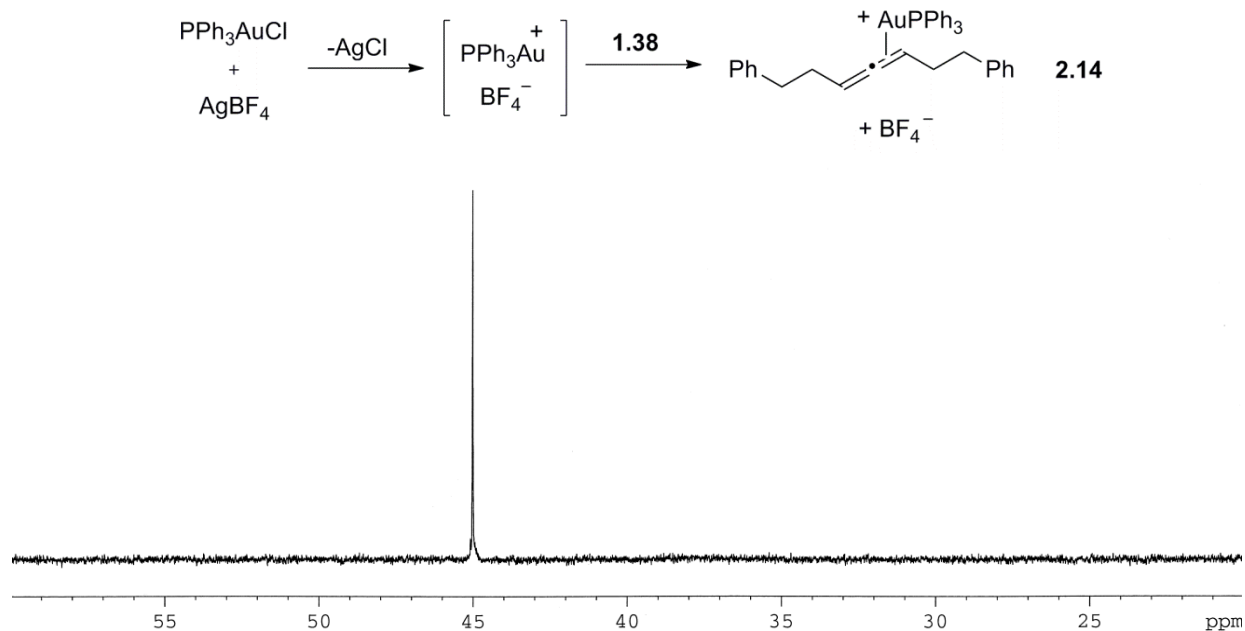
Figure S2.11 is a ³¹P NMR spectra of Ph₃PAuNTf₂ (6.0 mg, 8.12 μmol) and **1.38** (20.2 mg, 81.2 μmol) in 400 μL CD₃NO₂. The reaction turned yellow upon addition of the allene. In the absence of any nucleophile, this mixture showed ³¹P NMR resonance at 45.2 ppm (44.8 ppm in CD₂Cl₂), which resembled that of the resting state in the catalytic cycle, suggesting that the resting state of the catalyst was an allene-gold complex.

Figure S2.11. The gold-allene complex, generated from $\text{Ph}_3\text{PAuNTf}_2$ and **1.38**.



This complex was also independently generated from Ph_3PAuCl (6.0 mg, 20.1 μmol), AgBF_4 (11.7 mmol, 60.2 μmol) and 1,7-diphenylhepta-3,4-diene (15.0 mg, 60.4 μmol). Gold chloride was combined with the silver salt and sonicated for 2 minutes in 700 μL CD_2Cl_2 . The mixture was filtered through a micropipette filter fiber and added directly to **1.38**. The ^{31}P NMR spectra of the resulting solution showed the allene-gold complex (**2.14**) at δ 45.2 ppm (Figure S2.12).

Figure S2.12. The gold-allene complex, generated from Ph_3PAuCl , AgBF_4 and **1.38**.



In order to verify the NMR assignments, we compared M06-L predicted relative nuclear magnetic shielding constants⁴ to the measured chemical shifts. We calculated the isotropic nuclear magnetic shielding for phosphorus for $[\text{Ph}_3\text{PAu}]^+$ coordinated with MeNO_2 , penta-2,3-diene, and methyl carbazate. Using the chemical shift for the solvent coordinated species of $\delta=30.3$ ppm, we calculated a relative nuclear magnetic shielding for the allene coordinated structure of $\Delta\delta=+13.4$ ppm which compares well to the relative chemical shift $\Delta\delta=+15.5$ ppm observed.

Hammett Analysis of Formation of **1.39** from **1.38** and Methyl carbazate.

The rate of reaction for each catalyst was determined by monitoring the rate of disappearance of allene at 6 mol % catalyst loadings. The general procedure for kinetics was used with methyl carbazate (20.3 mg, 225 mmol), 0.4 mL of a standard solution containing **1.38** (22.4 mg, 90.0 mmol, per aliquot) and 1,3,5-tri-tert-butylbenzene (7.40 mg, 30.0 mmol, per aliquot) (internal standard) in CD_3NO_2 , and 0.2 mL of a standard solution containing $\text{PAR}_3\text{AuNTf}_2$ (3.99-5.09 mg, 5.40 mmol, per aliquot) in CD_3NO_2 . The reactions were heated to 45 °C and monitored by ^1H NMR until 80-85% conversion was reached. The rate data reported reflects an average of three independent kinetics experiments for reaction with each $\text{PAR}_3\text{AuNTf}_2$ catalyst. Hammett Analysis provide $\rho = 0.224$ and $R^2 = 0.9572$ (Figure S2.13, Table S2.3), suggesting that positive charge is diminishing in the rate determining transition state.

Figure S2.13. Hammett plot for the reaction, with 6 mol% catalyst loading.

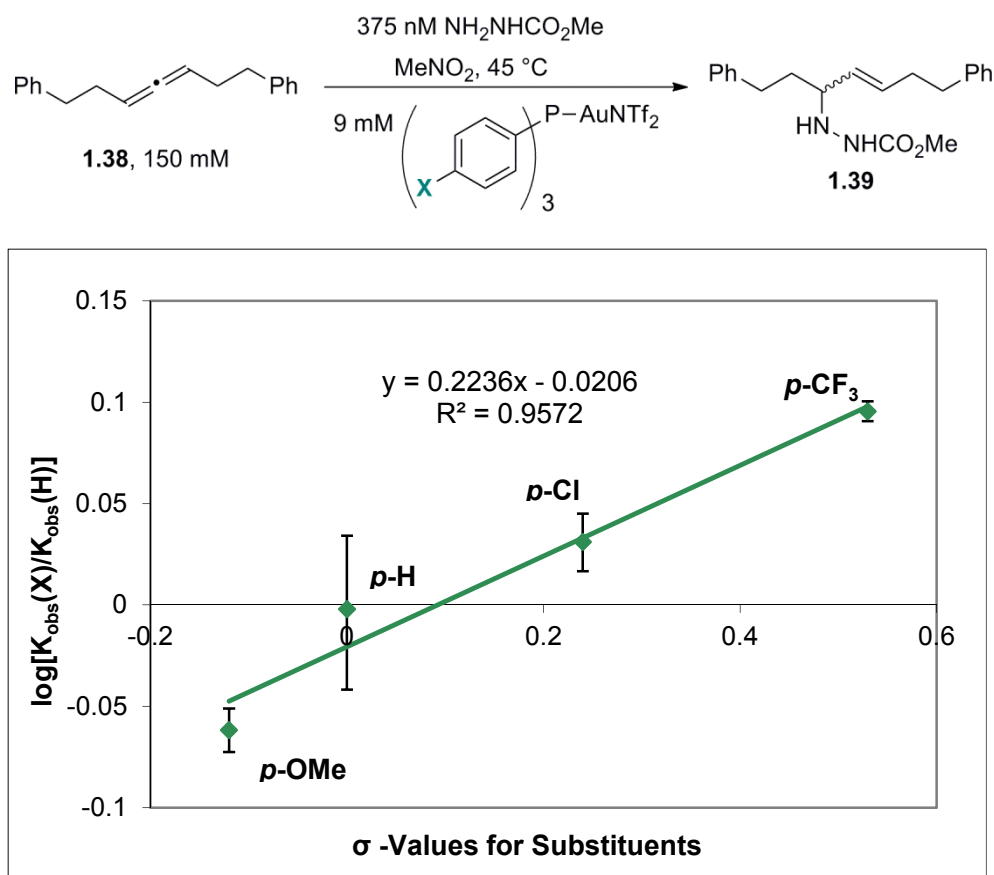
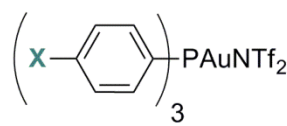


Table S2.3. Measured k_{obs} for various catalysts at 6 mol% catalyst loading.

	Trial 1 (h ⁻¹)	Trial 2 (h ⁻¹)	Trial 3 (h ⁻¹)	Average (h ⁻¹)
CF ₃	0.422(3)	0.415(5)	0.424(6)	0.420(5)
Cl	0.376(3)	0.355(6)	0.356(8)	0.362(11)
H	0.368(11)	0.311(6)	0.328(3)	0.336(29)
MeO	0.289(2)	0.288(6)	0.301(6)	0.292(9)

Reversibility of reaction.

Resubjecting Chiral Products to Racemic Reaction Conditions. Enantioenriched **1.39** (9.0 mg, 26.6 μmol , 56% ee) was added to a solution of methyl carbazate (4.79 mg, 53.2 μmol) and $\text{Ph}_3\text{PAuNTf}_2$ (1.97 mg, 2.66 μmol) in CH_3NO_2 in a scintillation vial equipped with magnetic stir bar and protected from ambient light. The resulting solution was stirred and heated to 45 °C for 6 h. The crude reaction mixture was passed through a silica plug, eluting with 1:1 EtOAc:hexanes. The organics were concentrated and flashed on SiO_2 , eluting with 1:4 EtOAc:hexanes, to obtain re-obtain **1.39** (9.0 mg, 99% yield, 56% ee). Enantioselectivity of the starting material and product was determined by HPLC on Chiralpak OD-H (90:10 hexanes:isopropanol, 0.5 mL/min) t_{R} 41.4 min (major), 47.2 min (minor).

Competition Experiments. To a solution of **1.38** (11.2 mg, 45.0 μmol), NH_2NHCOMe (4.1 mg, 45 μmol), and $\text{NH}_2\text{NHCO}t\text{Bu}$ (17.8 mg, 135 μmol) in 300 μL MeNO_2 , $\text{Ph}_3\text{PAuNTf}_2$ (3.99 mg, 5.4 μmol) was added. The solution was protected from light and stirred at 45 °C for 8 h. The crude reaction mixture was passed through a silica plug, eluting with 1:4 EtOAc:hexanes, to afford both **1.39** and **2.15** in a 15:85 ratio as determined by ^1H NMR with internal standard.

To a solution of **1.38** (10.0 mg, 29.5 μmol) and $\text{NH}_2\text{NHCO}_2t\text{Bu}$ (11.7 mg, 88.6 μmol) in 300 μL MeNO_2 , $\text{Ph}_3\text{PAuNTf}_2$ (2.20 mg, 2.95 μmol) was added. The solution was protected from light and stirred at 45 °C for 8 h. The crude reaction mixture was passed through a silica plug, eluting with 1:4 EtOAc:hexanes, to afford **1.39** as the only product (10.0 mg, 99% yield).

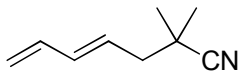
Chirality Transfer.

Enantioenriched **1.38** (87% ee) was prepared from the corresponding chiral propargyl alcohol by the method described previously. To a solution of **1.38** (10.9 mg, 40.3 μmol), methyl carbazate (3.6-29.0 mg, 40.3-322 μmol) in 400 μL MeNO_2 , $\text{Ph}_3\text{PAuNTf}_2$ (3.99 mg, 5.4 μmol) was added. The solution was protected from light and stirred at 45 °C for 12 h. The crude reaction mixture was flashed directly on 1:4 EtOAc:hexanes to provide the desired product (10.1 to 11.1 mg, 75-81% yield) (Table S2.4). The enantiomeric excess of the products were determined by chiral

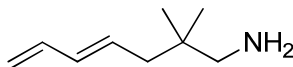
HPLC on a Chiral PAK OD-H column eluting with 90:10 *i*PrOH:hexanes with a flow rate of 0.5 mL/min.

III. Diene Hydroamination

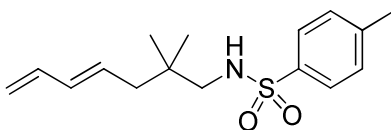
Synthesis of Starting Materials



(E)-2,2-dimethylhepta-4,6-dienitrile. To a solution of diisopropylamine (5.9 mL, 34.0 mmol) in THF (70 mL) was added 2.5M *n*-BuLi in hexane (14.3 mL, 35.7 mL) at 0 °C to prepare LDA solution in THF. The solution was stirred for 0.5h at the same temperature and then cooled to -78°C. Isobutyronitrile (14.3 mL, 35.7 mL) was added to the solution at -78°C and followed by an addition of a solution of (*E*)-5-bromopenta-1,3-diene (5.0 g, 34.0 mmol) in THF (15 mL) after 1hr. The mixture was stirred for 2h at -78°C and allowed to warm to room temperature. After quenching by saturated aq. NH₄Cl, the aqueous mixture was extracted with DCM (250 mL). The organic layer was washed with aq. NaHCO₃ and brine and then dried over Na₂SO₄. The solution was evaporated in vacuo and the residue was purified by silica gel column chromatography (hexane-EtOAc, 20:1) to afford (*E*)-2,2-dimethylhepta-4,6-dienitrile (2.85 g, 62%) as an oil. ¹H NMR (400 MHz, CDCl₃) δ 6.35 (dt, *J* = 16.9, 10.3 Hz, 1H), 6.16 (dd, *J* = 15.1, 10.4 Hz, 1H), 5.73 (dt, *J* = 15.1, 7.6 Hz, 1H), 5.19 (d, *J* = 16.8 Hz, 1H), 5.08 (d, *J* = 10.2 Hz, 1H), 2.31 (d, *J* = 7.6 Hz, 2H), 1.34 (s, 6H). ¹³C NMR (100 MHz, CDCl₃) δ 136.49, 135.86, 127.78, 124.92, 117.40, 44.07, 32.67, 26.46. MS (EI) calc. for [C₉H₁₃N]⁺: 135, found: 135.

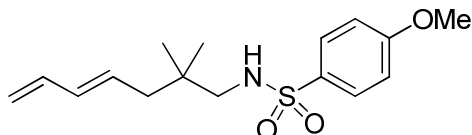


(E)-2,2-dimethylhepta-4,6-dien-1-amine. To a suspension of lithium aluminium hydride (LAH) (2.74g, 72.4 mmol) in Et₂O (36 mL) was added a solution of (*E*)-2,2-dimethylhepta-4,6-dienitrile (2.70g, 20.0 mmol) in Et₂O (18 mL) over 15min. at 0 °C. The mixture was allowed to warm to room temperature and stirred for 2 h at the same temperature. After adding Na₂SO₄·10H₂O to the mixture, the suspension was filtrated with Celite and the filtrate was evaporated in vacuo to afford (*E*)-2,2-dimethylhepta-4,6-dien-1-amine (2.60 g, 93%) as an oil. ¹H NMR (400 MHz, CDCl₃) δ 6.32 (dt, *J* = 17.0, 10.3 Hz, 1H), 6.06 (dd, *J* = 15.1, 10.4 Hz, 1H), 5.70 (dt, *J* = 15.3, 7.7 Hz, 1H), 5.10 (d, *J* = 16.9 Hz, 1H), 4.98 (d, *J* = 10.2 Hz, 1H), 2.47 (s, 2H), 2.00 (d, *J* = 7.6 Hz, 2H), 1.76 (br s, 2H), 0.87 (s, 6H). ¹³C NMR (100 MHz, CDCl₃) δ 137.29, 133.58, 131.71, 115.31, 52.77, 42.87, 35.62, 24.87. HRMS (EI) calc. for [C₉H₁₈N]⁺: 140.1434, found: 140.1434.

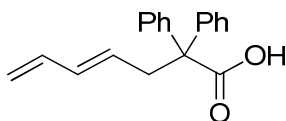


(E)-N-(2,2-dimethylhepta-4,6-dien-1-yl)-4-methylbenzenesulfonamide (2.20). To a solution

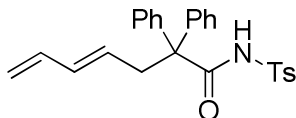
of (*E*)-2,2-dimethylhepta-4,6-dien-1-amine (200 mg, 1.44 mmol) and triethylamine (0.22 mL, 1.58 mmol) in DCM (8 mL) was added a solution of tosyl chloride (275 mg, 1.44 mmol) in DCM (5 mL) at 0 °C. The mixture was allowed to warm to room temperature and stirred for 12 h at the same temperature. After adding saturated aq. NaHCO₃ to the mixture, the aqueous mixture was extracted with EtOAc (150 mL). The organic layer was washed with brine and then dried over Na₂SO₄. The solution was evaporated in vacuo and the residue was purified by silica gel column chromatography (hexane-EtOAc, 10:1-3:1) to afford **2.20** (330 mg, 78%) as a solid. ¹H NMR (400 MHz, CDCl₃) δ 7.73 (d, *J* = 8.3 Hz, 2H), 7.31 (d, *J* = 8.0 Hz, 2H), 6.26 (dt, *J* = 17.0, 10.3 Hz, 1H), 6.00 (dd, *J* = 15.1, 10.4 Hz, 1H), 5.58 (dt, *J* = 15.1, 7.6 Hz, 1H), 5.10 (d, *J* = 16.9 Hz, 1H), 5.00 (d, *J* = 10.1 Hz, 1H), 4.38 (t, *J* = 6.6 Hz, 1H), 2.68 (d, *J* = 7.0 Hz, 2H), 2.43 (s, 3H), 1.98 (d, *J* = 7.6 Hz, 2H), 0.87 (d, *J* = 8.9 Hz, 6H). ¹³C NMR (100 MHz, CDCl₃) δ 143.55, 137.14, 137.02, 134.30, 130.38, 129.92, 127.29, 115.92, 53.04, 42.83, 34.86, 25.14, 21.74. HRMS (EI) calc. for [C₁₆H₂₄O₂NS]⁺: 294.1522, found: 294.1525.



(*E*)-N-(2,2-dimethylhepta-4,6-dien-1-yl)-4-methoxybenzenesulfonamide (2.21). Prepared from (*E*)-2,2-dimethylhepta-4,6-dien-1-amine in analogy to the procedure above for (*E*)-N-(2,2-dimethylhepta-4,6-dien-1-yl)-4-methylbenzenesulfonamide. ¹H NMR (400 MHz, CDCl₃) δ 7.78 (d, *J* = 8.7 Hz, 2H), 6.97 (d, *J* = 8.7 Hz, 2H), 6.26 (dt, *J* = 17.0, 10.2 Hz, 1H), 6.00 (dd, *J* = 15.0, 10.6 Hz, 1H), 5.58 (dt, *J* = 15.2, 7.6 Hz, 1H), 5.09 (d, *J* = 17.0 Hz, 1H), 4.99 (d, *J* = 10.0 Hz, 1H), 4.51 (t, *J* = 6.7 Hz, 1H), 3.87 (s, 3H), 2.66 (d, *J* = 6.9 Hz, 2H), 1.97 (d, *J* = 7.6 Hz, 2H), 0.85 (s, 6H). ¹³C NMR (100 MHz, CDCl₃) δ 162.96, 137.05, 134.24, 131.68, 130.44, 129.37, 115.84, 114.41, 55.79, 52.96, 42.77, 34.81, 25.13. HRMS (EI) calc. for [C₁₆H₂₄O₃NS]⁺: 310.1471, found: 310.1475.

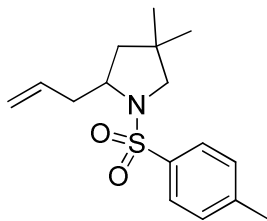


(*E*)-2,2-diphenylhepta-4,6-dienoic acid. To a solution of (*E*)-ethyl 2,2-diphenylhepta-4,6-dienoate (4.80 g, 15.7 mmol) in mixed solvent of MeOH (40 mL) and THF (40 mL) was added 50% aq. NaOH (12.6 g, 157 mmol) and the mixture was stirred for 18h at 60°C. After neutralization with 3M HCl, the pH of the solution adjusted to around 4. The aqueous mixture was extracted with EtOAc (200 mL, twice). The organic layer was washed with brine and then dried over Na₂SO₄. The solution was evaporated in vacuo and the crude product was purified by recrystallization from hexane-EtOAc, to afford (*E*)-2,2-diphenylhepta-4,6-dienoic acid (3.15 g, 72%) as a colorless crystal. ¹H NMR (400 MHz, CDCl₃) δ 7.37 – 7.22 (m, 10H), 6.16 (dt, *J* = 17.0, 10.3 Hz, 1H), 5.91 (dd, *J* = 15.2, 10.5 Hz, 1H), 5.53 – 5.40 (m, 1H), 5.00 (d, *J* = 17.0 Hz, 1H), 4.92 (d, *J* = 10.2 Hz, 1H), 3.19 (d, *J* = 7.2 Hz, 2H). ¹³C NMR (100 MHz, CDCl₃) δ 180.07, 142.04, 137.08, 134.81, 129.83, 129.27, 128.15, 127.33, 115.98, 60.66, 41.46. HRMS (EI) calc. for [C₁₉H₁₈O₂Na]⁺: 301.1199, found: 301.1199.

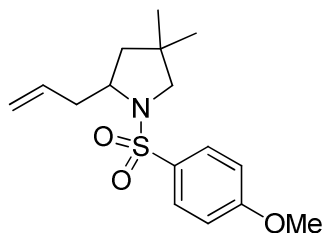


(*E*)-2,2-diphenyl-N-tosylhepta-4,6-dienamide (2.23). To a solution of (*E*)-2,2-diphenylhepta-4,6-dienoic acid (1.250 g, 4.50 mmol) and triethylamine (632 μ L, 4.50 mmol) in DCM (20 mL) was added 4-methylbenzenesulfonyl isocyanate (822 μ L, 5.40 mmol) at 0°C and the mixture was stirred for 18h at room temperature. After addition of water (10 mL) to the reaction mixture, the aqueous solution was extracted with EtOAc (250 mL). The organic layer was washed with 1 M HCl, aq. NaHCO₃ and brine and then dried over Na₂SO₄. The solution was evaporated in vacuo and the residue was purified by silica gel column chromatography (hexane-EtOAc, 10:1-5:1). This product was recrystallized from hexane-EtOAc to afford pure product (1.58 g, 81%). ¹H NMR (400 MHz, CDCl₃) δ 7.81 (br s, 1H), 7.77 – 7.69 (m, 2H), 7.37 – 7.23 (m, 9H), 7.18 – 7.08 (m, 4H), 6.06 (dt, *J* = 17.0, 10.3 Hz, 1H), 5.79 (dd, *J* = 15.2, 10.4 Hz, 1H), 5.44 – 5.29 (m, 1H), 4.95 (d, *J* = 17.0 Hz, 1H), 4.89 (d, *J* = 10.2 Hz, 1H), 3.07 (d, *J* = 7.2 Hz, 2H), 2.45 (s, 3H). ¹³C NMR (100 MHz, CDCl₃) δ 171.55, 145.20, 140.26, 136.76, 135.20, 129.63, 129.11, 128.98, 128.94, 128.62, 127.99, 116.32, 62.04, 41.73, 21.92. HRMS (EI) calc. for [C₂₆H₂₆O₃NS]⁺: 432.1628, found: 432.1635.

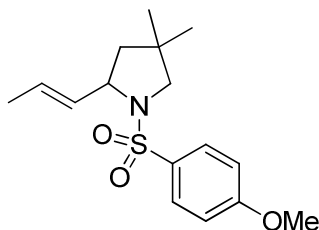
General procedure for Gold(I)-catalyzed hydroamination. A mixture of AgBF₄ (0.58mg, 3.0 μ mol) and the phosphine gold(I) chloride complex (1.5 μ mol) is suspended in 400 μ L of solvent in a sealed vial, and sonicated or stirred magnetically for 15 min at room temperature. The resulting suspension is filtered through a glassmicrofiber plug directly into a solution of substrate (0.05 mmol, unless otherwise specified) in 100 μ L of same solvent, through mixing is ensured and the resulting homogenous solution is stirred for 24h. The reaction was stopped by addition of one drop of triethylamine and the conversion was determined by ¹H NMR or HPLC of crude mixture after filtration through short silica gel column.



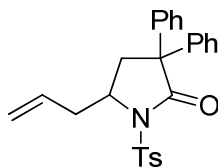
2-allyl-4,4-dimethyl-1-tosylpyrrolidine. ¹H NMR (400 MHz, CDCl₃) δ 7.74 (d, *J* = 8.3 Hz, 2H), 7.31 (d, *J* = 8.0 Hz, 2H), 5.82 – 5.68 (m, 1H), 5.14 – 5.03 (m, 2H), 3.71 – 3.60 (m, 1H), 3.14 (d, *J* = 10.6 Hz, 1H), 3.11 (d, *J* = 10.6 Hz, 1H), 2.88 – 2.70 (m, 1H), 2.43 (s, 3H), 2.43 – 2.37 (m, 1H), 1.68 – 1.61 (m, 1H), 1.52 (dd, *J* = 12.7, 8.9 Hz, 1H), 1.02 (s, 3H), 0.52 (s, 3H). ¹³C NMR (100 MHz, CDCl₃) δ 143.40, 135.59, 134.52, 129.73, 127.63, 117.91, 61.75, 59.68, 45.73, 40.77, 37.45, 26.57, 26.06, 21.75. HRMS (EI) calc. for [C₁₆H₂₄O₂NS]⁺: 294.1522, found: 294.1524.



2-allyl-1-((4-methoxyphenyl)sulfonyl)-4,4-dimethylpyrrolidine (2.22b). ^1H NMR (400 MHz, CDCl_3) δ 7.83 – 7.75 (m, 2H), 7.05 – 6.91 (m, 2H), 5.83 – 5.66 (m, 1H), 5.16 – 4.98 (m, 2H), 3.87 (s, 3H), 3.67 – 3.55 (m, 1H), 3.11 (s, 2H), 2.88 – 2.71 (m, 1H), 2.48 – 2.35 (m, 1H), 1.68 – 1.60 (m, 1H), 1.56 – 1.46 (m, 1H), 1.02 (s, 3H), 0.53 (s, 3H). ^{13}C NMR (100 MHz, CDCl_3) δ 162.98, 134.57, 130.45, 129.68, 117.87, 114.24, 61.78, 59.68, 55.78, 45.76, 40.79, 37.43, 26.61, 26.15. MS; exact mass calculated for HRMS (EI) calc. for $[\text{C}_{16}\text{H}_{24}\text{O}_3\text{NS}]^+$: 310.1471, found: 310.1479. HPLC; Chiralpak IC; hexane : EtOH : TEA = 97 : 3 : 0.01, 1 mL/min, 35.0 min. and 37.8 min.

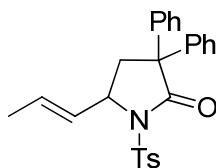


(E)-1-((4-methoxyphenyl)sulfonyl)-4,4-dimethyl-2-(prop-1-en-1-yl)pyrrolidine (2.22a). The general procedure for gold catalyzed hydroamination was used with **2.21** (50.0 mg, 0.162 mmol), AgBF_4 (1.9 mg, 0.0096 mmol), (*R*)-DTBMSEGPPOS(AuCl) $_2$ (7.9 mg, 0.0048 mmol) and 47.6 mg of products were isolated after chromatography on 20:1 hexanes:EtOAc (95% yield). ^1H NMR (400 MHz, CDCl_3) δ 7.81 – 7.66 (m, 2H), 7.03 – 6.88 (m, 2H), 5.58 (dq, J = 12.8, 6.4 Hz, 1H), 5.36 (dd, J = 15.2, 7.9 Hz, 1H), 4.07 – 3.96 (m, 1H), 3.87 (s, 3H), 3.17 (d, J = 10.1 Hz, 1H), 3.13 (d, J = 10.1 Hz, 1H), 1.76 – 1.67 (m, 1H), 1.65 (dd, J = 6.4, 1.3 Hz, 3H), 1.56 – 1.47 (m, 1H), 1.05 (s, 3H), 0.74 (s, 3H). ^{13}C NMR (100 MHz, CDCl_3) δ 162.80, 132.63, 131.03, 129.79, 126.85, 114.00, 62.10, 61.43, 55.76, 48.04, 37.49, 26.70, 26.32, 17.82. HRMS (EI) calc. for $[\text{C}_{16}\text{H}_{24}\text{O}_3\text{NS}]^+$: 310.1471, found: 310.1475. HPLC; Chiralpak IC; hexane : EtOH : TEA = 97 : 3 : 0.01, 1 mL/min, 53.6 min and 55.9 min.



5-allyl-3,3-diphenyl-1-tosylpyrrolidin-2-one (2.24b). ^1H NMR (400 MHz, CDCl_3) δ 7.82 (d, J = 8.3 Hz, 2H), 7.31 – 7.10 (m, 11H), 7.10 – 7.00 (m, 2H), 5.81 – 5.67 (m, 1H), 5.16 (d, J = 10.2 Hz, 1H), 5.05 (dd, J = 17.1, 1.4 Hz, 1H), 4.31 – 4.19 (m, 1H), 3.03 – 2.95 (m, 1H), 2.95 (dd, J = 13.5, 6.9 Hz, 1H), 2.57 (dd, J = 13.5, 6.7 Hz, 1H), 2.43 (s, 3H), 2.28 (dt, J = 13.6, 8.8 Hz, 1H). ^{13}C NMR (100 MHz, CDCl_3) δ 174.77, 145.11, 142.43, 140.18, 135.23, 132.62, 129.51, 128.72,

128.66, 128.61, 127.90, 127.64, 127.47, 127.40, 119.71, 57.92, 56.93, 39.24, 38.76, 21.88. HPLC; Chiralpak IC; hexane : EtOH = 93 : 7, 1mL/min, 12.3 min and 15.1 min. HRMS (EI) calc. for $[C_{26}H_{26}O_3NS]^+$: 432.1628, found: 432.1636.



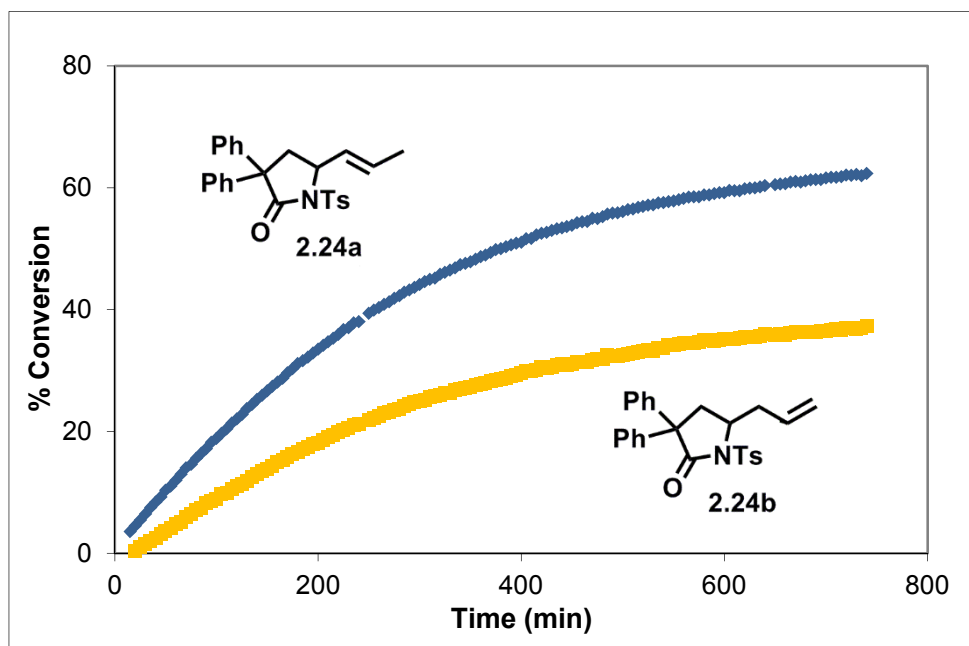
(E)-3,3-diphenyl-5-(prop-1-en-1-yl)-1-tosylpyrrolidin-2-one (2.24a). ^1H NMR (400 MHz, CDCl_3) δ 7.84 (d, J = 8.3 Hz, 2H), 7.31 – 7.08 (m, 12H), 5.80 (dq, J = 15.1, 6.8 Hz, 1H), 5.24 (dd, J = 15.1, 8.5 Hz, 1H), 4.66 – 4.55 (m, 1H), 3.01 (dd, J = 13.2, 6.8 Hz, 1H), 2.55 (dd, J = 13.3, 7.0 Hz, 1H), 2.44 (s, 3H), 1.69 (dd, J = 6.5, 1.6 Hz, 3H). ^{13}C NMR (100 MHz, CDCl_3) δ 174.32, 144.99, 141.92, 140.71, 135.97, 130.49, 129.82, 129.49, 128.84, 128.66, 128.56, 127.97, 127.57, 127.53, 127.38, 59.59, 58.12, 41.50, 21.88, 17.87. HPLC; Chiralpak IC; hexane : EtOH = 93 : 7, 1mL/min, 20.2 min and 28.1 min ((Z)-isomer, 19.1 min and 23.9 min). HRMS (EI) calc. for $[C_{26}H_{26}O_3NS]^+$: 432.1628, found: 432.1633.

Mechanistic Studies

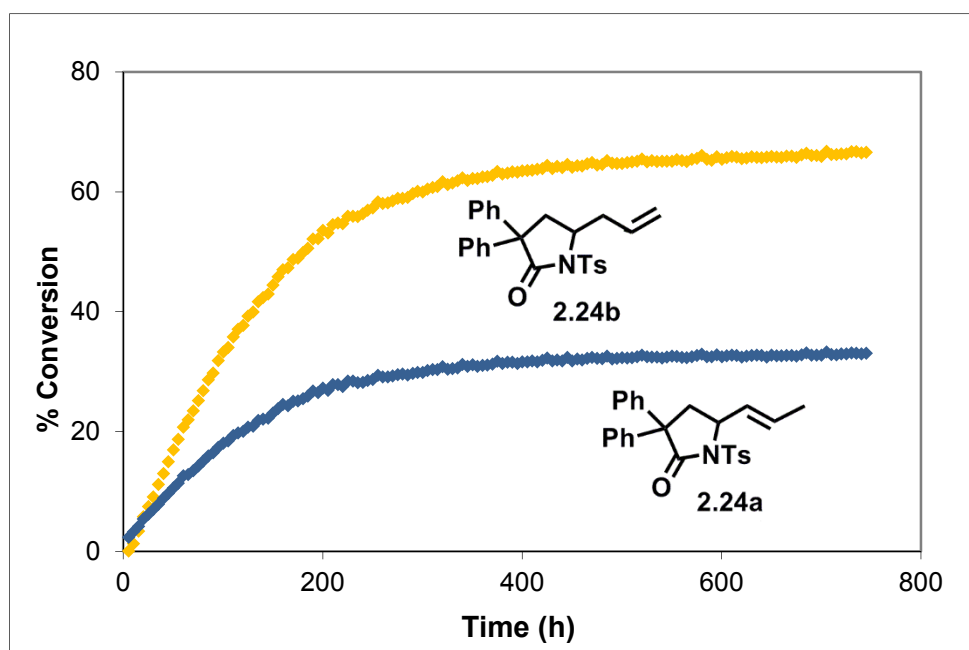
Procedure for monitoring the reaction with 2.23: A stock solution of **2.23** (42.0 mg, 0.097 mmol), (R)-DTBM-SEGPPOS(AuCl) $_2$ (4.8 mg, 0.0029 mmol), and toluene (internal standard, 10.3 μL , 0.097 mmol) in 2.1 mL CD_2Cl_2 was prepared. A second stock solution of AgBF_4 (11.5 mg, 0.058 mmol) was prepared in 0.69 mL CD_2Cl_2 and 0.04 mL EtOAc. At time $t = 0$, 0.073 mL of stock solution 2 was added to stock solution 1 and the resulting mixture was dispensed into three NMR tubes, two of which contained 2.0 equiv menthol or 2.0 equivalents of *i*PrOH, respectively. Both samples were monitored simultaneously by NMR on AV-500 and AV-600 spectrometers. The experiment was repeated twice and representative plots of the three reactions showing conversion to **2.24a** and **2.24b** as functions of time are shown in Figure S2.15. A plot showing the pseudo-first order kinetics of all three reactions is shown in Figure S2.16)

Figure S2.15. Monitoring hydroamination reaction with (a) 2.0 equiv. of menthol (b) 2.0 equiv. of *i*PrOH, and (c) in the absence of any additives. The allylic product is denoted by the blue line and the homoallylic product is denoted by gold line.

(a)



(b)



(c)

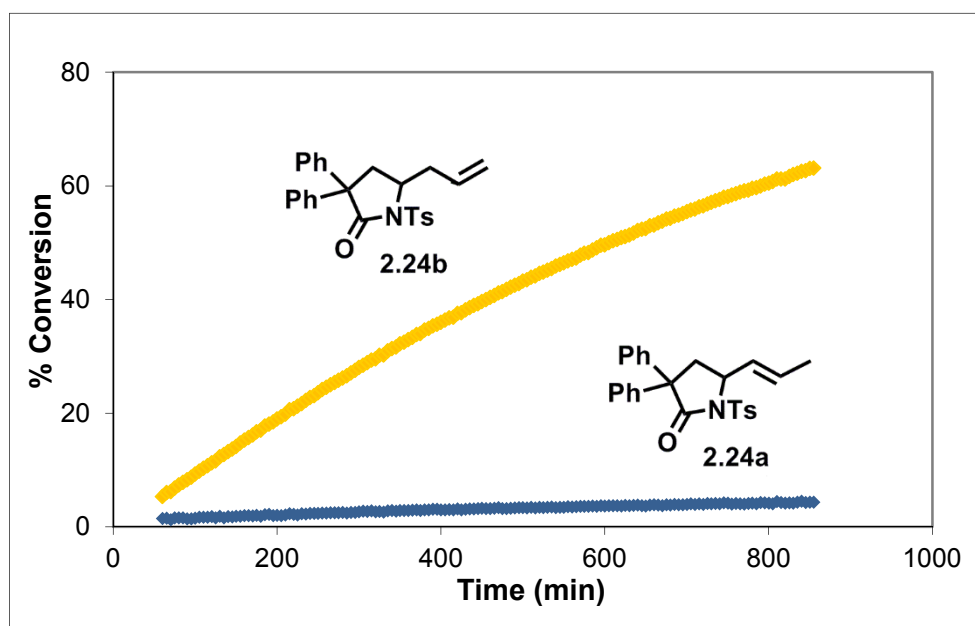
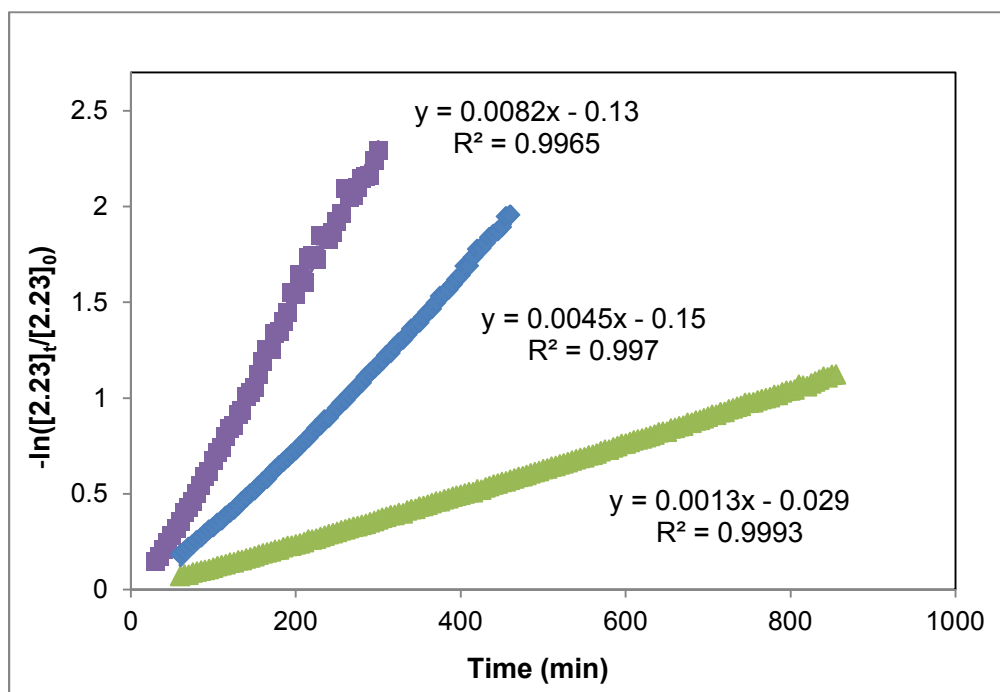
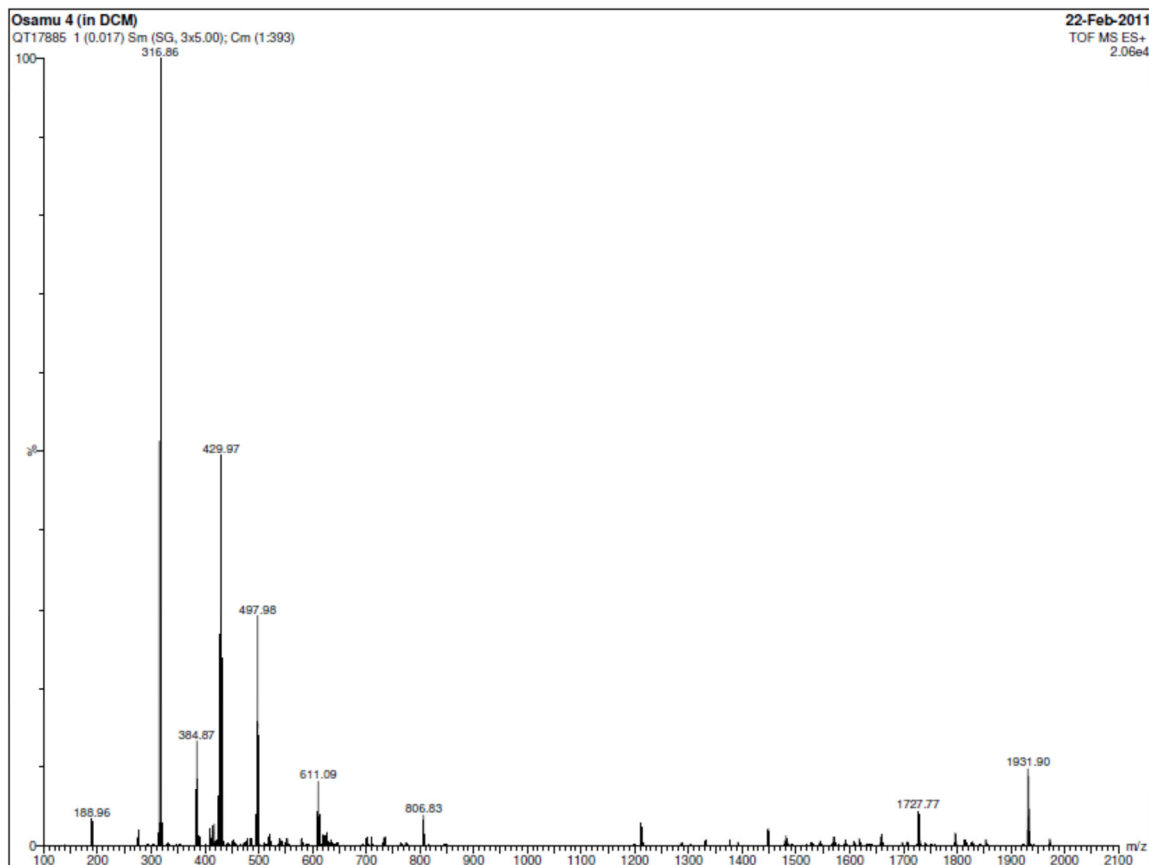
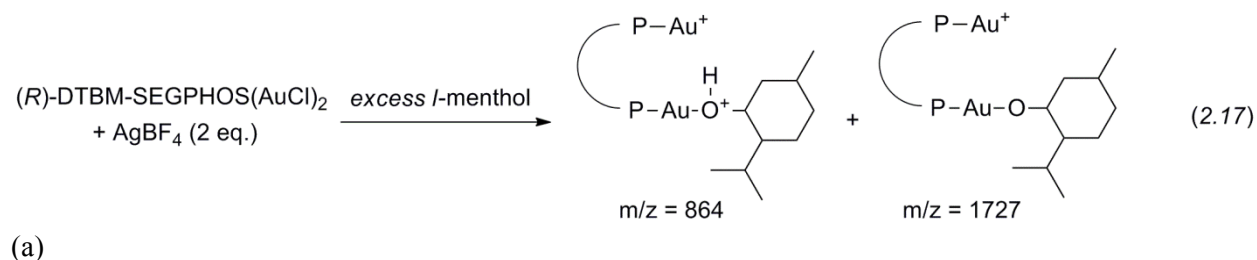


Figure S2.16. First order kinetic plots of $-\ln([2.23]_t/[2.23]_0)$ versus time (h). The slope of each line was taken to be the K_{tot} for the reaction.

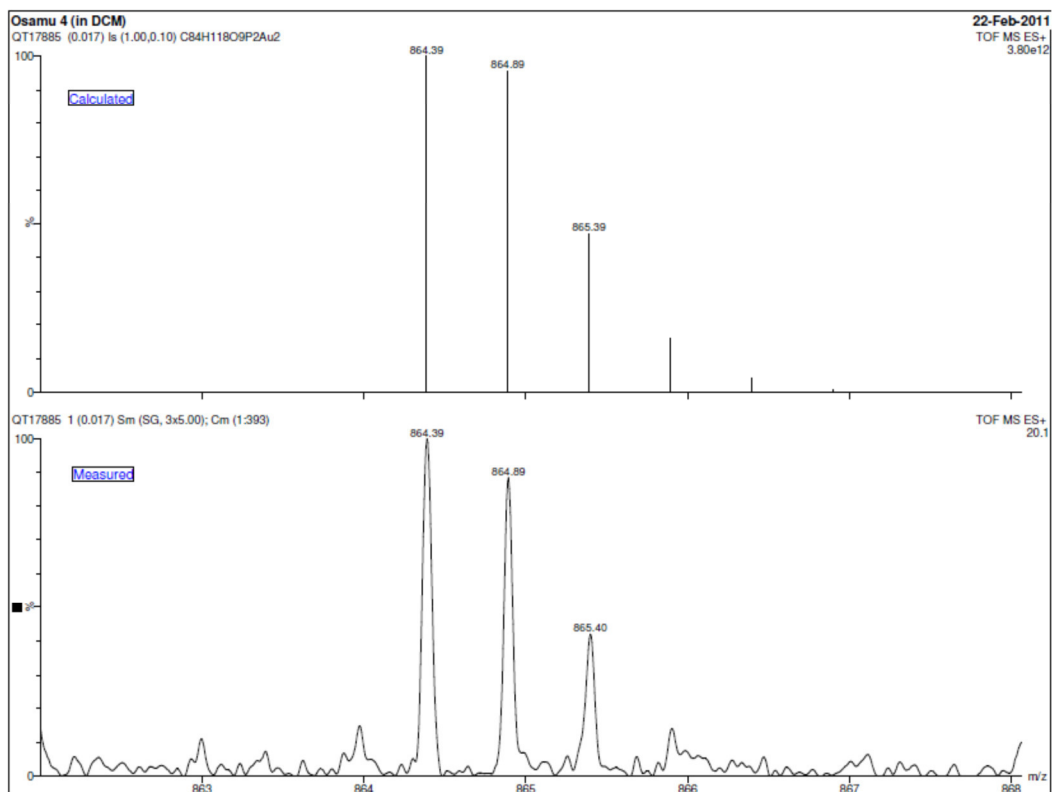


Mass Spectrometry. Mass spectrometry was carried on a Q-TOF Premier Spectrometer equipped with electrospray ionization source in positive ion mode. The sample was prepared by combining (R)-DTBM-SEGPHOS(AuCl)₂ with 2.0 equiv AgBF₄ and 66.0 equiv menthol in DCM so that a 50 μ M solution in gold complex was obtained. Both the +2 ion and +1 ion were observed by mass spectrometry. The full view of the mass spectrum is shown in Figure S2.17a. The simulated and collected data for and are shown in b and c, respectively.

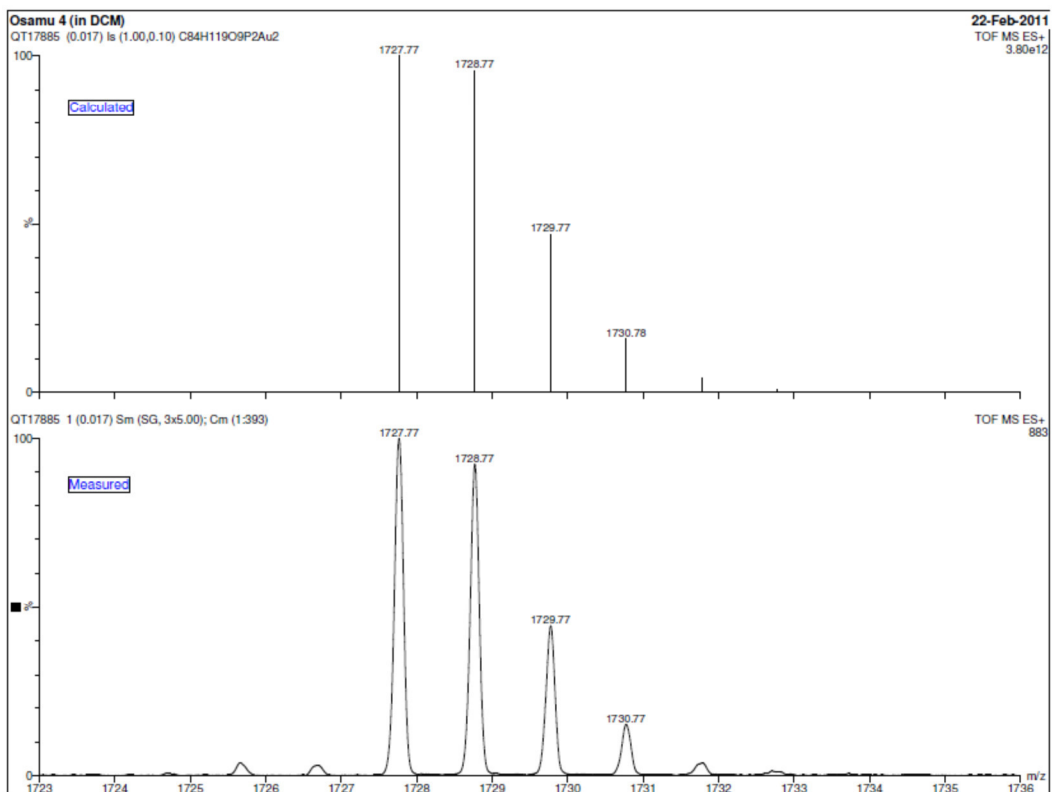
Figure S2.17. Mass spectrometry data via ESI for gold-menthol complexes.



(b)



(c)



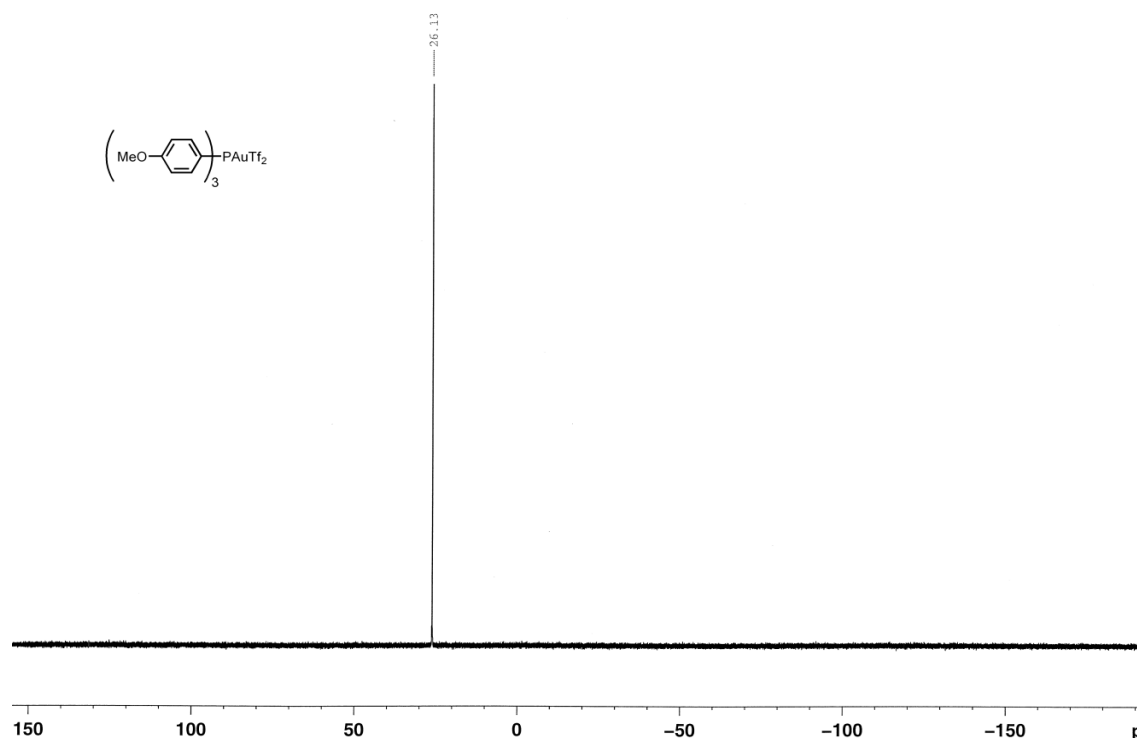
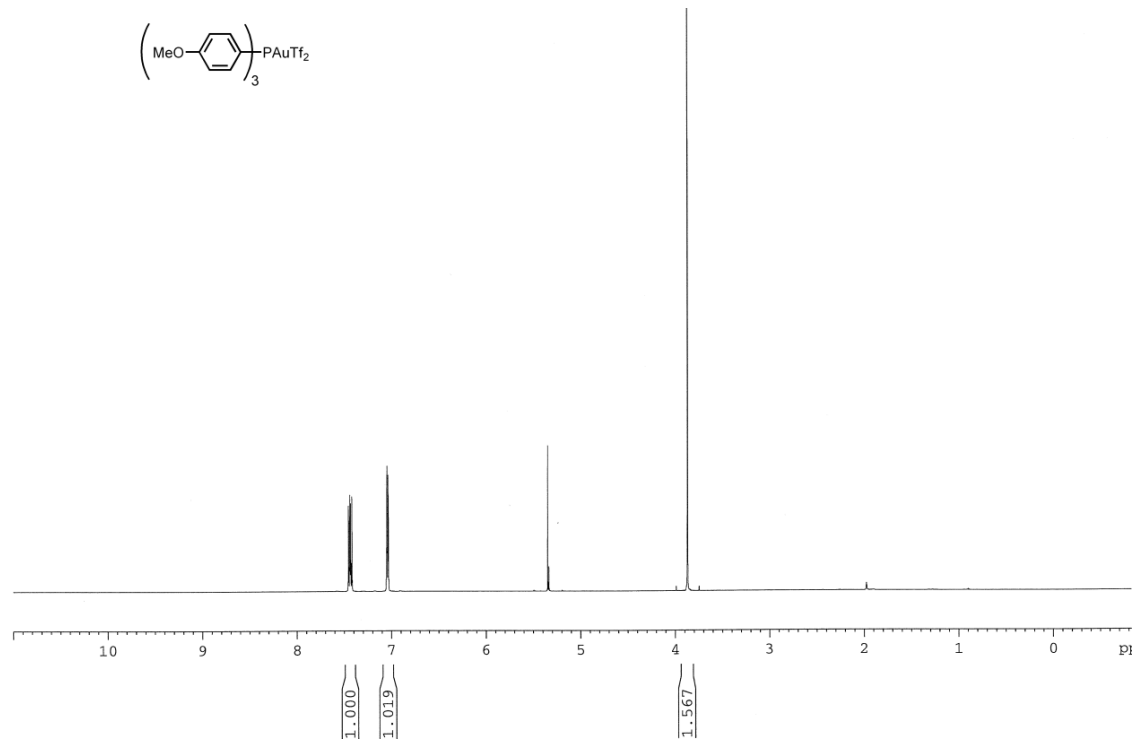
References

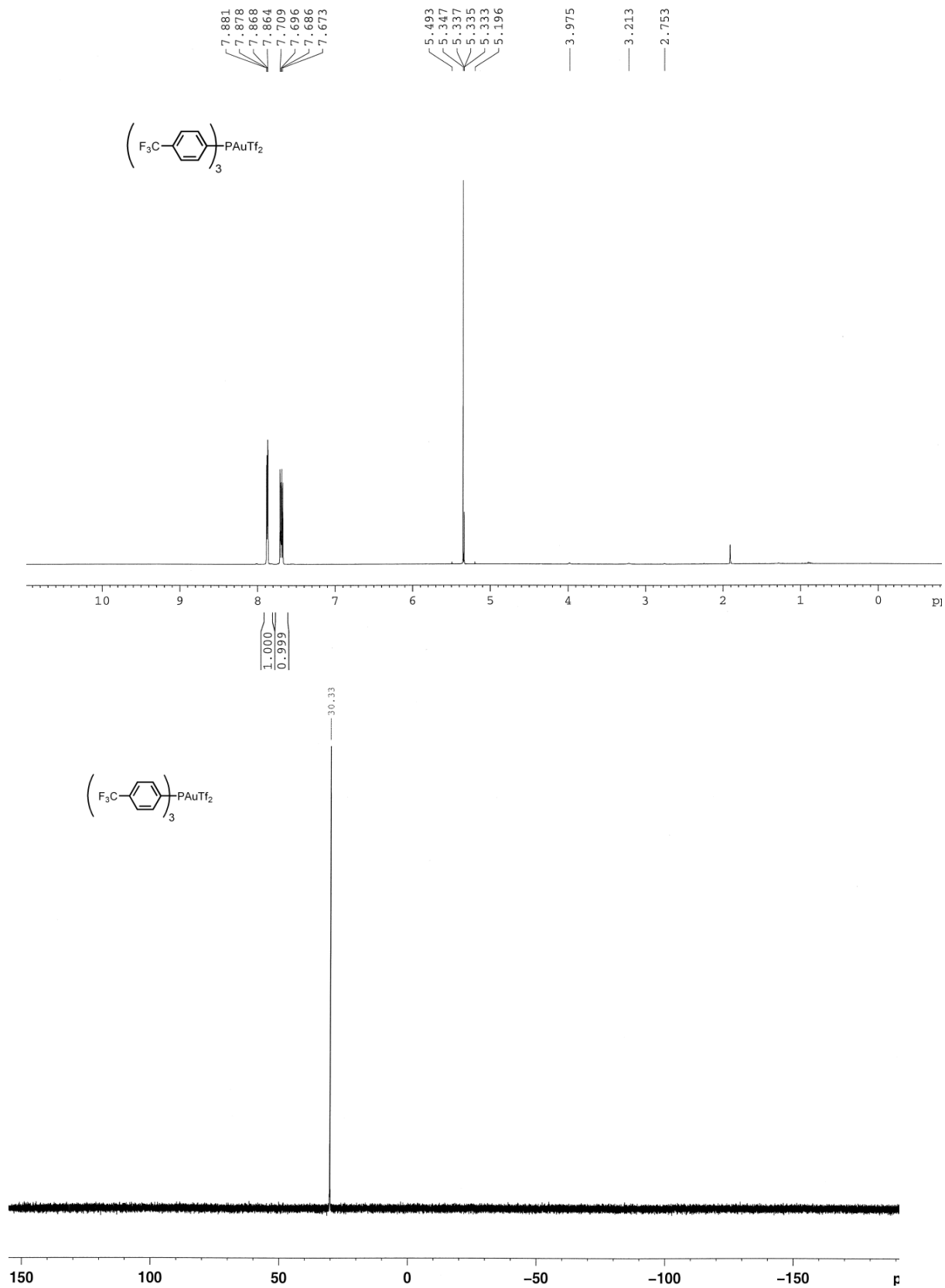
- (1) (a) Müller, T. E.; Beller, M. *Chem. Rev.* **1998**, *2*, 675. (b) Hultzsich, K. C. *Adv. Synth. Catal.* **2005**, *347*, 367.
- (2) Muller, T. E.; Hultzsich, K. C.; Yus, M.; Foubelo, F.; Tada, M. *Chem. Rev.*, **2008**, *108*, 3795.
- (3) (a) Zhang, Z.; Leitch, D. C.; Lu, M.; Patrick, B. O.; Schafer, L. L. *Chem. Euro. J.* **2006**, *7*, 2012. (b) Pohlki, F.; Doye, S. *Chem. Soc. Rev.* **2003**, *32*, 104.
- (4) Wang, X.; Widenhoefer, R. A. *Organometallics*. **2004**, *23*, 1649.
- (5) Hong, S.; Marks, T. J. *Acc. Chem. Res.* **2004**, *37*, 673.
- (6) (a) Walsh, P. J.; Baranger, A. M. *J. Am. Chem. Soc.* **1992**, *114*, 1708. (b) Johnson, J. S.; Bergman, R. G. *J. Am. Chem. Soc.* **2001**, *123*, 2923.
- (7) Pohlki, F.; Doye, S. *Angew. Chem. Int. Ed.* **2001**, *40*, 2305.
- (8) Straub, B. F.; Bergman, R. G. *Angew. Chem. Int. Ed.* **2001**, *40*, 4632.
- (9) Hesp, K. D.; Stradiotto, M. *Chem. Cat. Chem.* **2010**, *2*, 1192.
- (10) Casalnuovo, A.; Calabrese, J. C.; Milstein, D. *J. Am. Chem. Soc.* **1988**, *110*, 6738.
- (11) Zhou, J.; Hartwig, J. F. *J. Am. Chem. Soc.* **2008**, *130*, 12220.
- (12) Beller, M.; Trauthwein, H.; Eichberger, M.; Breindl, C.; Herwig, J.; Muller, T. E.; Thiel, O. R. *Chem. Eur. J.*, **1999**, *5*, 1306.
- (13) Hesp, K. D.; Tobisch, S.; Stradiotto, M. *J. Am. Chem. Soc.* **2010**, *132*, 413.
- (14) Utsunomiya, M.; Kuwano, R.; Kawatsura, M.; Hartwig, J. F. *J. Am. Chem. Soc.* **2003**, *125*, 5608.
- (15) Hartwig, J. F. *Pure Appl. Chem.* **2004**, *vol 76*, 507.
- (16) Nettekoven, U.; Hartwig, J. F. *J. Am. Chem. Soc.*, **2002**, *124*, 1166.
- (17) (a) Troups, K. L.; Widehoefer, R. A. *Chem. Commun.* **2010**, *46*, 1712. (b) Brunet, J. J.; Chu, N. C.; Diallo, O.; Vincendeau, S. *J. Mol. Catal. A: Chem.*, **2005**, *240*, 245.
- (18) (a) Robinson, R. S.; Dovey, M. C.; Gravestock, D. *Tet. Lett.* **2004**, *45*, 6787. (b) Sun, J.; Kozmin, S. A. *Angew. Chem. Int. Ed.* **2006**, *45*, 4991.
- (19) Bender, C. F.; Widenhoefer, R. A. *J. Am. Chem. Soc.* **2005**, *127*, 1070.
- (20) Rosenfeld, D. C.; Shekhar, S.; Takemiya, A.; Utsunomiya, M.; Hartwig, J. F. *Org. Lett.*, **2006**, *8*, 4179.
- (21) Bowring, M. A.; Bergman, R. G.; Tilley, T. D. *Organometallics*, **2011**, *30*, 1295.
- (22) For general reviews, see: (a) Gorin, D. J.; Sherry, B. D.; Toste, F. D.; *Chem. Rev.*, **2008**, *108*, 3351. (b) Jiménez-Núñez, E.; Echavarren, A. M.; *Chem. Commun.*, **2007**, 333. (c) Furstner, A.; Davies, P. W.; *Angew. Chem., Int. Ed.* **2007**, *46*, 3410. (d) Hashmi, A. S. K.; *Chem. Rev.* **2007**, *107*, 3180. (d) Li, Z.; Brouwer, C.; He, C.; *Chem Rev.*, **2008**, *108*, 3239.

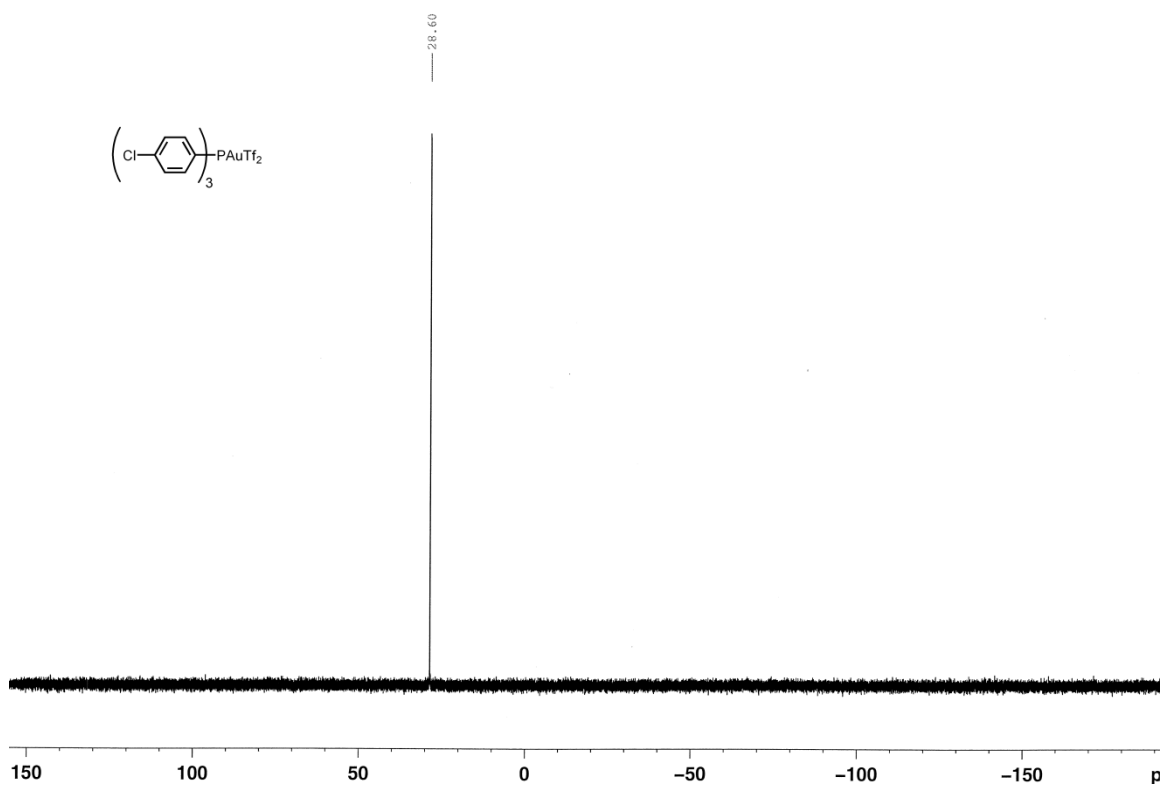
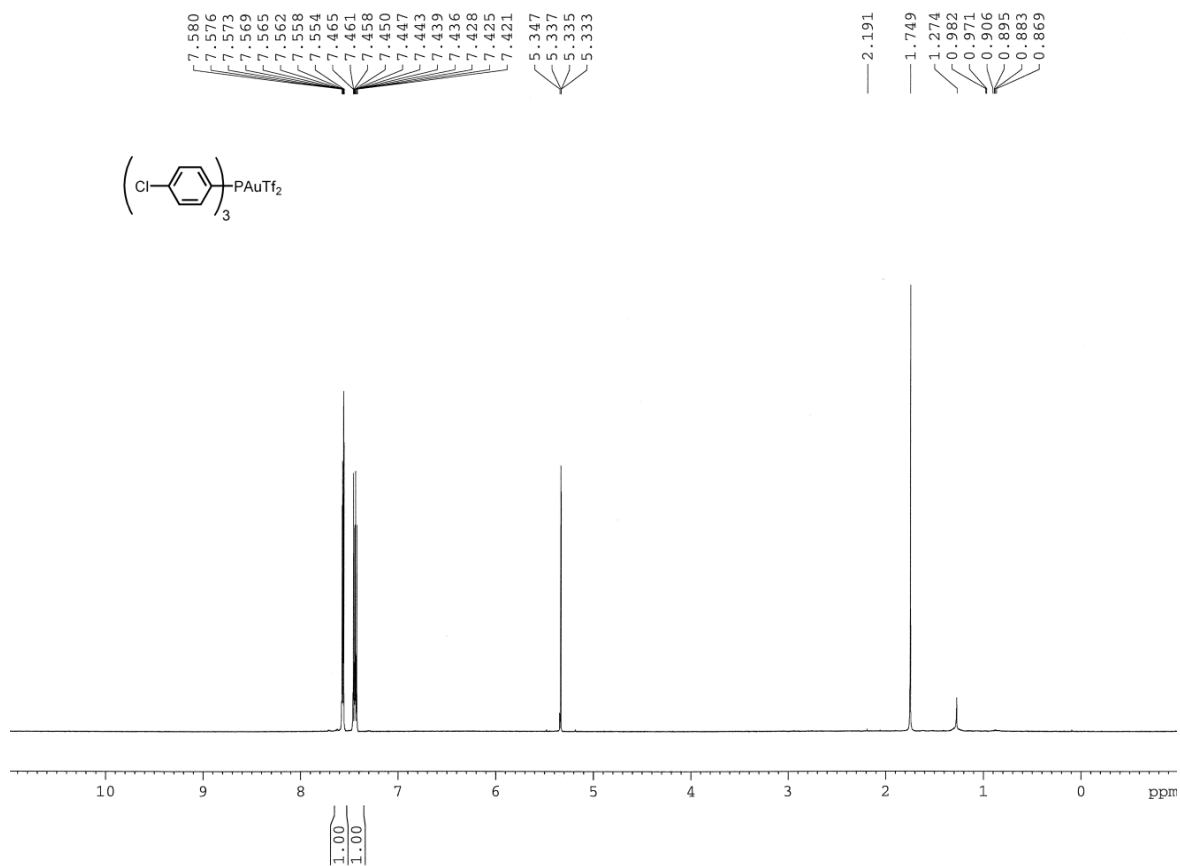
- (23) Gorin, D. J.; Toste, F. D.; *Nature*, **2007**, *446*, 395.
- (24) Zhang, Z.; Liu, Cong.; Kinder, R. E.; Han X.; Qian, H.; Widenhoefer, R. A. *J. Am. Chem. Soc.* **2006**, *128*, 9066.
- (25) Nishina, N.; Yamamoto, Y. *Tetrahedron* **2009**, *65*, 1799.
- (26) Duncan, A. N.; Widenhoefer, R. A. *Synlett* **2010**, 419.
- (27) Weber, D.; Tarselli, M. A.; Gagné, M. R. *Angew. Chem. Int. Ed.* **2009**, *48*, 5733.
- (28) Nishina, N.; Yamamoto, Y. *Angew. Chem. Int. Ed.* **2006**, *45*, 3144.
- (29) For proposed outer sphere mechanisms, see: Widenhoefer, R. A.; Han, Q. *Eur. J. Org. Chem.* **2006**, 4555. and reference 24.
- (30) For proposed inner sphere mechanisms, see: Zeng, X.; Soleilhavoup, M.; Bertrand, G. *Org. Lett.* **2009**, *11*, 3166 and reference 25.
- (31) (a) Schmidbaur, H. *Gold Bulletin*, **2000**, *33*, 3. (b) Scherbaum, F.; Grohmann, A.; Huber, Brigitte.; Kruger, C.; Schmidbaur, H. *Angew. Chem. Int. Ed.* **1988**, *27*, 1544.
- (32) Cheong, P. H.; Morganelli, P.; Luzung, M. R.; Houk, K. N.; Toste, F. D. *J. Am. Chem. Soc.* **2008**, *130*, 4517.
- (33) For selected examples of in situ catalyst generation with silver salts, see: (a) Hyland, C. T.; Hegedus, L. S. *J. Org. Chem.* **2006**, *71*, 8658. (b) Zhang, Z.; Bender, C. F.; Widenhoefer, R. A. *J. Am. Chem. Soc.* **2007**, *129*, 14148. (c) Liu, C.; Widenhoefer, R. A. *Org. Lett.* **2007**, *9*, 1935. (d) Piera, J.; Krumlinde, P.; Strübing, D.; Bäckvall, J. E.; *Org. Lett.* **2007**, *9*, 2235. (e) Hamilton, G. L.; Kang, E. J.; Mba, M.; Toste, F. D. *Science* **2007**, *317*, 496.
- (34) For an example of a gold(I) trimer precatalyst, see: (f) Sherry, B. D.; Maus, L.; Laforteza, B. N.; Toste, F. D. *J. Am. Chem. Soc.* **2006**, *128*, 8132.
- (35) Lalonde, R. L.; Wang, J. Z.; Mba, M.; Lackner, A. D.; Toste, F. D. *Angew. Chem. Int. Ed.* **2009**, *49*, 598.
- (36) Kanno, O.; Kuriyama, W.; Wang, Z. J.; Toste, F. D. *Angew. Chem. Int. Ed.*, **2011**, *50*, 9919.
- (37) (a) Mezailles, N.; Ricard, L.; Gagosz, F. *Org. Lett.* **2005**, *7*, 4133. (b) Toullec, P. Y.; Blarre, T.; Michelet, V. *Org. Lett.* **2009**, *11*, 2888.
- (38) (a) Grisé, C. M.; Barriault, L. *Org. Lett.* **2006**, *8*, 5905. (b) Grisé, C. M.; Rodrigue, E. M.; Barriault, L. *Tetrahedron* **2008**, *64*, 797. (c) Seidel, G.; Mynott, R.; Fürstner, A. *Angew. Chem. Int. Ed.* **2009**, *48*, 2510.
- (39) Mizushima, E.; Hayashi, T.; Tanaka, M. *Org. Lett.* **2003**, *5*, 3349. Also see reference 30.
- (40) For examples with gold(I), see: (a) Mauleon, P.; Krinsky, J. L.; Toste, F. D. *J. Am. Chem. Soc.* **2009**, *131*, 4513. (b) Benitez, D.; Tkatchouk, E.; Gonzales, A. Z.; Goddard, W. A., III; Toste, F. D. *Org. Lett.* **2009**, *11*, 4798. (c) Deutsch, C.; Gockel, B.; Hoffman-Roder, Anja, Krause, N. *Synlett*, **2007**, *11*, 1790.
- (41) For an example with gold(III), see: Morita, N.; Krause, N. *Org. Lett.* **2004**, *6*, 4121.

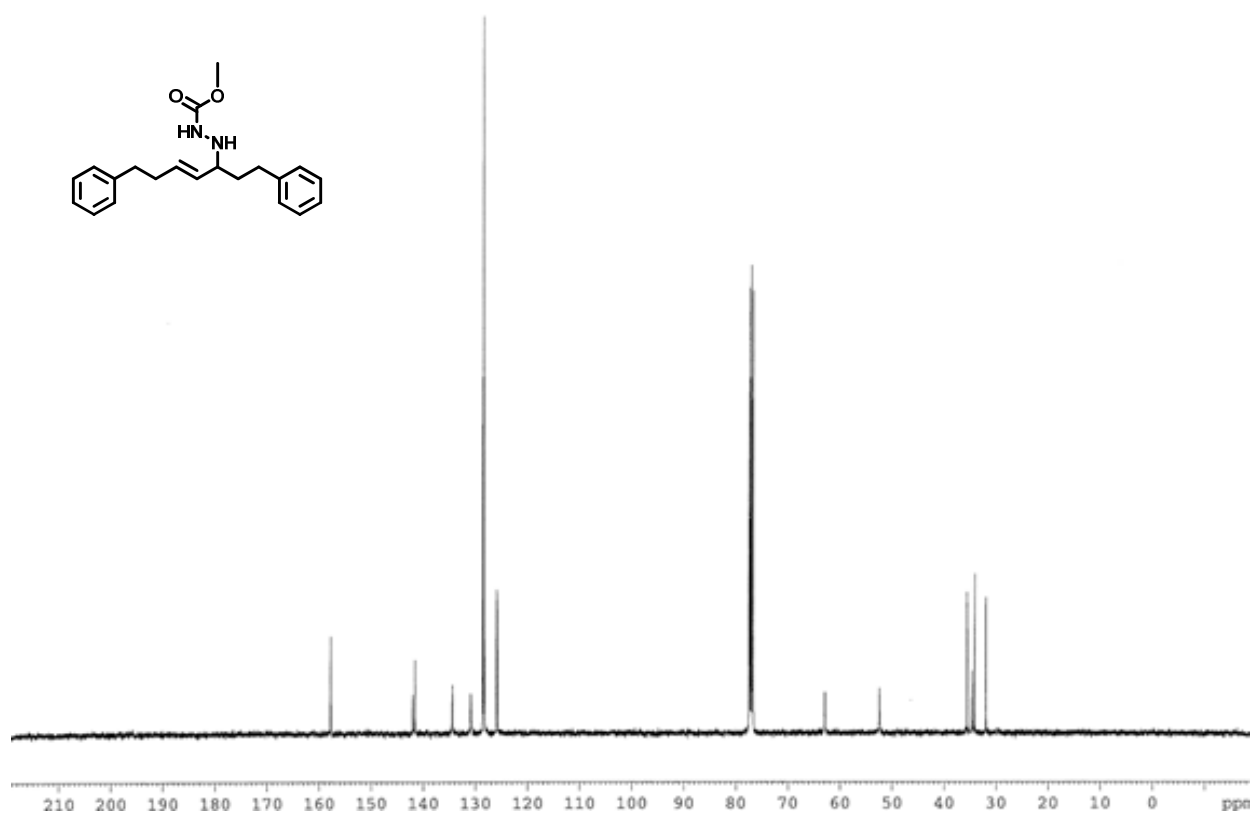
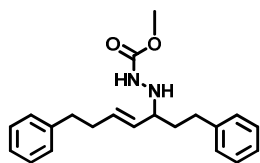
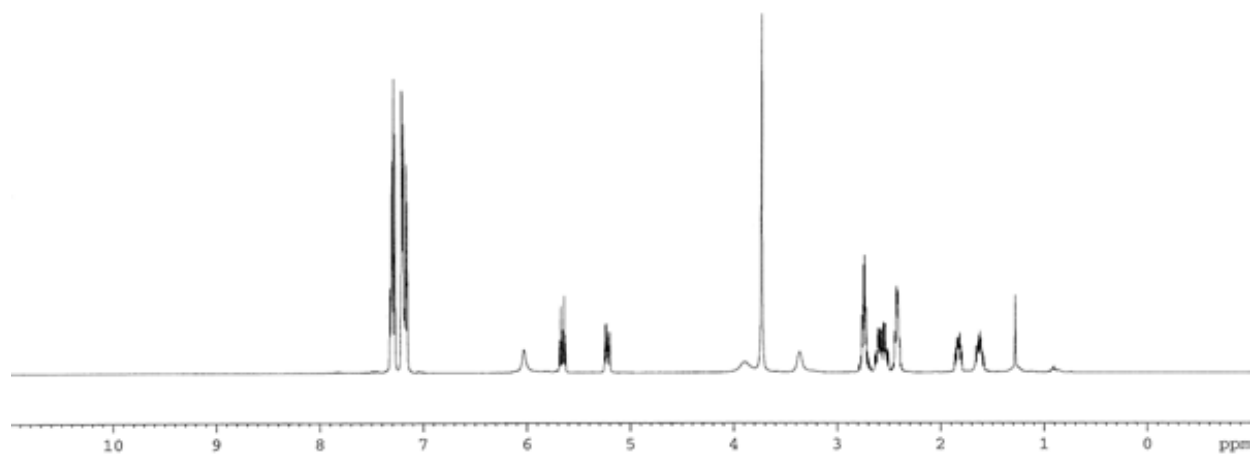
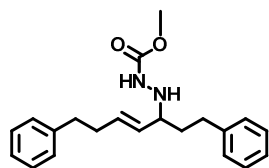
- (42) Hashmi, A. S. K.; Ramamurthi, T. D.; Rominger, F. *J. Organomet. Chem.* **2009**, 694, 592.
- (43) Shi, Y.; Ramgren, S. D.; Blum, S. A. *Organometallics* **2009**, 28, 1275.
- (44) Mohr, F.; Falvello, L. R.; Laguna, M. *Eur. J. Inorg. Chem.* **2006**, 833.
- (45) Porter, K. A.; Schier, A.; Schmidbaur, H. *Organometallics* **2003**, 22, 4922.
- (46) Herrero-Gómez, E.; Nieto-Oberhuber, C.; López, J. Benet-Buchholz, J.; Echavarren, A. M. *Angew. Chem. Int. Ed.* **2006**, 45, 5455.
- (47) Brown, T.J.; Dickens, M.G.; and Widenhoefer, R.A; *J. Am. Chem. Soc.*, **2009**, 131, 6350.
- (48) (a) Brown, T. M.; Sugie, A.; Leed, M. G. D.; Widenhoefer, R. A. *Chem. Euro. J.* **2012**, ASAP. DOI: 10.1002/chem.201103289. (b) Gandon, V.; Lemiére, G.; Hours, A.; Fensterbank, L.; Malacria, M. *Angew. Chem. Int. Ed.* **2008**, 47, 7534.
- (49) The pseudo first order rate constants (k_{obs}) measured reflects the rate of formation of both *trans* and *cis* hydroamination products.
- (50) For examples involving showing nucleophilic addition as the first irreversible step in the catalytic cycle, see reference 24 and Kinder, R. E.; Zhang, Z.; Widenhoefer, R. A. *Org. Lett.* **2008**, 10, 3157.
- (51) For studies of hydroamination of dienes and olefins, see Kovacs, G.; Ujaque, G.; Lledos, A. *J. Am. Chem. Soc.* **2008**, 130, 853. (b) LaLonde, R. L.; Brenzovich, W. E.; Benitez, D.; Tkatchouk, E.; Kelly, K.; Goddard, W. A.; Toste, F. D. *Chem. Sci.* **2010**, 1, 226.
- (52) Mauleon, P.; Zeldin, R. M.; Gonzalez, A.Z.; Toste, F. D. *J. Am. Chem. Soc.* **2009**, 131, 6348.
- (53) (a) Sherry, B. D.; Toste, F. D. *J. Am. Chem. Soc.* **2004**, 126, 15978. (b) Lee, J. H.; Toste, F. D.; *Angew. Chem. Int. Ed.* **2007**, 46, 912.
- (54) (a) Zhang, Z.; Widenhoefer, R. A. *Org. Lett.* **2008**, 10, 2079. (b) Patil, N. T.; Lutete, L. M.; Nishina, N.; Yamamoto, Y. *Tetrahedron Lett.* **2006**, 47, 4749.
- (55) Myers, A. G.; Zheng, B. *J. Am. Chem. Soc.* **1996**, 118, 4492.
- (56) Hadfield, M. S.; Lee, A. *Org. Lett.* **2010**, 12, 484.
- (57) We calculate isomer **2.14a** to be ~1 kcal/mol higher in free energy than **2.14b**.
- (58) Singleton, D. A.; Hang, C.; Szymanski, M. J.; Meyer, M. P.; Leach, A. G.; Kuwata, K. T.; Chen, J. S.; Greer, A.; Foote, C. S.; Houk, K. N. *J. Am. Chem. Soc.* **2003**, 125, 1319.
- (59) Garayalde, D.; Gomez-Bengoa, E.; Huang, X. G.; Goeke, A.; Nevado, C. *J. Am. Chem. Soc.* **2010**, 132, 4720.
- (60) Wang, Z. J.; Benitez, D.; Tkatchouk, E.; Goddard, W. A.; Toste, F. D. *J. Am. Chem. Soc.* **2010**, 132, 13064.
- (61) Yamaguchi, M.; Hayashi, A.; Minami, T. *JOC.* **1991**, 56, 4091.
- (62) Takaya, J.; Iwasawa, N.; *J. Am. Chem. Soc.* **2008**, 130, 15254.

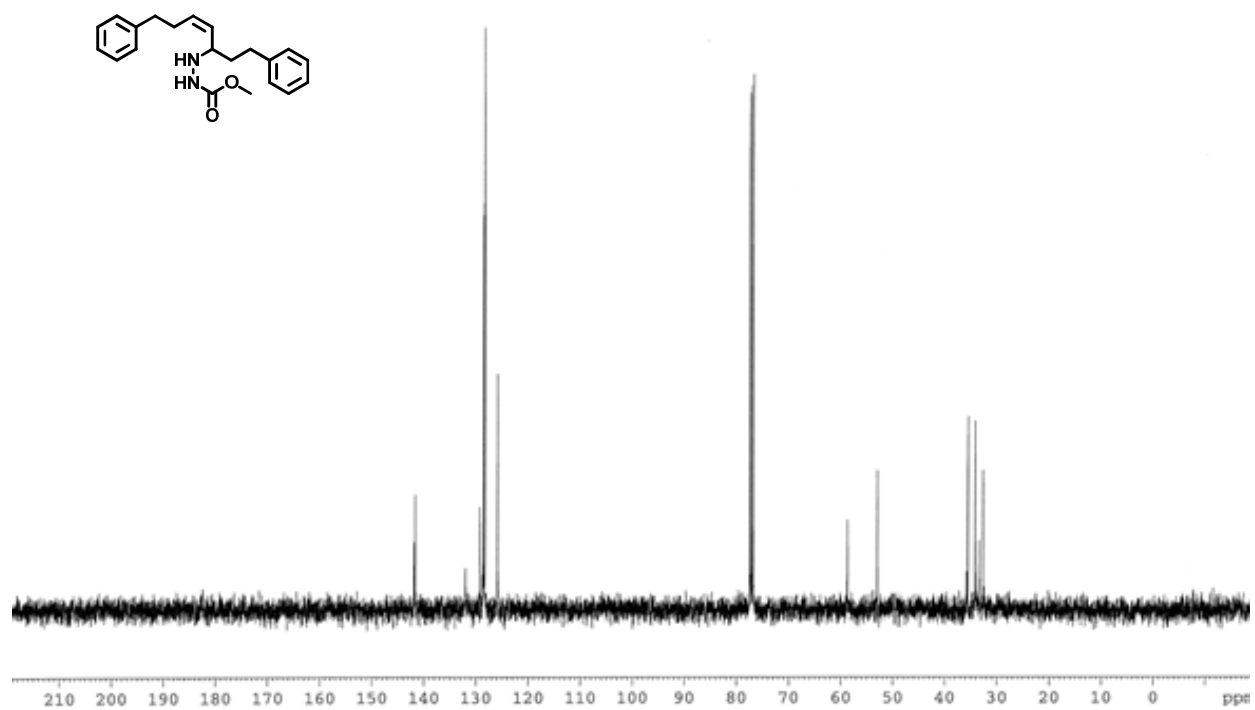
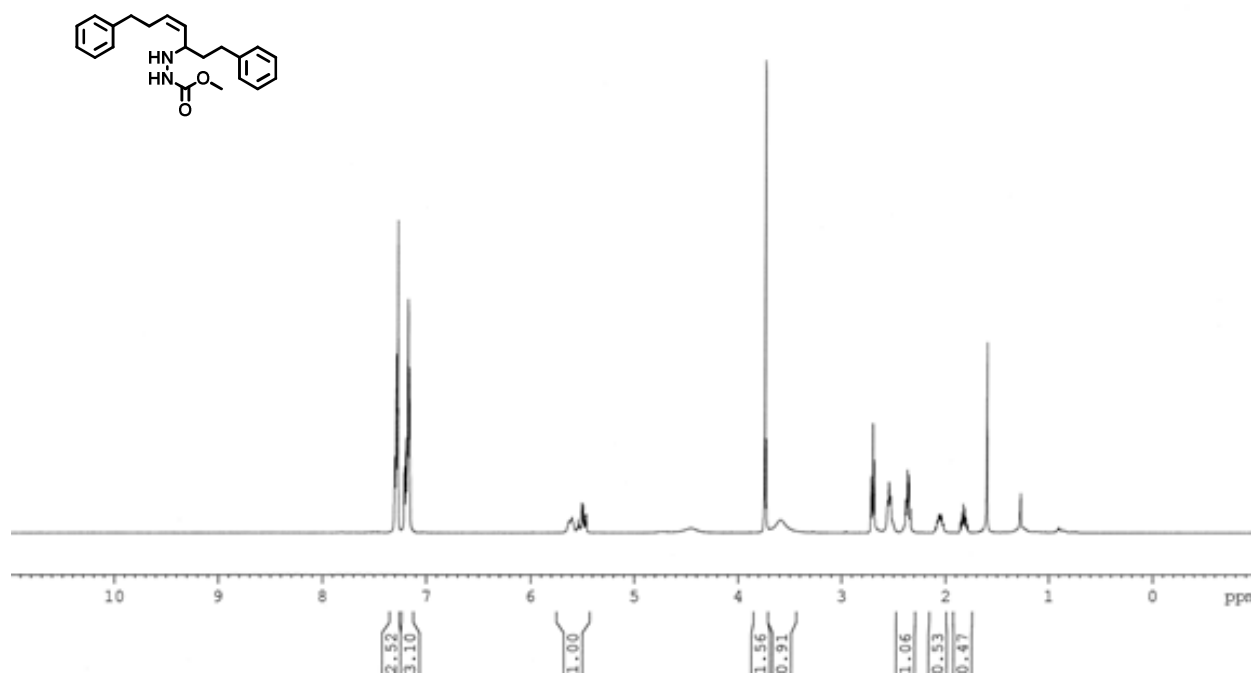
Appendix 2A: Additional NMR Spectra

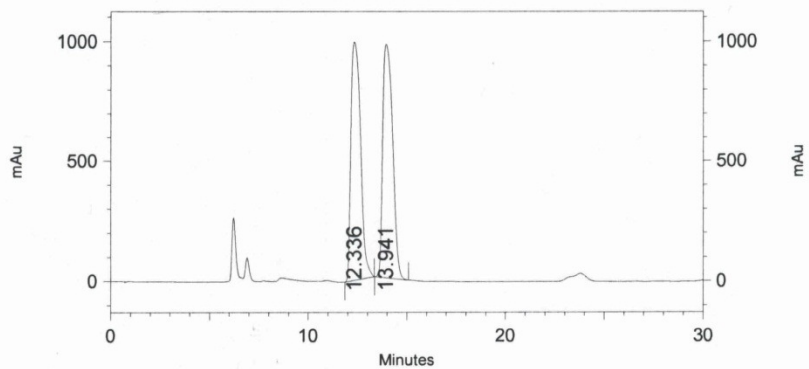
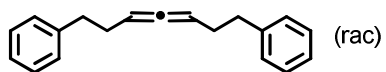






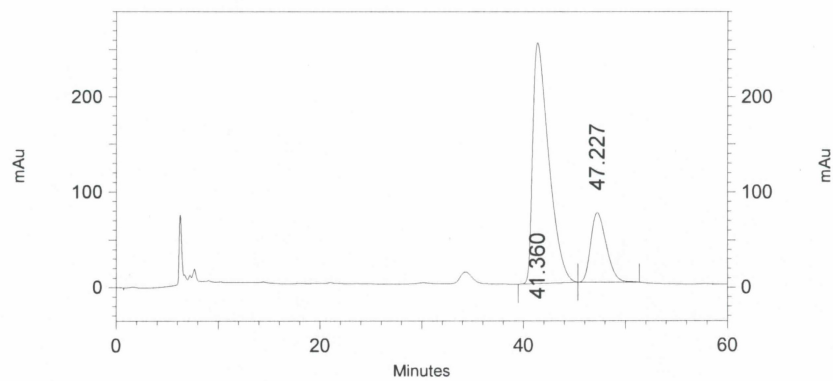
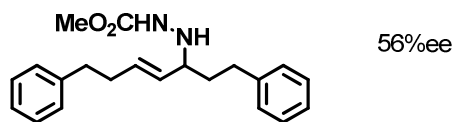






1: 210 nm, 4 nm Results

Retention Time	Area	Area Percent
12.336	33821406	49.769
13.941	34134794	50.231



1: 215 nm, 4 nm Results

Retention Time	Area	Area Percent
41.360	27700241	78.084
47.227	7774574	21.916

Chapter 3:

Catalysis by Gold(I) Complexes Encapsulated in a Supramolecular Cluster

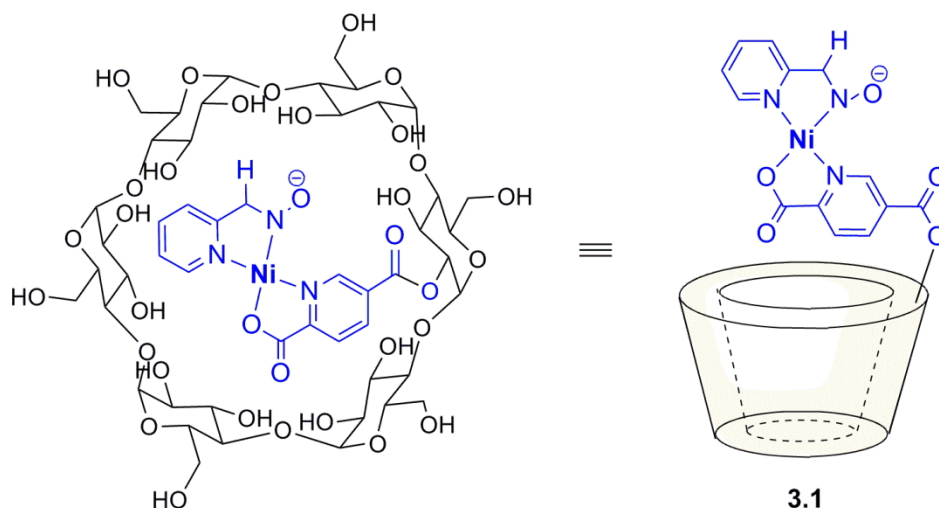
Portion of this work has been published in Wang, Z. J.; Casey, C. J; Bergman, R. G.; Raymond, K. N.; Toste, F. D. “Hydroalkoxylation Catalyzed by a Gold(I) Complex Encapsulated in a Supramolecular Host.” *J. Am. Chem. Soc.* **2011**, *133*, 7358-7360.

¹ The initial reaction discovery was performed with Dr. Casey Brown. Dr. Casey Brown also prepared the supramolecular cluster $K_{12}Ga_4L_6$ (**3.8**) used for catalysis.

Introduction to Supramolecular Catalysis

A longstanding goal of supramolecular and small molecule catalysis has been the design and preparation of assemblies that mimic the desirable catalytic qualities of enzymes.^{1,2} These qualities include the ability to (1) provide an “active site” for reaction removed from the bulk solvent, (2) select one substrate from a pool of molecules based on size, shape, or chirality, (3) produce one product with high regio-, chemo- and stereoselectivity, and (4) demonstrate dramatic rate enhancements relative to the uncatalyzed reaction.³ In contrast to small molecule catalysts, supramolecular complexes offer distinct advantages toward these goals as their three-dimensional cavities provide multiple points of interaction with a given substrate.⁴ The earliest supramolecular assemblies employed for catalysis were based on cyclodextrin frameworks, reported by Breslow over 4 decades ago (Figure 3.1).⁵ Cyclodextrin itself catalyzes a variety of hydrolysis reactions⁶ and the first “artificial enzymes” reported in the literature were cyclodextrins appended with nickel(II) complexes (3.1).

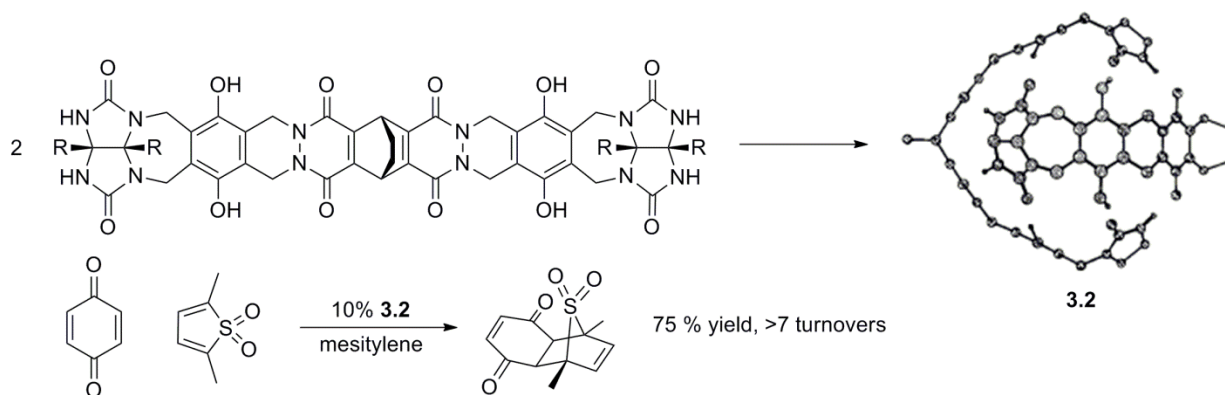
Figure 3.1. α -Cyclodextrin modified with Ni(II)-complex for hydrolysis of nitrophenyl acetate.



In recent years, several self-assembled supramolecular frameworks have emerged for catalysis.⁷ In contrast to the cyclodextrin and other early supramolecular hosts, many of these new assemblies are formed from metal-ligand coordination or hydrogen bond networks.^{8,9} The ability of these complexes to self-assemble is an important synthetic advantage over traditional covalent bond structures as complex three-dimensional scaffolds can be prepared from relatively simple subunits and the size and geometry of the scaffold can be dramatically altered via small changes in the organic ligand.¹⁰ Furthermore, the resulting assemblies often exhibit properties that are very different from the individual ligands or subunits.¹¹ While some of these frameworks act as “molecular flasks,” promoting the desired transformation by increasing the effective molarity of two reactants, others incorporate catalytically active guests into host-guest complexes.¹² In both of these cases, the interior of the molecular container is chemically distinct from the solvent and can help to mold substrates into reactive conformations or stabilize the reactive species.¹³

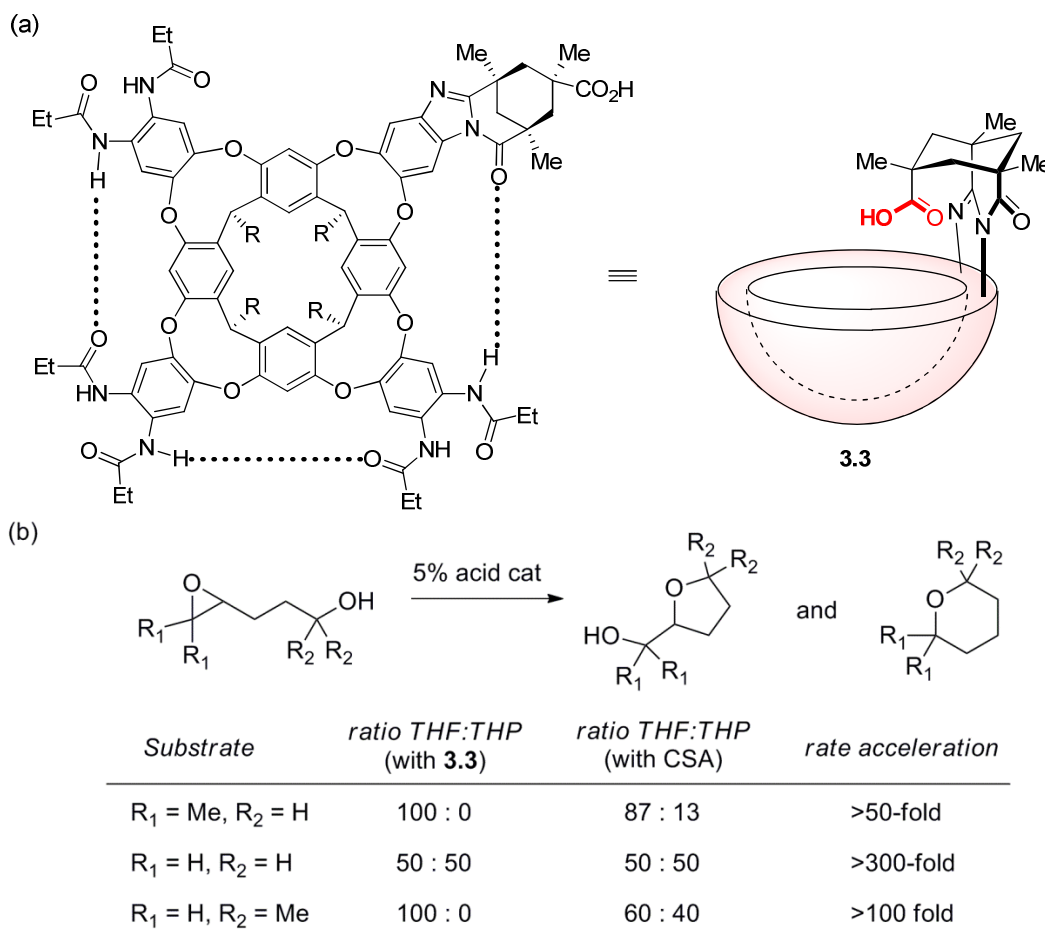
In 1997, Rebek reported a dimeric assembly for the Diels-Alder reaction of *p*-benzoquinone and cyclohexadiene.¹⁴ The supramolecular container (**3.2**) is comprised of two halves, containing two glycoluril subunits each and held together by intermolecular hydrogen bonds in the geometry of a “molecular softball” (Figure 3.2). The two halves assemble readily in organic solvent with a dimerization constant $> 10^6 \text{ M}^{-1}$ and interior volume of $\sim 300 \text{ \AA}^3$. The reaction of *p*-benzoquinone and cyclohexadiene is accelerated over 200-fold inside the capsule relative to the background reaction in the absence of cluster. Severe product inhibition prevented catalytic turnover and the overall reaction could only be run with low concentrations of starting materials. However, if the diene partner is changed to 2,5-dimethylthiophene dioxide, product inhibition was significantly reduced and up to 7 catalytic turnovers can be observed. This reaction was the first example of true catalysis by a molecular flask.

Figure 3.2. Catalytic Diels Alder reactions within a supramolecular “softball.”



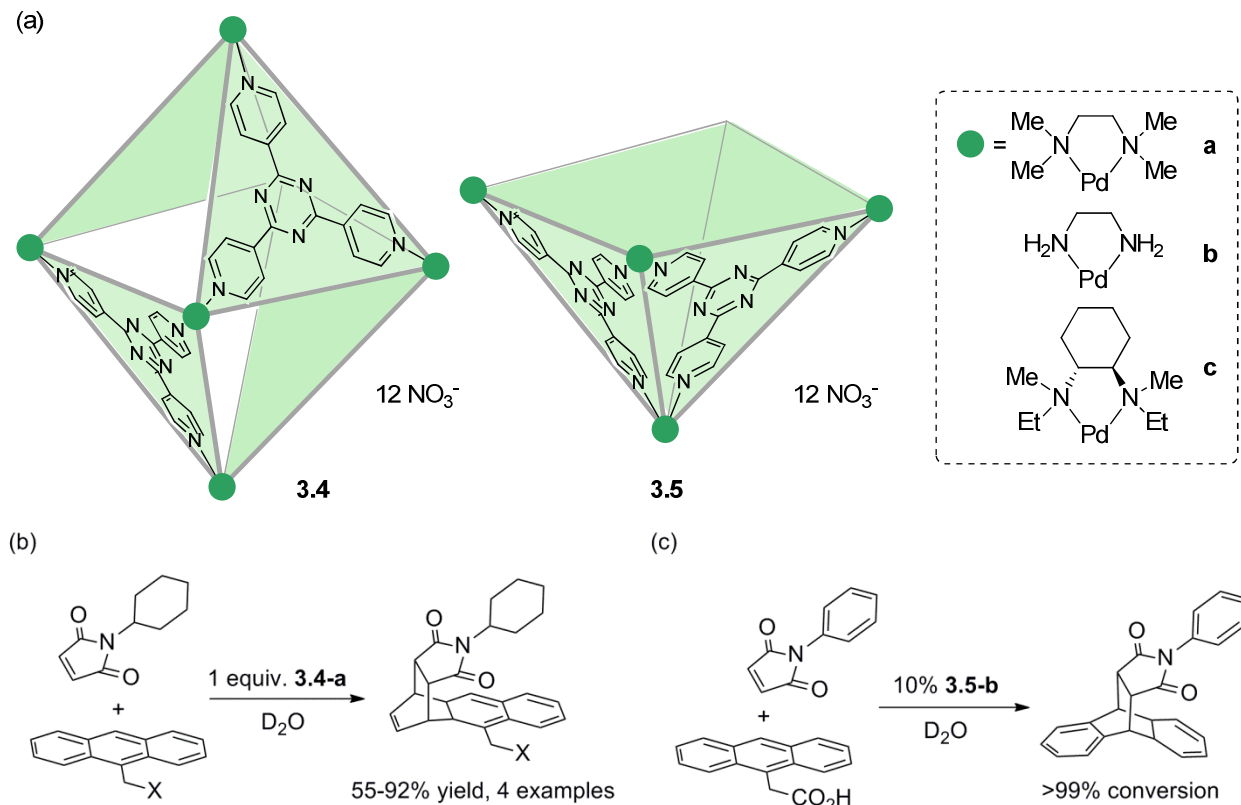
Since this seminal work, the Rebek group has reported several other hydrogen bonded assemblies, including **3.3**.¹⁵ In particular, Kemp's triacid derivative can be incorporated into one of the four subunits of **3.3** to form a bowl-shaped supramolecular Brønsted-acid catalyst (Figure 3.3). This catalyst was used for intramolecular epoxide opening and provided the desired product in high yield after 24 h with only 5 mol% catalyst loading. Remarkably, reaction inside the cavitand produced the tetrahydrofuran derivative as the sole product, while the reaction with CSA in organic solvent yielded both the 5 and 6-membered ring products. The selectivity and 50- to 300-fold rate enhancement observed were attributed to both the high concentration of Brønsted acid experienced by the substrate upon encapsulation and the cavitand itself in helping to coil the substrate into reactive cyclic conformations.

Figure 3.3. (a) Supramolecular Brønsted acid catalyst. Dashed lines indicate hydrogen bonds between the subunits. (b) Catalysis by **3.3** in ring opening of epoxides leads to rate acceleration and a product distribution different from that observed in the reaction catalyzed by CSA.



While hydrogen-bonded supramolecular assemblies have been used in a variety of organic reactions, they are unsuitable for reaction in polar protic or aqueous solvent, as protic solvents can disrupt the hydrogen bonding network holding the assembly together. In contrast, assemblies constructed from metal-ligand interactions are robust and can be used in both aqueous and nonaqueous solution. The Fujita group has prepared a variety of palladium and platinum clusters using pyridine-metal bonds (Figure 3.4a).¹⁶ The octahedral cage **3.4** self-assembles in the presence of end-capped Pd(II) complexes with triazine ligands, is highly charged (overall +12), and is readily soluble in water. In 2006, this complex was used as a catalyst in the Diels Alder reaction of anthracene and *N*-cyclohexyl maleimides.¹⁷ Encapsulation of the starting materials is promoted by the hydrophobic and pi-stacking effects and reaction occurs at room temperature with a rate improvement of up to 113-fold. The reaction with a stoichiometric amount of **3.4-a** yielded only the 1,4-addition product (Figure 3.4b), as opposed to the 9,10-adduct typically observed under typically thermal conditions. The selectivity observed was attributed to the restrictive environment within the supramolecular assembly, which organized the substrates into conformations favorable for reaction at the 1,4-positions.

Figure 3.4. Supramolecular octahedron (**3.4**) and “uncapped” assembly (**3.5**). Each green panel indicates one triazine ligand. Green circles at each apex indicates a Pd(II) center. (b) Diels-Alder reaction within **3.4-a** produces only the 1,4-adduct. (c) Diels-Alder reaction with catalytic **3.5-b** yields only the 9,10-adduct.

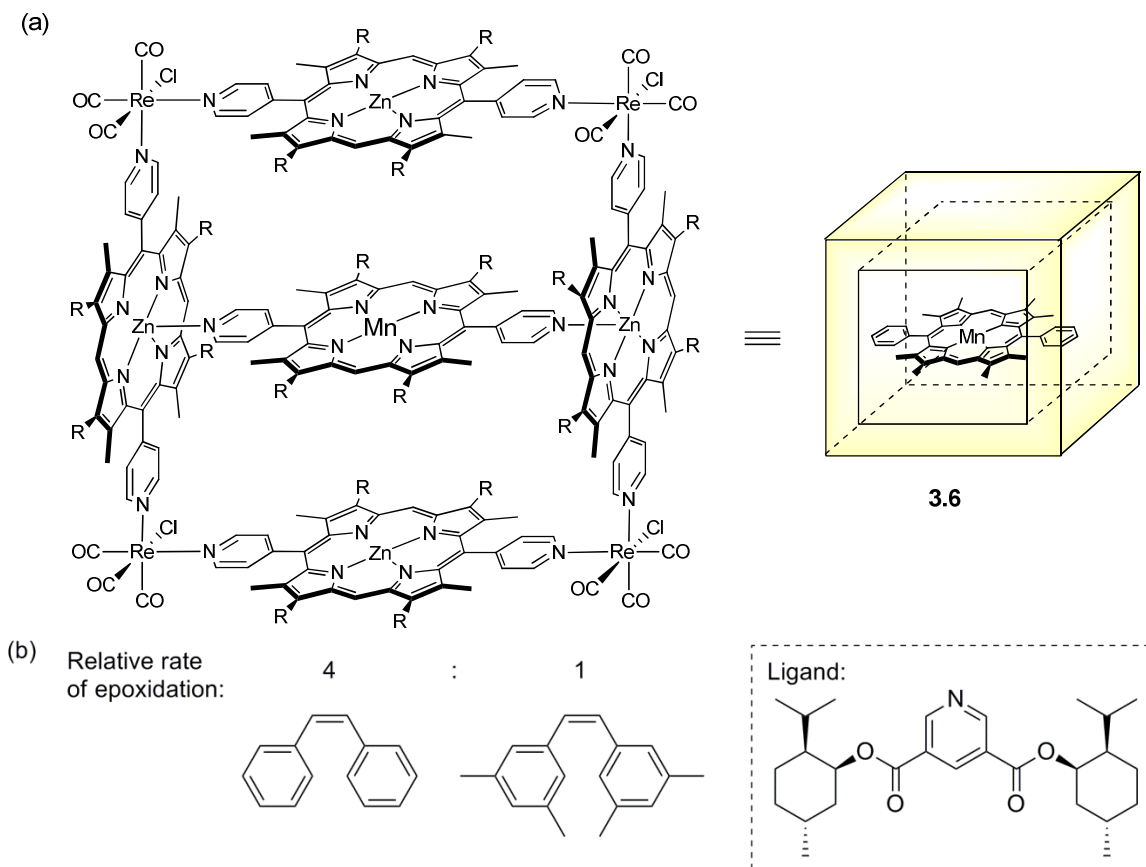


In contrast, the catalytic reaction of the maleimide and anthracene with the structurally related but “uncapped” complex **3.5-b** yielded the expected 9,10-adduct as the sole product (Figure 3.4b). The authors attribute this difference in product selectivity to the “open” face of complex **3.5**, which allows the phenyl maleimide to align with the 9,10-position prior to cycloaddition. The catalytic reaction was not inhibited by product formation, as the addition of maleimide introduced a bend in the product that prevented effective pi-stacking with the assembly. While **3.4** is not inherently chiral, introduction of chiral capping ligands on palladium (**3.4-c**) allowed the asymmetric [2+2] cross photoaddition of maleimide and fluoroanthrene to proceed in nearly 50% enantioselectivity.¹⁸

In addition to assemblies that act as supramolecular flasks, many supramolecular assemblies have been used as hosts for active metal complexes. In these examples the guest complex catalyzes the desired transformation, while the supramolecular host can improve the stability of the guest, restrict the space around the guest for improved selectivity, or increase the solubility of the guest in a given solvent. The first examples of transitional metal catalysts encapsulated in supramolecular frameworks were reported by the Hupp and Nguyen groups.¹⁹ In 2001, they reported encapsulation of a Mn(II) pyridyl-porphyrin complex inside a molecular square (**3.6**) comprised of four Zn(II) porphyrin units linked by four $\text{Re}(\text{CO})_3\text{Cl}$ corners (Figure 3.5).

Coordination of the pyridines on the catalytically active Mn(II)-porphyrin to the Zn(II) centers lock the complex within the square.

Figure 3.5. (a) Mn(II) porphyrin encapsulated in a supramolecular square comprised of Zn-porphyrins linked by Rh(I) corners. (b) Addition of ligands for Zn on **3.6** leads to substrate size selectivity.

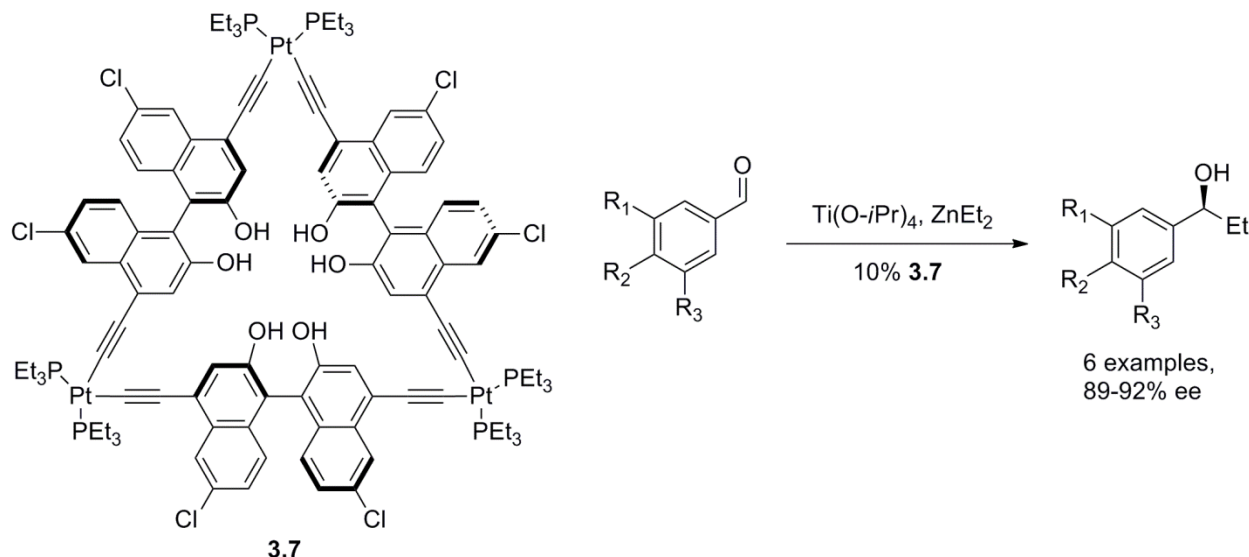


The host-guest complex **3.6** was used in the epoxidation of olefins. The lifetime of the Mn(II)-porphyrin complex in water was significantly improved from 10 min to 3 h upon encapsulation. This led to a 10-fold improvement in turnover number. Additionally, coordination of bulky pyridyl ligands to the remaining two Zn(II) centers on the interior of the square decreased the space within the square available for substrate binding and thus greatly improved the selectivity of the host-guest complex for reaction with smaller substrates.

The first chiral host-guest complex for catalysis was reported by Lin in 2002.²⁰ They prepared a molecular triangle comprised of three binol units ligated by three Pt(II) centers (**3.7**) which was then used in combination with $\text{Ti}(\text{O}-i\text{Pr})_4$ and ZnEt_2 for the asymmetric addition to aldehydes (Figure 7). The titanium center bound strongly to the binol subunits and the resulting host-guest complex acted as a chiral Lewis acid catalyst to produce enantioselectivities as high as 92% with six substrates. Host-guest complexes analogous to the Ti(IV)-**3.7** system based on direct ligation of the guest metal have been explored extensively by Reek and van Leeuwen.^{21,22}

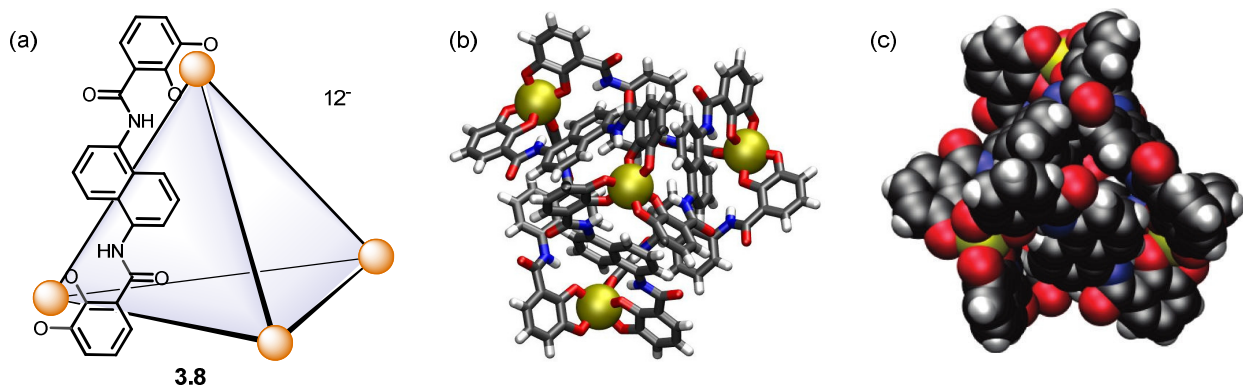
In these examples, a catalytically active metal such as Rh(I) or Pd(II) was used to template the supramolecular framework.

Figure 3.6. Binol-triangle **3.7** chelates Ti(IV), yielding a chiral Lewis acid catalyst for asymmetric aldehyde additions.

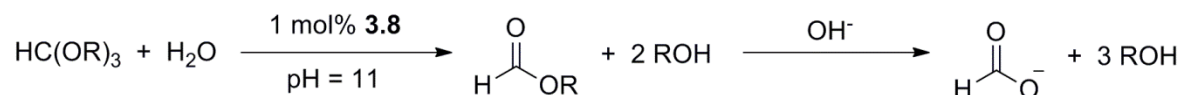


The Raymond and Bergman groups have reported a versatile supramolecular assembly that has functioned as a catalyst in organic reactions and has encapsulated a variety of organometallic guests. The assembly is comprised of four Ga(III) centers and six N,N'-bis(2,3-dihydroxybenzoyl)-1,5-diaminonaphthalene ligands that self-assemble into a tetrahedral cluster in water (Figure 3.7).²³ The complex is highly negatively charged (-12 overall), soluble in water, and has an interior volume of 350-500 Å³. While the cluster encapsulates monocationic guests most strongly, hydrophobic uncharged molecules and dicationic guests can also be bound internally.²⁴ The flexibility of the framework has allowed the formation of host-guest complexes with guests as small as tetramethylammonium and as large as Co(Cp)⁺₂.²⁵

Figure 3.7. (a) Cartoon depiction of Ga₄L₆ (**3.8**) where each vertex represents one Ga(III) center and each edge represents a naphthyl-catecholate ligand. (b) Molecular model of the Ga₄L₆ cluster, sighting down one of the C3-axes. (c) Space filling model of Ga₄L₆. (d) Orthoformate hydrolysis catalyzed by **3.8**.



(d)

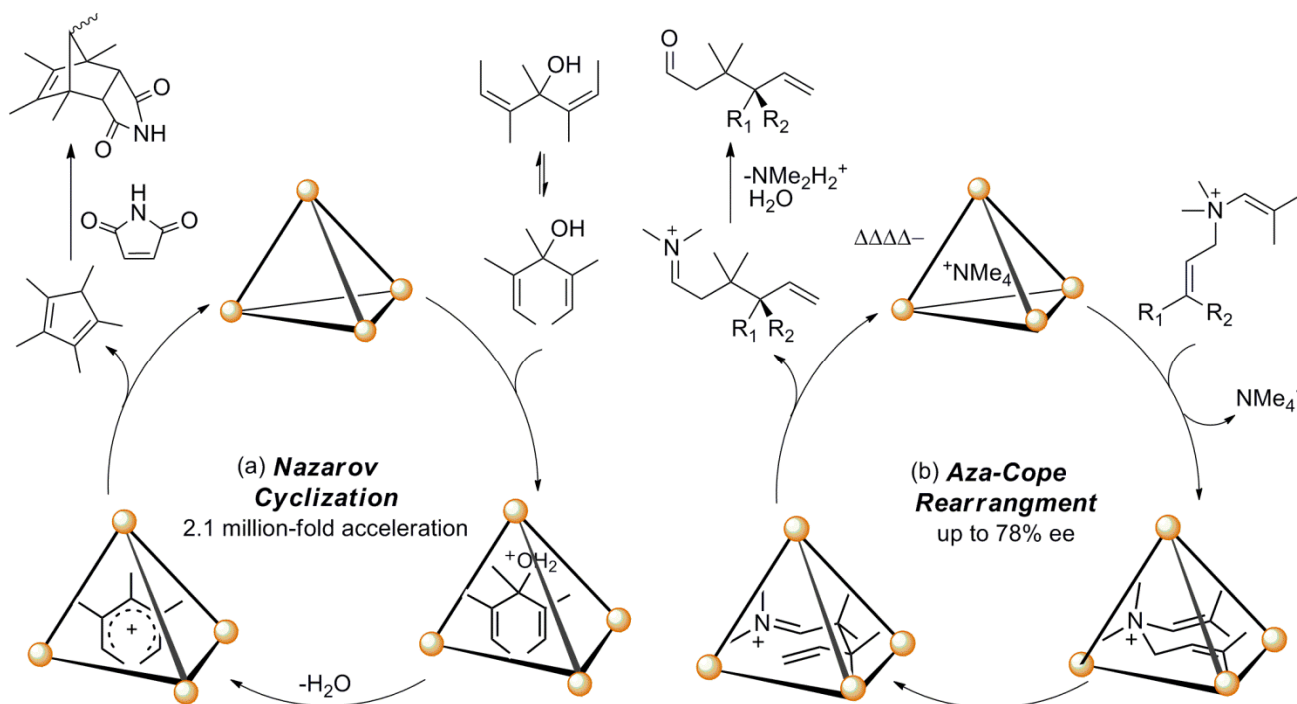


Due to the assembly's preference for binding monocations, the $\text{p}K_{\text{a}}$ of ammonium cations inside the cluster is raised by nearly 4 units²⁶ and acid-catalyzed reactions can occur even in basic solutions. For instance, the acid-catalyzed hydrolysis of orthoformates occurs at pH 11 at 50 °C in the presence of cluster **3.8** while no hydrolysis is observed if a “blocked” cluster bearing a strongly bound guest or no **3.8** is used.²⁷ Careful kinetic studies revealed that the system obeys Michaelis-Menten kinetics. The catalyst was found to rest as the orthoformate-encapsulated complex and protonation of the orthoformate in this complex was rate limiting. The kinetic data presented support the hypothesis that stabilization of the transition state leading to the protonated complex by the cluster was responsible for the rate enhancement observed.

The Ga_4L_6 cluster has also been used as a catalyst in Nazarov rearrangements (Figure 3.8a).²⁸ The reaction demonstrated a dramatic 2.1 million-fold rate acceleration relative to the uncatalyzed transformation and was the first example of acceleration by a supramolecular catalyst that approached the rate enhancement conferred by true enzymes. As the substrate could adopt both linear and U-shaped conformations, encapsulation helped to fold the substrate into the more reactive U-shaped conformation. Furthermore, the preference of the cluster for monocationic guests stabilized the transition state for ionization of the tertiary alcohol to the pentadienyl cation. Both of these factors are proposed to contribute to the acceleration observed. To alleviate product inhibition, maleimide was used as a trapping agent, which rapidly underwent Diels Alder cycloaddition with the cyclopentadiene product, shuttling it out of the catalytic cycle. Turnover numbers as high as 160 were achieved.

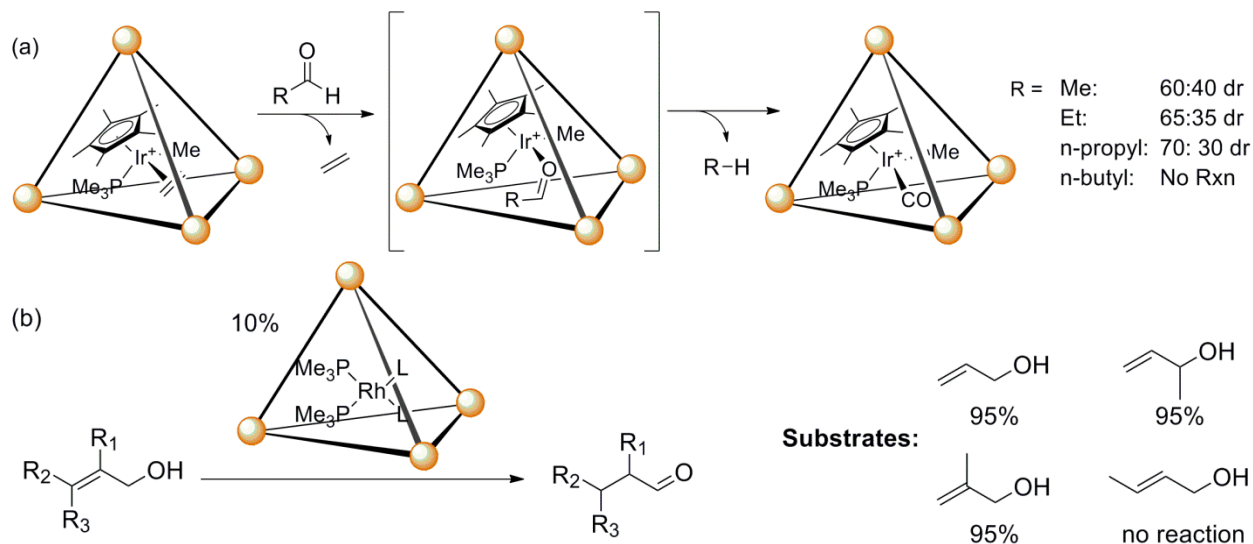
Additionally, **3.8** is inherently chiral due to the twist of the catecholate ligands and only enantiomeric homo-dimeric complexes ($\Delta\Delta\Delta\Delta$ and $\Lambda\Lambda\Lambda\Lambda$) are formed by self-assembly.²⁹ The enantiomeric complexes can be separated by introducing the chiral amine guest (-)-*N'*-methylnicotinium, and separating the resulting diastereomeric complexes. Ion exchange with tetramethylammonium can provide $\text{NMe}_4^+ \subset \Delta\Delta\Delta\Delta$ and $\text{NMe}_4^+ \subset \Lambda\Lambda\Lambda\Lambda$ (where \subset denotes encapsulation by the cluster). The isolated enantiopure assemblies have been used to catalyze the asymmetric Aza-Cope rearrangement of iminium substrates (Figure 3.8b). The iminium substrate is able to displace the tetramethylammonium cation and the imine product is hydrolyzed in solution to the neutral ketone, preventing competitive binding of the substrate and product. Molecular modeling of substrate binding showed that the prochiral conformation leading to the major product was 2.2 kcal/mol lower in energy than the conformation leading to its enantiomer. Synthetically, up to 78 % ee was observed. Currently, one limitation of asymmetric catalysis with **3.8** is that the resolved assemblies can only be isolated with the cationic amine guests (NMe_4^+ or *N'*-methylnicotinium). Thus, neutral and other weakly bound guests that cannot displace the ammonium guests cannot be incorporated into chiral host-guest complexes for catalysis.

Figure 3.8. Catalysis with Ga_4L_6 : (a) Nazarov cyclization of tertiary alcohols and (b) Enantioselective Aza-Cope Rearrangement with the enantio-resolved $\Delta\Delta\Delta\Delta$ -**3.8**.



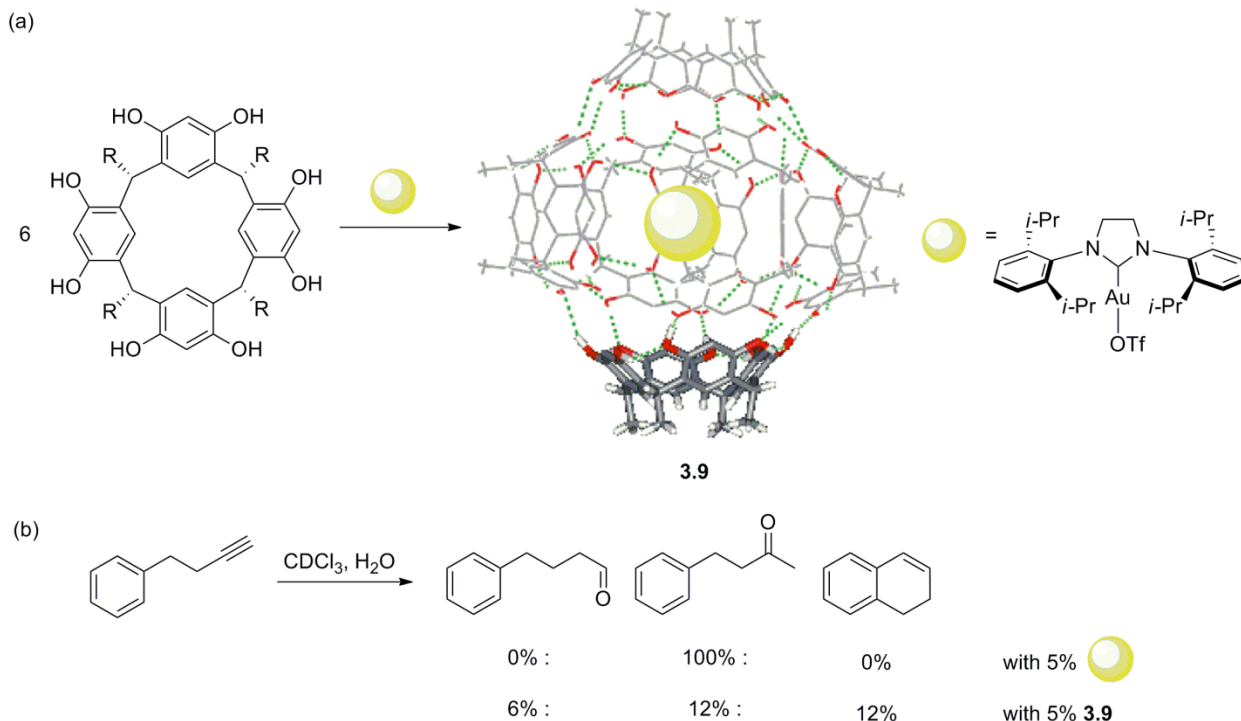
Cationic organometallic guests readily bind to **3.8** and in many cases exhibit selectivities not observed with the unencapsulated complexes. Host guest assemblies with iridium(I) half-sandwich complexes and rhodium(I) bisphosphine complexes have been prepared. The iridium(I) complex encapsulated in the supramolecular host³⁰ was stable inside the cluster for weeks, did not diffuse out into solution, and was able to activate primary aldehydes with loss of alkanes to provide the Ir(I)-CO complex with modest diastereo-, shape, and size selectivity (Figure 3.9a). While the overall transformation was not catalytic, this example was the first system to demonstrate that organometallic reactions can occur inside the Ga_4L_6 cluster. In contrast, the olefin isomerization reaction catalyzed by $(\text{Me}_3\text{P})_2\text{Rh}(\text{OD}_2)_2^+ \subset \text{3.8}$,³¹ could be achieved in high conversion with only 10 mol% catalyst loading (Figure 3.9b). However, due to the size of the rhodium complex, only the smallest substrates such as allyl alcohol and butene-ols could be employed. In both of these examples, the substrate selectivity observed provided evidence that reaction with the metal complex occurred on the inside of the cluster, rather than through aggregation of the metal to the cluster's exterior.

Figure 3.9. (a) C-H activation of aldehydes by $\text{Cp}^*\text{Ir}(\text{PMe}_3)(\text{Me})(\text{C}_2\text{H}_4) \mathbf{3.8}$. (b) Olefin isomerization of allylic alcohols by $(\text{PMe}_3)_2\text{Rh}(\text{OD}_2)_2^+ \mathbf{3.8}$.



Lastly, two reactions that were developed concurrently with the work described in this chapter are notable. In January 2011, Reek reported a hydrogen bonded supramolecular capsule comprised of six resorcin[4]arene units which was used to encapsulate a *N*-heterocyclic-carbene-Au(I) complex in chloroform (Figure 3.10a).³² The resulting host-guest complex was able to catalyze the hydration of alkynes and yielded three products in 12%, 6%, and 12% yield while the analogous reaction in the absence of the capsule yielded only the ketone hydration product in greater than 95% yield. Encapsulation greatly decreased the rate of hydration and less than 5 catalytic turnovers were observed before free NHC-Au(I) complex escaped from the capsule. Additionally, Brown et. al. developed a method for isomerization of allylic alcohols with $(\text{Me}_3\text{P})\text{CpRu}(\text{NCMe})_2^+ \mathbf{3.8}$ (Figure 3.10b).³³ While this reaction was slightly slower than the parallel reaction with free $(\text{Me}_3\text{P})\text{CpRu}(\text{NCMe})_2^+$, reaction with the encapsulated complex led to over 1000 catalytic turnovers, the highest observed for any organometallic host-guest complex. The lifetime of the Ru(II) catalyst was also greatly improved upon encapsulation.

Figure 3.10. (a) Hydrogen-bonded supramolecular capsule (**3.9**) reported by Reek for encapsulation of (NHC)AuOTf. (b) Reaction with **3.9** yielded different product ratios from reaction with free (NHC)AuOTf.

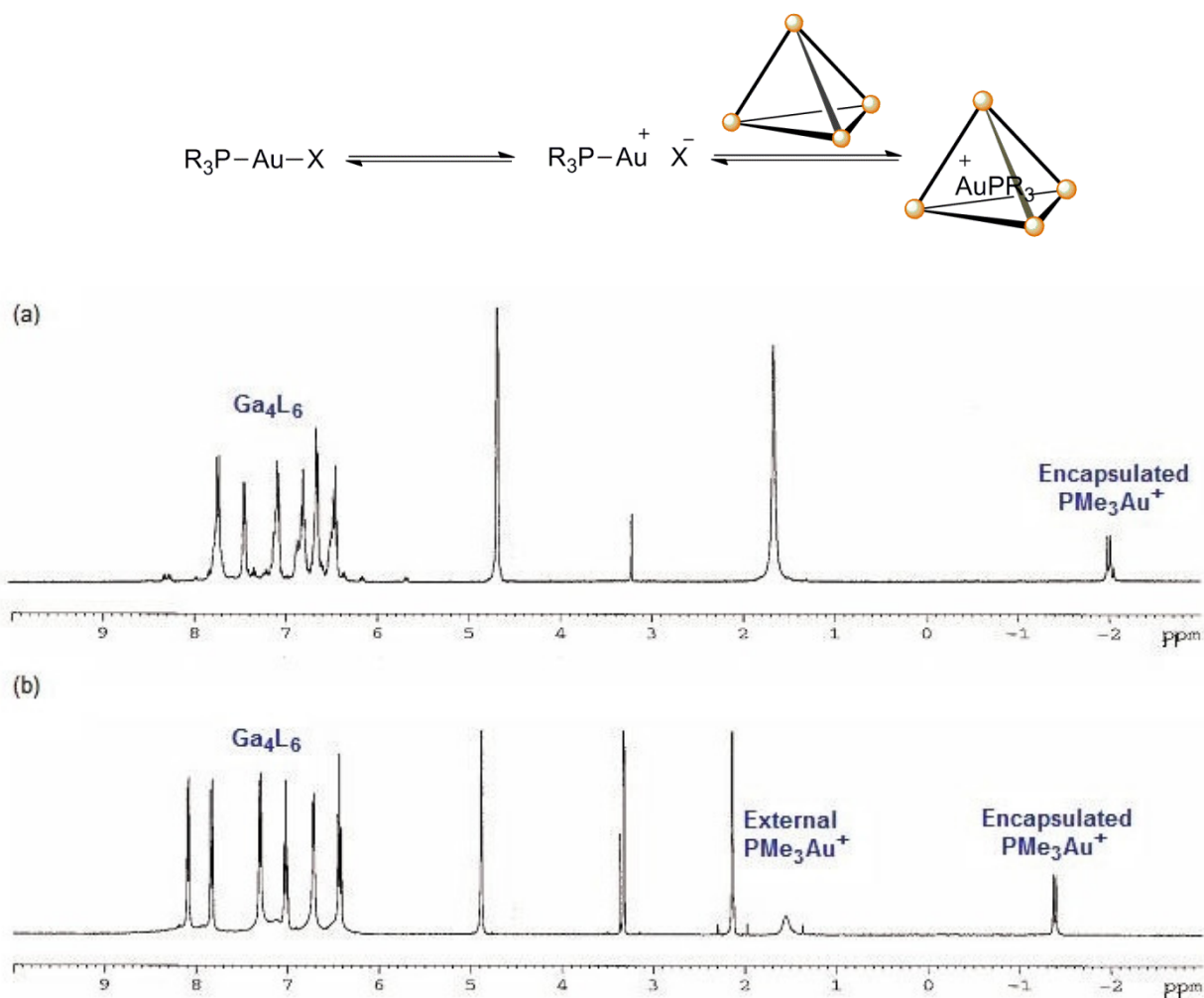


The reports discussed above highlight the potential of host-guest supramolecular complexes in transition metal catalysis. However, the goal of using host-guest complexes with organometallic guests as true synthetic analogues of enzymes requires not just the observation of changes in the selectivity of encapsulated systems (which has sometimes been effected by differential retardation, rather than acceleration, of reaction rates), but in the development of reactions that, like enzymes, exhibit enhanced reaction rates of the encapsulated substrates. Such acceleration has been demonstrated for several organic reactions, but had not been observed for any mediated by encapsulated metal catalysts. The Toste group has developed many methods using monocationic gold(I) complexes as π -acids for the activation of carbon-carbon multiple bonds.³⁴ Our work led us to consider whether gold(I)-phosphines would be suitable guests for the **3.8** host and whether this host-guest complex would exhibit “enzyme mimetic” qualities.

Results

We began our investigation by examining the affinity of gold(I)-phosphine complexes (R_3PAuX , where X is a halide) for encapsulation. Due to the tendency of the catechol ligands on **3.8** for oxidation, in situ generation of a more ionic gold(I) species via halide abstraction with $Ag(I)$ was unsuitable. However, we posited that the preference of **3.8** for cations could promote ionization of R_3PAuX to $R_3PAu^+ \subset \mathbf{3.8}$ and X^- in favor of the fully ionized form. Indeed, when Me_3PAuCl or Et_3PAuCl (1.0 equiv) was combined with the “empty” **3.8** (1.2 equiv) in D_2O or $MeOD$, encapsulation of the gold phosphine cation was observed by 1H and ^{31}P NMR. A representative spectrum of Me_3PAuCl with **3.8** in D_2O is shown below (Figure 3.11a).

Figure 3.11. (a) Reaction of **3.8** and PMe_3AuCl in D_2O . (b) Reaction of **3.8** and PMe_3AuCl in $MeOD$.

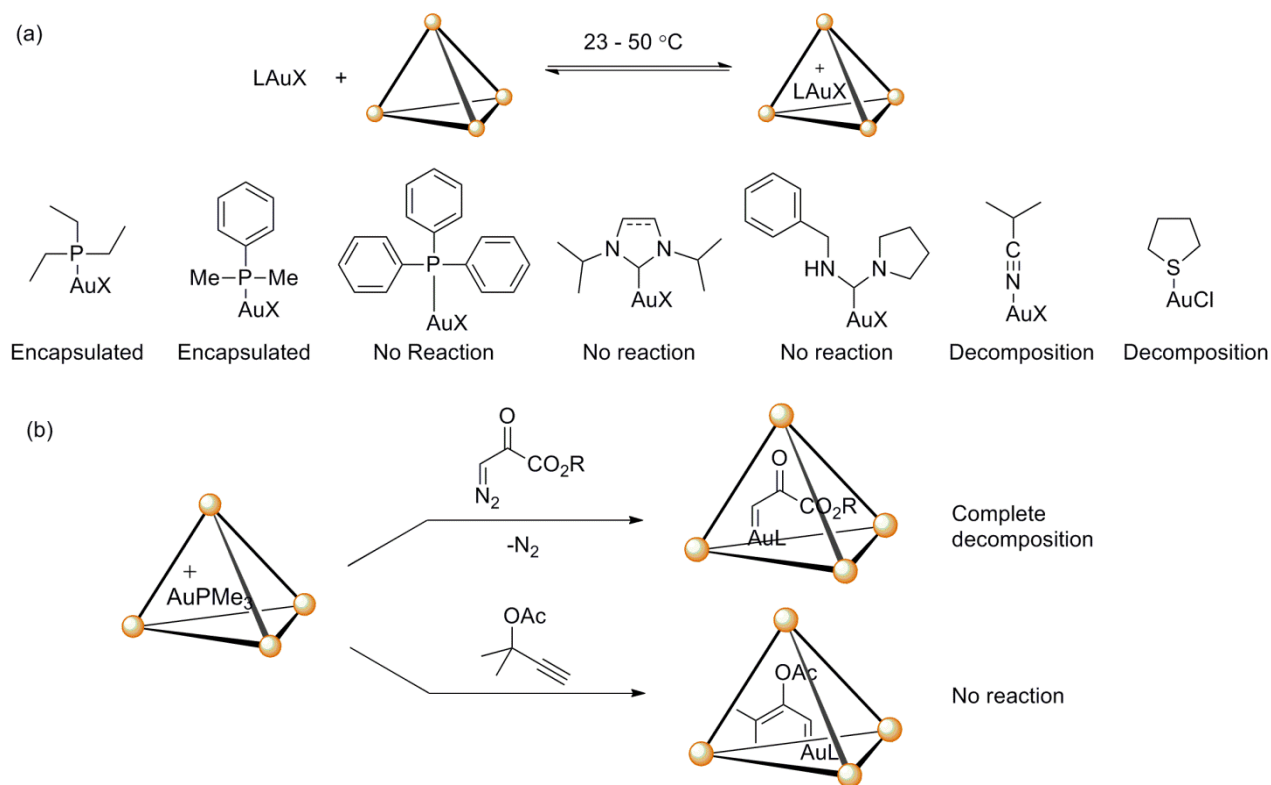


Characteristic of encapsulation, the phosphine alkyl peaks are shifted upfield from 1.64 ppm to -1.98 ppm and similar upfield shifts are also observed by ^{31}P NMR. We attribute the two overlapping doublets at -2.02 ppm and -1.98 ppm to be naked PMe_3Au^+ and the aquo complex, $Me_3PAu^+(OH_2)$, respectively. When $MeOD$ is used as solvent, peaks corresponding to both the

encapsulated and freely exchanging gold complex are observed (at -1.41 ppm and 1.65 ppm, respectively), indicating that the binding constant of Me_3PAu^+ to **3.8** is smaller in methanol than it is in water. Unsurprisingly, the overlapping peak believed to be the aquo complex is not present when methanol is used. Interestingly, reaction of Me_3PAuBr or $\text{Me}_3\text{PAuNTf}_2$ with **3.8** provided two complexes whose NMR spectra are identical to that generated from Me_3PAuCl and **3.8**. This suggested that the counterion (Cl^- , Br^- , or NTf_2^-) is fully dissociated from the encapsulated gold complex.

The encapsulated complex $\text{R}_3\text{PAu}^+ \subset \textbf{3.8}$ is stable for days at room temperature in water, but heating this solution to temperatures above 50 °C led to decomposition within hours. Encapsulation of the bulkier PEt_3AuCl or PMe_2PhAuX in D_2O or MeOD could also be observed by ^1H NMR. However, increasing the size of the catalyst further to PPh_3AuX ($\text{X} = \text{Cl}$ or NTf_2) led to no reaction. While we believe this is due to the size or rigidity of the phenyl phosphine ligands, insolubility of these gold complexes in water may also be responsible. Attempts to encapsulate N-heterocyclic carbene-, isopropyl nitrile-, and tetrahydrothiophene-gold complexes or to generate gold carbene complexes from $\text{Me}_3\text{PAu}^+ \subset \textbf{3.8}$ *in situ* were also unsuccessful. A summary of the encapsulation studies performed is presented in Figure 3.12.

Figure 3.12. (a) Encapsulation of gold(I) complexes in **3.8**. (b) Reaction of $\text{R}_3\text{PAu}^+ \subset \textbf{3.8}$ with substrates to generate gold(I)-carbene complexes *in situ*.

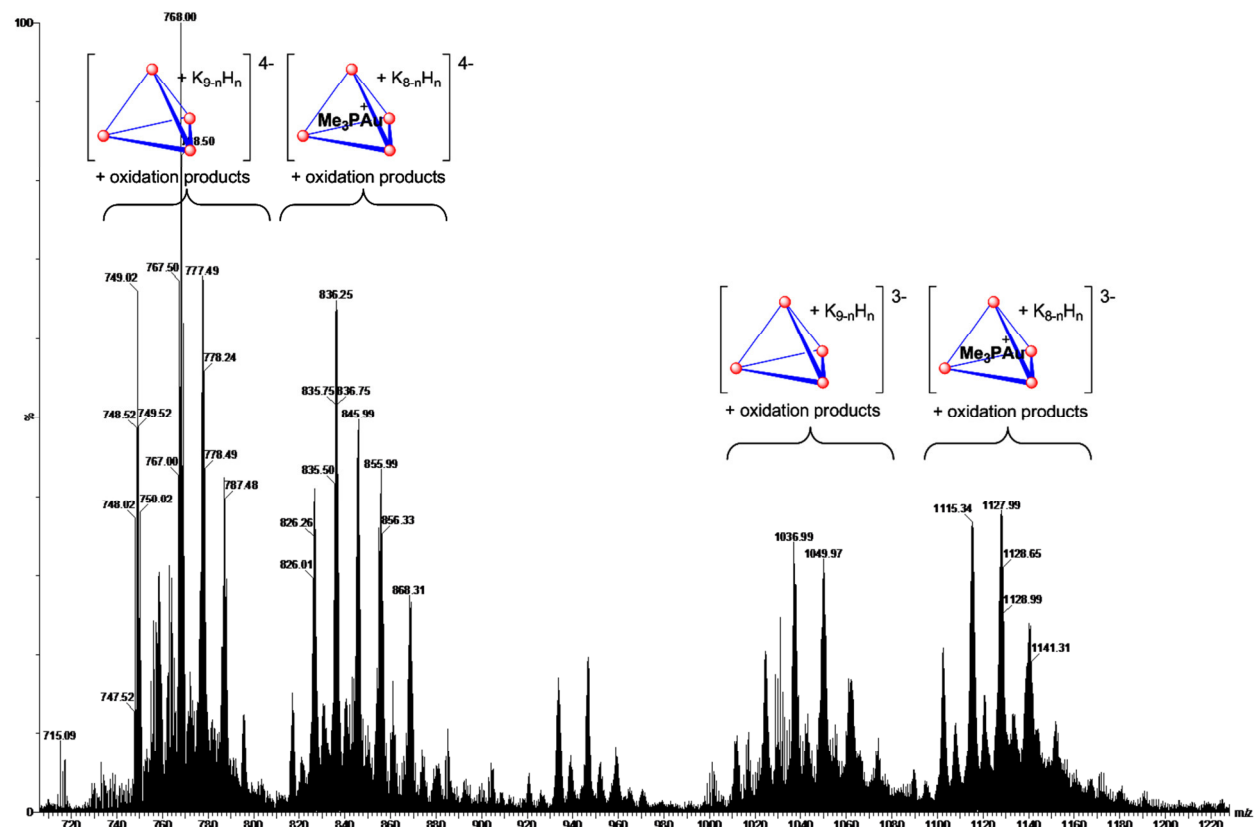


Attempts to precipitate and recrystallize the gold(I) host-guest complexes from acetone and water were unsuccessful. However, the encapsulated complex could be observed by ESI mass-spectrometry in negative ion mode. When a 1:1.5 ratio of Me_3PAuCl and **3.8** was stirred

rigorously at room temperature for 30 min then filtered through a microfilter fiber, peaks corresponding to both $\text{Me}_3\text{PAu}^+ \subset \mathbf{3.8}$ and empty $\mathbf{3.8}$ could be observed. The -3 and -4 charged states are particularly well-defined and the major peaks observed within each group correspond to different ratios of potassium and proton coordinated to the cluster (ie, $\{[\text{Me}_3\text{PAu}^+ \subset \mathbf{3.8}] \cdot \text{K}_8\text{H}_1\}^{-4}$, $\{[\text{Me}_3\text{PAu}^+ \subset \mathbf{3.8}] \cdot \text{K}_7\text{H}_2\}^{-4}$, etc.). The isotopic distributions for these peaks are in agreement with those simulated based on natural abundance of the composite atoms. Additional data from ESI mass spectroscopy are included at the end of the chapter.

Figure 3.13. ESI Mass spectroscopy of $\text{Me}_3\text{PAu}^+ \subset \mathbf{3.8}$, showing the -3 and -4 ion groups containing both of $\text{Me}_3\text{PAu}^+ \subset \mathbf{3.8}$ and empty $\mathbf{3.8}$.

Many transformations have been reported with gold(I) catalysts and we hypothesized that $\text{Me}_3\text{PAu}^+ \subset \mathbf{3.8}$ could also be a competent catalyst in some of these reactions. In particular, we focused on transformations involving substrates that would be compact or were at least sparingly soluble in water. Results from a survey of gold(I) mediated reactions are

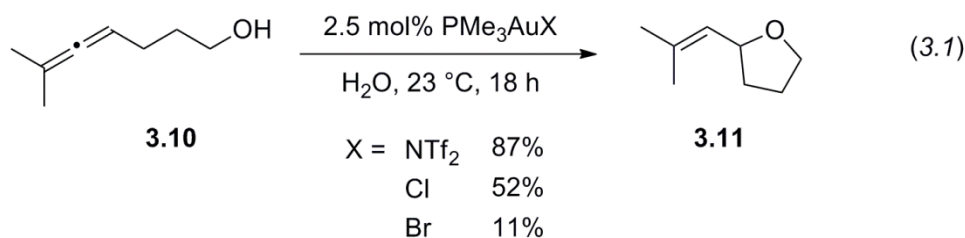


shown below. Interestingly, hydration reactions of allenes, alkynes or alkenes were not observed within the cluster, even though hydration of alkynes in the presence of gold is well-established. Of the reactions examined, the hydroalkoxylation of allenes showed appreciable conversion after 18 h by ^1H NMR with 2.5% catalyst loading. The hydroalkoxylation of allenes by gold(I) in organic solvent has been well investigated and we hypothesized that this transformation would be an ideal model system for our encapsulated catalyst.

Table 3.1. Reactions examined with $\text{Me}_3\text{PAu}^+ \subset \mathbf{3.8}$, using Me_3PAuCl as a precursor.

Substrate	Product	Transformation	Outcome
		Alkene Hydration	No reaction
		Alkyne Hydration	No reaction
		Allene Hydration	No reaction <10% allene isomerization observed
		Allene Hydroalkoxylation	52% Conversion
		Alkene Hydroalkoxylation	No reaction
		Acetylenic Schmidt	No reaction
		Cyclopropanation	No reaction

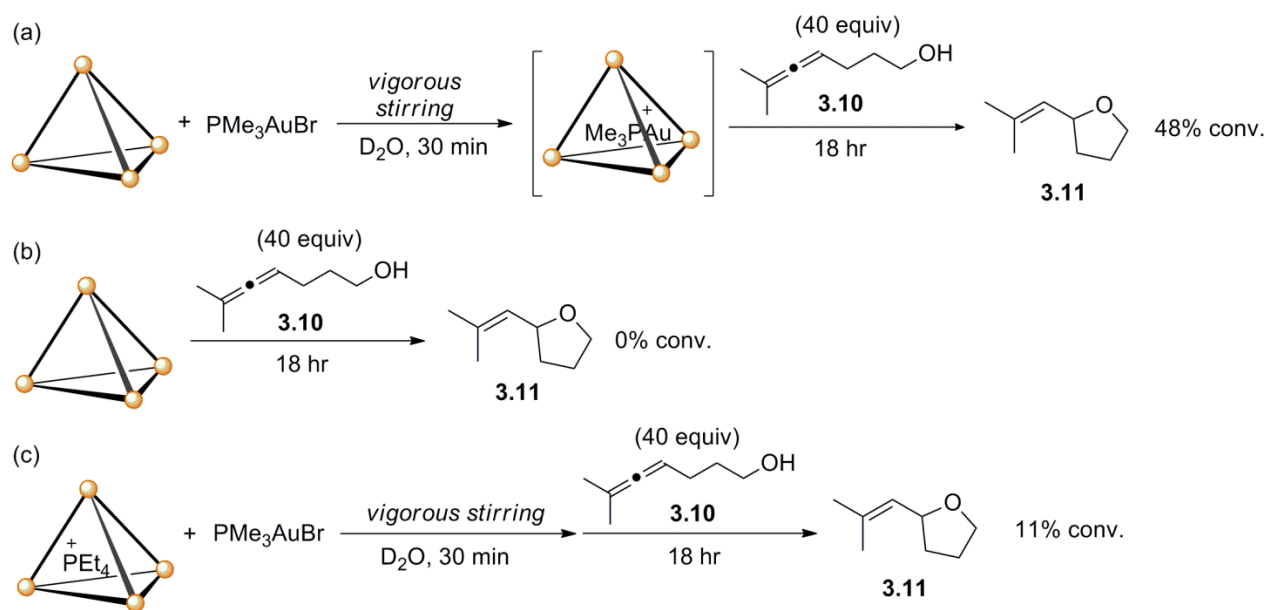
As a comparison, we examined the bulk-solution reactivity of Me_3PAuX with **3.8**, where $\text{X} = \text{Cl}$, Br , and NTf_2 (eq 3.1). While Me_3PAuCl and $\text{Me}_3\text{PAuNTf}_2$ catalyzed the reaction to appreciable conversion, Me_3PAuBr affected the cyclization in only 11% yield after 18 h, presumably due to the relative strength of the gold(I)-Br bond. However, all three Me_3PAuX complexes yield the same $\text{Me}_3\text{PAu}^+ \subset \text{Ga}_4\text{L}_6$ complex in the presence of Ga_4L_6 . Thus, encapsulation significantly enhances the reactivity of Me_3PAuBr .



When **3.10** (40.0 equiv) was added to an aqueous solution of $[\text{Me}_3\text{PAu}^+ \subset \text{Ga}_4\text{L}_6]^{11-}$, generated from **3.8** and PMe_3AuBr , 48% conversion of the allene to the desired product was

observed after 18 h at room temperature (Scheme 2a). This corresponds to 19 catalytic turnovers and is within error of the catalytic reaction with $[\text{Me}_3\text{PAu}^+ \subset \text{Ga}_4\text{L}_6]^{11-}$, generated from **3.8** and PMe_3AuCl . In the presence of **3.8** and **3.10** alone, no product was observed after 18 h, suggesting gold(I) was indeed necessary for reaction. To ensure that the enhanced rate of reaction was not due to changes in solvent polarity or counter anion effects^{10a} upon addition of the anionic assembly, another control experiment with a “blocked” cluster ($\text{PEt}_4^+ \subset \text{3.8}$) and free Me_3PAuBr was performed (Scheme 3.1). The tetraethyl phosphonium ion has a very high binding constant for Ga_4L_6 and, not surprisingly, no exchange between phosphonium and Me_3PAu^+ was observed when $\text{Et}_4\text{P}^+ \subset \text{3.8}$ and Me_3PAuBr were combined. When **3.10** was added to the solution containing $\text{Et}_4\text{P}^+ \subset \text{3.8}$ and Me_3PAuBr , only 11% conversion to the cyclized product was observed after 18 h. This experiment demonstrated that the majority of catalysis previously observed was due to a gold(I) complex bound to the interior of the cluster, rather than complexes associated with the exterior of the cluster or dissolved in solution. Thus, access to the interior of the cluster must be responsible for the activity enhancement observed.

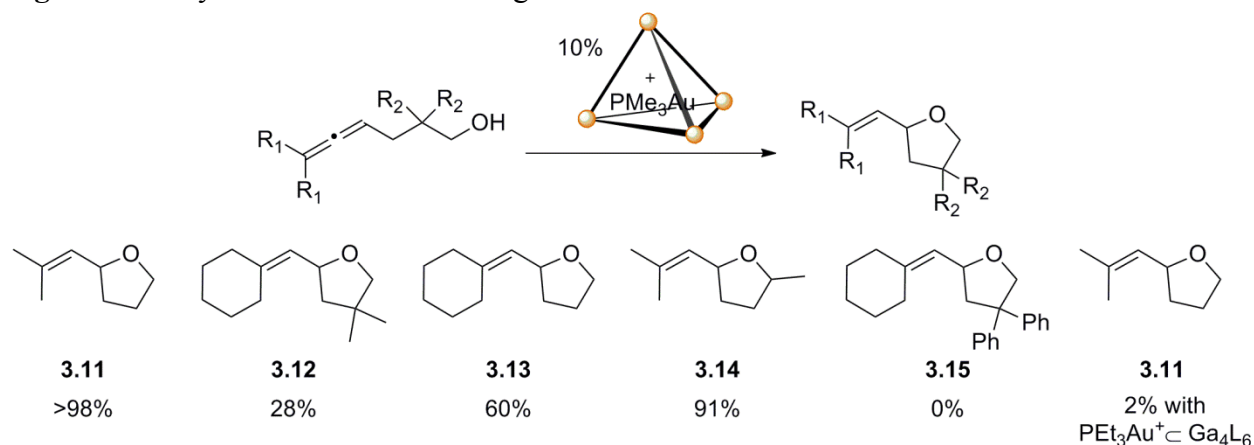
Scheme 3.1. (a) Hydroalkoxylation catalyzed by $\text{Me}_3\text{PAu}^+ \subset \text{3.8}$. (b) Background with **3.8** alone. (c) Background reaction with $\text{Et}_4\text{P}^+ \subset \text{3.8}$ and Me_3PAuBr .



Additionally, increasing the steric demand of the substrate or encapsulated gold decreased the rate of cyclization. For instance, the same reaction catalyzed by $\text{PEt}_3\text{Au}^+ \subset \text{3.8}$ proceeded to only 11% conversion after 18 h. Similarly, adding substitution along the backbone of the substrate and at the terminus of the allene slowed the reaction substantially. With $\text{Me}_3\text{PAu}^+ \subset \text{3.8}$ as a catalyst, only 28% conversion to the substituted product **3.12** was observed after 18 h even when catalyst loading was increased to 5 mol% $\text{Me}_3\text{PAu}^+ \subset \text{3.8}$. The same reaction in bulk solvent with PMe_3AuBr proceeded to 14% conversion. The modest rate enhancement observed with this more hindered substrate is consistent with cyclization taking place primarily within the cluster when $\text{Me}_3\text{PAu}^+ \subset \text{3.8}$ is used. Two other products (**3.13** and **3.14**) can also be formed in modest to good conversion. However, the hydrophobic and extremely bulky product **3.15** could

not be prepared with $\text{Me}_3\text{PAu}^+ \subset \mathbf{3.8}$, presumably due to the inability of the cluster to accommodate the size of the starting material leading to $\mathbf{3.15}$.

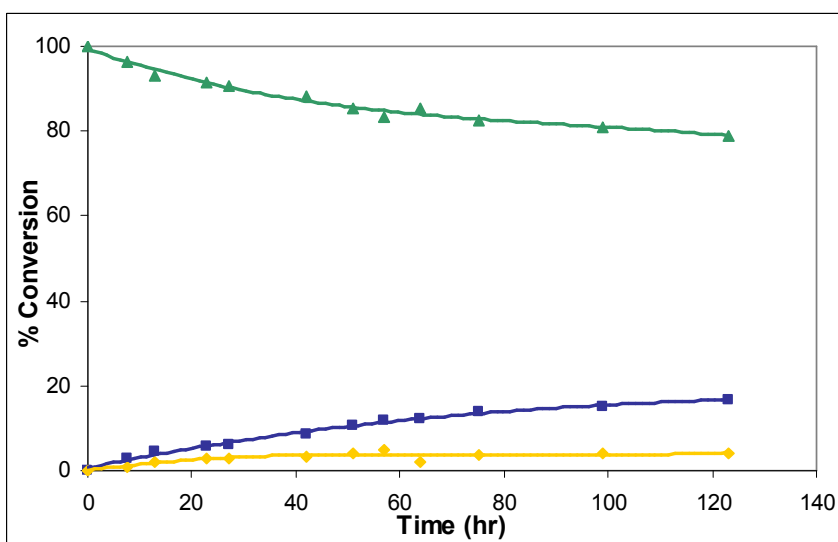
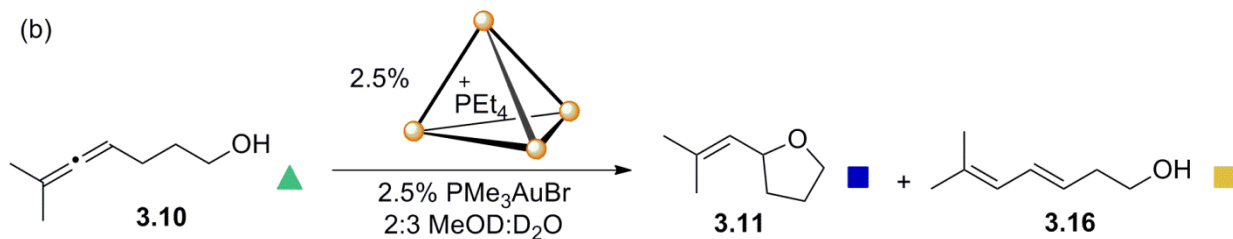
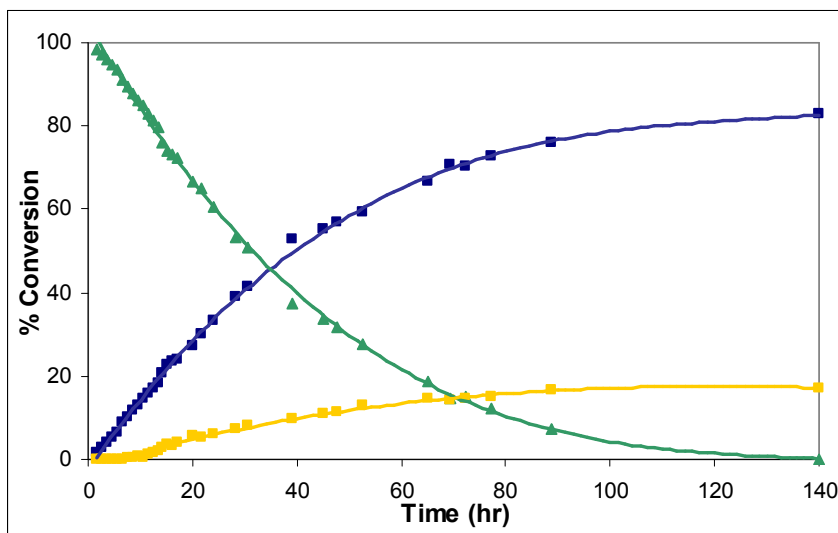
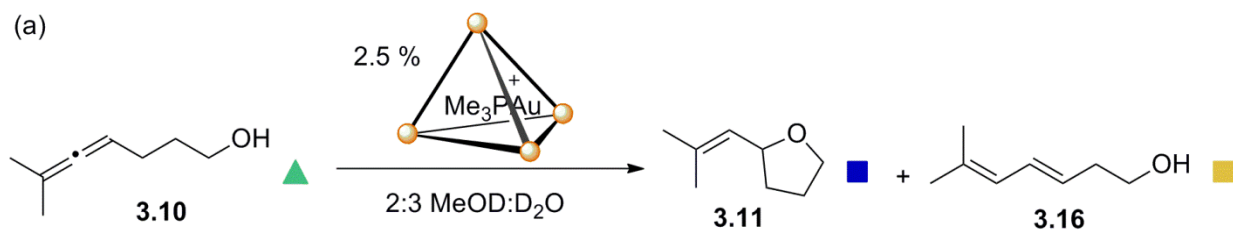
Figure 3.14. Cyclization with bulkier ligands and substrates.



To obtain a quantitative comparison of rates, we wanted to monitor the reaction of **3.11** with $\text{Me}_3\text{PAu}^+ \subset \mathbf{3.8}$ or PMe_3AuBr and the blocked cluster ($\text{PET}_4^+ \subset \mathbf{3.8}$). To obtain a homogeneous reaction mixture, approximately 20% DMSO was added to a solution of $\text{Me}_3\text{PAu}^+ \subset \mathbf{3.8}$ in D_2O . However, this shifted the equilibrium between $\text{Me}_3\text{PAu}^+ \subset \text{Ga}_4\text{L}_6$ and Me_3PAu^+ such that the latter could be observed by ^1H NMR. After screening a variety of mixtures of organic solvent and D_2O , we found that a mixture of MeOD: D_2O in 2:3 ratio was suitable for kinetic studies. At this combination the substrate is soluble up to 16.5 mg/mL and no externally bound or exchanging Me_3PAu^+ was observed.

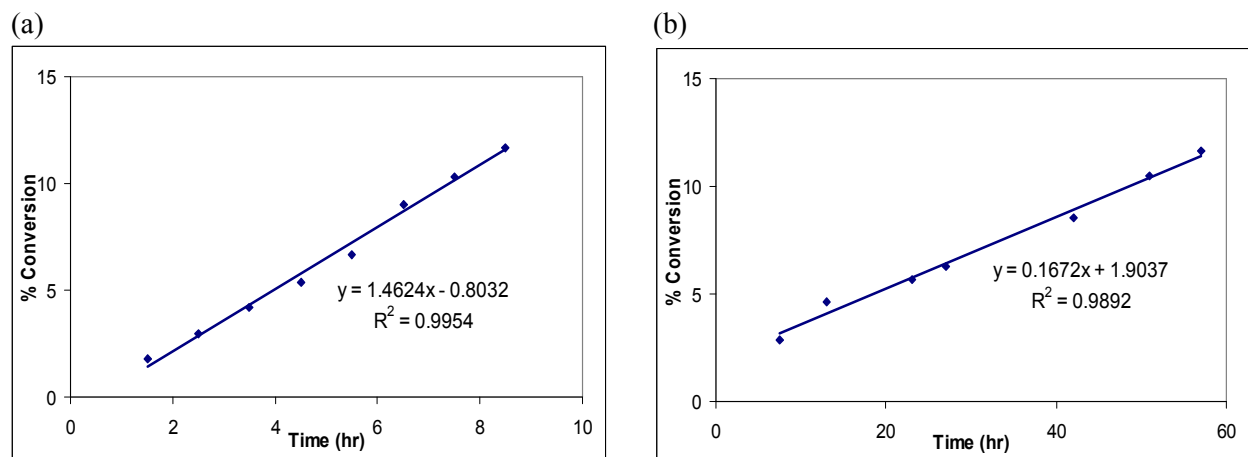
When the reaction mixture in MeOD and D_2O was protected from air oxidation, the $\text{Me}_3\text{PAu}^+ \subset \mathbf{1}$ complex maintained catalytic activity over 5 days and completely consumed the starting allene (Figure 3.15a). Complete conversion to a 4.8:1 ratio of **3.11** to **3.16** was observed, where **3.16** is a side product from allene isomerization. In contrast, the background reaction with the blocked assembly and Me_3PAuBr progressed to less than 20% total conversion. Additionally, whereas the reaction with $\text{Me}_3\text{PAu}^+ \subset \mathbf{3.8}$ obeyed a first order rate law for the entire duration of the experiment, the reaction with the blocked assembly and Me_3PAuBr began to slow after 48 h, even when conversion was still low. This tapering is likely caused by catalyst decomposition and this hypothesis is supported by the observation of purple precipitates in the reaction mixture after only 8 h. Lastly, to obtain a maximum turnover number, we added 250 equiv of **3.10** to a solution of the catalyst in 2:3 MeOD: D_2O . After 6 days of vigorous stirring of the biphasic mixture, **3.11** was isolated in 27% yield, corresponding to 67 turnovers.

Figure 3.15. Monitoring the cyclization of **3.10** with (a) $\text{Me}_3\text{PAu}^+ \subset \text{Ga}_4\text{L}_6$ and (b) $\text{PEt}_4^+ \subset \text{Ga}_4\text{L}_6$ and PMe_3AuBr .

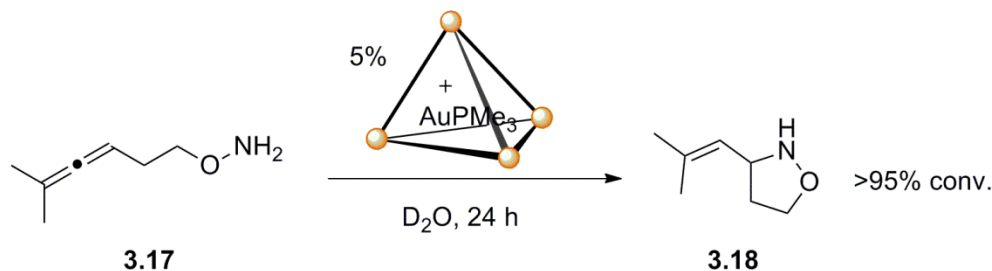


Using the method of initial rates, we plotted the percent conversion of the reaction from 0-12% conversion vs. time (h). As $[3.10] \approx [3.10]_0$ at low conversion, the slope of the graphs below are directly proportional to the relative rate constants for the two reactions. Because the reactions are run at the same concentration of gold(I) and **3.10**, taking a ratio of the two slopes provided us with a relative rate of 8.0 ± 0.9 , as an average of 3 independent runs. A representative set of initial rate experiments is shown in Figure 3.16.

Figure 3.16. (a) Initial rates plot of reaction of **3.10** with $\text{PMe}_3\text{Au}^+ \subset \mathbf{3.8}$. (b) Initial rates plot of reaction of **3.10** with PMe_3AuBr and $\text{PEt}_4^+ \subset \mathbf{3.8}$.



Cyclization of a related unprotected hydroxylamine substrate **3.17** could also be achieved under similar reaction conditions (eq. 3.2). Indeed, nearly quantitative conversion to the desired product was observed after 24 h. However, monitoring this reaction by NMR, showed that the reaction with $\text{Me}_3\text{PAu}^+ \subset \mathbf{3.8}$ was actually slightly slower than the reaction with Me_3PAuBr alone.

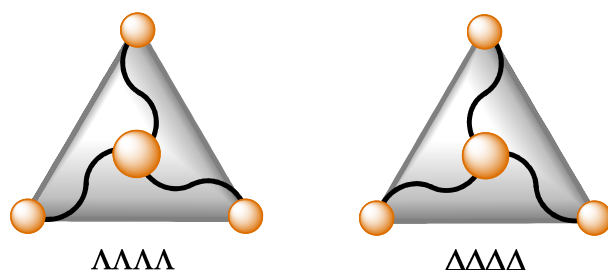


In conclusion, we have shown that three phosphine gold(I) complexes are readily encapsulated in Ga_4L_6 in both methanol and water. While the bulkier $\text{Et}_3\text{PAu}^+ \subset \mathbf{3.8}$ was substantially less catalytically active, the $\text{Me}_3\text{PAu}^+ \subset \mathbf{3.8}$ complex generated in situ can be used to affect the hydroamination and hydroalkoxylation of allene substrates. Notably, the encapsulation of Me_3PAu^+ , generated from Me_3PAuBr in water, led to enhancement in catalytic activity in the hydroalkoxylation of allenes. This reaction constitutes the first example of acceleration of a gold-catalyzed process in which reactivity and lifetime of the catalyst are enhanced by supramolecular encapsulation. The $\text{Me}_3\text{PAu}^+ \subset \mathbf{3.8}$ complex generated remains catalytically active for over 5 days and performs up to 67 turnovers.

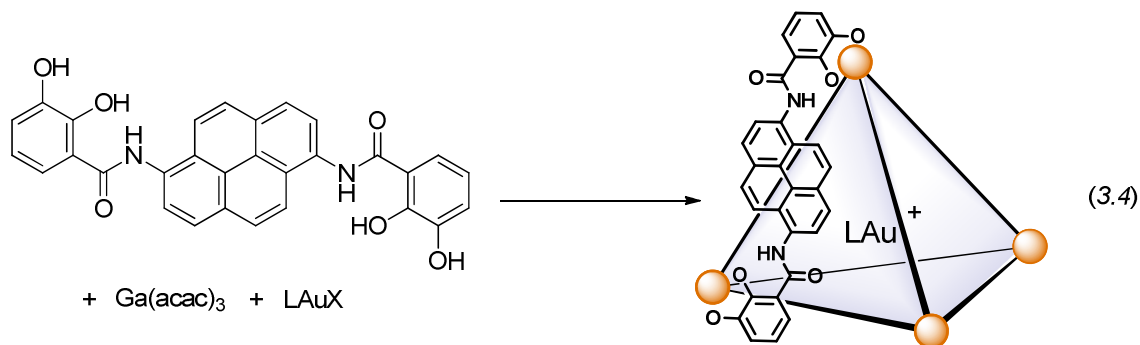
Future Directions

In recent years, many methods for asymmetric gold(I) catalysis have been reported. As the Ga_4L_6 assemblies are inherently chiral, encapsulation of gold(I) in $\Delta\Delta\Delta\Delta$ - Ga_4L_6 or $\Lambda\Lambda\Lambda\Lambda$ - Ga_4L_6 (Figure 3.17) would yield chiral gold(I) complexes, which may be used for enantioselective transformations. Using a chiral capsule around an achiral gold(I) catalyst for enantio-induction would be an orthogonal approach to existing methods. The hydroamination and hydroalkoxylation reactions reported in this chapter are excellent model reactions for such an asymmetric transformation as enantioselective cyclizations with both substrates have been performed in organic solvent. Our preliminary results with $\text{NMe}_4^+ \subset \Delta\Delta\Delta\Delta$ and PMe_3AuX has shown that the gold cation is not strongly bound or kinetically reactive enough to displace NMe_4^+ from the interior of the chiral cluster. Thus, formation of $\text{PMe}_3\text{Au}^+ \subset \Delta\Delta\Delta\Delta$ or $\Lambda\Lambda\Lambda\Lambda$ may require isolation of the “empty” $\Delta\Delta\Delta\Delta$ or $\Lambda\Lambda\Lambda\Lambda$.

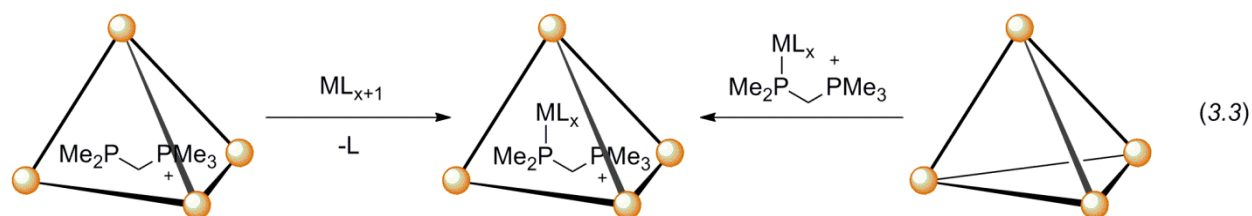
Figure 3.17. Cartoon showing $\Delta\Delta\Delta\Delta$ and $\Lambda\Lambda\Lambda\Lambda$ -**3.8**. Each orange ball represents a Ga(III) center and the twist of the catechol ligands (black lines) are exaggerated to show helical chirality.



A major limitation in the development of new reactions with $\text{PMe}_3\text{Au}^+ \subset \mathbf{3.8}$ is the size and shape of the tetrahedral cluster. Incorporation of gold(I) compounds into larger assemblies may improve the scope of hydroalkoxylation, expand the range of complexes that can act as hosts, and allow the development of new reactions in supramolecular clusters. For instance, formation of a gold(I) complex encapsulated in a Ga_4L_6 assembly, where $\text{L} = \text{N,N}'\text{-(pyrene-1,6-diyl)bis(2,3-dihydroxybenzamide)}$, would increase the interior volume available for catalysis by approximately 40%. However, our initial efforts to form this assembly have not been fruitful, as the pyrene assembly cannot be formed by self-assembly, and must be templated with a strongly bound cation.



One possible approach toward this problem would be to tether the metal catalyst to a cation that is strongly bound such as a phosphonium or ammonium cation. The phosphonium cations are among the most strongly bound guests within the naphthyl-Ga₄L₆ cluster, while ammonium cations have previously been used to template the pyrene-Ga₄L₆ assembly. Either the phosphonium or ammonium cations could in theory be tethered to a neutral or cationic metal complexes (eq. 3.3), but as the cluster prefers mono-cationic guests and di-cations are better solvated by the bulk solvent, a neutral metal complex would be more suited for this approach. As no neutral metals have been previously used as guests, tethering them to a phosphonium cation could greatly expand the range of metal complexes that could be used inside the cluster.



For instance, a ruthenium metathesis catalyst such as the Grubbs 1st generation complex could be prepared and encapsulated inside pyrene- or naphthyl-Ga₄L₆. Metathesis in water and cis-selective metathesis are important goals in transition metal catalysis and supramolecular encapsulation may provide a solution for both; encapsulation will greatly improve the solubility and stability of ruthenium catalysts, and reaction within a restrictive space may provide selectivity for formation of cis olefins. The tethering approach may also allow us to introduce neutral or less strongly bound cationic metals into the chiral assemblies without resolution of an “empty” $\Delta\Delta\Delta\Delta$ - or $\Lambda\Lambda\Lambda\Lambda$ -Ga₄L₆. In such an event, the metal itself will not need to be a strongly bound guest, as long as the cationic ligand tether has a high affinity for **3.8**.

Experimental

General Experimental Procedure and Instrumentation

All reagents and solvents were obtained from commercial suppliers and used without further purification, unless otherwise specified. All air-sensitive reactions were carried under positive N₂ pressure in a glove box with degassed solvent. ¹H and ³¹P NMR spectra were recorded with Bruker AV-500, AV-600, and DRX-500 spectrometers relative to residual protonated solvent resonances. Mass spectra of the clusters were measured in negative ion mode using a quadrupole time-of-flight mass spectrometer (Q-tof Premier, Waters, Milford, MA) equipped with an electrospray ionization source. The ion source voltages were adjusted for optimum mass spectral signal of the cluster ions of interest prior to recording data.

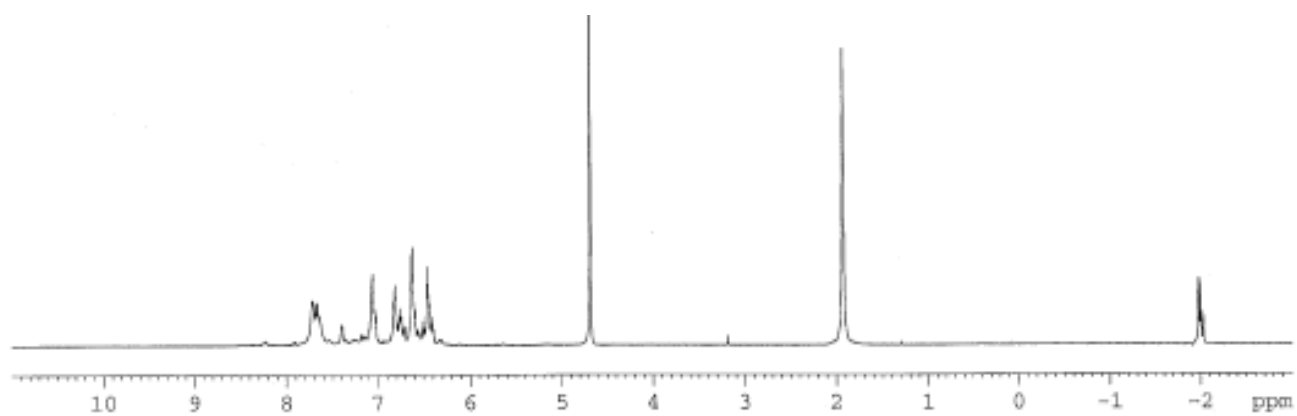
Gold bromide complexes were prepared as reported by the Toste group,³⁶ and used without further purification. Gold triflimide complexes were prepared as described previously in Chapter 2. Substrate **2** (6-methylhepta-4,5-dien-1-ol) was prepared by the method described by Widenhoefer.³⁶ Substrate **5** was prepared by the method described by Mikami.³⁷ The “empty” host assembly, K₁₂[Ga₄L₆] (**3.8**) was prepared using modified literature procedures.³⁸ All flash chromatography was performed on Merck 60 silica gel (32-63 μm). Thin-layer chromatography (TLC) analysis was performed using Merck silica gel 60 F254 TLC plates, and visualized by staining with I₂, UV, anisaldehyde, and/or potassium permanganate.

Encapsulation of PR₃AuX.

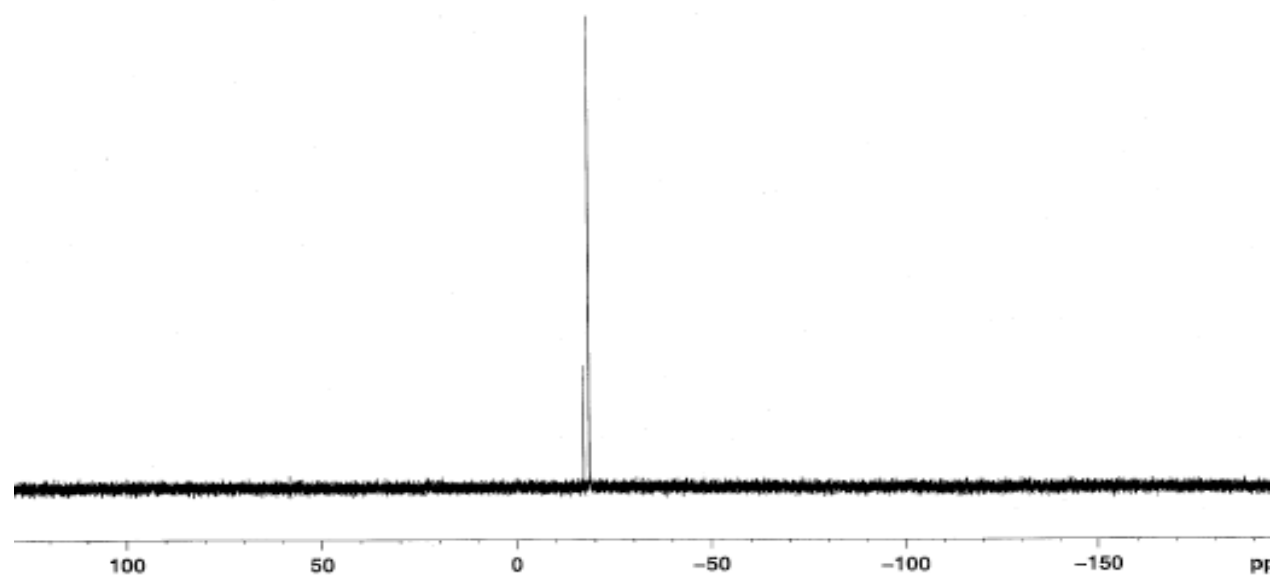
General Procedure: To a vial containing cluster **3.8** (1.2 equiv) and PR₃AuX (1.0 equiv) as solids, D₂O and/or methanol was added under N₂. The solution was stirred vigorously at room temperature for 30 min, before spectroscopic measurements were taken. ¹H NMR data from the reaction of **1** with various PMe₃Au⁺ sources are depicted in Figure S3.1 and data from **3.8** with PR₃AuCl in MeOD are shown in Figure S3.2.

Figure S3.1. Proton and ³¹P NMR of reaction of **3.8** (12.0 mg, 0.00333 mmol) with PMe₃AuX in 0.6 mL D₂O, where (a) X = NTf₂ (1.5 mg, 0.0028 mmol), (b) X = Cl (0.9 mg, 0.0028 mmol) and (c) X = Br (1.0 mg, 0.0028 mmol)

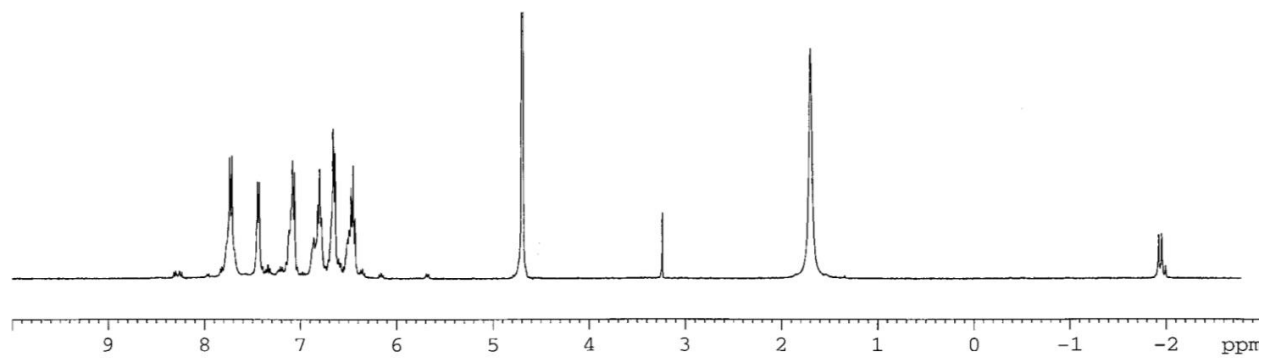
(a) ^1H NMR:



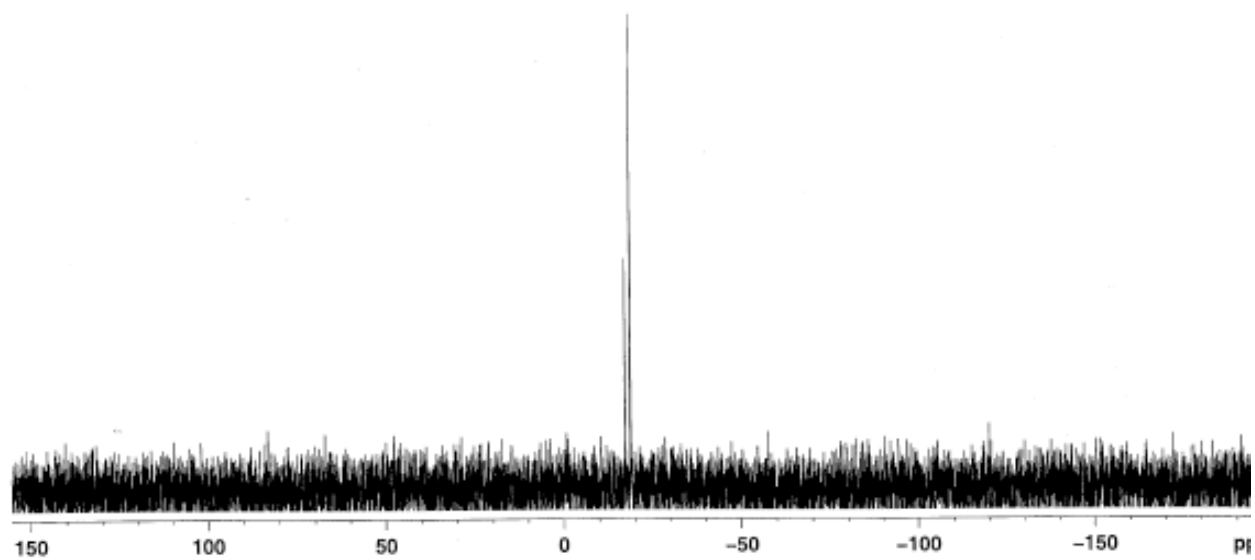
^{31}P NMR:



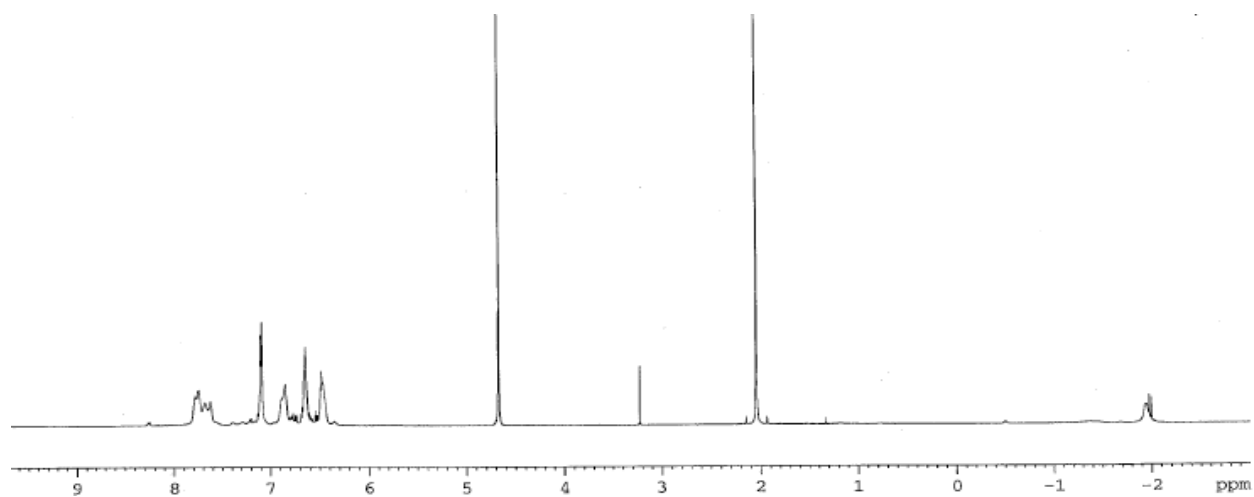
(b) ^1H NMR:



^{31}P NMR:



(c) ^1H NMR:



^{31}P NMR:

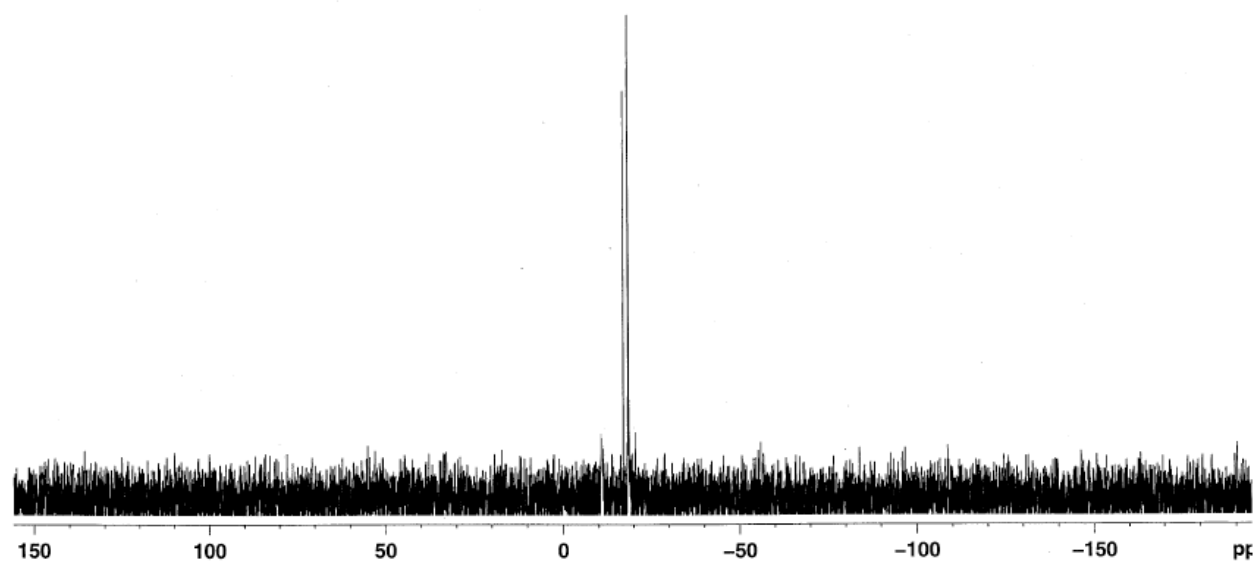
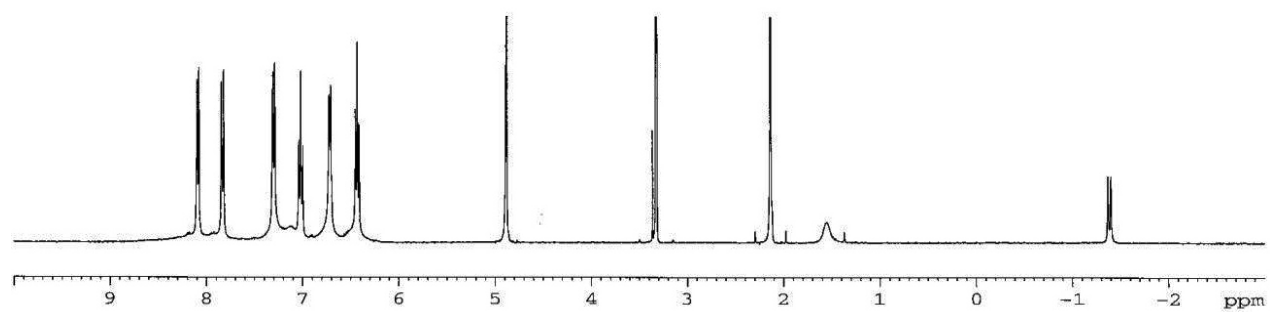
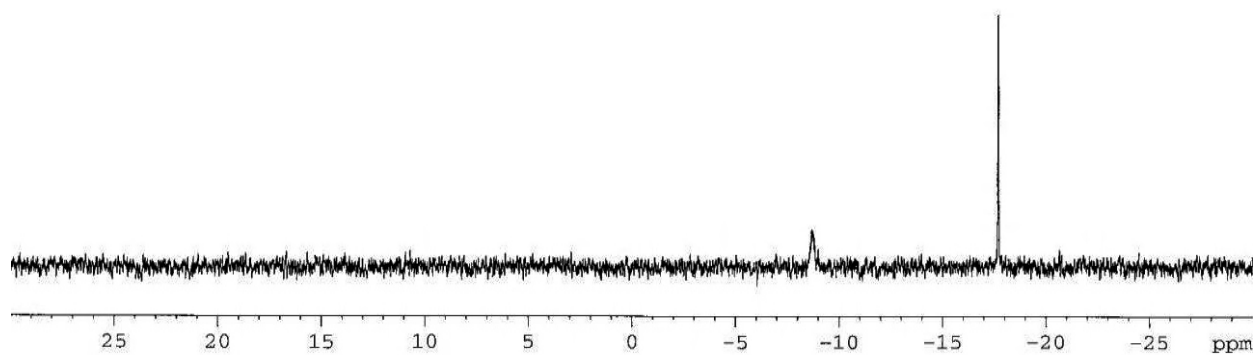


Figure S3.2. (a) Reaction of **1** with PMe_3AuCl in 0.6 mL MeOD. (b) Reaction of **1** with PEt_3AuCl in MeOD.

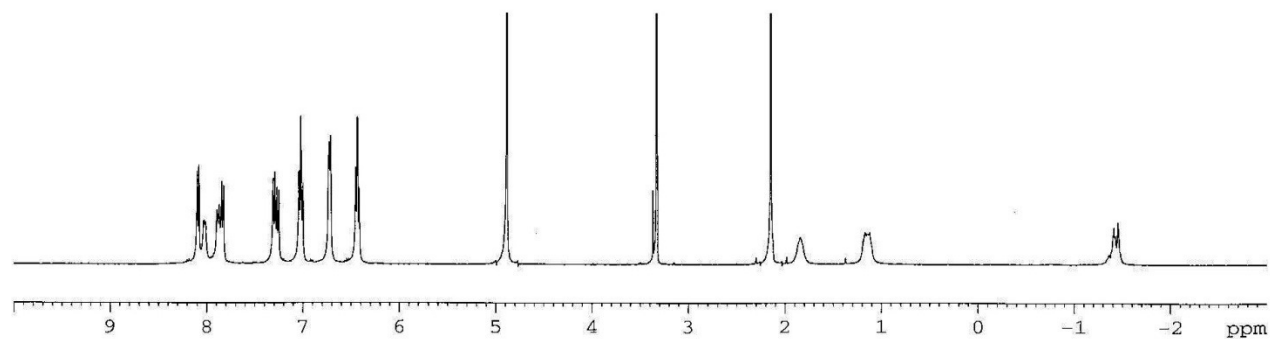
(a) ^1H NMR



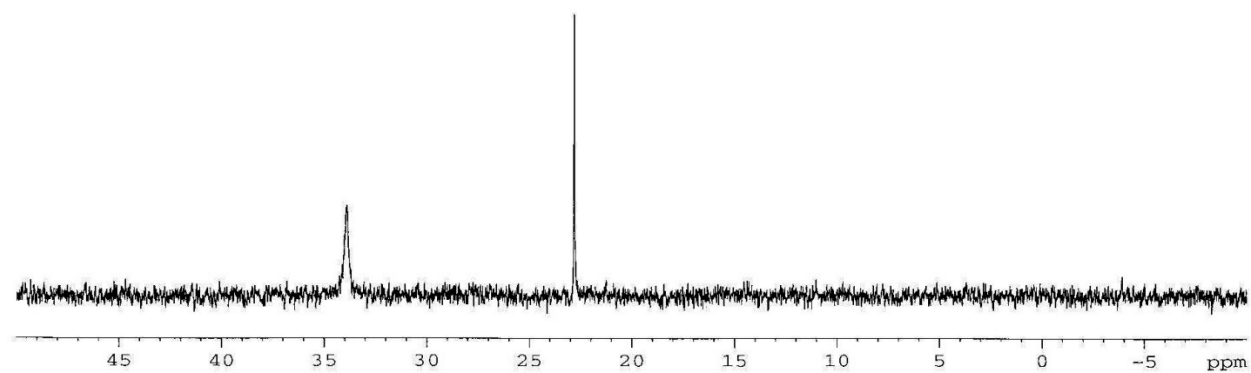
^{31}P NMR:



(b) ^1H NMR:



^{31}P NMR:



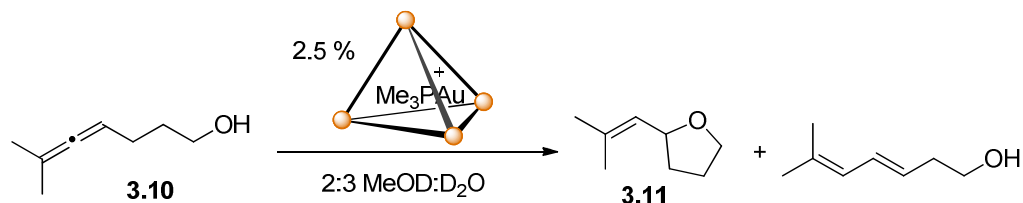
Hydroalkoxylation by Gold(I)

Procedure for reaction catalyzed by $\text{Me}_3\text{PAu}^+ \mathbf{3.8}$:

A vial was charged with Me_3PAuX (1.0 equiv) and **3.8** (1.2 equiv) in a glove box under N_2 atmosphere. Deuterated solvent was added and the solution was stirred vigorously for 30 min at 23 °C. The solution was transferred to a sealed NMR tube and ^1H NMR spectrum was recorded to ensure encapsulation had occurred. The sample was taken back into the glove box and the solution was filter through a microfilter fiber directly into a vessel containing the substrate. The reaction mixture was stirred at room temperature for the specified time and the products were extracted with 1 mL water and 1 mL CDCl_3 . The organic fractions were dried and the % conversions reported reflect the ratio of starting material to products in the organic extracts.³⁹

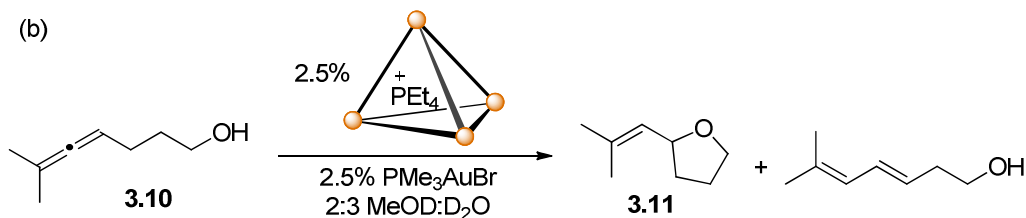
To obtain isolated yields and to confirm the identity of the product, the CDCl_3 solution was concentrated and the resulting residue was chromatographed on SiO_2 using 1:9 Et_2O : pentanes as eluent. Proton NMR of the isolated product matches that reported in the literature.³ ^1H NMR (CDCl_3 , 600 MHz): δ 4.51 (t, $J = 7.3$ Hz, 1H), 3.90 (q, $J = 5.5$ Hz, 1H), (q, $J = 7.3$ Hz, 1H), 3.75 (q, $J = 5.5$ Hz, 1H), 2.06 – 2.00 (m, 1H), 2.00 – 1.95 (m, 1H), 1.95-1.89 (m, 1H), 1.75 (s, 3H), 1.72 (s, 3H), 1.57 – 1.51 (m, 1H).

Procedure for Monitoring the Reaction by Point Kinetics:



Following the general procedure above, **3.8** (14.8 mg, 0.0041 mmol) and PMe_3AuBr (1.2 mg, 0.0034 mmol) were combined in 0.4 mL MeOD and 0.6 mL D_2O . The solution was stirred vigorously for 30 min then filtered into an NMR tube containing **3.10** (17.3 mg, 0.137 mmol) and internal standard (iPrOH or dioxane, 0.0686 mmol). The NMR tube was sealed with parafilm and Teflon tape and the reaction mixture was shaken vigorously until a homogeneous mixture was reached. The reaction mixture was stored at 23 °C and monitored via point kinetics for 140 h by ^1H NMR. The percent conversion calculated at each time point is based on relative integration to the internal standard.

Procedure for Monitoring the Background Reaction by Point Kinetics:



To an NMR tube containing PMe_3AuBr (1.2 mg, 0.0034 mmol) and $\text{PET}_4^+ \subset \mathbf{3.8}$ (15.1 mg, 0.0041 mmol), 0.4 mL MeOH and 0.6 mL D_2O were added, followed by $\mathbf{3.10}$ (17.3 mg, 0.137 mmol). The tube was sealed under N_2 and the reaction mixture was monitored via point kinetics for 123 h by ^1H NMR. The percent conversion calculated at each time point is based on relative integration to the internal standard.

Calculation of Relative Rates

Using the method of initial rates, we plotted the percent conversion of the reaction from 0-12% conversion vs. time (h). As $[\mathbf{3.10}] \approx [\mathbf{3.10}]_0$ at low conversion, the slope of the graphs below are directly proportional to the relative rate constants for the two reactions. As the reactions are run at the same concentration of gold and $\mathbf{3.10}$, taking a ratio of the two slopes provided a relative rate acceleration of 8.0 ± 0.9 , as an average of 3 independent runs. See Table S3.1 for rate constants for each individual run.

Table S3.1. Measured rate constants for reaction, assuming a first order rate law.

Reaction with $\text{PMe}_3\text{Au}^+ \subset \mathbf{3.8}$	Reaction with $\text{PET}_4^+ \subset \mathbf{3.8}$ and PMe_3AuBr	Relative Rate Acceleration
0.025 h^{-1}	0.0035 h^{-1}	7.2
0.024 h^{-1}	0.0029 h^{-1}	8.3
0.015 h^{-1}	0.0017 h^{-1}	8.6

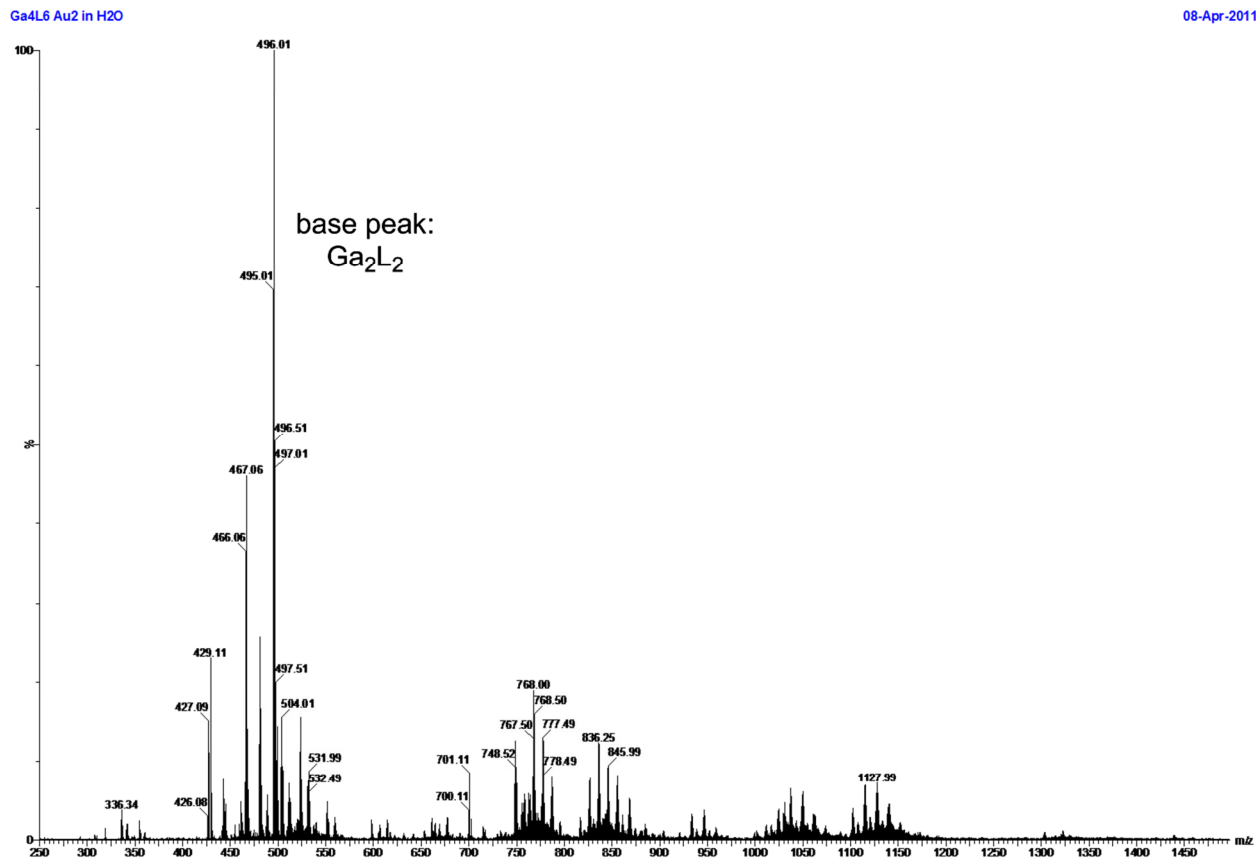
Average: 8.0 ± 0.9

Mass Spectrometry:

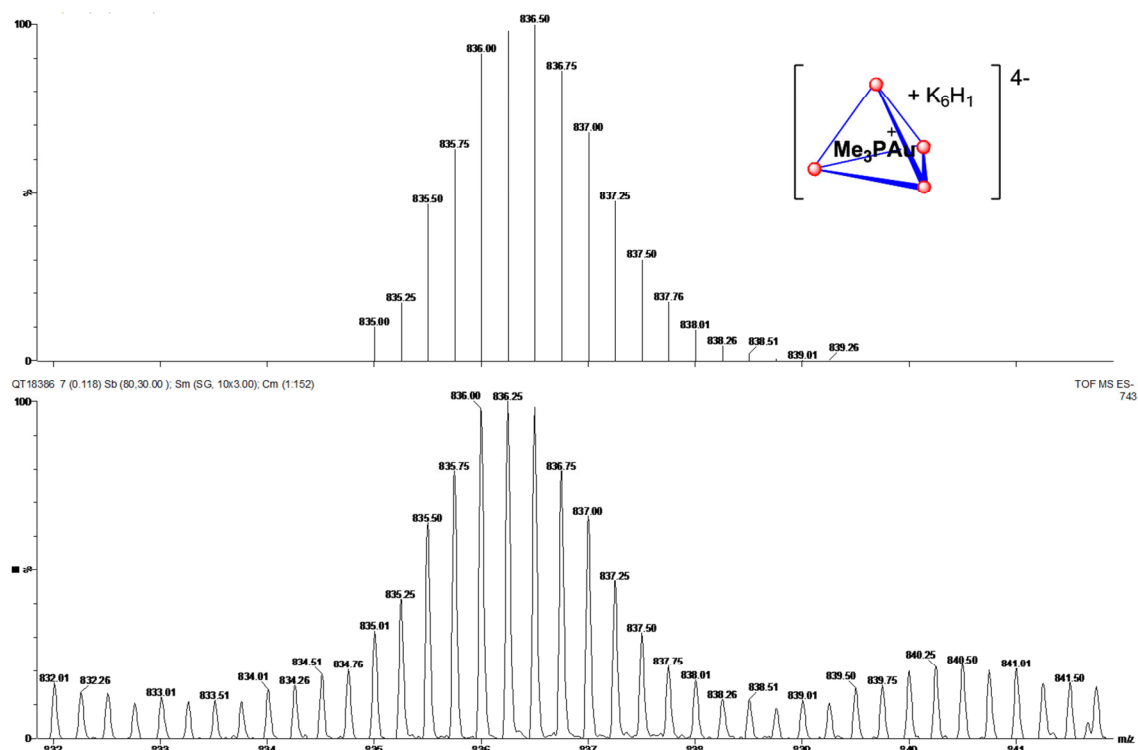
Mass spectrometry was carried on a Q-TOF Premier Spectrometer equipped with electrospray ionization source in negative ion mode. The sample was prepared by combining PMe_3AuBr (1.0 equiv) and $\mathbf{3.8}$ (1.75 equiv) in 2:3 MeOH:H₂O to obtain a 3mM solution in gold. The solution was stirred vigorously at room temperature under N_2 atmosphere for 30 min then filtered through a 20 μm filter before injection onto the mass spectrometer (Figure S3.3). Multiple charged states of $\text{PMe}_3\text{Au}^+ \subset \mathbf{3.8}$ are observed, corresponding to the 3⁻, 4⁻, and 5⁻ ion groups. The base peak corresponds to GaL_2^{2-} .

Figure S3.3. (a) Full view of the ESI mass spectrum. (b) Theoretical (top) and observed (bottom) masses for $(\text{PMe}_3\text{Au}^+ \subset \mathbf{3.8})\text{K}_6\text{H}_1$. (c) Theoretical (top) and observed (bottom) masses for $(\text{PMe}_3\text{Au}^+ \subset \mathbf{3.8})\text{K}_6\text{H}_2$.

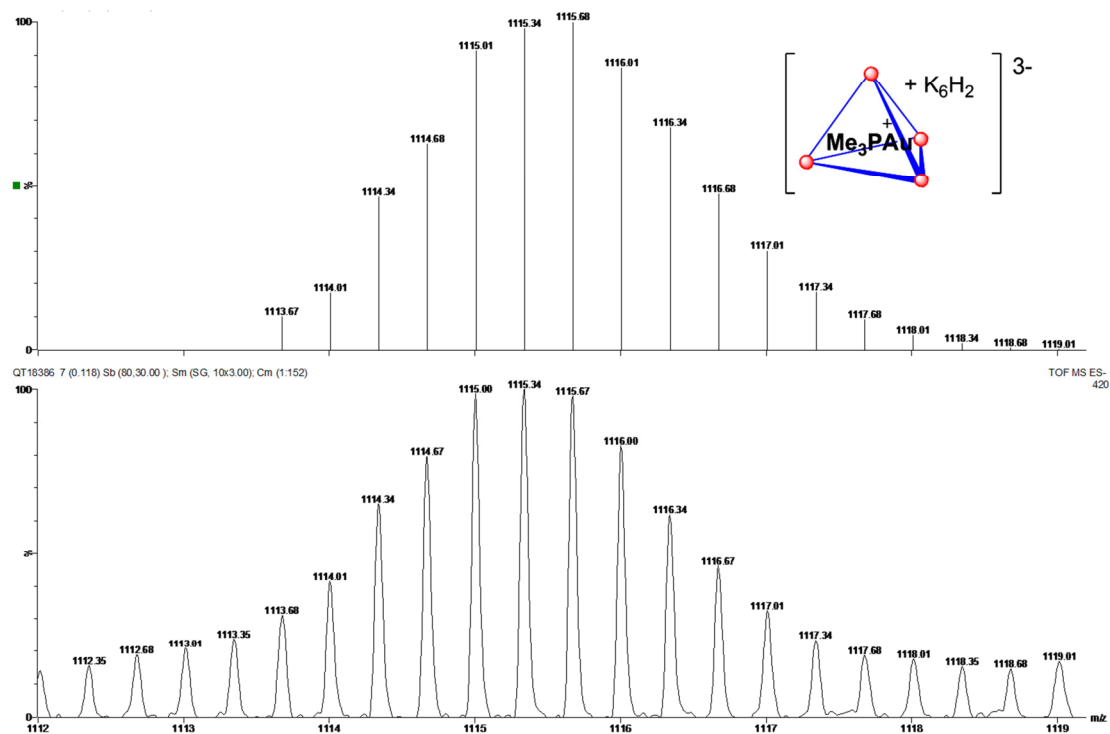
(a)



(b)



(c)



References

- (1) Elemans, J. A. A. W.; Cornelissen, J. J. L. M.; Feiters, M. C.; Rowman, A. E.; Nolte, R. J. M. Bio-inspired Supramolecular Catalysis. *Supramolecular Catalysis*. Wiley-VCH: Weinheim, **2008**.
- (2) Oshovsky, G. V.; Reinhoudt, D. N.; and Verboom, W. *Angew. Chem. Int. Ed.* **2007**, *46*, 2366.
- (3) Atwood, J. L.; Davies, J. E. D.; MacNicol, D. D.; Voegtle, F.; Lehn, J.-M. *Comprehensive Supramolecular Chemistry*, Pergamon: Oxford, **1996**.
- (4) Schneider, H.-J. Yatsimirsky, A. K.; *Chem. Soc. Rev.*, **2008**, *37*, 263.
- (5) Breslow, R.; Overman, L. *J. Am. Chem. Soc.*, **1970**, *92*, 1075.
- (6) Tabushi, I. *Acc. Chem. Res.* **1982**, *15*, 66.
- (7) Wiester, M. J.; Ulmann, P. A.; Mirkin, C. A. *Angew. Chem., Int. Ed.* **2010**, *50*, 114.
- (8) Davis, A. V.; Yeh, R. M.; Raymond, K. N. *PNAS*, **2002**, *99*, 4793.
- (9) Hof, F.; Rebek, J. Jr. *PNAS*, **2002**, *99*, 4775.
- (10) Sun, Q.-F.; Iwasa, J.; Ogawa, D.; Ishido, Y.; Sato, S.; Ozeki, T.; Sei Y.; Yamaguchi, K.; Fujita, M. *Science*, **2010**, *328*, 1144.
- (11) Vriezema, D. M.; Aragonés, M. C.; Elemans, J. A. A. W.; Cornelissen, J. J. L. M.; Rowan, A. E.; Nolte, R. J. M. *Chem. Rev.*, **2005**, *105*, 1445.
- (12) Yoshizawa, M.; Klosterman, J. K.; Fujita, M. *Angew. Chem., Int. Ed.* **2009**, *48*, 3418.
- (13) (a) F. Hof, S. L. Craig, C. Nuckolls, J. Rebek, Jr., *Angew. Chem. Int. Ed.* **2002**, *41*, 1488.
(b) W.-Y. Sun, M. Yoshizawa, T. Kusukawa, M. Fujita, *Curr. Opin. Chem. Biol.* **2002**, *6*, 757.
- (14) (a) Kang, J.; Rebek, J. Jr. *Nature*, **1997**, *385*, 50. (b) Kang, J.; Santamaría, J.; Hilmersson, G.; Rebek, J. Jr. *J. Am. Chem. Soc.* **1998**, *120*, 7389.
- (15) Shenoy, S. R.; Pinacho Crisóstomo, F. R.; Iwasawa, T.; Rebek, J., Jr. *J. Am. Chem. Soc.* **2008**, *130*, 5658.
- (16) Fujita, M.; Oguro, D.; Miyazawa, M.; Oka, H.; Yamaguchi, K.; Ogura, K. *Nature*, **1995**, *378*, 469.
- (17) Yoshizawa, M.; Tamura, M.; Fujita, M. *Science*, **2006**, *312*, 251.
- (18) Nishioka, Y.; Yamaguchi, T.; Kawano, M.; Fujita, M. *J. Am. Chem. Soc.* **2008**, *130*, 8160.
- (19) Merlau, M. L.; Pilar Mejia, M.; Nguyen, S.-T.; Hupp, J. T. *Angew. Chem. Int. Ed.*, **2002**, *40*, 4239.
- (20) Lee, S. J.; Hu, A.; Lin, W. *J. Am. Chem. Soc.*, **2002**, *124*, 12948.
- (21) Meeuwissen, J.; Reek, J. N. H. *Nature Chem.* **2010**, *2*, 615.

- (22) Wilkinson, M.; van Leeuwen, P. W. N. M.; Reek, J. N. H. *Org. Biomol. Chem.* **2005**, *3*, 2371.
- (23) Caulder, D. L.; Brückner, C.; Powers, R. E.; König, S.; Parac, T. N.; Leary, J. A.; Raymond, K. N. *J. Am. Chem. Soc.* **2001**, *123*, 8923.
- (24) Leung, D. H.; Bergman, R. G.; Raymond, K. N. *J. Am. Chem. Soc.* **2008**, *130*, 2798.
- (25) Davis, A. V. and Raymond, K. N. *J. Am. Chem. Soc.* **2005**, *127*, 7912.
- (26) Pluth, M. D.; Bergman, R. G.; Raymond, K. N. *J. Am. Chem. Soc.* **2007**, *129*, 11459.
- (27) (a) Pluth, M. D.; Bergman, R. G.; Raymond, K. N. *Science* **2007**, *316*, 85. (b) Pluth, M. D.; Bergman, R. G.; Raymond, K. N. *Angew. Chem. Int. Ed.* **2007**, *46*, 8587.
- (28) Hastings, C. J.; Bergman, R. G.; Raymond, K. N. *J. Am. Chem. Soc.* **2010**, *132*, 6938.
- (29) (a) Brown, C. J.; Bergman, R. G.; Raymond, K. N. *J. Am. Chem. Soc.* **2009**, *131*, 17530. (b) Fiedler, D.; Bergman, R. G.; Raymond, K. N. *Angew. Chem. Int. Ed.* **2004**, *43*, 6748.
- (30) Leung, D. H.; Fiedler, D.; Bergman, R. G.; Raymond, K. N. *Angew. Chem. Int. Ed.* **2004**, *43*, 963.
- (31) Leung, D. H.; Bergman, R. G.; Raymond, K. N. *J. Am. Chem. Soc.* **2007**, *129*, 2746-2747.
- (32) Cavarzan, A.; Scarso, A.; Sgarbossa, P.; Strukul, G.; Reek, J. N. H. *J. Am. Chem. Soc.*, **2011**, *133*, 2848.
- (33) Casey J. Brown, Gregory M. Miller, Miles W. Johnson, Robert G. Bergman, and Kenneth N. Raymond, *J. Am. Chem. Soc.* **2011**, *133*, 11964.
- (34) See chapter 1 and 2 and references therein for examples of gold(I) activation of allenes and alkynes for nucleophilic addition.
- (35) Brenzovitch, W. E.; Benitez, D.; Lackner, A. D.; Shunatona, H. P.; Tkatchouk, E.; Goddard, W. A.; Toste, F. D. *Angew. Chem. Int. Ed.* **2010**, *49*, 5519.
- (36) Zhang, Z.; Liu, C.; Kinder, R. E.; Han, X.; Qian, H.; Widenhoefer, R. A. *J. Am. Chem. Soc.* **128**, 9066.
- (37) Aikawa, K.; Kojima, M.; Mikami, K. *Adv. Synth. Catal.* **2010**, *352*, 3131.
- (38) Caulder, D. L.; Bruckner, C.; Powers, R. E.; König, S.; Parac, T. N.; Leary, J. A.; Raymond, K. N. *J. Am. Chem. Soc.* **2001**, *123*, 8923.
- (39) As the starting material **3.10** and product **3.11** and diene show different solubilities in water, no internal was employed in heterogeneous reactions (ie, those that employed D₂O as solvent).

Chapter 4:

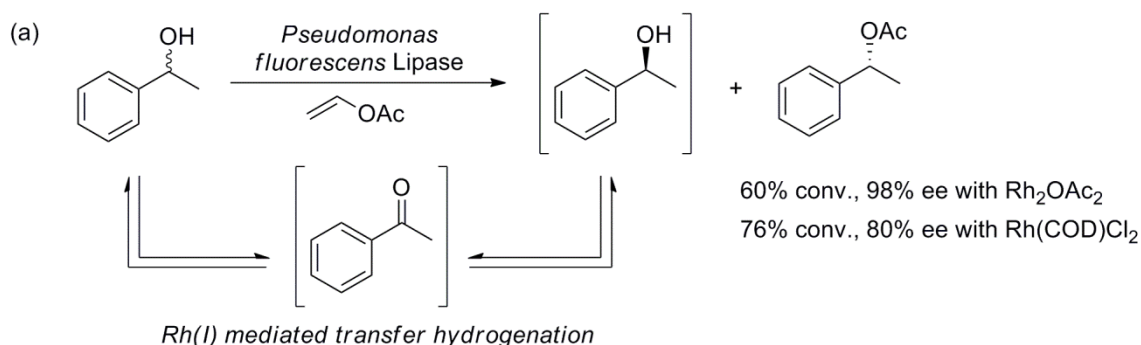
A Supramolecular Approach to Combining Enzymatic and Transition Metal Catalysis

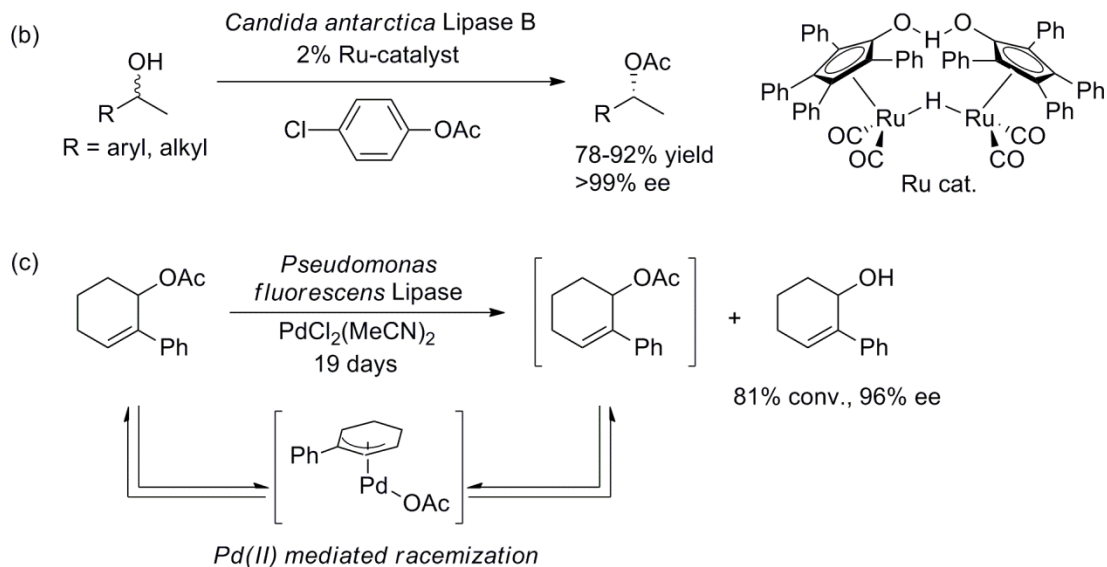
Introduction

Over the last two decades, research on supramolecular enzyme mimics has been largely directed toward developing scaffolds that showcase the selectivity and catalytic properties of enzymes.¹ The frameworks that have been reported as a result of these efforts² operate as molecular flasks in analogy to the binding site of proteins. Despite these reports, one hallmark of catalysis by true enzymes in a complex metabolic pathway has been much less explored: the ability to catalyze transformations in the presence of many other biocatalysts.³ The integration of enzymatic and chemo-catalysis in one-pot sequences can result in powerful transformations.⁴ One pot procedures can minimize solvent waste and materials used for purification.⁵ However, combined chemo-enzymatic processes are rare as they require the catalysts to be compatible with each other while operating under similar conditions and rates.⁶ This presents a challenge as many natural enzymes (with the exception of some lipases) are not stable in organic solvent⁷ and denature at high temperatures. However, most synthetic processes are performed in these solvents and span a wide range of reaction temperatures.

A few interesting examples of transition metal catalyst working in parallel with enzymes have been reported.⁸ The bulk of these reported methods have relied on relatively promiscuous and robust lipases and esterases as the enzyme partner. One transformation that has showcased the power of the chemo-enzymatic approach is the dynamic kinetic resolution of alcohols first reported by Williams and Bäckvall in the late 90s.^{9,10} Williams examined the racemization and acetylation of phenethyl alcohol with *Pseudomonas fluorescens* lipase and a variety of organometallic transfer hydrogenation catalysts and found that Rh_2OAc_4 and $\text{Rh}(\text{COD})\text{Cl}_2$ were competent catalysts for the desired tandem transformation (Figure 4.1a). By using a $\text{Ru}(\text{II})$ transfer hydrogenation catalyst and changing the acyl donor from vinyl acetate to *p*-chlorophenyl acetate, Bäckvall was able to significantly improve both the enantioselectivity and the yield of the overall transformation (Figure 4.1b).¹⁰ The kinetic dynamic resolution can also be run in “reverse” with *Pseudomonas fluorescens* starting from a racemic mixture of allyl acetates (Figure 4.1c).¹¹ The racemization process is achieved by a palladium(II) catalyst via a (π -allyl)-palladium intermediate.

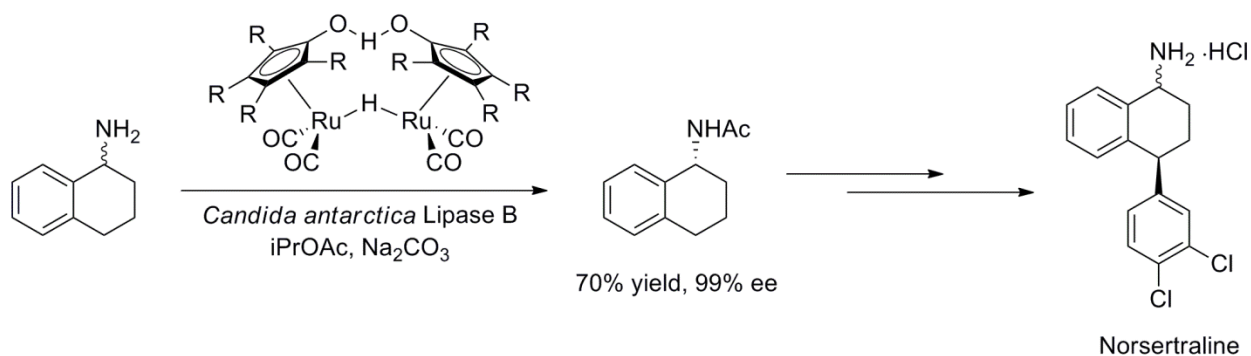
Figure 4.1. Dynamic kinetic resolution of secondary alcohols via tandem racemization and acylation reported by (a) Williams and (b) Bäckvall. (c) Dynamic kinetic resolution of allylic acetates in the presence of $\text{Pd}(\text{II})$ catalyst.





Since these early reports, a variety of organometallic complexes have been used in these transformations and kinetic dynamic resolution of diols, hydroxyl esters, hydroxyl nitriles, hydroxyphosphates, azido alcohols and amines has been achieved.¹² In particular, the chemoenzymatic dynamic kinetic resolution of amines was an important step in the total synthesis of Norsertraline by Bäckvall (Scheme 4.1).¹³ Once again, Ru(II)-catalyzed transfer hydrogenation of the amine enabled the racemization step.

Scheme 4.1. Kinetic dynamic resolution of amines in the total synthesis of Norsertraline.

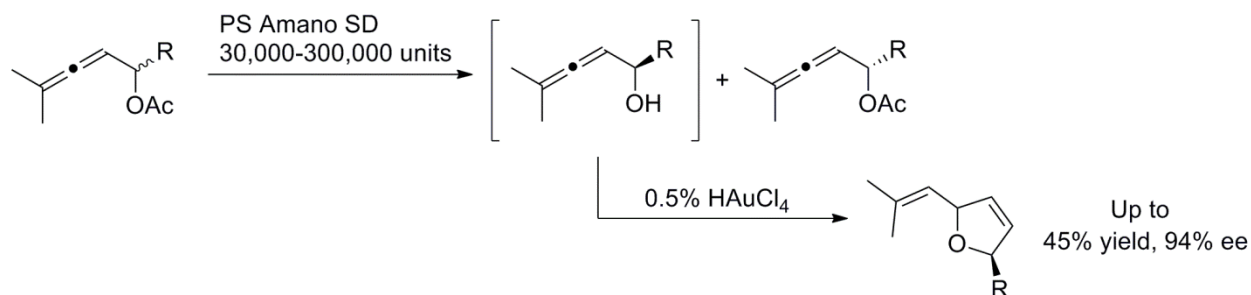


Additionally, Pd(II) complexes and Pd-nanoparticles have been used in one pot Suzuki¹⁴ or Heck¹⁵ cross coupling, followed by asymmetric reduction by a dehydrogenase. While both of these reactions require addition of the enzyme half way through the reaction, they nonetheless demonstrate the ability of the enzyme to catalyze transformations in the presence of transition metals and transition metal nanoparticles. Interestingly, while the Pd(II) complex itself did not affect enzymatic activity, excess phosphine or boronic acid used for cross coupling greatly diminished product yield. Thus, dehydrogenase from *Rhodococcus* sp. could not be added until all boronic acid was consumed, as determined by gas chromatography.

In 2009, Krause was able to use a gold(III) catalyst for the tandem hydrolysis and cyclization of allenic acetates (Figure 4.2).¹⁶ The racemic acetates were enantioselectively resolved by PS

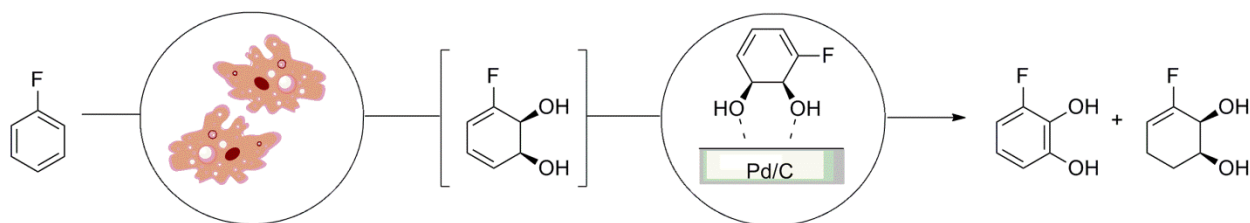
Amano SD enzyme via hydrolysis and then cyclized by HAuCl_4 . The transformation provided the dihydrofuran product in moderate to good yields and high enantioselectivity. However, a low ratio of gold(III) to enzyme was critical to reaction yield and the optimized reaction conditions required up to 100 mg (300,000 units) of enzyme for the reaction with only 10 mg substrate. Despite these drawbacks, this report highlighted the potential of enzymatic resolution for the synthesis of enantioenriched heterocycles.

Figure 4.2. Tandem hydrolysis and cyclization with HAuCl_4 .



While lipases and esterases are robust and easy to handle, the majority of catalytic enzymes found in nature cannot be isolated as solids and are not suitable for benchtop chemical synthesis. To expand the range of enzymes used in tandem processes Hardacre and coworkers have used cell cultures of a mutant strain of *Pseudomonas putida* in conjunction with Pd/C for the synthesis of catechols from monosubstituted benzenes (Figure 4.3).¹⁷ Mutant strains of *Pseudomonas putida* do not express cis-dioldehydrogenase and thus cell cultures of these strains build up an excess of cis-dihydrodiols as a result of benzene oxidation by toluene dioxygenase. Addition of Pd/C to the cell medium led to formation of both catechols and tetrahydrodiols. This procedure was used to synthesize gram quantities of fluoro-catechol from fluorobenzene.

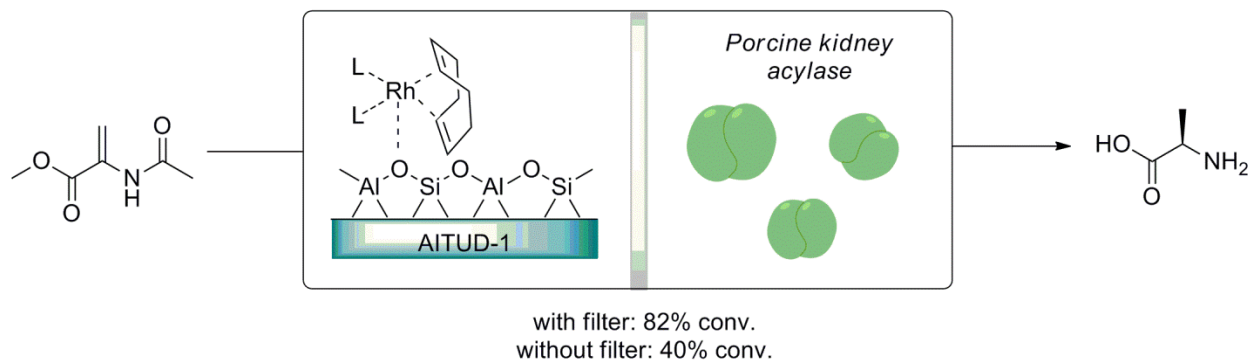
Figure 4.3. One pot procedure for synthesis of catechols and cyclic diols with *Pseudomonas putida* and Pd/C from fluorebenzene.



In nature, enzymes are able to compartmentalize their reactive sites such that series of chemically incompatible reactions can be performed in tandem. This idea of “site isolation” has inspired a number of approaches using polymers, gels, and solid support to isolate reactive catalysts from one another. In one such example, cationic $\text{Rh}(\text{COD})_2\text{L}_2^+$ complexes were immobilized on A1TUD-1, a mesoporous aluminosilicate and used in a tandem hydrogenation and hydrolysis process with two acylases (Figure 4.4).¹⁸ Despite immobilization the optimized conditions required a filter between two compartments of the reaction vessel to separate the

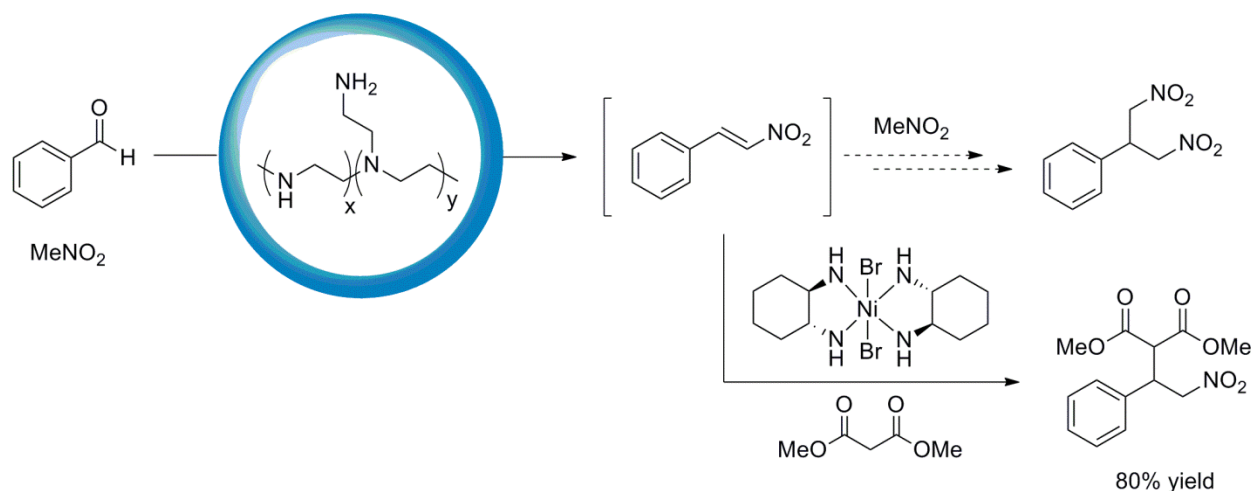
enzyme and the hydrogenation catalyst. This hybrid engineering and chemical approach was able to provide L-alanine from methyl 2-acetamidoacrylate in high conversion after 24 h.

Figure 4.4. Tandem catalysis by Rh(I) catalysts immobilized on AITUD-1 and porcine kidney acylase.



In a molecular approach to the problem of site isolation, encapsulation of polymeric amine poly(ethyleneimine) in a capsule formed via polymerization at water-oil interfaces allowed tandem catalysis to be performed with a nickel Lewis acid (Figure 4.5).¹⁹ The polymer catalyst is able to activate benzaldehyde for the addition of nitromethane and the nickel catalyst activates the resulting product for Michael addition with dimethyl malonate. Interestingly, in the absence of a competent Ni(II) Lewis acid (for instance, when the polymer is not sequestered and allowed to coordinate to the nickel center or when no nickel complexes are added), a product different from that resulting from Michael addition of nitromethane is observed. While neither catalyst employed in this transformation is a true enzyme, encapsulation nonetheless allowed two incompatible catalysts to work in one-pot. Other polymer approaches, including encapsulation of enamine and imine catalysts within star-polymer cores have also been reported.

Figure 4.5. One pot additions with nitromethane and dimethyl malonate. Compartmentalization of the amine polymer catalyst allows for formation of desired product, instead of the side product from double addition.



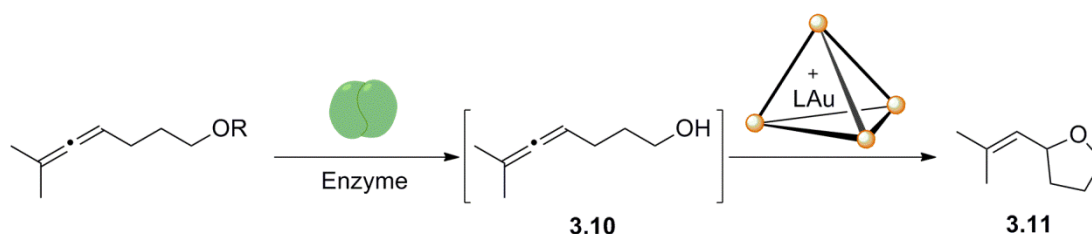
A supramolecular approach to the problem of tandem catalysis with organometallic complexes has many advantages. Firstly, the ability of supramolecular assemblies to stabilize reactive metal centers via host-guest interactions may improve the lifetime of the organometallic complex.^{20, 21} Secondly, supramolecular hosts that demonstrate high water solubility can “pull” metal complexes with hydrophobic organic ligands into the aqueous solution such that reactions traditionally performed in organic solvent can be achieved in water.²² Thirdly, the cluster itself can prevent the reactive metal catalyst from diffusing into solution where it can interact directly with residues on a protein, negating the need for high enzyme loading. These advantages make supramolecular host-guest complexes an attractive target for the development of synthetic catalysts that can work collaboratively with true enzymes.

We have examined organometallic complexes encapsulated in the tetrahedral $K_{12}Ga_4L_6$ ($L = N,N'$ -bis(2,3-dihydroxybenzoyl)-1,5-diaminonaphthalene, **3.8**) cluster. The complexes are stable at neutral pH in water and the cluster itself provides a well-defined cavity for reaction.²³ In particular, the gold(I)- Ga_4L_6 host-guest complex ($PMe_3Au^+ \subset \mathbf{3.8}$) exhibits an eight-fold rate enhancement relative to the free gold complex in the hydroalkoxylation of allenes, and shows higher reactivity toward unsubstituted substrates like **3.10** than those bearing substitution along the alkyl chain.²⁴ Additionally, Brown and coworkers have demonstrated that $(Me_3P)CpRu(NCMe)_2^+ \subset Ga_4L_6$ catalyzes the isomerization of allyl alcohols and showed the complex can perform >1000 catalytic turnovers.²⁵ In both cases, the encapsulation improved the lifetime of the organometallic guest. We hypothesized that these host-guest assemblies would be excellent platforms to test whether a Ga_4L_6 host-guest complex could function in a multi-step reaction containing an enzyme-mediated step.

Results

We have previously studied the hydroalkoxylation of allenes with gold(I)-phosphines encapsulated in Ga_4L_6 (**3.8**).²⁴ As many enzymes yield alcohols as products, we hypothesized that enzymatic reaction with of an alcohol precursor could yield **3.10** which could then be cyclized with our gold catalyst in one pot to afford **3.11**. This overall transformation is shown in the scheme below. Both esterases and lipases are promiscuous enzymes that accept a range of substrates²⁶ and we posited that these enzymes could be incorporated into our proposed sequence and used to hydrolyze the ester of **3.10**.

Scheme 4.2. One-pot enzyme reaction to reveal **3.10**, followed by hydroalkoxylation with $\text{LAu}^+ \subset \mathbf{3.8}$.



To ensure that the enzymatic hydrolysis of **4.1** is independently viable, we monitored the reaction of **4.1** with a few representative esterases and lipases (Table 4.1). High conversion to the hydrolyzed product was observed at room temperature for rabbit liver esterase. However, reaction with *Candida rugosa* and *Rhizopus arrhizus* lipases proceeded much less readily. As the triglyceride triolein is the standard substrate for both of these enzymes, we posited that a long-chain ester may be a better substrate match for these enzymes. Indeed, when we changed from acetate to octanoate (**4.2**), higher conversion was observed for both lipases.

Table 4.1. Ester hydrolysis to generate alcohol **3.10**.

The reaction scheme shows the hydrolysis of an allene-ester (4.1) to an allene-alcohol (3.10) using an enzyme in a buffer.

Substrate	Enzyme	Conversion
R = Ac (4.1)	rabbit liver esterase (12 U)	88%
R = Ac	<i>Rhizopus arrhizus</i> lipase (3 U)	30%
R = Ac	<i>Candida rugosa</i> lipase (3 U)	74%
R = (4.2)	<i>Rhizopus arrhizus</i> lipase (3 U)	80%
R = (4.2)	<i>Candida rugosa</i> lipase (3 U)	100%

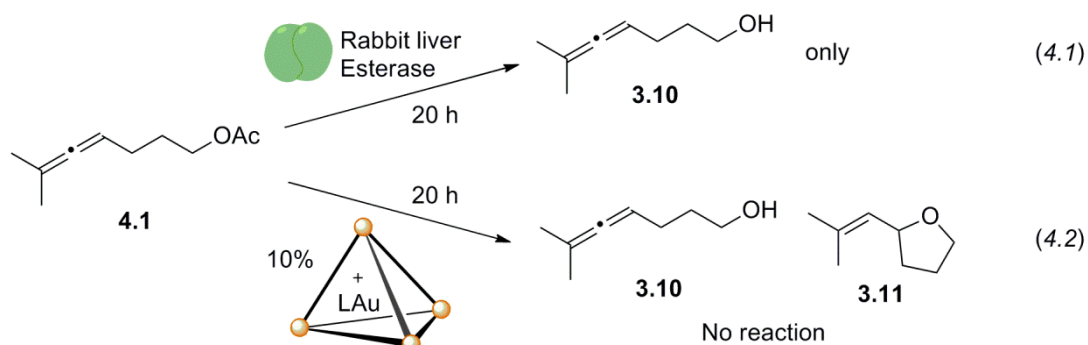
Turning to the tandem reaction, we combined **4.1** with rabbit liver esterase and 10 mol% $\text{PMe}_3\text{Au}^+ \text{3.8}$ in tris buffer pH 8 and 12% conversion (based on remaining starting material) to the cyclized product was observed after 20 h (Table 4.2, entry 1). Neither phosphate buffer nor unbuffered milipore water was suitable as solvent for the reaction (entry 2 and 3). However, addition of 5% DMSO to the reaction mixture greatly improved the solubility of **4.1** and resulted in a dramatic improvement in conversion to 88% after 20 h (entry 4). The same effect on yield was observed when 5% MeOH was used (entry 5). Increasing the reaction temperature to 37 °C allowed the reaction to proceed to complete conversion (entry 6) and high isolated yield (based on internal standard after extraction, see experimental section) using only 6 units of enzyme.

Table 4.2. Optimization for tandem reaction with rabbit liver esterase and $\text{PMe}_3\text{Au}^+ \text{3.8}$.

Entry	Enzyme loading	Solvent	Temperature (°C)	Additive	% Conversion ^a
1	25 U	tris buffer pH 8	23	none	12
2	25 U	phos buffer pH 7.5	23	none	0
3	25 U	H ₂ O	23	none	0%
4	25 U	tris buffer pH 8	23	5% DMSO	88%
5	25 U	tris buffer pH 8	23	5% MeOH	89%
6	6 U	tris buffer pH 8	37	5% DMSO	>98%
7	3 U	tris buffer pH 8	37	5% DMSO	62%

^aDetermined by integration relative to internal standard after extraction with CDCl_3

Significantly, treating **4.1** with rabbit liver esterase under identical conditions afforded only the alcohol product **3.10** (eq 4.1) and subjecting **4.1** to 5 mol% of $\text{PMe}_3\text{Au}^+ \text{3.8}$ alone led to no reaction (eq. 4.2). Thus, catalytic formation of the cyclized product **3.11** required both rabbit liver esterase and $\text{PMe}_3\text{Au}^+ \text{3.8}$. When PMe_3AuCl was used instead of $\text{PMe}_3\text{Au}^+ \text{3.8}$, only 62% conversion to the cyclized product was observed: the remaining material consisted of 14% unreacted **4.1** and 24% allenic alcohol **3.10** (Table 4.3, entry 16).

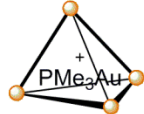


Following these initial results, we examined the tandem reaction sequence with a variety of esterases and lipases. While in some cases, addition of cluster resulted in lower conversion to product (relative to reaction with PMe_3AuCl), the encapsulated complex $\text{PMe}_3\text{Au}^+\text{C}^-\text{3.8}$ performed as well or better than the free catalyst in others. Additionally, a few lipases have been known to cleave amide bonds²⁷ and we were able to exploit this property to furnish isoxazolidine **3.18** in good yield after amide hydrolysis of **4.3** and hydroamination. Interestingly, tandem reactions with $\text{PMe}_3\text{Au}^+\text{C}^-\text{3.8}$ and rabbit, hog or horse liver esterase showed a small to moderate amount of starting material after 20 h when PMe_3AuCl was used, suggesting that PMe_3AuCl inhibits activity of the esterase. Amino acids like cysteine, histidine and asparagine have been known to coordinate free gold(I) ions,^{28,29} and we hypothesize that decrease in yield of hydrolysis observed is a result of direct interactions between gold(I) and amino acid residues on the esterase. In contrast, the encapsulated gold complex sequesters PMe_3Au^+ and prevents it from diffusing into the bulk solvent where it can complex to the protein.

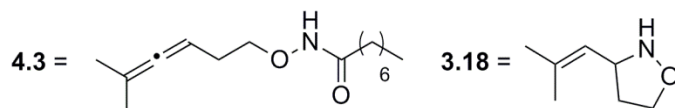
Table 4.3. Tandem reaction with esterases and lipases.

Reaction scheme showing the tandem reaction of substrate **4.1** (an allylic ester) with Rabbit liver Esterase (4.1) and 10% $\text{PMe}_3\text{Au}^+\text{C}^-\text{3.8}$ (4.2) over 20 h. The reaction with the esterase alone yields product **3.10** (an allylic alcohol). The reaction with the encapsulated complex yields both **3.10** and **3.11** (an isoxazolidine), with no reaction observed for the free catalyst.

Entry	Substrate	Enzymes (1-6 units) ^a	ester : alcohol: prod ^b	ester : alcohol: prod ^b
1	4.1	rabbit liver (E)	0 : 0 : 100	14 : 24 : 62
2	4.1	horse liver (E)	4 : 43 : 53	11 : 35 : 54
3	4.1	hog liver (E)	3 : 3 : 94	35 : 22 : 42
4	4.1	Candida lipolytica (E)	43 : 43 : 14	58 : 36 : 6
5	4.1	Mucor meihei (E)	59 : 28 : 13	12 : 48 : 40
6	4.1	Pseudomonas fluorescens (E)	93 : 2 : 5	30 : 34 : 36
7	4.1	Streptomyces diastatochromogenes (E)	13 : 12 : 75	44 : 22 : 34
8	4.1	Bacillus stearothermophilus (E)	Significantly higher conv. with PMe_3AuCl	
9	4.1	Rhizopus oryzae (E)		

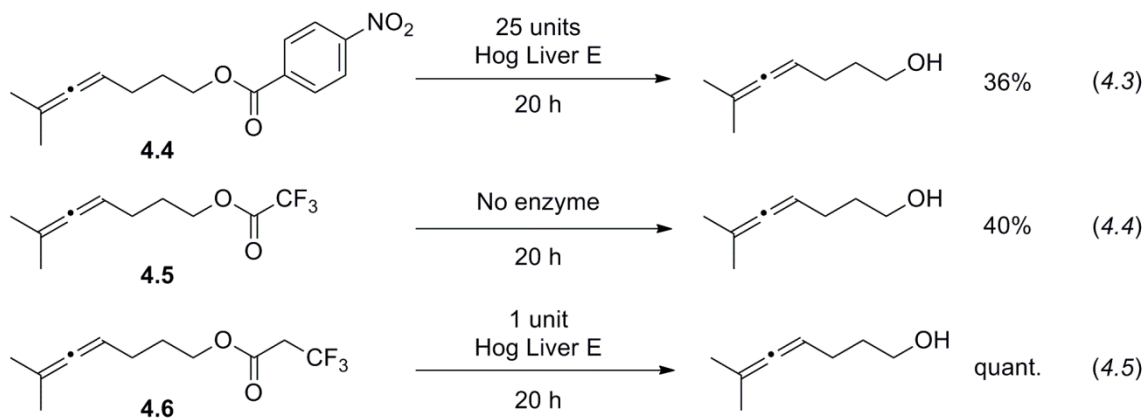

PMe₃AuCl

Entry	Substrate	Enzymes (1-6 units) ^a	ester : alcohol: prod ^b	ester : alcohol: prod ^b
10	4.1	<i>Candida rugosa</i> (L)	0 : 0 : 100	0 : 0 : 100
11	4.1	<i>Mucor miehei</i> (L)	0 : 0 : 100	0 : 0 : 100
12	4.1	<i>Pseudomonas cepacia</i> (L)	24 : 3 : 73	26 : 15 : 59
13	4.1	<i>Pseudomonas fluorescens</i> (L)	15 : 3 : 82	14 : 5 : 81
14	4.1	<i>Candida antartica</i> (L)	0 : 0 : 100	0 : 0 : 100
15	4.2	<i>Rhizopus arrhizus</i> (L)	80 : 11 : 9	80 : 10 : 10
16	4.2	<i>Candida rugosa</i> (L, 3 units)	0 : 0 : 100	15 : 0 : 85
17	4.3	<i>Mucor miehei</i> lipase (L, 3 units)	38 : 2 : 60	32 : 2 : 66



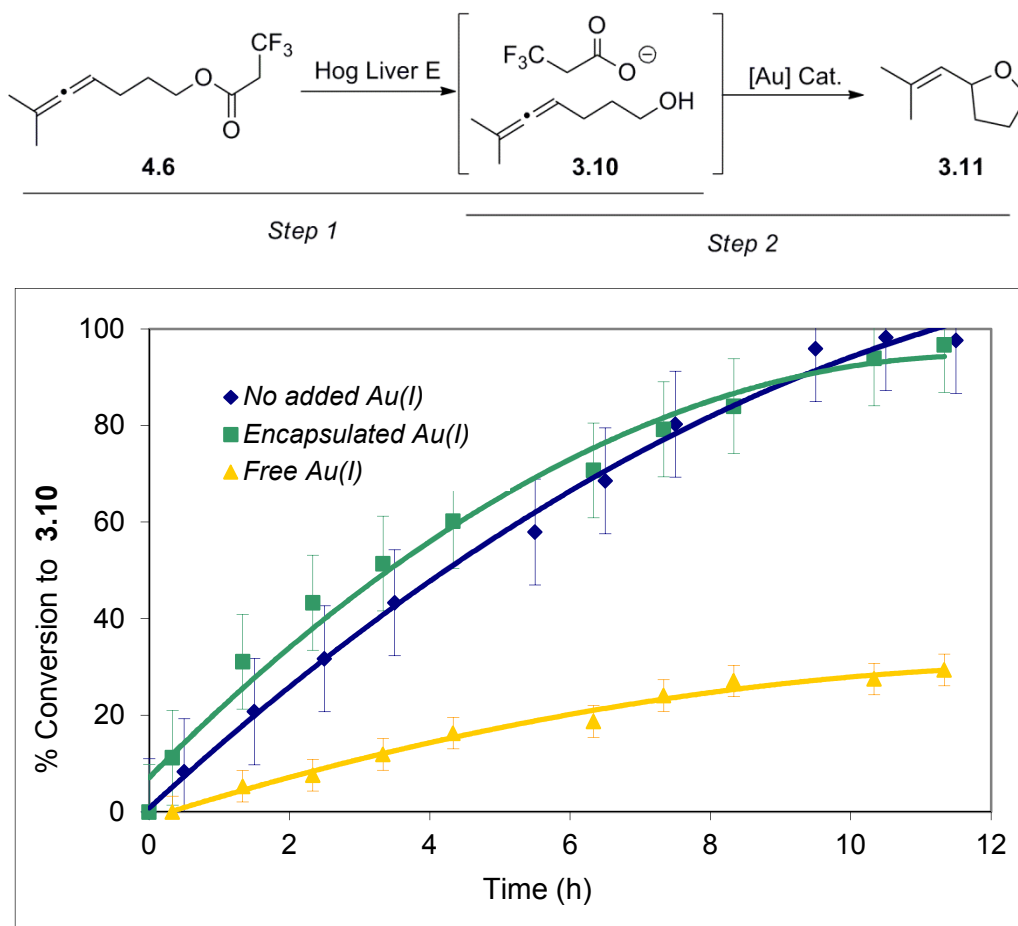
^a(E) = esterase (1 unit), (L) = lipase (6 units, unless otherwise specified). ^bBased on NMR integration relative to unreacted starting material

To further explore this hypothesis, we wanted to monitor the rate of enzymatic hydrolysis. We prepared the *p*-nitrobenzoate ester of **3.10** and subjected it to optimized reaction conditions with hog liver esterase. The nitrobenzoate fluorophore provided a functional handle for us to follow the reaction by UV-visible spectroscopy. However, hydrolysis of this substrate was extremely slow and only 36% conversion was observed after 20 h with 25 units of enzyme (eq. 4.3). As this rate of reaction was unsuitable for kinetic measurements, we turned to ¹⁹F NMR for analysis and prepared the trifluoro acetate of **3.10**. However, this substrate showed appreciable hydrolysis in buffered solution, even in the absence of enzyme (eq. 4.4). Finally, we synthesized the trifluoro-propanoate ester **4.3**. Gratifyingly, this substrate exhibited rates of hydrolysis similar to **4.1** (eq. 4.5), was readily distinguishable from the trifluoro-propanoate by NMR, and allowed us to monitor the rate of enzymatic hydrolysis step in the tandem transformation.



We performed the transformation under three reaction conditions: (1) with hog liver esterase and $\text{PMe}_3\text{Au}^+ \mathbf{3.8}$, preformed from PMe_3AuCl and $\mathbf{3.8}$ (2) with hog liver esterase and PMe_3AuCl and (3) with hog liver esterase alone. The reaction trace below demonstrates the effect of the catalyst in the cyclization step (step 2, Figure 4.6) on the kinetics of the first step (step 1, Figure 4.6) in the sequence. Conversion from $\mathbf{3.10}$ to product is not measured directly. While the rate of hydrolysis in the presence of $\text{PMe}_3\text{Au}^+ \mathbf{3.8}$ is within error of the inherent rate of hydrolysis in the absence of any gold species, the rate of esterase catalysis is significantly reduced when PMe_3AuCl is used as catalyst. This result provides evidence that the supramolecular host guest complex has little effect on enzyme activity, while the free $\text{PMe}_3\text{Au}^+ \mathbf{3.8}$ is deleterious to enzyme catalysis. We conclude that the supramolecular cluster may prevent undesired direct interactions between the enzyme and gold catalysts, preserving the activity of both.

Figure 4.6. Enzymatic hydrolysis of $\mathbf{4.3}$ monitored by ^{19}F NMR, relative to trifluoroethanol internal standard: (■), PMe_3AuCl (▲ free Au), or no additional gold complexes (●).



In addition to esterase and lipase hydrolysis, we posited that reduction of an aldehyde by a dehydrogenase could generate the alcohol functionality required for cyclization. There are few examples of tandem chemoenzymatic reactions involving dehydrogenases and most of these require sequential addition of the metal and enzyme catalysts.^{14,15} We prepared aldehyde **4.7** and

treated it with horse liver dehydrogenase (2 units) and a stoichiometric amount of NADPH cofactor in phosphate buffer. Gratifyingly, 96% conversion to the desired alcohol was observed. However, attempts to incorporate aldehyde reduction into a sequence with $\text{PMe}_3\text{Au}^+ \mathbf{3.8}$ led to complete decomposition of the aldehyde. Indeed, suspension of the aldehyde in buffer at room temperature for 20 h led to the same result. Thus, we reason that instability of the aldehyde under reaction conditions could be at least partially responsible for the decomposition we observed. As secondary alcohols can also be cyclized by $\text{PMe}_3\text{Au}^+ \mathbf{3.8}$, reduction of ketone **4.8** by dehydrogenase could also unveil a competent nucleophile for our reaction. However, reduction with up to 150 units of dehydrogenase failed to furnish the secondary alcohol in appreciable conversion. Addition of bovine serum albumin to the reaction mixture did not improve conversion to the desired product and resulted in formation of an unidentified side product.

Figure 4.7. Tandem reduction and cyclization.

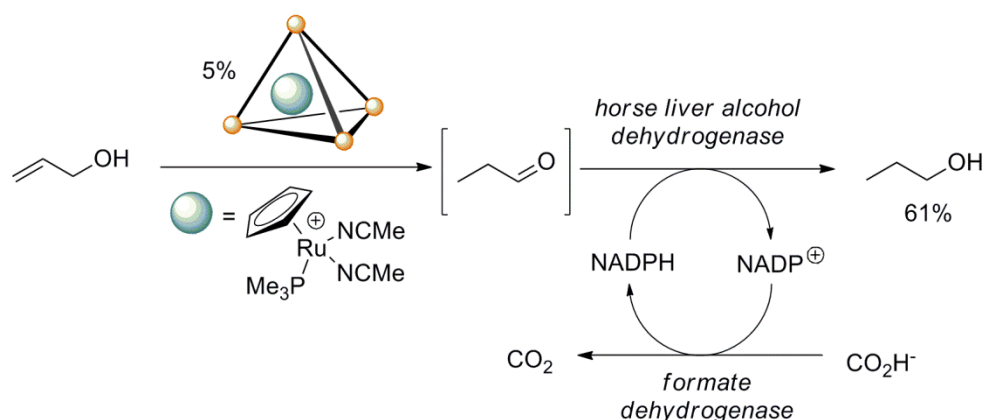
Substrate	Enzyme	[Au] cat.	Conversion
R = H (4.7)	horse liver alcohol dehydrogenase (2 U)	none	96% to 3.10
R = H	horse liver alcohol dehydrogenase (2 U)	$\text{PMe}_3\text{Au}^+ \mathbf{3.8}$	decomposition
R = H	horse liver alcohol dehydrogenase (2 U)	PMe_3AuCl	decomposition
R = H	none	none	decomposition
R = Me (4.8)	horse liver alcohol dehydrogenase (up to 12 U)	none	<10% to 4.9
R = Me	yeast alcohol dehydrogenase (up to 150 U)	none	<10% to 4.9
R = Me	horse liver alcohol dehydrogenase (up to 12 U)	none	trace 3.14
R = Me	horse liver alcohol dehydrogenase (2 U) + bovine serum albumin	$\text{PMe}_3\text{Au}^+ \mathbf{3.8}$	33% to unidentified product

We have previously shown that $(\text{Me}_3\text{P})\text{CpRu}(\text{NCMe})_2^+ \mathbf{3.8}$ is a high-turnover catalyst for isomerization of allylic alcohols. The aldehyde product from this reaction provided another opportunity to incorporate a dehydrogenase-reduction step into a sequence with **3.8**. In particular, the enzyme step proceeds first followed by the metal-catalyzed step, in reverse of the hydrolysis-hydroalkoxylation sequence discussed previously. However, as both the propen-ol (substrate), propionaldehyde (intermediate), and propanol (product) are all highly soluble or miscible with water, organic extraction cannot be used to determine conversion. Furthermore, as enzymes are incompatible with deuterated solvent, performing the tandem reaction in buffered D_2O was also unsuitable. Fortunately, the transformation can be monitored directly in water, using an external standard filled with D_2O and operating under solvent suppression parameters

for ^1H NMR. Diagnostic peaks for the propen-ol, propionaldehyde (and its hemi-acetal), and propanol can all be observed.

When propen-ol was added to a solution of $(\text{Me}_3\text{P})\text{CpRu}(\text{NCMe})_2^+ \mathbf{3.8}$ (5 mol%), horse liver dehydrogenase (1 unit), and a stoichiometric amount of NADPH, 70% conversion to the desired product was observed after 6 h. Additionally, we found that the reduction can be coupled to oxidation of sodium formate by formate dehydrogenase with little decrease in the yield of reaction (61%). The overall transformation used 0.15 equivalents of NADPH and required that the supramolecular catalyst work well in concert with both dehydrogenases. Once again, neither the enzyme couple nor the encapsulated ruthenium catalyst alone could carry out both reactions in the sequence. The analogous reaction with free $(\text{Me}_3\text{P})\text{CpRu}(\text{NCMe})_2^+$ proceeds to slightly higher conversion under the same conditions. However, we attribute the difference in yield to the isomerization step, as the olefin isomerization proceeds faster with $(\text{Me}_3\text{P})\text{CpRu}(\text{NCMe})_2^+$ than $(\text{Me}_3\text{P})\text{CpRu}(\text{NCMe})_2^+ \mathbf{3.8}$. As this step occurs first, the concentration of propionaldehyde increases more rapidly, and higher conversion is observed after the same time.

Figure 4.7. Tandem olefin isomerization and enzymatic reduction.

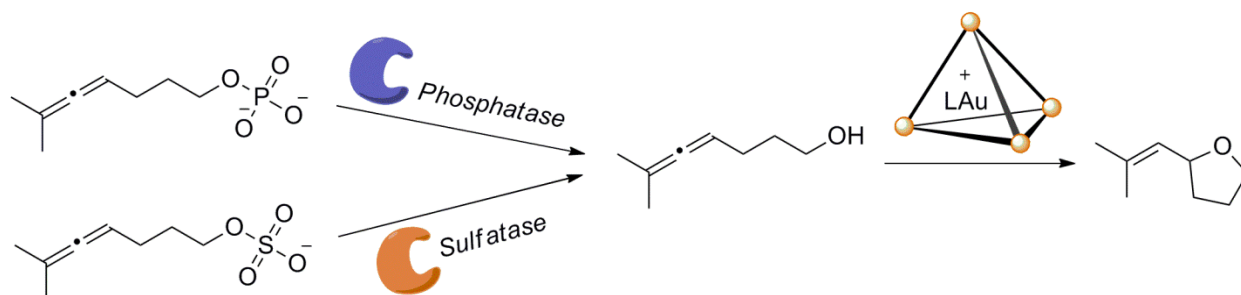


The examples reported here demonstrate the ability of a variety of enzymes to catalyze reactions in tandem with a supramolecular enzyme mimic. Notably, this combination is viable independent of whether the enzymatic or metal-catalyzed reaction proceeds first. While not all the enzymes we examined were affected by the presence of free gold(I) and ruthenium(II) complexes, encapsulation of a gold(I) catalyst can improve the rate of catalysis of the enzyme relative to that of the free cationic complex in some cases. While the mechanism of interaction between the free gold cation and hog liver esterase is not well understood at this time, the ability of free gold(I) to coordinate strongly to a variety of amino acids led us to believe that direct coordination by gold(I) to the enzyme is responsible for the significant decrease in catalytic activity observed in the presence of PMe_3AuCl . These results suggest that encapsulation can prevent adverse interactions from occurring and provides a method for tandem catalysis with reactive transition metal complexes. Our studies have important implications for the development of new supramolecular hosts for catalysis and demonstrate a key advantage of supramolecular catalysis in integrated chemical and biological synthetic sequences.

Future Directions

To determine whether encapsulation can be used as a more general approach to tandem catalysis, sequences with other enzymes should be examined. For instance, the hydroalkoxylation reaction can be incorporated into sequences with phosphatases or sulfatases with mono-phosphates and mono-sulfates, respectively. These enzymes are important in biological signaling pathways and tandem reactions with these enzymes would highlight the bio-compatibility of our supramolecular approach. Another avenue of research is the incorporation of other bio-incompatible metal complexes into a chemo-enzymatic sequence: for instance copper(I). The inability to use copper(I) in biological studies has inspired many methods, such as copper-free click reactions with cyclooctynes. Encapsulation of copper complexes that cannot diffuse into bulk solution but are still catalytically active may provide an orthogonal approach to the problem of copper cytotoxicity.

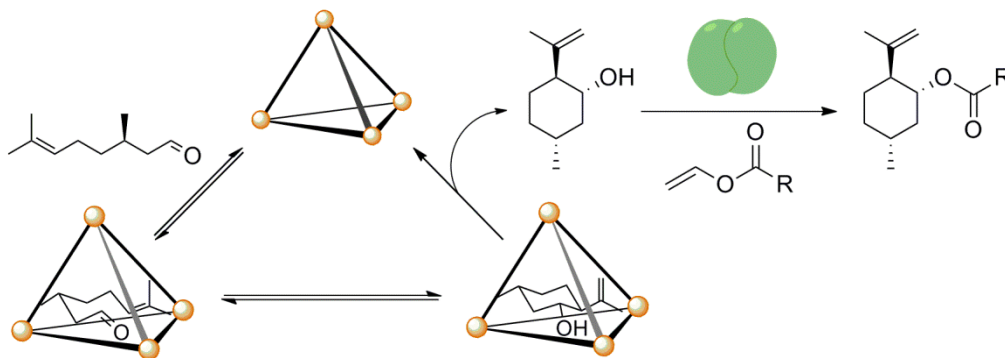
Figure 4.8. Chemo-enzymatic reactions with phosphatases and sulfatases.



The concept of “compartmentalization” via a supramolecular encapsulation has enormous potential in tandem catalysis beyond tandem reactions with enzymatic catalysts. For instance, many homogeneous metal catalysts readily absorb or coordinate to nanoparticles and mesoporous silicates. Indeed, this property has been exploited to immobilize homogeneous catalysts on solid support. Thus, introduction of a homogeneous metal catalyst is unsuitable under these conditions, as this catalyst may also become absorbed onto the solid support. However, compartmentalization may be able to prevent an encapsulated small molecule metal catalyst from coordinating directly to the heterogeneous surface and allow tandem homogeneous and heterogeneous reactions to take place.

Lastly, the ability of enzymes to operate well in concert with encapsulated metal complexes can be exploited as a general method to prevent product inhibition in supramolecular catalysis. In many examples of supramolecular catalysis where the capsule itself serves as a molecular reaction vessel, product can bind competitively with the starting material. Currently, the methods reported that show high turnover numbers have relied on changes in product shape to prevent binding, or addition of external reagents to trap out the product. These approaches are very specific to a given substrate and greatly limit the number of substrates suitable for catalysis by supramolecular complexes.

Figure 4.9. Cyclization of citronellal and enzymatic processing to remove the product out of equilibrium with the cluster.



In contrast, enzymes catalyze reactions with a range of functional groups. Thus, in situ enzymatic modification of a product by an enzyme may provide a more general solution for the problem of product inhibition. For instance, we recently reported the cyclization of citronellal by **3.8** and kinetic studies showed that the reaction began to slow at 40% conversion. However, if the secondary alcohol on the product can be esterified with a greasy ester, the resulting species would show much lower affinity for **3.8**. This may improve the product yield of this cyclization, and also allow us to perform detailed kinetic studies on the system in the absence of product inhibition.

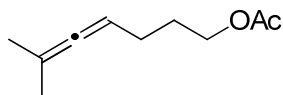
Experimental

General Experimental Procedure and Instrumentation

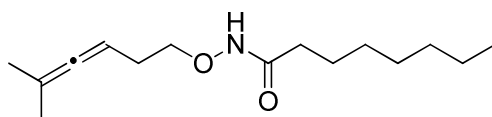
All reagents, catalysts and solvents were obtained from commercial suppliers and used without further purification, unless otherwise specified. All air-sensitive reactions were carried under positive N₂ pressure in a glove box with degassed solvent. All milligram quantities of substrate, complex, or enzyme were massed in an XP26 micro balance by Toledo-Mettler. Proton, ¹⁹F, and ³¹P NMR spectra were recorded with Bruker AVQ-400, DRX-500, AV-500, and AV-600 spectrometers and chemical shifts are reported in parts per million (ppm) relative to residual protonated solvent resonances. All enzymes and cofactors were obtained from Sigma Aldrich and used without further purification. Unit values reflect the rate of catalysis by the given enzyme on a standard substrate per unit time at defined pH and temperature, as reported by Sigma Aldrich.

Chloro(trimethylphosphine)gold(I) was prepared following standard protocols³⁰ or else obtained from Sigma Aldrich. The ruthenium complex [RuCp(PMe₃)(MeCN)₂][PF₆] and host guest complex [RuCp(PMe₃)(MeCN)₂]⁺ **3.8** was prepared following reported literature procedures.³¹ Compound **3.10** (6-methylhepta-4,5-dien-1-ol) was prepared as described previously in Chapter 3. The “empty” host assembly, K₁₂[Ga₄L₆] (**3.8**) was prepared using modified literature procedures.³² All flash chromatography was performed on Merck 60 silica gel (32-63 μm). Thin-layer chromatography (TLC) analysis was performed using Merck silica gel 60 F254 TLC plates, and visualized by staining with iodine, short wavelength UV, anisaldehyde, and/or potassium permanganate.

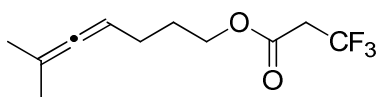
Substrate Synthesis



Preparation of 6-methylhepta-4,5-dien-1-yl acetate (4.1): To a solution of 6-methylhepta-4,5-dien-1-ol (100 mg, 0.79 mmol) in DCM (10 mL) at 0 °C, NEt₃ (154 μL, 1.11 mmol), acetic anhydride (90 μL, 0.96 mmol) and DMAP (20 mg, 0.16 mmol) was added. The solution was warmed to 23 °C and stirred for 2 h. The reaction mixture was diluted with DCM (10 mL) and quenched on a solution of saturated aqueous NaHCO₂ (15 mL). The organics were extracted and washed twice with water (15 mL), dried over MgSO₄, and concentrated by rotary evaporation. The crude oil was chromatographed on SiO₂ eluting 4% Et₂O in pentanes which provided purified **4** as a clear oil in 90% yield. ¹H NMR (CDCl₃, 500 MHz): δ 4.98 (m, 1H), 4.12 (t, *J* = 7.0 Hz, 2H), 2.10 (s, 3H), 2.04 (q, *J* = 7.0 Hz, 2H), 1.72 – 1.78 (m, 2H), and 1.70 (d, *J* = 3.0 Hz, 2H). ¹³C NMR (CDCl₃, 500 MHz): δ 201.8, 171.7, 95.7, 87.7, 64.0, 27.9, 25.5, 21.1, and 20.7.



Preparation of N-((5-methylhexa-3,4-dien-1-yl)oxy)octanamide (4.3): The starting unprotected hydroxylamine (O-(5-methylhexa-3,4-dien-1-yl)hydroxylamine) was prepared following literature precedent.^X To a solution of this amine (50 mg, 0.40 mmol) at 0 °C in DCM (10 mL), octanoic acid (70 μ L, 0.41 mmol) and DCC (85 mg, 0.41 mmol) was added. The reaction was warmed to 23 °C and stirred for 14 h. The crude reaction was filtered through a pad of silica to remove urea precipitates, concentrated by rotary evaporation, and chromatographed on SiO₂ eluting 20-30% Et₂O in hexanes. The desired product was isolated as pale yellow oil in 67% yield. ¹H NMR (CDCl₃, 500 MHz): δ 8.75 (broad s, 1H), 4.94-4.98 (m, 1H), 3.86-3.98 (m, 2H), 2.32 (q, J = 6.5, 2H), 2.07-2.13 (m, 2H), 1.68 (d, J = 3.0 Hz, 6H), 1.62-1.68 (m, 2H), 1.26-1.32 (m, 8H), and 0.89 (t, J = 3.5 Hz, 3H). ¹³C NMR (CDCl₃, 500 MHz): δ 202.7, 171.9, 96.0, 84.6, 76.3, 34.8, 33.6, 32.0, 29.5, 29.3, 25.7, 22.9, 21.0, 14.4.



Preparation of 6-methylhepta-4,5-dien-1-yl 3,3,3-trifluoropropanoate (4.6): To a solution of 6-methylhepta-4,5-dien-1-ol (100 mg, 0.79 mmol) in DCM (10 mL) at 0 °C, 3,3,3-trifluoropropanoic acid (111.4 mg, 0.87 mmol), DMAP (97 mg, 0.79 mmol), and DCC (180 mg, 0.87 mmol) was added. The reaction was warmed to 23 °C and stirred for 3 h. The crude mixture was filtered through a pad of silica to remove urea precipitates, concentrated by rotary evaporation, and chromatographed directly on SiO₂ eluting 2-4% Et₂O in hexanes. The desired product was isolated as a clear oil in 54% yield. ¹H NMR (CDCl₃, 500 MHz): δ 4.97 (m, 1H), 4.24 (t, J = 6.5 Hz, 2H), 3.20 (q, J = 10.5 Hz, 2H), 2.03-2.09 (m, 2H), 1.73 – 1.80 (m, 2H), 1.70 (d, J = 3.0 Hz, 6H). ¹³C NMR (CDCl₃, 500 MHz): δ 202.2, 164.5 (q, J = 15 Hz), 123.7 (q, J = 1100 Hz) 96.2, 88.0, 64.3, 40.0 (q, J = 125 Hz), 28.3, 25.8, and 21.0.

General Procedure for Tandem Enzyme Reactions with PMe₃Au⁺ 3.8:

Chloro(trimethylphosphine) gold(I) (0.50 mg, 1.6 μ mol) was combined with K₁₂[Ga₄L₆] (3.8) (7.0 mg, 1.6 μ mol) in tris buffer pH 8 (0.7 mL) in an oxygen-free glove box. The solution was stirred rapidly at room temperature for 20 min and then filtered through a micro syringe filter. A portion of the filtered catalyst solution (1.2 μ mol, 500 μ L) was added to a second vial equipped with silicon septa cap and stir bar and removed from the glove box. A stock solution of the allene substrate and internal standard (in a 3:1 ratio) in degassed MeOH or DMSO was made. A second stock solution of the enzyme in buffer solution was made such that the final concentration of enzyme is 1 unit per 10 μ L. To the solution of PMe₃Au⁺Ga₄L₆, the enzyme (1-6 units) and substrate solutions (12.0 μ mol of substrate in 25 μ L MeOH or DMSO) are added. Additional buffer is added such that the final volume of reaction is 550 μ L and the resulting mixture was stirred gently (60-100 rounds per minute) for 20 h. The aqueous reaction is extracted three times with CDCl₃ (0.5 mL, each) dried with Na₂SO₄, and ¹H NMR of the organic solution is recorded to determine conversion and yield, relative to internal standard. Proton NMR data of the product matches that previously reported.³ NMR yields of the products are reported in Table S1 below and representative spectra are included for each tandem reaction performed: tandem hydroalkoxylation with rabbit liver esterase, tandem hydroalkoxylation with

hog liver esterase, and tandem hydroamination with a *Mucor miehei* lipase (spectra 1-3, respectively).

Table S4.1. NMR yields of tandem reactions with lipases and esterases with $\text{PMe}_3\text{Au}^+ \subset \mathbf{3.8}$.

Enzyme (1-6 U)
5% MeOH, 20 h

3.10 **3.11**

Entry	Substrate	Product	Enzyme	Conditions	NMR Yield of 3
1	4.1	3.11	rabbit liver esterase ^c	6 U enzyme, 37 °C, tris pH 8	95%
2	4.1	3.11	hog liver esterase ^d	1 U enzyme, 23 °C, tris pH 8	82%
3	4.1	3.11	horse liver esterase ^d	1 U enzyme, 23 °C, tris pH 8	51%
4	4.2	3.11	<i>Candida rugosa</i> lipase	3 U enzyme, 37 °C, phos. pH 7	86%
5	4.3	3.18	<i>Mucor miehei</i> lipase ^e	3 U enzyme, 37 °C, phos. pH 7	56%

4.3 = **3.18** =

Reaction of Alcohol and Formate Dehydrogenase with $[\text{RuCp}(\text{PMe}_3)(\text{MeCN})_2]^+ \subset \mathbf{3.8}$:

Solid NADPH (2.0 mg, 2.7 μmol), alcohol dehydrogenase (1 unit), formate dehydrogenase (1 unit), and sodium formate (3.3 mg, 53.0 mmol) are massed into a NMR tube using a micro balance. The NMR tube is equipped with an external standard containing D_2O and DMF as standard and taken into an oxygen-free glove box. A solution of $[\text{RuCp}(\text{PMe}_3)(\text{MeCN})_2]^+ \subset \mathbf{3.8}$ (3.2 mg, 0.88 μmol) in phosphate buffer pH 7 is prepared and added to the NMR tube containing the solid components. Propen-1-ol is added (1.2 μL , 17.7 μmol) is added last. The reaction mixture is shaken gently until homogeneous and then incubated at 37 °C for 6 h. Water suppression ^1H NMR is taken to determine NMR yield relative to DMF external standard of known concentration (spectrum 4). The relevant product peaks are indicated.

Following Reaction of Fluorinated Substrate **4.6** with Hog Liver Esterase by ^{19}F NMR:

Stock solutions: Substrate **4.6** and trifluoroethanol (internal standard, 1.0 equiv. rel. to **4.6**) was dissolved in degassed DMSO such that a 26.4 mM solution of **7** was formed (stock 1). In another vial, a stock solution of hog liver esterase (1 unit per 10 μL) was prepared in tris buffer pH 8 (stock 2). In a separate vial in an oxygen free glove box equipped with stir bar, PMe_3AuCl (0.50 mg, 1.6 μmol) and $\text{K}_{12}[\text{Ga}_4\text{L}_6]$ (7.0 mg, 1.9 μmol) are dissolved in tris buffer pH 8 (615 μL) and stirred vigorously for 20 min. The solution is filtered (stock 3).

Sample with $\text{PMe}_3\text{Au}^+ \subset \mathbf{3.8}$: Under N_2 , stock solution 3 (450 μL , 1.2 μmol of $[\text{Au}]^+$) was transferred to an NMR tube equipped with rubber septa cap and a D_2O external standard. The sample is removed from the glove box and at $t = 0$, stock solution 2 (10 μL) and stock solution 1 (55 μL) was added. NMR tube was sealed with parafilm and shaken gently until all components were combined.

Sample with PMe_3AuCl : A sample of PMe_3AuCl (0.37 mg, 1.2 μmol) was added to an NMR tube equipped with and a D_2O external standard and a rubber septa cap. Tris buffer pH 8 (450 μL) was added. At time $t = 0$, stock solution 2 (10 μL) and stock solution 1 (55 μL) was added and the NMR tube was sealed with parafilm and shaken gently until all components were combined.

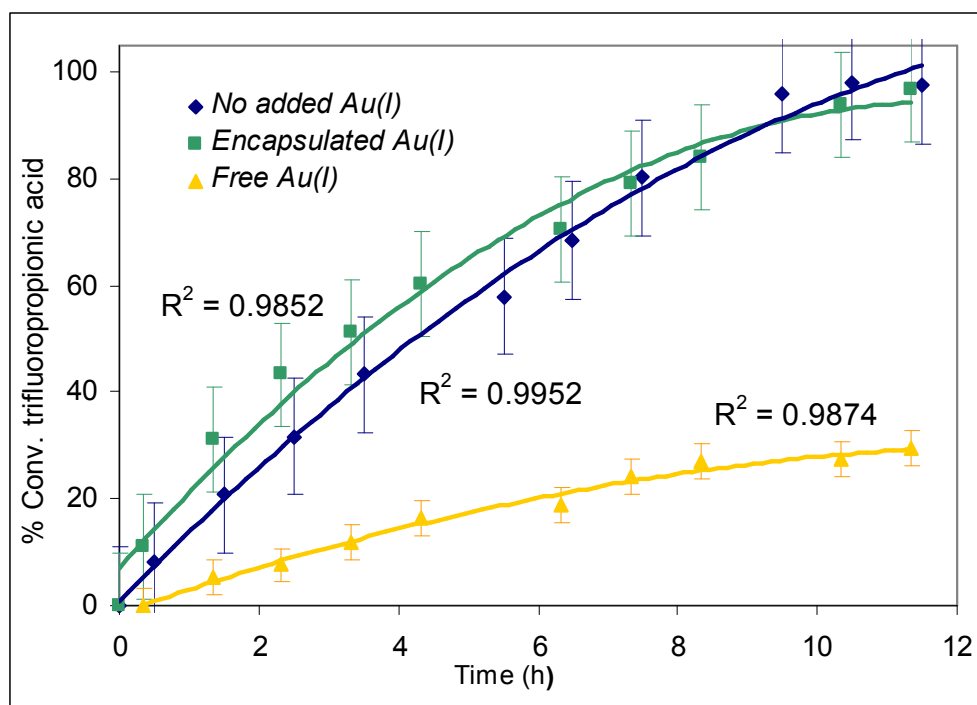
Sample with no $[\text{Au}]^+$: Tris buffer pH 8 (450 μL) was added to an NMR tube equipped with rubber septa cap and a D_2O external standard. At time $t = 0$, stock solution 2 (10 μL) and stock solution 1 (55 μL) was added and the NMR tube was sealed with parafilm and shaken gently until all components were combined.

Percent conversion from **4.6** to **3.**, as determined by the appearance of trifluoropropionic acid, was measured relative to internal standard. The ^{19}F NMR peaks monitored are as follows (tris buffer pH 8 with D_2O external standard, 400 MHz): substrate **4.6** (-63.7 ppm), trifluoropropionic acid (-62.4 ppm), and trifluoroethanol internal standard (-75.6 ppm). The kinetic data collected is shown in Table S2 and plotted in Figure S1.

Table S4.2. Kinetic data of reaction of **4.6** with Hog Liver esterase from ^{19}F NMR. Three conditions were examined: (1) reaction in the presence of $\text{PMe}_3\text{Au}^+ \subset \mathbf{3.8}$, (2) reaction in the presence of PMe_3AuCl and (3) reaction in the absence of any gold complexes.

<i>Time (h)</i>	<i>% Conv. (No $[\text{Au}]^+$)</i>	<i>Time (h)</i>	<i>% Conv. (Encapsulated $[\text{Au}]^+$)</i>	<i>%Conv. (Free $[\text{Au}]^+$)</i>
0	0	0	0	0
0.5	8.3	0.33	11.2	0
1.5	20.7	1.3	31.1	5.3
2.5	31.7	2.3	43.3	7.6
3.5	43.3	3.3	51.4	11.9
5.5	58	4.3	60.2	16.3
6.5	68.6	6.3	70.7	18.7
7.5	80.3	7.3	79.2	24.1
9.5	95.9	8.3	84.0	27.1
10.5	98.2	10.3	93.9	27.5
11.5	97.6	11.3	96.7	29.4

Figure S4.1. Plot of the conversion of the three reactions versus time (h).



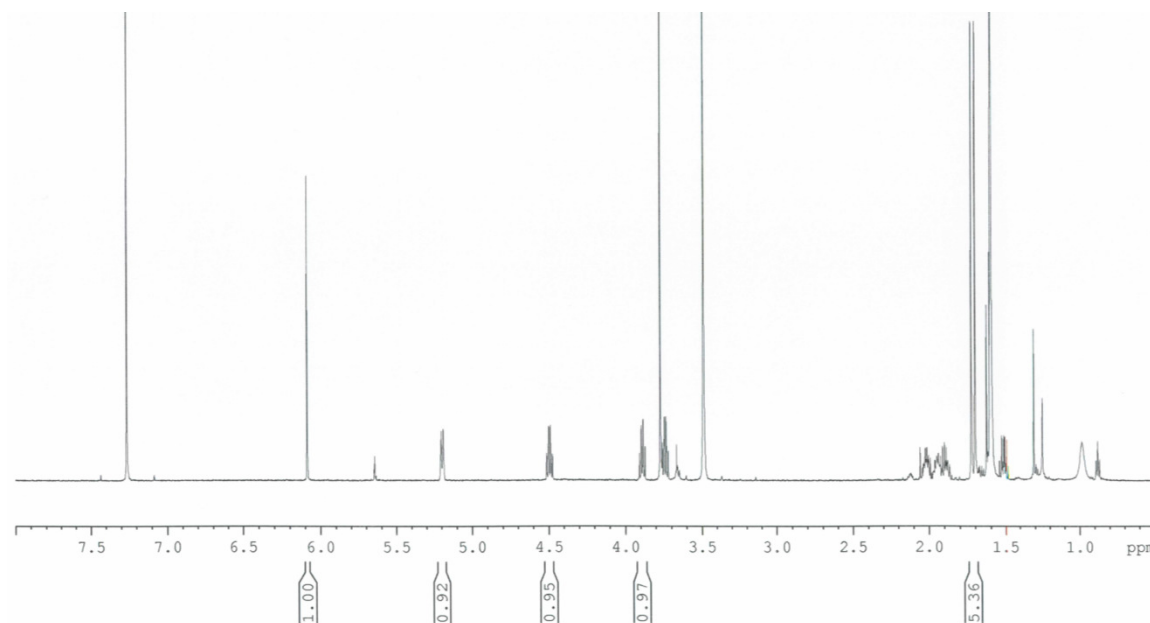
References

- (1) Wiester, M. J.; Ulmann, P. A.; Mirkin, C. A. *Angew. Chem., Int. Ed.* **2010**, *50*, 114.
- (2) Yoshizawa, M.; Klosterman, J. K.; Fujita, M. *Angew. Chem., Int. Ed.* **2009**, *48*, 3418.
- (3) Dalby P. A.; Lye G. J.; Woodley J. M. One-pot synthesis and the integration of chemical and biocatalytic conversions. *Handbook of Chiral Chemicals*, 2nd Ed., CRC Press, Boca Raton, **2005**.
- (4) Pollard D. J.; Woodley J. M. *Trends Biotechnol.* **2007**, *25*, 66.
- (5) Gröger, H. *Chem. Cat. Chem.* **2011**, *3*, 239.
- (6) Hailes, H. C.; Dalby, P. A.; Woodley, J. M. *J. Chem. Technol. Biotechnol.* **2007**, *82*, 1063.
- (7) Ogino H.; Ishikawa, H. *J Biosci Bioeng*, **2001**, *91*, 109.
- (8) Pamies, O.; Bäckvall, J.—E. *Chem. Rev.* **2003**, *103*, 3247.
- (9) Dinh, P. M.; Howarth, J. A.; Hudnott, A. R.; Williams, J. M. J.; *Tetrahedron. Lett.* **1996**, *37*, 7623.
- (10) Larsson, A. L. E.; Persson, B. A.; Bäckvall, J. E. *Angew. Chem., Int. Ed. Engl.* **1997**, *36*, 1211.
- (11) Allen, J. V.; Williams, J. M. J. *Tetrahedron Lett.* **1996**, *37*, 1859.
- (12) Kim, Y.; Park, J.; Kim, M.-J. *Chem. Cat. Chem.* **2011**, *3*, 271.
- (13) Thalen, L. K.; Zhao, D.; Sortais, J-B.; Paetzold, J.; Hoben, C.; Bäckvall J.-E. *Chem. Eur. J.* **2009**, *15*, 3403.
- (14) Burda, E.; Hummel, W.; Gröger, H. *Angew. Chem. Int. Ed.*, **2008**, *47*, 9551.
- (15) Boffi, A.; Cacchi, S.; Ceci, P.; Cirilli, R.; Fabrizi, G.; Prastaro, A.; Niembro, S.; Shafir, A.; Vallribera, A. *Chem. Cat. Chem.* **2011**, *3*, 347.
- (16) Asikainen, M.; and Krause, N. *Ad. Syn. Cat.* **2009**, *351*, 2305.
- (17) Berberian, V.; Allen, C. C. R.; Sharma, N. D.; Boyd, D. R.; Hardacre, C. *Adv. Synth. Catal.* **2007**, *349*, 727.
- (18) Simons, C.; Hanefeld, U.; Arends, I. W. C. E.; Maschmeyer, T.; Sheldon, R. A. *Topics in Cat.*, **2006**, *40*, 35.
- (19) Poe, S. L.; Kobaslija, M.; McQuade, D. T. *J. Am. Chem. Soc.* **2006**, *128*, 15586.
- (20) Fiedler, D.; Bergman, R. G.; Raymond, K. N. Stabilization of Reactive Organometallic Intermediates inside a Self-Assembled Nanoscale Host. *Angew. Chem. Int. Ed.*, **2006**, *45*, 745.
- (21) Merlau, M. L.; del Pilar Mejia, M.; Nguyen, S. T.; Hupp, J. T. *Angew. Chem., Int. Ed.*, **2001**, *40*, 4239.
- (22) For a general review of supramolecular chemistry in water, see Oshovsky, G. V.; Reinhoudt, D. N.; and Verboom, W. *Angew. Chem. Int. Ed.* **2007**, *46*, 2366.
- (23) Fiedler, D.; Leung, D. H.; Bergman, R. G.; Raymond, K. N. *Acc. Chem. Res.* **2005**, *38*, 351.

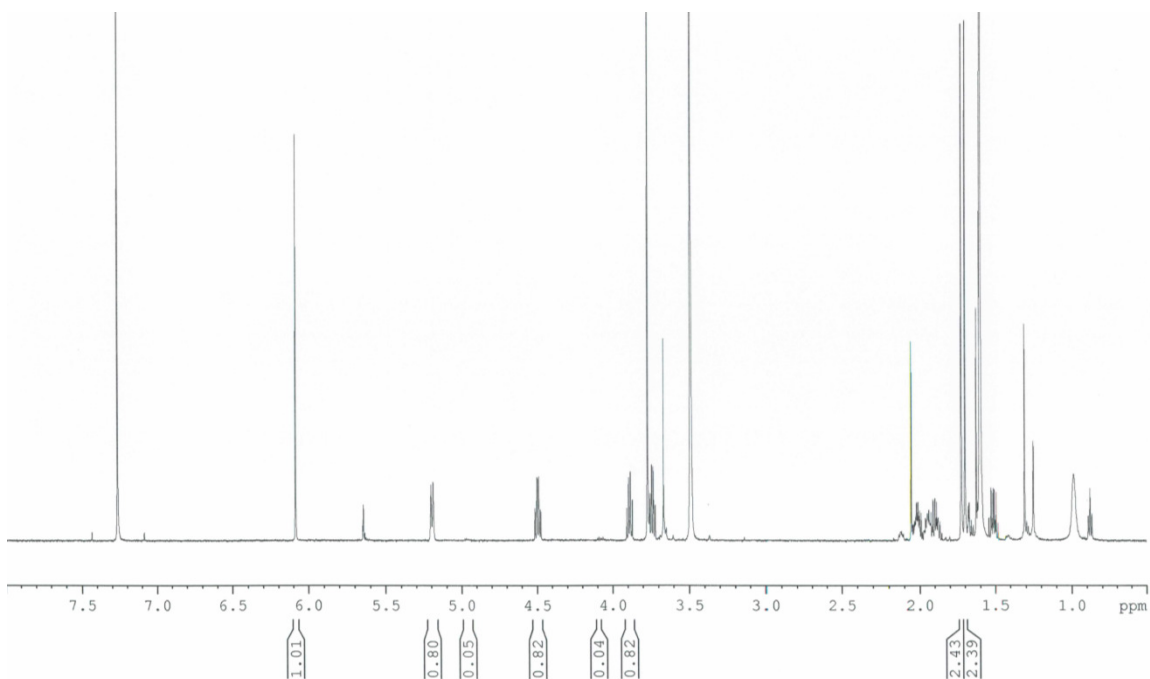
- (24) Wang, Z. J.; Casey, C. J.; Bergman, R. G.; Raymond, K. N.; Toste, F. D. *J. Am. Chem. Soc.* **2011**, *133*, 7358.
- (25) Brown, C. J.; Miller, G. M.; Johnson, M. W.; Bergman, R. G.; Raymond, K. N. *J. Am. Chem. Soc.* **2011**, *133*, 11964.
- (26) Drauz, K.; Waldmann, H. *Enzymes Catalysis in Organic Synthesis: a Comprehensive Handbook*. Wiley-VCH: New York, **2002**, vol. 2-3.
- (27) Bornscheuer, U. T.; Kazlauskas, R. J. *Angew. Chem. Int. Ed.* **2004**, *43*, 6032-6040.
- (28) Brooks, R. R. Watterson, J. R.; *Noble Metals and Biological Systems*. CRC Press: Florida, **1992**, p. 180.
- (29) Bhabak, K. P.; Bhuyan, B. J.; Mugesh, G. *Dalton Trans.*, **2011**, *10*, 2099.
- (30) (a) H. Schmidbaur and R. Franke, *Chem. Ber.* *105* (1972) 2985. (b) Angermaier, K., Zeller, E., Schmidbaur, H. *J. Org. Met.*, **1994**, *472*, 371.
- (31) C. Slugovc, E. Ruba, R. Schmid, K. Kirchner, *Organometallics*, **1999**, *18*, 4230-4233.
- (32) Caulder, D. L.; Bruckner, C.; Powers, R. E.; Konig, S.; Parac, T. N.; Leary, J. A.; Raymond, K. N. *J. Am. Chem. Soc.* **2001**, *123*, 8923-8938.

Appendix 4A: NMR Spectra

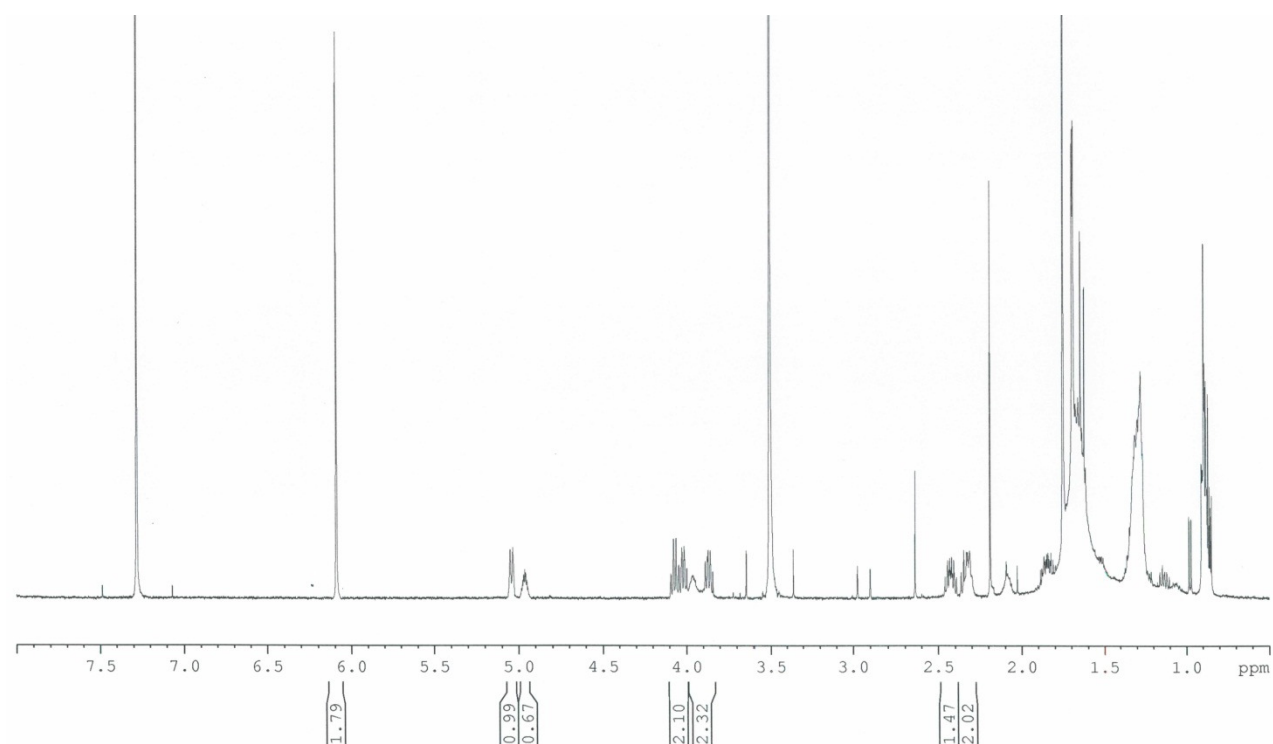
Spectrum 1: Tandem reaction of **4.1** with rabbit liver esterase and $\text{PMe}_3\text{Au}^+ \mathbf{3.8}$



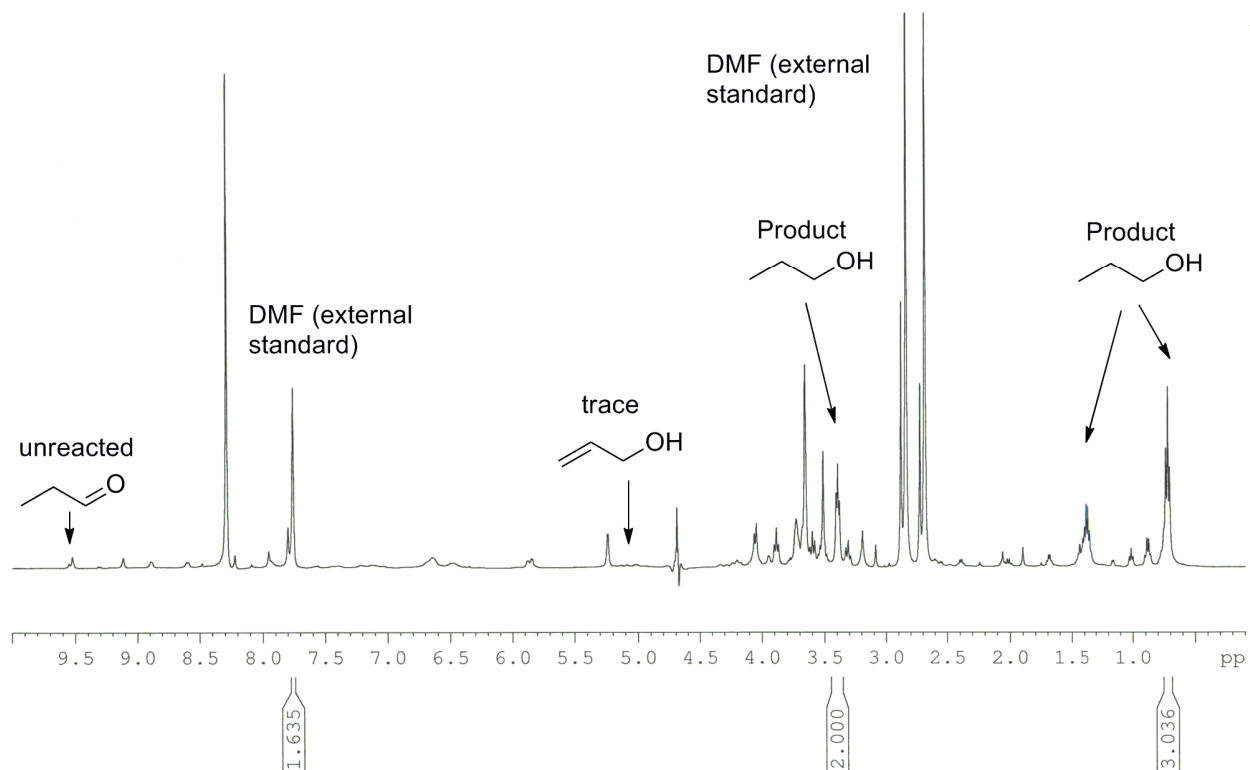
Spectrum 2: Tandem reaction of **4.1** with hog liver esterase and $\text{PMe}_3\text{Au}^+ \mathbf{3.8}$



Spectrum 3: Tandem Reaction of **4.3** with *Mucor meihie* lipase and $\text{PMe}_3\text{Au}^+ \text{3.8}$



Spectrum 4: Reaction of 2-propene-1-ol with $[\text{Ru}]^+ \text{3.8}$, HLADH, FDH, NADPH, and



NaHCO_2 .